Geodynamics of the Andaman - Sumatra - Java Trench - Arc System Based on Gravity and Seismotectonic Study

Thesis submitted to the

Cochin University of Science and Technology

By

Lasitha S

In partial fulfillment of the requirement for the award of the degree of

DOCTOR OF PHILOSOPHY

Under The Faculty of Marine Sciences

Department of Marine Geology & Geophysics
Cochin University of Science and Technology
Cochin - 682 016, Kerala, India.

September 2007

DEPARTMENT OF MARINE GEOLOGY & GEOPHYSICS
COCHIN UNIVERSITY OF SCIENCE AND TECHNOLOGY
COCHIN- 682 016, KERALA, INDIA.

CERTIFICATE

This is to certify that the research work presented in the thesis entitled **"GEODYNAMICS OF THE ANDAMAN-SUMATRA-JAVA TRENCH-ARC SYSTEM BASED ON GRAVITY AND SEISMOTECTONIC STUDY"** is an authentic record of research work carried out by Ms. Lasitha S. under my supervision and guidance at the Department of Marine Geology & Geophysics, Cochin University of Science and Technology, Cochin-682016 in partial fulfillment of the requirements for the degree of Doctor of Philosophy in Geophysics and that no part thereof has been included for the award of any other degree.

Dr. M. Radhakrishna
(Research Supervisor)

Cochin 682 016
September 2007

DECLARATION

I hereby declare that the thesis entitled **"GEODYNAMICS OF THE ANDAMAN-SUMATRA-JAVA TRENCH-ARC SYSTEM BASED ON GRAVITY AND SEISMOTECTONIC STUDY"** is the bonafide report of the original work carried out by me under the supervision of Dr. M. Radhakrishna at the Department of Marine Geology and Geophysics, Cochin University of Science and Technology, and no part thereof has been included in any other thesis submitted previously for the award of any degree.

Lasitha. S

September,2007,
Cochin-16.

Lasitha S

ACKNOWLEDGEMENT

As days pass by, life convinces me more and more of the blessings and tender love Lord has showered upon me, strengthening and leading me through hardships and trials.

I am extremely grateful to my guide Dr. M. Radhakrishna, for the excellent guidance through out the entire course of this work. I express my sincere gratitude for his valuable advices and motivation ever since my M.Sc days in CUSAT.

Also my gratitude to Dr. C.G. Nambiar, Head and doctoral committee, Department of Marine Geology & Geophysics, for his timely suggestions and advices.

My sincere thanks are due to Prof. K.T. Damodaran, Director, School of Marine Sciences, Cochin University of Science and Technology, for granting necessary permission to avail of the facilities of the school during the course of my research.

I relish the blessings and encouragement of faculty members of the Department of Marine Geology & Geophysics, Cochin University of Science & Technology, Prof. A. C. Narayana, P. Seralathan, S. Rajendran, K. Sajan and Dr. M. Ravisankar.

I also thank to Staff members of the Department of Marine Geology and Geophysics and staff members of Directors Office for the help rendered by them during the course of this study.

I express my heartfelt gratitude to Shri. T.M. Mahadevan, former Director, Atomic Mineral Division for his valuable advice and directions and critical comments during the various stages of this work.

Also, I am thankful to Dr. C. Subrahmanyam, NGRI, Hyderabad for many of his ideal and valuable suggestions.

I memorize that this venture would not have materialized without the wholehearted help of Dr. Sanu T D, Scientist, ONGC.

I am thankful to both university and Council of Scientific and Industrial Research for the financial support through fellowship.

This work would not have been accomplished without the tremendous help and assistance rendered by Sheena V.Dev and Shinu N. No words to explain my gratefulness towards them who are always with me in highs and lows.

Many thanks to my friends Drs. Arts K P, Ajayakumar P, N. R. Nisha, Su P. S, C. P. Priju, Mr. Babu Nalluswamy, Sijin kumar A. V, Nilof S. Pasha, Arunkur V.S, Subeer A, Baiju K. R, Sunilkumar, V, Venkiteswaran, G, Gireesh R, Dil Amarnath, Mashood, , Ms. Vinu Prakash, Sreela, Rekha, Subha and Subitha for t help in different stages of my work.

My sincere thanks due to Dr. S.Rajan, NCAOR, Goa for the support in final stages of my work.

I dedicate this for the love, belief, hope, dreams and prayers of my fam that could only make what I am today.

Lasitha

CONTENTS

List of Figures

Chapter 1

Chapter 2

Chapter 3

Chapter 4

Chapter 6

Figure 6.5 Gravity anomaly maps along Andaman arc and the Andaman Sea region used in the analysis / interpretation for delineating lithosphere structure. A) Free-air anomaly map (GEOSAT 2'x2' gravity) B) Slab Residual Gravity Anomaly (SRGA) deduced by subtracting the slab effect from the Free-air map C) Mantle Bouguer Anomaly (MBA) map. Details are discussed in text.

Figure 6.6-6.13: Gravity derived crustal models along the profiles AA'-HH in the Andaman arc region. The post-tsunami earthquakes are projected on to the crustal section to understand the relation of crustal structure and seismogenic behaviour. Open circles are events without any mechanisms, filled circles have focal mechanisms and stars are >5.5 magnitude events with type of faulting shown Thrust (T), Normal (N),Strike-slip (S)

List of Tables

CHAPTER 1

INTRODUCTION

1.1. General Introduction

The Burmese- Indonesian arc system extends from the Eastern Himalayan syntaxis southward through Burma, Andaman-Nicobar, Sumatra and eastward through Java to at least Sumba (Figure 1.1). The eastern edge of the Indo-Australian plate is being subducted beneath the Burmese plate along the Sunda subduction zone. This region is a classical example of a subduction system, composed of the down going Indo-Australian slab along the Andaman-Sumatra-Java trench, an accretionary wedge, the outer arc ridge, the Bengkulu - Mentawai fore arc basin off Sumatra and Java fore arc basin in front of the volcanic arc (Pubellier et al, 1992; Samuel and Harbury, 1996). The geometry of the subducting plate varies from Andaman in the north to Java in the south and the age and thickness of the subducted oceanic crust varies in terms of increase in dip and depth of penetration (Newcomb and McCann, 1987). This zone of interference is associated with strong volcanism and earthquakes causing occasional Tsunamis.

The Andaman-Burmese arc system serves as an important transitional link between the Himalayan collision zone to the north and the Sumatra – Java trench system in the south (Hamilton, 1979). The Andaman Sea is an extensional basin marking the edge between the China and Burma plates (Curray et al, 1977). Fitch (1972) viewed the Sunda strait as a tectonic as well as physiographic break in the arc that marks the limit between Java trench frontal subduction and Andaman-Sumatra

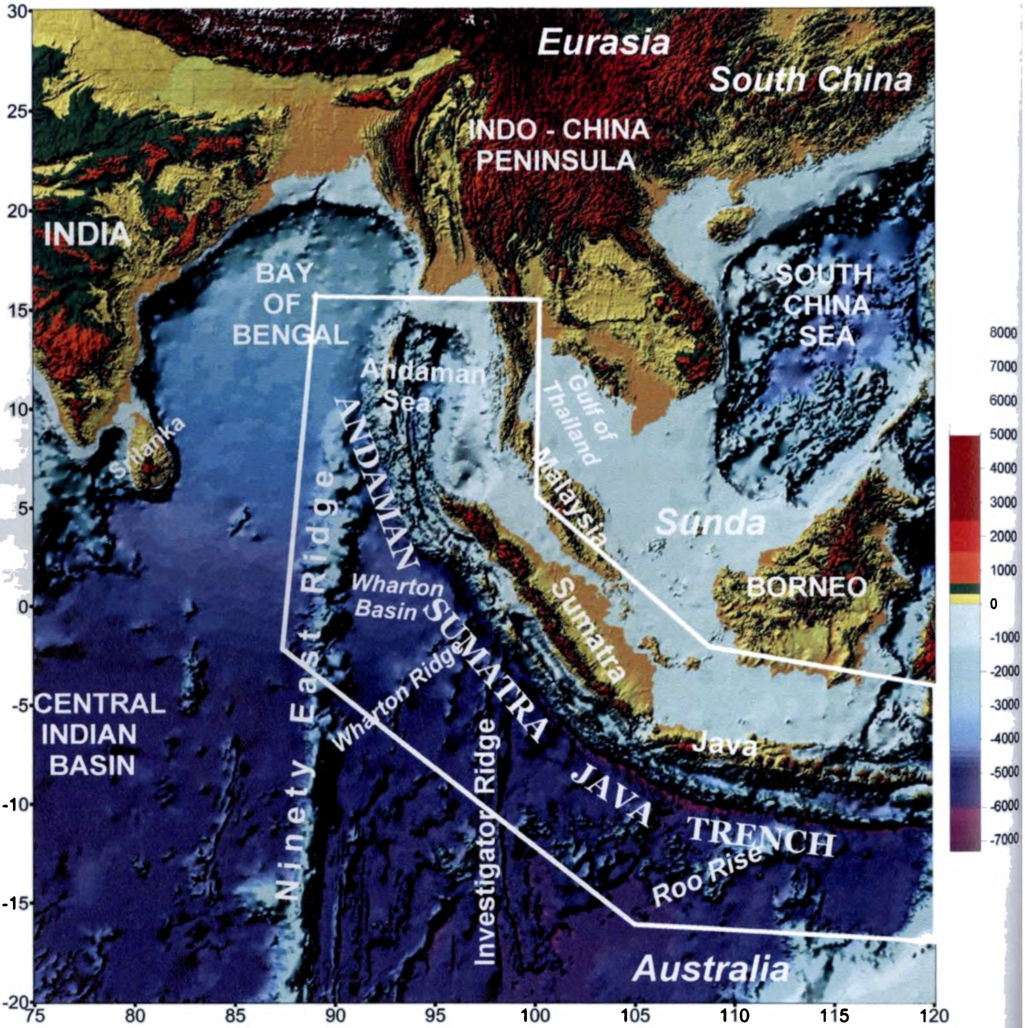

Figure 1.1. Topographic relief map as seen from GEBCO digital bathymetry data in the eastern Indian Ocean. Major morpho-tectonic elements in the region are indicated. The region covered by white line is the area of present study along the Andaman-Sumatra-Java trench-arc system.

oblique subduction. The geologic and tectonic history of the region is very complex due to the presence of several active faults/tectonic features, which have strong genetic linkage to the regional tectonics of the NE Indian Ocean and the Indian subcontinent. Hence, it is important to know more about the ongoing geodynamic process in the region.

1.2. Definition of the Problem

Earthquakes are powerful manifestations of sudden releases of strain energy accumulated due to tectonic movements and radiate seismic waves of various types that propagate in all directions through the earth's interior. The theory of plate tectonics gives a satisfactory explanation for the observed pattern of earthquakes emanating from plate boundaries. According to the theory, the relative movement between the lithospheric plates is considered to be the basic cause of earthquakes. At the boundary of these moving plates, they collide with each other and form large mountain belts or move away from each other forming spreading ridges. Large areas of moving plates that cannot move further are consumed at deep ocean trenches or subduction zones which mark sites of convective down welling of the earth's lithosphere (Figure 1.2).

The deepest earthquakes are always associated with subduction zones, where they occur at depths as great as 700 km. These earthquakes define inclined zones of seismicity known as Wadati-Benioff Zones, which outline the descending lithosphere. Studies of many volcanic arcs around the world have revealed that they tend to form above subduction zones at a location where the subducted slab has reached a depth of about of 100km. The introduction of cold oceanic crust into the mantle depresses the local geothermal gradient and causes a large portion of the earth to deform in a brittle fashion than it would in a normal geothermal gradient setting. Because earthquakes can only occur when a rock is deforming in a brittle fashion, subduction zones have the potential to create very large earthquakes. Subduction zones vary dramatically in their ability to store elastic strain energy. Such variation has been explained by

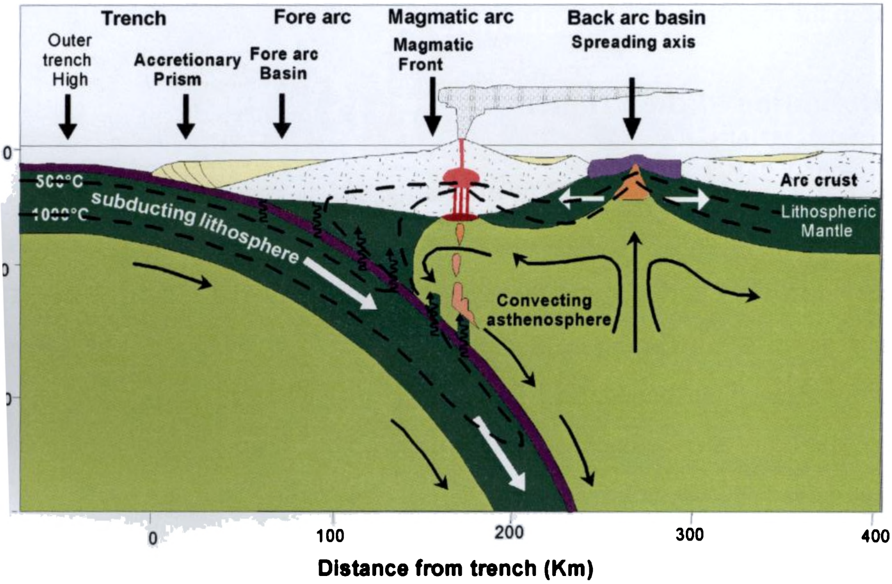

Figure 1.2. Schematic representation of a Subduction zone

differences in convergence rates and subducting plate ages (Kanamori, 1983), presence of subducting sediments and seamounts (Ruff, 1989; Cloos, 1992), upper plate deformation (McCaffrey, 1993), motion of the subducting slab through the mantle (Scholz and Campos, 1995), and temperature of the plate interface (Hyndman and Wang, 1993).

1.3. Study area

The Sunda arc extends about 5600 km between Andaman islands to the northwest and Banda arc to the east resulting from the convergence between the Indo-

Australian plate and South west Asia (Newcomb and McCann, 1987). While normal subduction prevails in the Java arc region, the subduction becomes progressively more oblique towards Sumatra and Andaman arc. Due to this oblique subduction, the tectonic deformation significantly varies in the different segments of the Indonesian arc-trench system. Also, the depth, dip and age of the Subducting slab vary significantly from north towards south that further complicates the geodynamic setting in the region. As the region is characterized by the large magnitude earthquakes similar to the other subduction zones of the world oceans, and in view of the 26th December 2004 giant mega thrust earthquake of Sumatra, the region has drawn the attention of international geo scientific community for more detailed understanding of the ongoing deformation and geodynamics. It is, therefore, important to know about the tectonic processes, deformation and geologic evolution of the area in order to assess future hazard. Because of this importance, the region pertaining to the Andaman-Sumatra-Java trench-arc system falling between 15°S-15°N and 90°E-118°E has been considered for detailed gravity and seismotectonic study (Figure 1.3).

1.4. Objectives

The Andaman-Sumatra-Java trench-arc and the adjoining region are seismically very active, characterized by earthquakes with depth of up to around 700 km. Many previous workers have studied the overall tectonics of the region and their studies gave valuable information on seismotectonics, subduction process and plate kinematic setting of the region (Rodolfo et al., 1969; Fitch, 1970, 1972; Curray et al., 1977, 1979, 1982; Hamilton, 1979; Moore and Curray, 1980; Huchon and Le Pichon, 1984; Chandra, 1984; Mukhopadhyay and Krishna, 1991; Curray, 1987, 2005; Maung, 1987; Newcomb and McCann, 1987; Mukhopadhyay and Dasgupta, 1988; Mc Caffery, 1991; Dasgupta, 1992; Diament et al., 1992; Dasgupta and Mukhopadhyay, 1993, Dasgupta et al., 2003; Mukhopadhyay and Krishna, 1995;

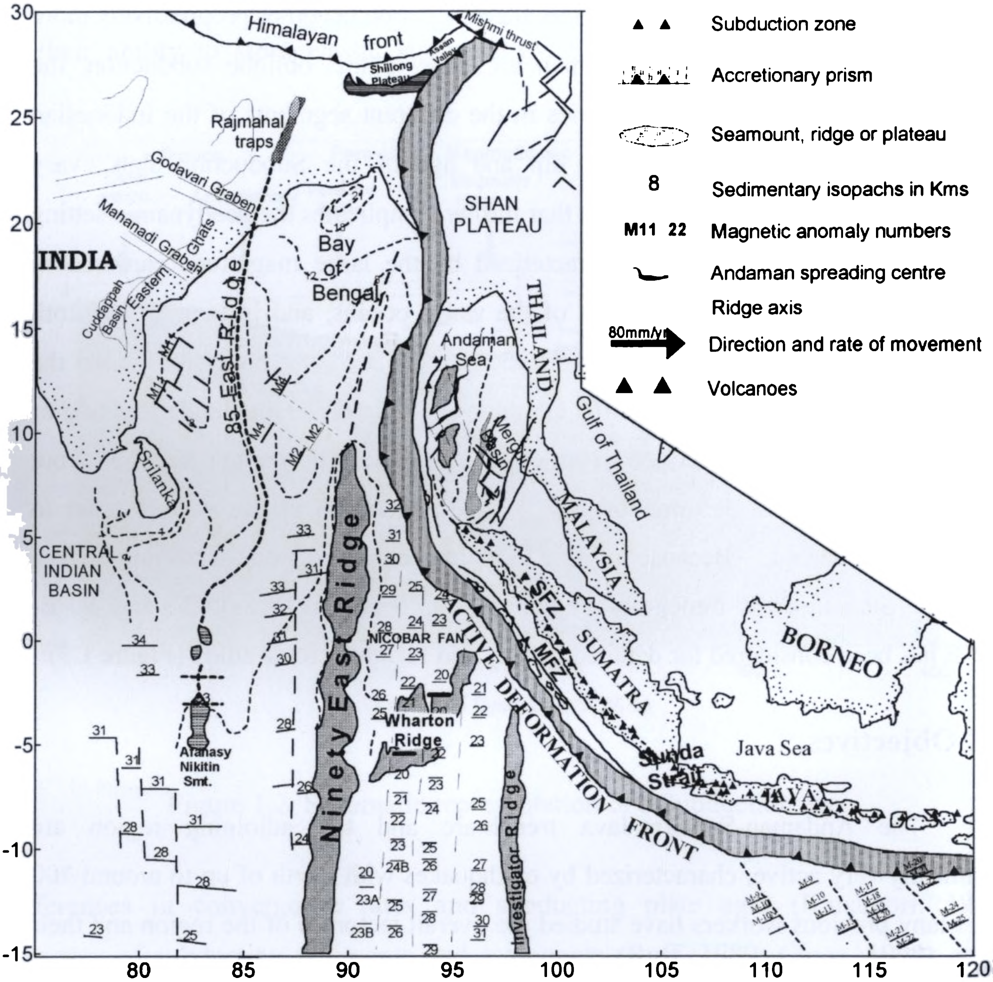

Figure 1.3. Tectonic sketch map showing various physiographic and tectonic features in the eastern Indian Ocean.

Malod et al.,1995; Krishna et al., 1995; Ravikumar et al., 1996; Slancova et al., 2000; Sieh, 2000; Prawirodirjo, 2000; Schluter et al., 2002; Kamesh Raju, 2005; Khan and Chakraborty, 2005 among others). A first order segmentation of the Burmese-

Indonesian arc has been presented by Chandra (1984), who suggested two transverse boundary zones, the north Andaman Boundary zone and the Sunda Boundary zone. Newcomb and McCann (1987) observed that the entire length of Sumatra has the potential to produce great thrust earthquakes whereas the plate interface near Java and Lesser Sunda islands can be considered to have low seismic potential. Slancova et al. (2000) identified seismically active domains within the overriding plates in the Sumatra fault zone (SFZ) and Java fault zone (JFZ).

Though many of these previous geophysical investigations have brought out significant variations on the tectonics operative in different segments of the arc, a unified picture through detailed Seismotectonic regionalization to understand the upper plate deformation, geometry of the subducting lithosphere is required. The recent mega thrust earthquake of 26 December 2004 has devastated the region and strongly ruptured plate boundary over a length of 1300 km along the Andaman-Sumatra arc. This resulted in a need for reassessment of the long-term deformation pattern as well as understanding the crustal mass anomalies in this segment of the arc. Therefore in the present study, the following aspects have been focused through detailed evaluation of the seismotectonics and interpretation of the gravity data.

- To understand the present day kinematics along the eastern plate boundaries of the Indian Ocean that is associated with strong volcanism and earthquake activity.
- To study the Benioff zone configuration and the stress distribution all along the arc.
- To attempt detailed seismotectonic regionalisation through a compilation of geological, tectonic and faulting pattern, which helps in identifying various active seismogenic zones of homogeneous deformation.

- Estimation of deformation velocities for the identified seismogenic zones to understand the present day tectonics in the overall realm of geodynamics of the region.
- To study the variation in the crustal deformation rates prior and after the tsunami event along the Andaman-Sumatra region.
- To delineate the crustal structure and density heterogeneities along and across the Andaman arc and its correlation with the seismogenic behaviour through analysis of seismotectonics, slab residual gravity and mantle Bouguer anomalies.

1.5. Data

A study of this nature requires compilation of vast amount of tectonic as well as geologic information, compilation of seismicity catalog, focal mechanism solutions, gravity, bathymetry and other geophysical information.

We have adopted the valuable information on geology, tectonics and overall geodynamics of the region given by many previous workers. For the study of the upper plate deformation and stress distribution pattern, we have compiled the hypocentral data of earthquakes from ISC and PDE listings. All available focal mechanisms pertaining to the area have been taken from Harvard CMT solutions and also from other important works related to the area. Although the region is covered by vast amount of ship-borne geophysical measurements, the available data is very sparse and does not cover the region uniformly. Therefore, the 2-minute gridded GEOSAT gravity data of Sandwell and Smith (1997) and the 1-minute gridded GEBCO bathymetry data have been considered for the present study.

1.6. Scope of the Present study

Altogether 7 chapters constitute this thesis. Chapter 1 gives the introduction on the objectives of the study, data used and the study area. Chapter 2 deals with the regional geologic setting and evolutionary history of the area. Here, the geotectonic framework of the Andaman-Sumatra-Java trench-arc system in the eastern Indian Ocean is described.

Chapter 3 describes the Benioff zone configuration and stress distribution in the Benioff zone all over the arc. This work aims to study the variation in subduction zone geometry along and across the arc and the fault pattern within the subducting plate. Depth of penetration as well as the dip of the Benioff zone varies considerably along the arc which corresponds to the curvature of the fold- thrust belt which varies from concave to convex in different sectors of the arc. The entire arc is divided into 27 segments and depth sections thus prepared are utilized to investigate the average dip of the Benioff zone in the different parts of the entire arc, penetration depth of the subducting lithosphere, the subduction zone geometry underlying the trench, the arc-trench gap, etc.

Chapter 4 describes how different seismogenic sources are identified in the region, estimation of moment release rate and deformation pattern. The region is divided into broad seismogenic belts. Based on these previous studies and seismicity pattern, we identified several broad distinct seismogenic belts/sources. These are 1) the outer arc region consisting of Andaman-Nicobar islands 2) the back-arc Andaman Sea 3) The Sumatran fault zone (SFZ) 4) Java onshore region termed as Java Fault Zone (JFZ) 5) Sumatran fore arc sliver plate consisting of Mentawai fault (MFZ) 6) The offshore Java fore arc region 7) The Sunda Strait region. As the seismicity is variable, it is difficult to demarcate individual seismogenic sources. Hence, we employed a moving window method having a window length of 3–4° and with 50% overlapping starting from one end to the other. We succeeded in defining 4 sources each in the Andaman fore arc and Back arc region, 9 such sources (moving windows) in the Sumatran Fault zone (SFZ), 9 sources in the offshore SFZ region and 7 sources in the offshore Java region. Because of the low seismicity along JFZ, it is separated into three seismogenic sources namely West Java, Central Java and East Java. The Sunda strait is considered as a single seismogenic source.The deformation rates for each of the seismogenic zones have been computed. A detailed error analysis of velocity tensors using Monte–Carlo simulation method has been carried out in order to obtain uncertainties. The eigen values and the respective eigen vectors of the velocity tensor are computed to analyze the actual deformation pattern for different zones. The results obtained have been discussed in the light of regional tectonics, and their implications in terms of geodynamics have been enumerated.

In the light of recent major earthquakes (26th December 2004 and 28th March 2005 events) and the ongoing seismic activity, we have recalculated the variation in the crustal deformation rates prior and after these earthquakes in Andaman–Sumatra region including the data up to 2005 and the significant results has been presented in Chapter 5.

Modeling of the lithospheric structure in the Andaman arc and the Andaman sea region using gravity and earthquake data constitutes the Chapter 6. In this chapter, the down going lithosphere along the subduction zone is modeled using the free air gravity data by taking into consideration the thickness of the crustal layer, the thickness of the subducting slab, sediment thickness, presence of volcanism, the proximity of the continental crust etc. Here a systematic and detailed gravity interpretation constrained by seismicity and seismic data in the Andaman arc and the Andaman Sea region in order to delineate the crustal structure and density heterogeneities along and across the arc and its correlation with the seismogenic behaviour is presented.

Chapter 7 is the summary and conclusion of the study.

CHAPTER 2

REGIONAL GEOLOGY AND TECTONIC HISTORY

2.1. Introduction

The seafloor created by spreading processes and aseismic ridges originating by mantle plumes from the Early Cretaceous to the Present document the tectonic history of break up of eastern Gondwanaland, major plate reorganizations, directions and rates of plate motions; interactions of hotspots with spreading centers, intra plate deformation and collision history of Indian plate with Eurasia and Himalayan orogeny (Krishna et al., 1995). The active tectonics of central eastern Asia exhibits a varied and complicated combination of styles of deformation. Much of this region appears to experience shortening in N-S direction, but both normal faulting associated with E-W or NW-SE crustal extension, and strike-slip faulting on major faults appear to play a key role in the overall deformation of Asia (Deng et al., 1979; Molnar and Tapponnier, 1975, 1978; Tapponnier and Molnar, 1977, 1979). These observations led to the suggestion that Asia deforms in response to the collision and subsequent penetration of India into Eurasia and that much of China is pushed eastward out of the way of the impinging continents (Molnar and Tapponnier, 1975, 1978; Tapponnier and Molnar, 1977, 1979).

The island arcs, trenches and marginal basins associated with Sunda arc form one of the most tectonically active and complex regions of the world (Purdy and Detrick, 1978). Stretching from Burmese arc nearly to Timor, the Sunda Island Arc delineates a subduction zone separating the Indian-Australian plate from the southward projection of the Eurasian plate. The Sunda Island arc, displays the characteristic relationship of a deep trench, a sedimentary arc, and a gravity minimum inside the trench, earthquake hypocenters along a dipping Benioff zone, and a volcanic arc above the Benioff zone. It continues to be an area of high interest for studies of the complexities created in a zone of plate convergence (Curray et al., 1977).

2.1. Regional geotectonic setting

The island arc extends over some 5600 km and separates the Indo-Australian plate and the Eurasian plate. This sector of the subduction system has been active since middle Tertiary time, as inferred from dating of the Sunda system volcanism by Hamilton (1988). Hamilton suggests that along the arc, the collision system changes from oceanic-continental in Sumatra through transitional in Java to intra-Oceanic in Bali. A morphological map of the study area is shown in Figure 2.1

On the northeastern side of the study area, the slow slipping Red River Fault of Vietnam and Southern China separates the Southeast Asian plate and the Eurasian plate. The Burmese-Andaman arc system forms an important transitional tectonic link between the Himalayas in the north and the Sunda arc in the south (Hamilton, 1979). Towards north, the Burmese arc meets the Himalayan arc at the syntaxis zone along the Mishmi hills block forming a major thrust zone. The Burmese arc is bounded on its west by the tectonically active belts of northeast India wherein, currently uplifting Shillong plateau is the most important tectonic feature. The Burma plate covering the Burmese plains, the Andaman and north Sumatra basins separate the Indian plate and the Eurasian plates. The eastern periphery of this Burma plate lies, the relatively high standing areas that include the Shan plateau, the Malay Peninsula and its western shelf, the Malacca strait and Sumatra. The Shan-Sagaing fault is a major right lateral fault along the eastern edge of the Burmese arc where the western Burma seems to slide past the rest of Indo-China (LeDain et al., 1984).

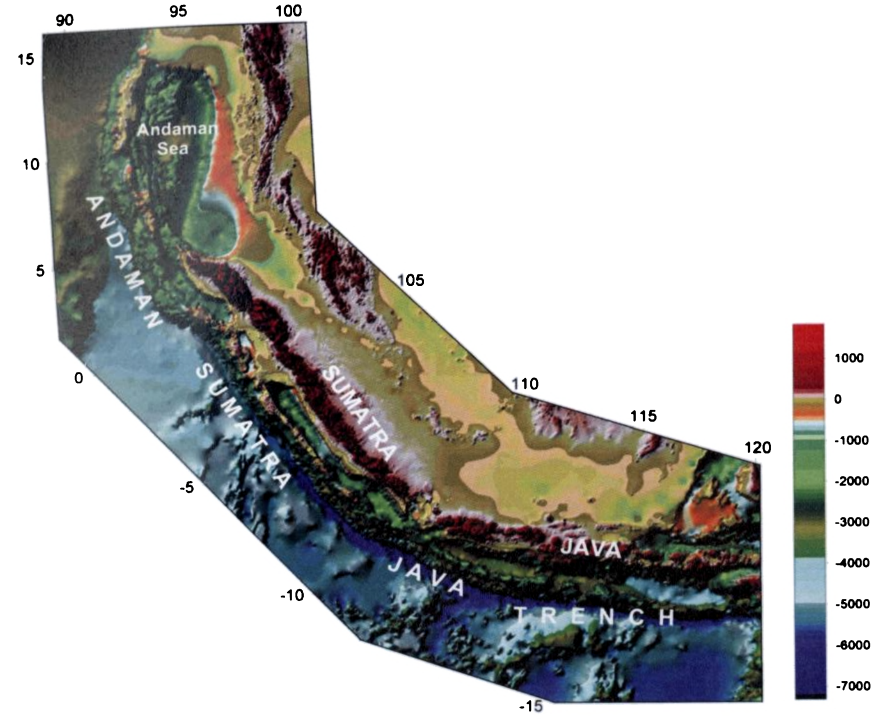

Figure 2.1. Morphology map of the Andaman-Sumatra-Java trench-arc system.

The Andaman basin is an extensional basin spreading in a NW-SE direction marking the edge between the Eurasia and Burma plates in the north to Indonesia in the south, situated between 6°N and 14°N and 91°E and 94°E. Win Swe (1972) inferred that the Sagaing fault turns southward into the spreading axis of Andaman Sea. This back arc-spreading center in the Andaman Sea is transformed southward into the Sumatra fault system that cuts the entire length of Sumatra (Curray et al., 1977). The western side of the Burmese and Andaman trench-arc region is bordered by Bay of Bengal and Ninety East Ridge. The Andaman basin comprising of Andaman Sea in the back-arc extends nearly 1200 km from Burma to Sumatra in the N–S and around 650 km from the Malay Peninsula to the Andaman and Nicobar Islands in the E–W. The central Andaman Sea is marked by steep and elongate sea valleys and seamounts such as the Nicobar Deep, Barren–Narcondam volcanic islands, Invisible bank, Alcock and Sewell seamounts (Rodolfo, 1969). Curray et al. (1982) suggested that the Andaman Sea and the central lowlands of Burma are parts of a single structural province.

Towards south, the Sumatra fault system extends for 1900 km along the volcanic chain of western Sumatra from 10°N to 7°S (Sieh and Natawidjaja, 2000). In the southwestern part, there is a 300 km wide strip of lithosphere between the Sumatran fault and the Sumatran deformation front called the Sumatran fore arc sliver plate. The SFZ is also considered as the limit between the Eurasian plate and the fore arc sliver plate. The fore arc ridge (outer arc high) is characterized by islands such as Enggano, Pagai, Siberut, and Nias that provide considerable geological information.

Java (8° S ,110° E) is part of the Sunda Island Arc, which includes Sumatra to the North West and Bali to the East. It is the world's 13th largest island formed mostly as the result of volcanic events. Java Sea and Borneo lies to the north and Indian Ocean to the south of Java. Its southern edge is marked by the presence of the Wharton Basin and the north Australian Basin. (Figure 2.2).

Since this area is associated with strong earthquake activity and volcanism, it is important to understand the tectonics, geological history as well as the ongoing geodynamic processes in order to assess the future hazards.

2.3. Geotectonic Framework and evolution of the Andaman-Sumatra-Java trench-arc system in the Eastern Indian Ocean

The zone of active convergent margin along the Andaman – Sumatra-Java arc in the eastern Indian Ocean is geodynamically quite complex and interesting in view

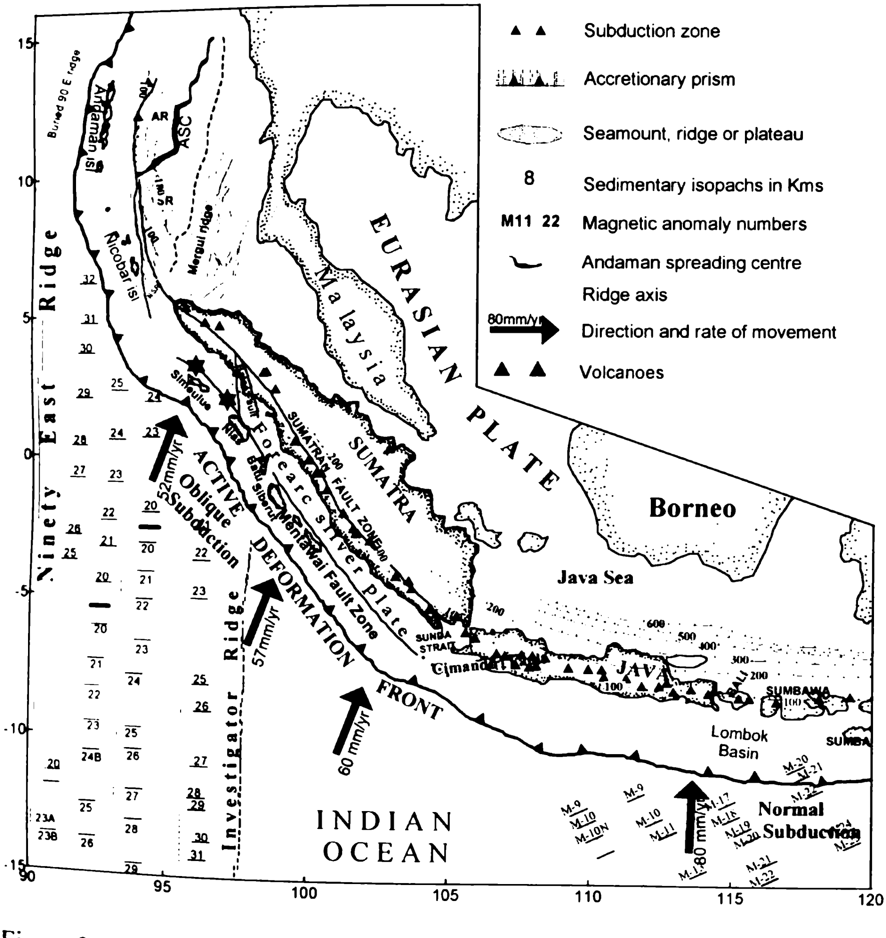

Figure 2.2. Generalised tectonic map of the Andaman-Sumatra-Java trench-arc and adjacent regions.

of wide variation in subduction geometry, morphology and stress field in both along and across the arc and the presence of active back-arc spreading in the Andaman Sea.

Major tectonic features in the eastern Indian Ocean were inherited from the break-up of the eastern Gondwanaland and subsequent spreading of the Indian Ocean floor. Some of these features which are important in the evolutionary history of the region (see Fig. 1.3- generalized tectonic map) are: (1) the large sediment filled basin called the Bengal fan in the Bay of Bengal, 2) the Ninety East ridge, a 4500 km long aseismic ridge trending N–S along the 90° E meridian (3) The fold mountain belt of Andaman and Indo-Burman ranges formed by eastward subduction and motion along the Shan-Sagaing transform and the Neogene back-arc spreading in the Andaman Sea (4) the Sumatran Fault Zone (SFZ), a northwest trending active strike-slip fault that cuts the entire length of Sumatra and Indonesia (5) Java onshore region termed as Java Fault Zone (JFZ) (6) Sumatran fore arc sliver plate consisting of Mentawai fault zone (MFZ) (7) The offshore Java fore arc region, which is characterized by typical fore arc basins and (8) The Sunda strait, which is considered as a transition zone between the normal subduction in front of Java to the east and oblique subduction to the west. Most of these features came into existence during the northward flight of India since the late Cretaceous. McKenzie and Sclater (1971) studied the evolution of the Indian Ocean since the Late Cretaceous based on magnetic anomaly identifications and concluded that during 75–35 m.y., the movement of the Indian plate was very rapid (18 cm/yr) mostly in northward direction. They infer that this movement was taken up by the Chagos-Laccadive transform fault on the West and by the Ninety East Ridge on the East. Johnson et al. (1976) have studied the spreading history of the eastern Indian Ocean, where the oldest magnetic anomalies are aligned sub-parallel to the East Coast of India corresponding to about 2 km isobath. A schematic illustration of age and history of oceanic crust in the eastern Indian Ocean (Figure 2.3) is given by Hamilton (1979).

The details on various prominent stages of geological evolution and resultant formation of major tectonic/structural elements are discussed here for better understanding of present day geodynamics of the region.

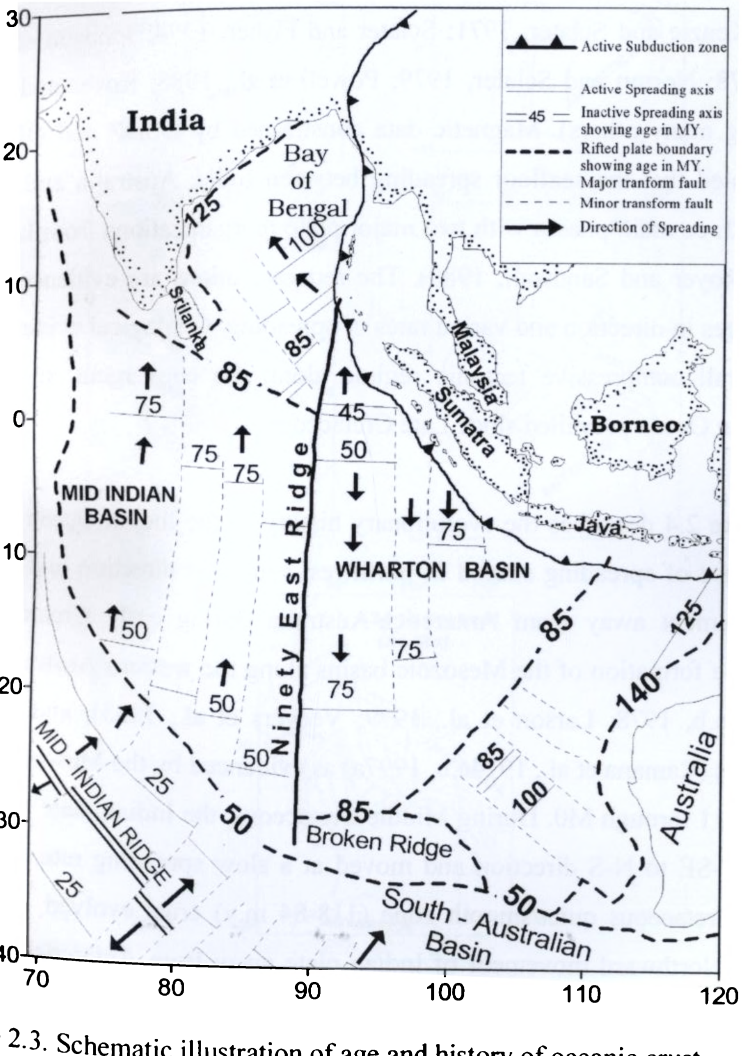

Figure 2.3. Schematic illustration of age and history of oceanic crust in the eastern Indian Ocean as given by Hamilton (1979).

2.3.1. Geologic Evolution of the Eastern Indian Ocean

Break up of eastern Gondwanaland during the Early Cretaceous resulted in the evolution of the Indian Ocean. The plate tectonic theory has been used for the eastern Gondwana reconstruction to unravel the evolutionary history of the Indian Ocean (McKenzie and Sclater, 1971; Sclater and Fisher, 1974; Johnson et al., 1976; Duncan, 1978; Norton and Sclater, 1979; Powell et al., 1988; Royer and Sandwell, 1989; among many others). Magnetic data constrained by DSDP and ODP drilling results revealed that the seafloor spreading between India, Australia and Antarctica occurred in three main phases with two major plate reorganizations from late Jurassic to present (Royer and Sandwell, 1989). The reorganizations are evidenced by ridge jumps, changes in direction and varied rates of spreading. Geological evidences reveal that an overall compressive tectonic regime along the convergent margin in the eastern Indian Ocean prevailed since Late Cretaceous.

Figure 2.4 describes the evolutionary history of the Indian Ocean in general. The first phase of spreading started in northwest-southeast direction and resulted in India's movement away from Antarctica-Australia during early Cretaceous. This resulted in the formation of the Mesozoic basins along the western Australian margin (Markl 1974a,b, 1978; Larson et al., 1979; Veevers et al., 1985), and the eastern Indian margin (Ramana et al., 1974a,b, 1997a) as evidenced by the Mesozoic anomaly sequences M11 through M0. During Middle Cretaceous, the Indian plate rotated from its early NW-SE to N-S direction and moved at a slow spreading rate. During this period, the Cretaceous quiet/smooth zone (118-84 m.y) crust evolved in the distal Bengal Fan. Northward movement of Indian plate away from Antarctica took place during Middle Cretaceous to Middle Eocene. The first major reorganization of the plates took place during Middle Cretaceous time, evidenced by the change in India's motion from NW-SE to N-S (McKenzie and Sclater, 1971; Norton and Sclater, 1979;

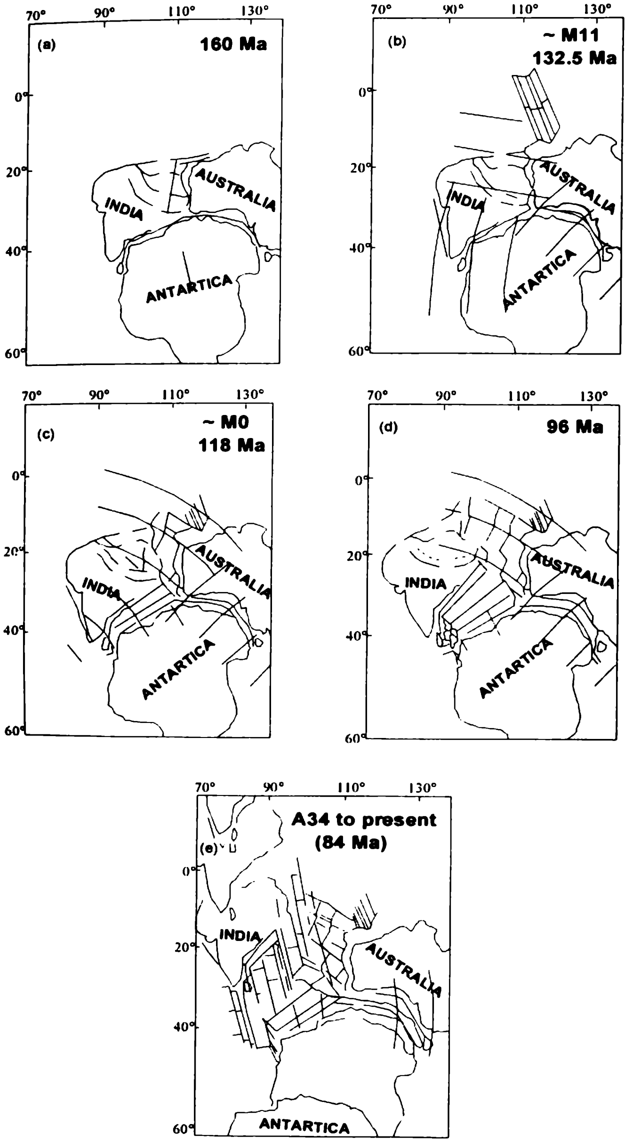

Figure 2.4. Sketch model of the evolution of the northeastern Indian Ocean (after Ramana et al., 2001).

Powell et al., 1988; Cande and Mutter, 1982; Veevers et al., 1986; Scotese et al., 1988). The second phase of spreading started in the N-S direction and continued up to formation of anomaly 19 (about 24 m.y) in the central Indian Ocean. During this period, India drifted in the N-S direction from Antarctica with a rapid speed of 11 to 7 cm/yr. The magnetic lineations 34 through 19 have evolved in the east-west direction with large lateral offsets, giving rise to the major fracture zones. During this phase of drifting, major parts of the central Indian and Crozet basins have evolved (McKenzie and Sclater, 1971; Schlich, 1975, 1982). The initiation of seafloor spreading between Australia and Antarctica (Cande and Mutter, 1982) and the opening of Wharton basin (Sclater ánd Fisher, 1974; Liu et al., 1983) also took place during this period. The second major plate reorganization occurred in the middle Eocene time when Indian and Australian plates merged and formed as a Single Indo-Australian plate (magnetic anomaly 20 to 18) (Liu et al., 1983; Royer et al., 1989a; Krishna et al., 1995). The third phase of spreading initiated in northeast-southwest direction in the middle Eocene and appears to continue since then. The Australian and Antarctica basins (Weissel and Hayes, 1972) were formed along the SE Indian ridge (SEIR) in the third phase.

2.3.2. Tectonics

The 2004 and 2005 witnessed two mega earthquakes that have ruptured the boundary between the Indo-Australian plate, which moves generally northward at 40-50 mm/yr, and the southeastern portion of Eurasian plate, which is segmented into the Burma and Sunda sub plates. East of Himalayas, the plate boundary trends southward through Myanmar, continuing offshore as a subduction zone along the Andaman-Nicobar islands and further south to Sumatra, where it turns eastward along the Java trench. This zone of convergence is characterized by the occurrence of numerous earthquakes, both shallow and deep (Figure 2.5). The area is a classical example of a subduction system, composed of the down going Indo-Australian slab along the Sumatra-Java trench, an accretionary wedge, the outer arc ridge forming the backstop (Pubellier et al., 1992; Samuel and Harbury, 1996), the Bengkulu - Mentawai fore arc

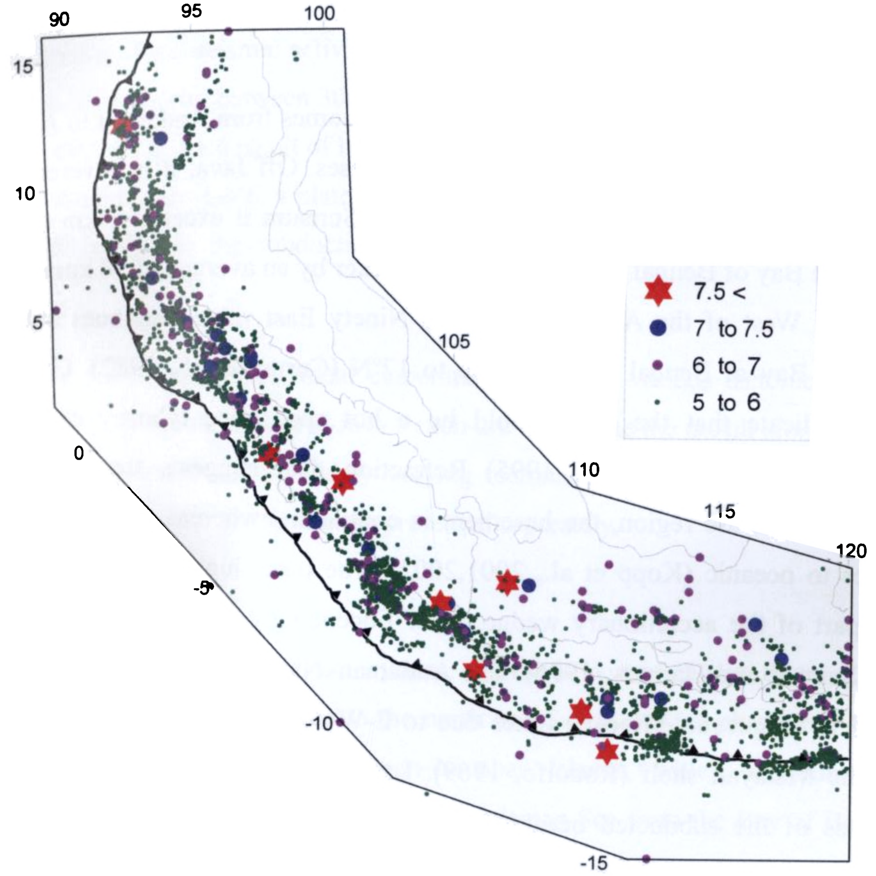

Figure 2.5. Seismicity map of the Andaman - Sumatra – Java arc region showing epicenters with magnitude ≥ 5.0. Both shallow upper plate and deeper Benioff zone events have been included in the map.

basin off Sumatra and Java fore arc basin in front of the Volcanic arc (Schluter et al., 2002). The Andaman-Sumatra-Java arc system has evolved through mainly subduction related processes responding kinematically to the plate reorganizations and other tectonic adjustments taking place during the evolution of the Indian Ocean as well as the Philippine Sea region.

The geometry of the subduction plate varies as it comes from Andaman to Java as the sediment thickness of the subducted plate decreases. Off Java, it is covered by only few hundred meters of sediments, whereas, off Sumatra it exceeds 1 km and at the head of the Bay of Bengal the sediments are thicker by an average of 10 km (Curray et al., 1977). West of the Andaman arc, the Ninety East ridge continues subsurface below the Bay of Bengal sediments up to 17°N (Curray et al., 1982). Geophysical studies indicate that the ridge could be a hot spot trace (Curray et al., 1982; Mukhopadhyay and Krishna, 1995) Refraction data suggests that off Southern Sumatra, in the arc region, the basement is continental whereas, off western Java it changes to oceanic (Kopp et al., 2001,2002). The outer high, which represents the fossil part of the accretionary wedge, is of Eocene-Oligocene age (Pubellier et al., 1992; Samuel and Harbury, 1996). The Andaman–Nicobar ridge is believed to have formed in Oligocene–Miocene times due to E-W compression of sediments derived from the Malayan shelf (Rodolfo, 1969). Lay et al. (2005) observed that age and thickness of the subducted oceanic crust and the convergence rate increase from Andaman towards Java along the arc. The increasing dip and depth of penetration of the Benioff zone reflects this change as well as changes in slab geometry. Oblique, but predominantly thrust motion occurs in the Andaman trench with a convergence rate of about 1.4 cm/yr (Lay et al., 2005). The Andaman back-arc spreading ridge-transform system accommodates the remaining plate motion, joining with the Sumatra fault to the south. The subducting oceanic crust off Sumatra is 46-60 m.y old and has a present convergence rate of 6.81cm/yr, while the crust off Java with an age ranging from 70 to 100 m.y. (Hamilton, 1979, Ghose et al., 1990) converges at a rate of 7.23 cm/yr (DeMets et al., 1994). According to Newcomb and McCann (1987), the slab configuration is ambiguous in the northern Sumatra, where as, in the south the observed dip is 40-50°. West of Sunda strait, seismic activity does not extend below 300 km. But by Java, seismic activity extends from the surface to a depth of 650 km with a gap in seismicity between 300 and 500 km (Fitch and Molnar, 1970; Newcomb and McCann, 1987). As a result of highly oblique motion between the Indo-Australian plate and the Eurasian plate, a plate sliver, referred to as the Burma micro plate, has sheared off parallel to the subduction zone from Myanmar to Sumatra (Lay et al., 2005).

The following sections deal elaborately about the various tectonic features associated with Andaman-Sumatra-Java trench-arc region. As the arc all along contain morpho-tectonic features with widely varying tectonic history and also for clarity, different segments of the arc have been presented separately.

2.3.2.1. ***Andaman arc region***

The Andaman-Burmese arc system serves as a transitional tectonic link between Himalayan Collision zone to the north and Sunda arc–trench system in the south (Hamilton, 1979). The Andaman–Nicobar Islands, which are sub-aerial expressions of the fore-arc ridge separate the Andaman Sea from the Bay of Bengal. The region is dominated by youthful structures which are either tensional in origin or have resulted from combined tensional and strike-slip movements. The Andaman basin comprising of Andaman Sea in the back-arc extends nearly 1200 km from Burma to Sumatra in the N–S and around 650 km from the Malay Peninsula to the Andaman and Nicobar Islands in the E–W. It is an extensional basin spreading in NW-SE direction marking the edge between the Eurasia and Burma plates in the north and Indonesia in the south, situated between 6° N and 14°N and 91° E to 94°E.

The Indo-Burman ranges and the Andaman–Nicobar ridges are a northward continuation of the Mentawai ridge of the Sumatran subduction zone. Rodolfo (1969) suggested that the east-west compression of sediments derived from the Malayan shelf resulted in the formation of the Andaman–Nicobar ridge in Oligocene–Miocene age. The central Andaman Sea is marked by steep and elongate sea valleys and seamounts such as the Nicobar Deep, Barren–Narcondam volcanic islands, Invisible bank, Alcock and Sewell seamounts (Rodolfo, 1969). Curray et al. (1982) inferred that the formation of the Andaman Sea has a definite genetic linkage with the evolution of the Bay of Bengal. During this evolution, modifications to the subduction zone geometry have produced considerable mass anomalies at depth. The rock types in the Andaman –Nicobar islands mainly constitute: Cretaceous serpentinites, ophiolites with radiolarian cherts, Cretaceous to Eocene cherty pelagic limestone and a thick section of Eo-Oligocene flysch overlain by Neogene shallow water sediments (Chatterjee, 1967; Eremenko and Sastri, 1977; Roy, 1983). The western base of the Andaman–Nicobar ridge is marked by the trench that is filled with the sediments of the Bay of Bengal (Curray et al., 1979). The structure along the arc in the Andaman–Nicobar ridge region is dominated by east dipping nappes having gentle folding, while tighter folding and intense deformation is observed off Sumatra (Weeks et al., 1967; Moore and Curray, 1980). Eremenko and Sastri (1977) observed that the deformation is more intense in Cretaceous–Oligocene sequences than the younger sequences. Several north –south faults and thrusts have been observed in the Andaman–Nicobar ridge and the adjacent offshore areas, among them, the most significant are the Jarwa thrust developed on the main islands (Roy, 1983) and the West Andaman fault, east of the Andaman–Nicobar ridge (Curray et al., 1979). Mukhopadhyay (1984) observed that some of these faults/thrusts are seismically active. Curray et al. (1982) suggested a relation between thickness of sediments on the subducting plate and height and volume of the outer sedimentary arc or non–volcanic ridge of the arc. Curray et al.

(1982) inferred that the Andaman Sea and the central lowlands of Burma are parts of a single structural province.

The Andaman Sea is a complex back arc extensional basin that differs from most other such basins in that it is west facing and that it was formed by transtension (Curray, 2005). It lies along a highly oblique convergent margin between the northeastern moving Indo-Australian plate and nearly stationary Eurasian plate. Uyeda and Kanamori (1979) related the back-arc spreading activity in the Andaman Sea to leaky transform tectonics. Eguchi et al. (1979) inferred collision of the Ninety East ridge with the Sunda trench in the middle or late Miocene which transmitted compressional stresses into the back-arc area and at the same time the drag exerted by the collision of India with Eurasia caused opening of the Andaman Sea, whereas, Curray (2005) is of the opinion that as the greater Indian continental mass converged on the SE Asian margin, it caused clockwise rotation of the subduction zone and increase in obliquity to the point that transtension along a sliver plate has resulted in oblique rhombo chasm like opening of the Andaman Sea during the Neogene. General structure in the Mergui north Sumatra basin consists of a series of horsts and grabens. Seismic refraction studies by Kieckhefer (1978) indicate that a thin continental crust underlies the basin. Structures in the basin are suggestive of rotated fault blocks indicating rifting of an older sedimentary section during the opening of this part of the Andaman Sea. The identified magnetic anomalies in the central Andaman Sea indicate a spreading rate of 3.72 cm/yr with opening started about 13 m.y. or in Middle Miocene (Curray et al., 1979). Total opening since that time has been 460 km (Curray et al., 1982). Raju et al. (2004) has arrived at a conclusion that the present full rate spreading in the central Andaman Basin is about 38 mm/yr and that it has opened 118 km in about the last 4 m.y, which agrees with the recent observation of Curray (2005). Win Swe (1972) inferred that this spreading axis is in turn transformed northward onto the Sagaing fault. Curray et al. (1977) proposed that opening of the Andaman

Sea is transformed southward into the Sumatra fault system. In the geologic past, some of the motion of this opening may possibly have been taken up by a southern continuation of the West Andaman Fault.

Curray(2005) excellently synthesized all available geological and geophysical data and proposed different stages of opening of the Andaman Sea region. His reconstruction involves separation of India from Australia and Antarctica in the eastern Gondwanaland and its northward flight since the Cretaceous. Some salient aspects of the reconstruction history (Figure 2.6) have been presented below; as outlined in Curray (2005).

- Before the departure of India from Australia and Antarctica, the South Tibet, Burma and SIBUMASU Blocks had already spun off northward and had docked against Asia. Prior to initiation of the subduction system, this could have been a passive continental margin, the source of some of the older sediments found in Myanmar and the Andaman-Nicobar Ridge.
- The northeastern corner of 'Greater India' hit this subduction zone at about 59 Ma (Klootwijk et al., 1992), the so-called 'soft collision', and India underwent some counter clockwise rotation from about 59 to 55 Ma, at which time the suture was completely closed. During this time and until about 44 Ma, India was indenting the Asian margin and rotating the subduction zone in a clockwise direction. With this rotation the direction of convergence became increasingly more oblique. Finally, probably in the middle to late Eocene, about 44 Ma, a sliver fault formed, the forerunner of the Old West Andaman and Sagaing Fault systems. Right-lateral motion started on the Khlong Marui and Ranong Faults at about this same time (Lee and Lawver, 1995) prior to the opening of the Mergui Basin during the Oligocene. The northern strand of the Mergui fault may have crossed the Mergui

Ridge as a splay of the Sagaing Fault (Figure 2.6a). The Mergui Ridge was probably part of the original volcanic arc.

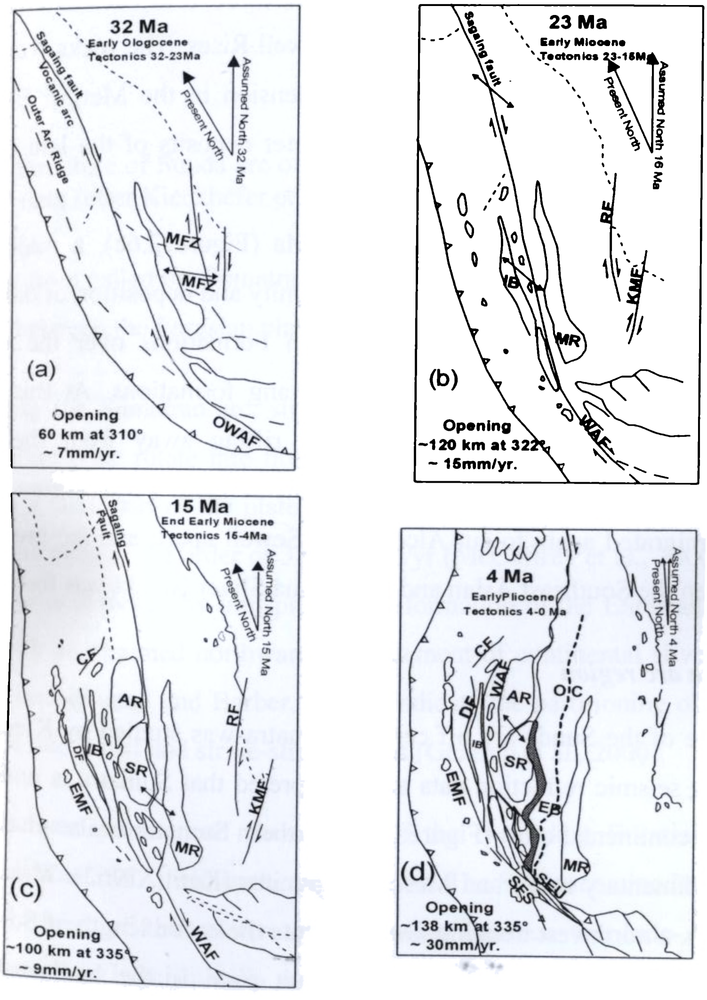

Figure 2.6. Sketch model of the reconstruction history showing different stages of opening of the Andaman Sea region (after Curray, 2005).

- By early Miocene, about 23 Ma (Figure 2.6b) , the plate convergence was oblique enough that extension and back arc sea floor spreading moved westward to the sliver fault running approximately along the magmatic arc, which had by that time migrated westward. The sea floor spreading and creation of oceanic crust formed the rock masses comprising of Alcock and Sewell Rises. The rocks from Alcock are early Miocene. With abandonment of extension in the Mergui Basin area, rapid subsidence occurred and the shallow water deposits of the late Oligocene were buried by deeper water facies.
- At the end of early Miocene, about 15-16 Ma (Figure 2.6c), a major change occurred in the Mergui Basin with an unconformity and deposition of dark gray to black shales of the Baong, Trang and Surin Formations over the carbonate sediments of the Peutu, Tai, Katang and Payang formations. At this time the conjoined Alcock and Sewell Rises started rifting away from the edge of continental crust forming East Basin. And finally at about 4 Ma (Figure 2.6d), the plate edge migrated again to cut Alcock and Sewell apart, and the present plate edge between the Southeast Asian and the Burma Sliver Blocks was formed.

2.3.2.2. *Sumatra arc region*

Structure of the Sunda arc off central Sumatra was studied by Kieckhefer et al. (1980), using seismic refraction data and interpreted that Sumatra is underlain by older, Paleozoic continental crust (Figure 2.7). Northern Sumatra is also characterized by Paleozoic sedimentary rocks and Mesozoic granites (Katili, 1962). The Sumatran fault Zone (SFZ), a northwest trending fault that cuts the entire length of Sumatra and Indonesia is a major dextral active strike-slip fault zone. In the southwestern part, there is a 300 km wide strip of lithosphere between the Sumatran fault and the

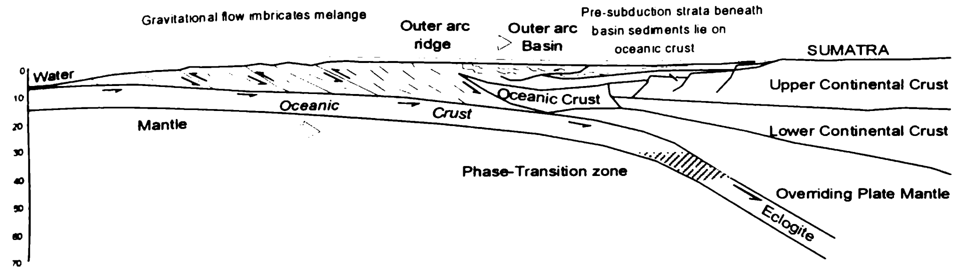

Figure 2.7. Structure of Sunda arc off the central Sumatra based on seismic refraction data (after Kieckhefer et al, 1980).

deformation front called the Sumatran fore arc sliver plate. The SFZ is also considered as the limit between the Eurasian plate and the fore arc sliver plate.

Along the Sumatran arc, slip vectors for earthquakes of the under thrusting Indo-Australian plate rotate into north east direction suggesting that convergence is oblique and a large part of the plate motion is taken up by right-lateral shear within the overriding plate in the order of 3.6-4.9 cm/yr (McCaffrey et al., 2000). The trench parallel shear is absorbed by transpressive deformation of the Eurasian plate leading edge and with an assumed northward displacement of continental slivers (Baroux et al., 1998; Simandjuntak and Barber, 1996), indicate the partitioning of oblique plate convergence into thrust and strike-slip motions (Genrich et al., 2000).

The most pronounced shear zone of the overriding Eurasian plate is the Sumatra fault zone (SFZ) within the volcanic arc. The SFZ accommodates most of the right lateral stress of the relative plate motion between the Indo-Australian and Eurasian plates and is seismically active (Schluter et al., 2002). The Sumatran fault system consisting of 20 en echelon segments (Tjia, 1978) is the world's clearest example of major shear fault system adjacent to a convergent margin (Fitch, 1970a; 1972). The fault extends for 1900 km along the volcanic chain of western Sumatra from 10° N to 7° S (Sieh and Natawidjaja, 2000). It turns into a complex pattern of extensional faults in the fore arc south of Sumatra. North of Sumatra, the SFZ seen to be continuing into the Andaman Sea and joins with the fracture zones of back arc spreading center (Curray et al., 1978). The oblique subduction beneath Sumatra results in partitioning of the convergent motion. The variation of slip rates along the various segments of SFZ ranging from 1.1cm/yr to 2.8cm/yr (Baroux et al., 1998) was accommodated by fore arc sliver deformation (Diament et al., 1992; McCaffrey, 1992). Slip rates as determined by SPOT images along stream offsets along the fault infer movements of 0.6 cm/yr in the south to 2.3 cm/yr in the north (Bellier and Sebrier, 1995). According to Malod and Kermel (1996), the right lateral slip is not only taken up by SFZ with a rate of 2 cm/yr, but also, by the Mentawai fault zone (MFZ) identified by Diament et al. (1992) in the fore arc basin. The MFZ give rise to a slip rate of up to 1.1 cm/yr off Nias Island. The northern part of the MFZ seems to be connected to SFZ by the Batee fault and terminates within the accretionary wedge, indicating two slivers (Mentawai and Aceh slivers) on top of which the fore arc basin has developed. If this is correct, the accretionary wedge and the outer arc high with the islands of Enggano and Nias must be a separate northward moving feature along the Mentawai fault (Malod et al., 1995; Van der weff, 1996). The shape and location of the Sumatran fault and the active volcanic arc are highly correlated with the shape and character of the underlying subducting lithosphere (Sieh and Natawidjaja, 2000).

Arc-normal extension is known to be an important mechanism in bringing high pressure, low temperature metamorphic rocks to shallow levels in accretionary wedges (Platt, 1986). Arc-parallel extension is also important because the estimated strain parallel to the Sumatran fore arc implies thinning of the fore arc at 1-2 mm/yr, which could result in rapid rise of rocks from deep in the accretionary wedge (McCaffrey, 1991).

A grid of multi channel seismic profiles and well data from the Sumatra fore arc basin revealed stratigraphic framework for the northern and central basins (Beaudry and Moore, 1981, 1985; Izart et al., 1994; Malod et al., 1995). According to these data a wide spread uplift and erosion occurred during the Paleogene followed by fore arc subsidence since the latest Oligocene-earliest Miocene as evidenced by two transgressive- regressive sequences of limestone and shale due to eustatic changes and tectonism. During Pliocene-Paleocene, two more sequences of deltaic, clastic and clay mineral were shed from the Sumatra margin into the subsiding basin segmented by traverse ridges into several sub basins (Natawidjaja and Sieh, 1994; Genrich et al., 2000). According to Dickinson (1995), these basins were formed in the Oligocene. However, older basin sediment (Early Eocene) is found on some islands (Pubellier et al., 1992; Schluter et al., 2002)

The fore arc ridge (outer arc high) is characterized by islands such as Enggano, Pagai, Siberut, and Nias provide considerable geological information. During Eocene and Oligocene an increase in the subduction rate led to the formation of mélange (Karig et al., 1980), containing ultrabasic oceanic components. Early Miocene sediments were initially deposited in deep water and since the Middle Miocene shallow water clastic and carbonate sequences dominate. On Enggano Island, late Paleogene to Pliocene successions are folded and thrusted (Schluter et al., 2002).

2.3.2.3. *Sunda Strait*

The Sunda strait is historically famous due to the explosion of the Krakatau volcano in 1883 and is an important area to understand the geodynamic evolution of the western Indonesia. The Sunda strait is interpreted either as related to rotation of Sumatra relative to Java with the rotation axis close to the strait during the late Cenozoic (Zen, 1983; Ninkovich, 1991) or as an extensional feature (Huchon and Le

Pichon, 1984; Harjono et al., 1992) resulting from the northwestward displacement of the southern block along the SFZ as a consequence of oblique subduction in Sumatra. Schluter et al (2002) suggest that the initial transtension and the formation of pull-apart basins of the Sunda strait are due to a clockwise rotation of Sumatra with respect to Java since the lower Miocene. The southeastern part of the SFZ, the Semangko fault, ends in the Sunda strait in a complex pattern of dominantly normal faults associated with subsidence, seismicity and volcanism (Huchon and Le Pichon, 1984). The Sunda strait is mostly covered by quaternary volcanic products (Harjono et al., 1991; Nishimura et al., 1986). The amount of extension of the Sunda strait is estimated to 50-70 km (Malod and Kemel, 1996) and presumably occurred during Pliocene (Diament et al, 1992). The region south of the Sunda strait is a transition zone between two steady state tectonic regimes: to the east, normal subduction in front of Java with well developed fore arc basins, and to the west, oblique subduction with sliver plates and strike slip faults accommodating the lateral component of the oblique subduction (Malod, 1995). Fitch (1972) proposed the Sunda strait as a tectonic as well as physiographic break in the arc. Within the Sunda strait, a typical pull-apart basin, that widens to the south, was initiated during the early Miocene along the southern part of the Sumatran fault (Diament et al., 1990; Huchon and Le Pichon, 1984; Lassal et al., 1989). Huchon and Le Pichon (1984) estimated that the subduction in the Sunda strait started at 13 Ma, whereas, according to Harjono and Suparka (1992) initiation of subduction is around 7-10 Ma.

2.3.2.4. *Java arc region*

Formed mostly as the result of volcanic events, Java is the 13th largest island in the world and the fifth largest island of Indonesia. Curray et al. (1977) examined the structure of central Java from seismic refraction data and interpreted that the apparently normal oceanic crust of the Wharton basin is being subducted beneath central Java. The fore arc basin is underlain by either thickened oceanic crust (Figure

2.8a and b) or thinned continental crust with slightly anomalous velocities. Java is underlain by a thin young continental crust formed during the Tertiary as the roots of the magmatic arc. The current subduction system, located offshore south of present day Java began in Late Oligocene (Hamilton, 1979). Along the central Java, the oceanic crust converges at a rate of 6-7cm/yr in a direction N11°E and is approximately orthogonal to the trench. At present, 135 m.y old oceanic crust subduct off eastern Java and crustal ages decreases to 96 m.y off western Java.

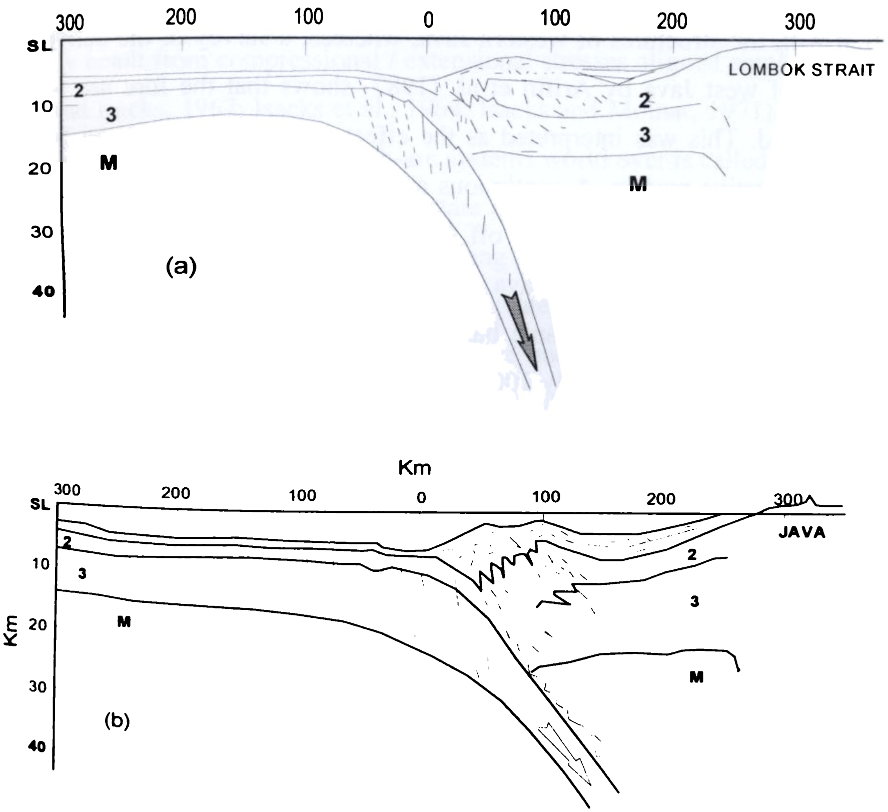

Figure 2.8. Structure of central Java and Bali from seismic refraction data (after Curray et al., 1977).

Tectonic stress and extension, resulting from northward movement of the Australian and Indian plates and rotation of Borneo, formed rifts or half graben complexes along much of the southern margin of the Sunda shelf plate (now Sumatra and Java) in Eocene to Oligocene time (Hall, 1977a,b; Longley, 1997; Sudarmono and others, 1977). These complexes are aligned north-south and are separated by faulted plateaus. The normal subduction below Java is characterized by the development of typical fore arc basins. It has been proposed that the transition between the two regimes of subduction zones occurs south west of Java, raising the question of continuation of the Sumatra and Mentawai faults into the accretionary prism and their connection with the structures of western Java, whereas, a survey of the active plate margin south of west Java by Arifin et al. (1987) shows that the fore arc basin is poorly developed. This was interpreted as the effect of continuation of the Sumatra fault within the active margin. A continuous accretionary wedge, outer arc high and fore arc basin are recognized along off Sumatra and western Java, but are not developed further east in off central Java. A large scale uplifts and segmentation of the fore arc due to subduction of oceanic basement relief leads to isolated bathymetric highs reaching water depths of only 1000 m compared to 2000 m in the western part of Java (Wittwer et al., 2006).

On land, a large fault zone known as the Cimandiri fault is interpreted as a large sinistral strike slip fault initiated during the Miocene (Dardji et al., 1994). No shear faulting of regional extent similar to that of SFZ exists in Java (Newcomb and McCann, 1987). The spatial variations in the slip vector azimuths at the Java trench suggest that arc parallel stretching of the fore arc occurs (McCaffrey, 1991).

CHAPTER 3

SEISMOTECTONICS OF THE LITHOSPHERIC SUBDUCTION IN THE EASTERN INDIAN OCEAN

3.1. Introduction

The occurrence of deep and intermediate depth earthquakes along a trench – arc system marking slab like geometry of the descending oceanic lithosphere essentially result from compressional / extensional stresses aligned parallel to the slab (Oliver and Isacks, 1967; Isacks et al., 1969; Isacks and Molnar, 1971). This inclined seismic zone associated with all trench-arc systems world over is called as the Wadati-Benioff Zone (WBZ) and knowledge on state of stress in these zones is important in understanding the geodynamic processes along convergent margins in general, and ongoing tectonic deformation within the upper plate, in particular. The latter aspect is more significant due to the fact that the negative buoyancy of the dense rocks of the descending lithosphere results in a downward body force which gets transmitted to the surface plate.

Earthquake focal mechanism solutions give valuable information on the state of stress and their spatial variations, in turn, help to identify contortions and disruptions in the descending lithosphere. According to Isacks and Molnar (1971), focal mechanisms in the WBZ show the following pattern: i) either P- or T- axes are parallel to the dip of the WBZ ii) slab-dip-parallel compression in the deepest parts of the WBZ iii) slab-dip-parallel compression or extension in the intermediate parts of the WBZ. However, deviations from this general pattern have been observed in the

WBZ of various arc systems (Isacks and Molnar, 1971; Giardini and Woodhouse, 1986; Apperson and Frolich, 1987; Slancova et al., 2000).

Recently, the Andaman-Sumatra-Java arc (together referred as Sunda arc) region came to the attention of international geo-scientific community for more detailed studies on geodynamics of the region after the occurrence of giant mega thrust earthquake of Mw ~ 9.3 on 26 December 2004 and the subsequent sequence of earthquakes with another mega event on 28 March 2005. In view of the extent of rupture and the significantly large deformation the events had caused in the upper plate, a close study of spatial variations in the geometry of WBZ is very useful. Several earlier workers had analyzed the nature of WBZ in terms of seismicity trends and Seismotectonic patterns along various segments of the arc (Fitch, 1970, 1972; Isacks and Molnar, 1971; Chandra, 1984; Mukhopadhyay 1984; Jarrard, 1986; McCaffrey, 1991; Dasgupta and Mukhopadhyay, 1993; McCaffrey, 1994, 1996; Guzman-Speziale and Ni, 1996; Schoffel and Das, 1999; Slancova et al., 2000; Dasgupta et al., 2002; Radhakrishna and Sanu, 2002; among many others), systematic analysis of entire arc was never looked into. In this chapter, a detailed Seismotectonic evaluation of the WBZ has been made to delineate the three-dimensional geometry of the WBZ as well as spatial variations in the stress distribution pattern which will throw light on the on-going geodynamic processes along the arc.

3.2. Lithosphere dynamics and associated processes at subduction zones

As the Oceanic lithosphere moves away from the ocean ridge, it cools, thickens and becomes denser because of thermal contraction. Even though the basaltic rocks of the oceanic crust are lighter than the underlying mantle rocks, the colder sub crustal rocks in the lithosphere become sufficiently dense to make old oceanic lithosphere heavy enough to be gravitationally unstable with respect to the hot mantle rocks immediately underlying the lithosphere. As a result of this gravitational instability the oceanic lithosphere begins to sink into the interior of the earth at ocean trenches. As the lithosphere descends into the mantle, it encounters increasingly denser rocks. However, the rock of the lithosphere also becomes increasingly dense as a result of the increase of pressure with depth. The descending lithosphere continues to subduct as long as it remains denser than the immediately adjacent mantle rocks at any depth.

The negative buoyancy of the dense rocks of the descending lithosphere results in a downward body force. Because the lithosphere behaves elastically, it can transmit stresses and act as stress guide. The body force acting on the descending plate is transmitted to the surface plate, which is pulled toward the ocean trench. This slab pull force is one of the important driving forces in plate tectonics and continental drift (Liu et al., 1995)

Prior to subduction, the lithosphere begins to bend downward. The convex curvature of the seafloor defines the seaward side of the ocean trench. The oceanic lithosphere bends continuously and maintains its structural integrity as it passes through the subduction zone. As a result of the bending lithosphere, the near surface rocks are placed in tension, and block faulting often results. This block faulting allows some of the overlying sediments to be entrained in the upper part of the basaltic crust. Some of these sediments are then subducted along with the basaltic rocks of the oceanic crust, but the remainder of the sediments is scraped off at the base of the trench. These sediments form an accretionary prism that defines the landward side of many ocean trenches. Mass balances show that only a fraction of the sediment that make up layer 1 of the oceanic crust are incorporated into the accretionary prisms. Since these sediments are derived by the erosion of the continents, the subduction of sediments is a mechanism for subducting continental crust and returning it into the mantle.

Ocean trenches are the sites of many of the largest earthquakes. These earthquakes occur on the fault zone separating the descending lithosphere from the overlying lithosphere. Great earthquakes such as the 1960 Chilean earthquake, 1964 Alaskan earthquake, 2004 Sumatra earthquake etc accommodate about 20m of down dip motion of the oceanic lithosphere (Lay et al., 2005). A large fraction of the relative displacement between the descending lithosphere and the overlying mantle wedge appears to be accommodated by great earthquakes of this type. A typical velocity of subduction is 0.1mm/yr so that a great earthquake with displacement of 20 m would be expected to occur at intervals of about 200 years (Turcotte and Schubert, 2002).

The lithosphere appears to bend continuously as it enters an ocean trench and then appears to straighten out and descend at a near constant dip angle. A feature of some subduction zones is paired belts of deep seismicity. The earthquakes in the upper seismic zone, near the upper boundary of the descending lithosphere are associated with compression. The earthquakes within the descending lithosphere are associated with tension. These double seismic zones are attributed to the 'unbending' i.e., straightening out of the descending lithosphere (Kawakatsu, 1986). The double seismic zones are further evidence of the rigidity of the subducted lithosphere. They are also indicative of the forces on the subducted lithosphere that are straightening it out so that it descends at a typical angle of 45°.

One of the key questions in plate tectonics is the fate of the descending plates. Earthquakes terminate at depth of about 660 km (Bina and Okal, 1998), but the termination of seismicity does not imply cessation of subduction. This is the depth of a major seismic discontinuity associated with the solid-solid phase change from spinel to perovskite and magnesiowustite; this phase change could act to prevent penetration of the descending lithosphere. In some case seismic activity spreads out at this depth, and in some cases it does not. Shallow subduction earthquakes generally indicate extensional stresses whereas the deeper earthquakes indicate compressional stresses. This is also an indication of resistance to subduction. Seismic velocities in the cold descending lithosphere are significantly higher than in the surrounding hot mantle.

Volcanism is also associated with subduction. A line of regularly spaced volcanoes closely parallels the trend of the ocean trench in almost all the cases. These volcanoes may result in an island arc or they may occur on the continental crust and lie125 -175 km above the descending plate. The bulk of the volcanic rocks at island arcs has near basaltic compositions and erupts at temperatures very similar to eruption temperatures at accretionary margins. These volcanoes are primarily the result of the partial melting of rocks in the mantle wedge above the descending lithosphere. Geochemical evidences indicate that the partial melting of subducted sediments and oceanic crust does important role in island arc volcanism. Isotopic studies have shown that subducted sediments participate in the melting process. Also, the locations of the surface volcanic lines have a direct geometrical relationship to the geometry of subduction. In some cases, two adjacent slab segments subduct at different angles, and an offset occurs in the volcanic line; for the shallower dipping slab, the volcanic line is farther from the trench keeping the depth to the slab beneath the volcanic line nearly constant. Processes associated with the subducted oceanic crust trigger subduction zone volcanism. The bulk of the volcanism is directly associated with the melting of the mantle wedge in a way similar to the melting beneath an accretionary plate margin. A possible explanation is that 'fluids' from the descending oceanic crust induce melting and create sufficient buoyancy in the partially melted mantle wedge rock to generate an ascending slab and enhance melting through pressure release. This process may be three dimensional with ascending diapers associated with individual volcanic centers (Turcotte and Schubert, 1982).

3.3. Regional geotectonic setting of the Sunda Arc

The Sunda arc extending over a distance of 5600 km from Andaman islands in the north to the Banda arc in the east, constitutes a major subduction zone and separates the Indo-Australian plate and the Eurasian plate. This subduction system in the eastern Indian Ocean has been active since middle Tertiary (Hamilton, 1988). Significant along strike variations in style and geometry of subduction as well as geophysical characteristics occur from west to east along the Sunda arc (Newcomb and McCann, 1987). Hamilton (1988) suggested that the subduction system changes from oceanic – continental in Sumatra through transitional in Java. Hamilton (1979) pointed out that the Andaman arc system together with Burmese arc forms an important transitional tectonic link between the Himalayas in the north and the Indonesian part of the arc in the south. A small lenticular plate, called the Burma plate, covering the Burmese plains, the Andaman and north Sumatra basins, separate the Indian and Eurasian plates (Curray et al., 1979). The Andaman basin comprising of Andaman Sea in the back-arc extends nearly 1200 km N-S from Burma to Sumatra and around 650 km E-W between Andaman Nicobar Islands and the Malay Peninsula. Win Swe (1972) inferred that the Sagaing fault, a major right lateral fault along the eastern edge of the Burmese arc, continues southward and joins the spreading axis in the Andaman Sea. Curray et al. (1977) proposed that the back-arc spreading system in the Andaman Sea transforms southward into the Sumatran fault system.

The Sumatran fault system, a 1900 km long trench parallel fault passing the entire length of Sumatra, is one of the World's major shear fault adjacent to a convergent zone (Fitch, 1972), and accommodates motion parallel to the arc by dextral strike-slip displacement (Newcomb and McCann, 1987). These observations suggests that the highly oblique convergence in the Burma-Andaman-Sumatra arc is accompanied by large-scale right lateral shear along the Sagaing fault and the Sumatran fault through ridge-transform systems in the Andaman Sea (Curray et al., 1979, 1982; Karig et al., 1979, 1980; Curray , 2005). Between the Sumatran fault and the Sumatran deformation front in the offshore, a 300 km wide strip of the lithosphere exists as a fore arc sliver plate, in which, the 600 km long Mentawai fault is located (Diament et al., 1992). Further southeast, the Sunda strait separates the arc into the Sumatra and Java segments, where, the trend o the trench-arc system changes from NW-SE in Sumatra region to E-W in Java region an seems to be a transition zone in the morphology of the fore arc domain (Malod et al., 1995).The Sunda Strait is a consequence of northwestward motion of the southwestern part of the Sumatran block along the Sumatra fault. The area is subjected to NW-SE extension because of the motion along Sumatran fault and to NE-SW compression because of subduction (Huchon and Le Pichon, 1984). The age and thickness of the subducting oceanic crust increases from Sumatra to Java and normal subduction prevails below the Java arc. The Java arc represents a typical subduction zone, displaying the outer bulge and a deep trench. A trench slope break separates the accretionary prism into a frontal wedge and the outer high (Kopp et al., 2002). The outer high off Java is completely submerged and generally 2000-3000 m deep, with isolated highs reaching depths around 1000 m (Moore et al., 1980). The fore arc basin is located adjacent to the volcanic arc. The seismic refraction line off central Java suggests the presence of oceanic crust beneath the fore arc basin (Curray et al., 1977). Hamilton (1988) observed that this segment of the subduction system has been active since the Oligocene and evolved after the late Eocene collision of India with Asia.

3.3.1. Various characteristics of the Arc

Many geological and tectonic characteristics of the Andaman–Sumatra–Java arc change significantly along strike. Fore arc geometry systematically varies from west to east (the depth of the fore arc basins, trench slope break and trench increase towards Java) as the sediment thickness on the subducting plate increases (Newcomb and McCann, 1987). A complex tectonic system exists in the Andaman Islands, where convergence is essentially sub parallel to the arc of the Lesser Sunda Islands and the Australian continent occurs (Sliver et al., 1983). But a relatively simple style of subduction occurs where oceanic crust is subducted beneath the continental platform of Sumatra and western Java as well as the island arc of eastern Java.

3.3.1.1. *Rheology*

Fore arc rheology appears to correlate with arc type (whether the upper plate is oceanic or continental) and arc age. Elastic fore arcs appear to correlate with the occurrence of great earthquakes, suggesting that rheology rather than stress controls fore arc deformation and where great subduction zone thrust earthquakes occur. The Java –Sumatra fore arc displays elastic-perfectly plastic behavior. It is elastic up to obliquity of about 20° and at higher obliquities it deforms at a rapid enough rates and keeps the slip vectors at a nearly constant angle relative to the trench-normal. In Java - Sumatra, the arc parallel strike slip fault takes up the motion of the fore arc relative to the upper plate. It is apparently the only one of the world's fore arcs that displays this behavior (McCaffrey, 1994).

3.3.1.2. *Compression / Extension*

Perhaps, the most difficult variable to quantify is the strain regime of the overriding plate. The stress or strain at any point in a subduction zone is optimally described as a stress or strain tensor. Subduction zones can be ranked to some extent in terms of their positions along a continuum from strongly extensional to strongly compressional (Uyeda and Kanamori, 1979).

Subduction zones with highly extensional environment in the overriding plate exhibit back arc spreading, the formations of oceanic crust in a marginal basin behind the arc (Karig, 1971; Packam and Falvey, 1971) such as in Andaman subduction zone. Back arc spreading in the Andaman Sea has averaged 3.7 cm/yr for the last 13 my, prior spreading is poorly known because of very subdued magnetic anomalies (Curray et al, 1982; Lawver and Curray, 1981). A few focal mechanisms from behind the Andaman Nicobar ridge are interpreted by Mukhopadhyay (1984) as indicating fore arc thrusting. For every back arc basin except Andaman, the spreading direction is approximately perpendicular to the trench. Indeed, the oblique spreading and major transform faults of the Andaman Sea are often interpreted (Curray et al, 1982; Weissel, 1981; Taylor and Karner, 1983) as evidence that it may not be appropriate to consider the origin of this marginal basin as typical back arc spreading.

Sumatra and Java subduction zones are considered to be mildly compressional. The back arc region of eastern Sumatra exhibits moderate but pervasive Pliocene- Pleistocene folding and some quaternary thrusting, both with compression approximately parallel to the plate convergence direction (Katili, 1974). The eastern end of Java indicates intra plate thrusting (Fitch, 1972). Deformation is active in the foreland basin of North Java and the nearby offshore area, with mild open folds in north Central Java and Miocene to Quaternary northward-directed folds and thrusts in the west Java basin (Hamilton, 1979). He suggests that, much of this deformation may be attributable to magmatism rather than subduction related compression, as the folds arc around large volcanic edifices. Back arc thrusting east of Java is probably caused by continental collision of Australia with Banda subduction zone and is not relevant to the strain regime of Java.

3.3.1.3. *Convergence rates*

The convergence directions at subduction zones used to be indicated by slip vectors of shallow interplate thrust earthquakes (Jarrard, 1986). However, developments in the studies related to world wide plate motion models gave rise to accurate convergence rates between the major plates (Minster and Jordan, 1978), more recently the NUVEL – 1A plate motion model (DeMets et al., 1990; Argus and Gordon, 1991). These plate motion models are based on inversion of Pliocene-Pleistocene spreading rates, transform fault azimuths and earthquake slip vectors and from GPS measurements.

According to these models, the Indo-Australian plate is subducting under the Eurasian plate with a convergence rate of 75 mm/yr (Minster and Jordan, 1978; DeMets et al., 1990). Analysis of slip vectors obtained from focal mechanisms suggests a approximately N-trending convergence between these two plates (Jarrard, 1986; McCaffrey, 1991). But because of the variation in local trench azimuth, this convergence is normal to the Java and becomes progressively more oblique at Sumatra and further north. DeMets et al. (1994) estimated convergence rates of 72 mm/yr near Java and 68 mm/yr off Sumatra. Lay et al. (2005) noticed predominantly thrust motion with a convergence rate of 14 mm/yr along the Andaman trench.

3.3.1.4. *Slab age and configuration*

The age and thickness of the subducted oceanic crust increases from Sumatra to Java and it is reflected by the increasing dip and depth of penetration of the Benioff zone. In the Sumatra and Andaman segments, ages increase northward, but because of the oblique convergence and closely spaced fracture zones, age probably decreases discontinuously down dip. West of Sunda Strait, seismic activity does not extend below 200 km. Slab configuration is ambiguous in northern Sumatra while in the south a plane dipping 40° - 50° is apparent. By Java, seismic activity extends from the surface to a depth of 650 km with a gap in seismicity between 300 and 500 km. Trench depth can be affected by thickness of the sedimentary trench fill, thickness of sediments on the oceanic crust before entering the trench, and presence of aseismic ridges (Jarrard, 1986).

3.3.1.5. *Arc age*

Initiation of subduction is usually followed in less than 5 my by initiation of arc volcanism (Gill, 1981). Therefore, the oldest arc related rocks in a subduction zone provide an estimate of duration of subduction. Initiation of the subduction pattern in Andaman–Sumatra-Java is controversial. In Sumatra, scattered Cretaceous and Paleogene K-Ar ages are found for granitic rocks, but the orientation of these belts is not reliably known. Hamilton (1979) suggested that the belt may be strongly oblique to the modern trench and truncated at the trench. He interpreted Late Cretaceous and Paleogene mélanges and igneous rocks in Java as forming an arc trending from western Java through Borneo. In both Java and Sumatra, late Oligocene calc- alkaline rocks are the oldest arc related rocks that are clearly part of the present subduction geometry (Hamilton, 1979). The poorly dated Andaman region is at least as old as the Late Oligocene start of continental thinning, and probably cretaceous (Curray et al, 1982). The age of the lithosphere along different portions of the arc varies greatly, aging progressively eastward. It varies from 49-96 Ma under Sumatra to the west to 96- 134 Ma under Java.

3.4. Data and Analysis

As already stated the Sunda arc region is seismically active and characterized by the occurrence of shallow as well as deeper earthquakes. A compilation of both historical and recent events has been made from the NOAA epicentral listing. A preliminary analysis of the catalogue indicated that the events prior to 1900 lacked proper depth information. As depth is a very important parameter in a study of this kind, the time period of data has been confined to the period during 1900-2005.

3.4.1. Seismicity

From the list of earthquakes considered during 1900-2005, for the events before 1964, their magnitudes have been compiled from Rothe (1969) and Gutenberg and Richter (1954). For the period during 1953-1965, magnitudes from Rothe listing have been recalculated by Newcomb and McCann (1987). Similarly Engdahl et al (1998) precisely determined hypo central parameters from ISC listing for the period 1964-1995. We considered these revised magnitudes with events Ms $\geq$4.5 for the present analysis. For events where Ms value is not available, it is obtained from Mb using Mb-Ms relation derived for the region. The magnitudes estimated by Gutenberg and Richter (1954) and Rothe(1969) are equivalent to 20-s Ms(Geller and Kanamori, 1977). As the events related to the upper plate mostly confine to depths < 70 km, they have been divided into shallow ($\leq$ 70 km) or deeper WBZ events (> 70 km) for the purpose of showing on a seismicity map (Figure 3.1).

3.4.2 Focal Mechanism solutions

Source mechanisms of earthquakes have been known to provide valuable information on the distribution of stresses and deformation pattern in seismically active regions. For the purpose of understanding the stress distribution pattern in the WBZ, a large number of focal mechanism solutions, nearly 1173 have been compiled from the Harvard CMT catalogue. From the total compiled events, it is seen that around 926 events belong to the shallow upper plate while 247 events are from the

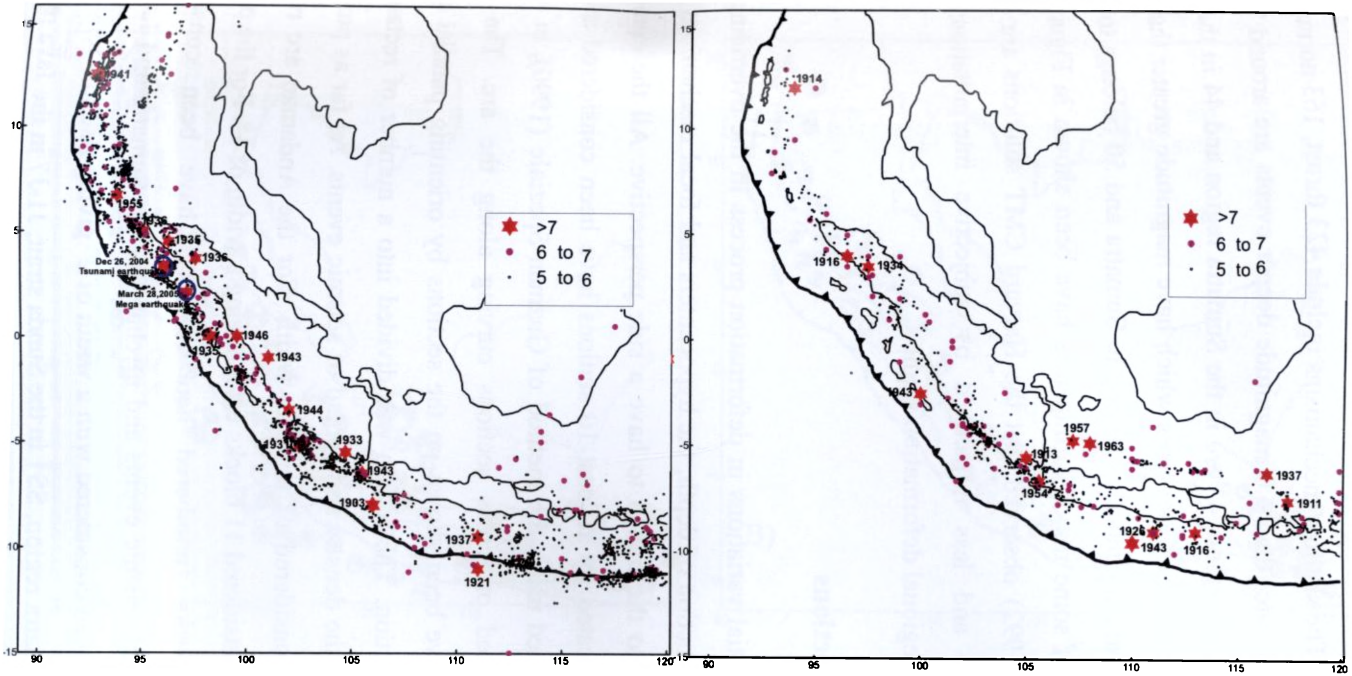

Figure 3.1. Seismicity map of the Sunda Arc showing events with magnitude Ms > 4.5 occurred during 1900 – 2005. A) shallow upper plate events (h≤70 km), and B) deeper events within the subducted plate (h > 70 km). The year of occurrence is shown for selected significant earthquakes in the region.

Out of the 247 deeper events, 105 events are thrust, 57 events are normal and 85 are strike - slip mechanisms. The shallow mechanisms include 423 thrust, 163 normal and 340 strike- slip events. Greater than 6.0 magnitude deeper events are around 95, of which 8 are in the Andaman region, 43 are in the Sumatra region and 44 in the Java region. There are around 188 shallow events which have magnitude greater than 6.0. Among them, 41 belong to Andaman, 97 belong to Sumatra and 50 belongs to Java. The focal mechanisms of some major earthquakes have been shown in Figure 3.2. Frolich and Apperson (1992) observed that the Harvard CMT solutions are better representative, complete and less influenced by subjective interpretations and therefore can be used in regional deformation studies.

3.4.3. Seismological sections

To study the spatial variations in deformation process in the overriding and subducting plates as a function of depth, the hypocenters and focal mechanisms have to be projected normal to the trench to have a side perspective. All the events of magnitude > 4.5 and located by at least 10 stations have been considered and the events have been projected using the method of Guzman-Speziale (1990), in which hypocenters are projected on cross sections curving along the arc. The focal mechanism solutions have been shown on the sections by orienting parallel to the azimuth of the cross section. The region was divided into a number of rectangular shaped blocks based on the density and spread of seismic events. As far as possible, the blocks have been considered of uniform width. For the Andaman arc region, Dasgupta et al. (2003) considered 11 blocks each having a width of 1°. For the present purpose, the same blocks (numbered here A1-A11) have been considered incorporating more recent seismic events and mechanisms. In Sumatra and Java arc region, the blocks have been considered with a width of 2° giving rise to a total of 16 blocks (S1-S8 in the Sumatra region, SS1 in the Sunda strait, J1-J7 in the Java region)

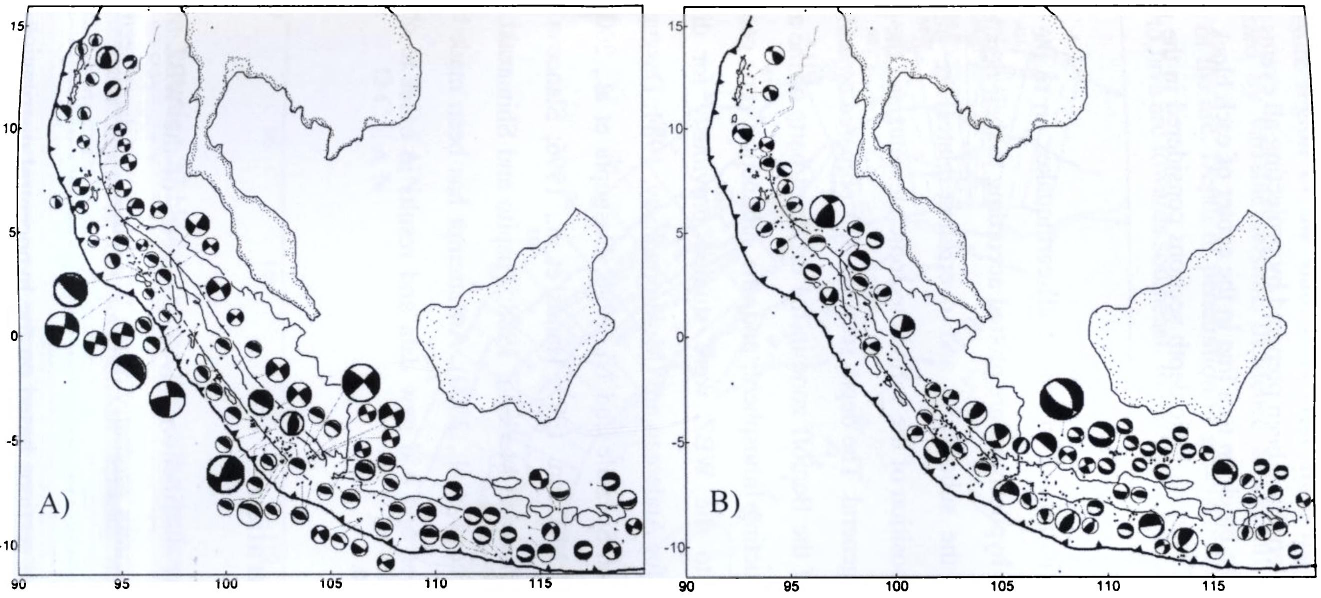

Figure 3.2. Map showing the focal mechanisms of earthquakes (Ms > 5.5) compiled from Harvard CMT catalogue in the Sunda arc region. A) Shallow upper plate events (h≤70 km), and B) Deeper events within the subducted plate (h > 70 km).The size of the mechanism is in accordance to the magnitude of the earthquake

The 27 seismologic depth sections have been prepared by projecting all events as well as mechanisms pertaining to the block on to a line in the center of each block. Figure 3.3 shows the location of all 27 seismologic depth sections considered in the present study.

A computer program is utilized to project all earthquakes on to the central plane of each block where the hypocenters are plotted according to their depths. The enveloping surface defining the subducting and overriding plates are manually adjusted using the surface disposition of the various tectonic elements and the pattern of hypocentral distribution in general. The depth sections thus prepared are utilized to investigate, the average dip of the Benioff zone in the different parts of the arc; the penetration depth of the subducting lithosphere; and, the subduction zone geometry. The earthquakes pertaining to the WBZ were studied previously for different segments of the arc; such as, for Andaman arc (Mukhopadhyay, 1984; Dasgupta and Mukhopadhyay, 1993; Guzman-Speziale and Ni, 1996; Dasgupta et al., 2003), for Sumatran arc (Newcomb and McCann, 1987; Hanus et al., 1996; Slancova et al., 2000) and for Java arc (Cattaneo and Merlanti, 1988; Puspito and Shimazaki, 1995; Schoffel and Das, 1999; Slancova et al., 2000). An attempt has been made here to synthesize all these information and add new data and results in order to obtain a holistic picture of the entire arc.

3.5. Benioff zone configuration

Earthquake hypocenter distributions reveal geometry of the WBZ in most subduction zones. Figure 3.4 shows geometry of the WBZ in all 27 depth sections in Andaman-Sumatra-Java arc region. The horizontal lower boundary of the lithosphere is placed at about 80 km in all sections based on the hypocentral distribution in the initial flexure region of the slab. It is clear from the sections that the WBZ is characterized by variable seismic incidence and depth of penetration in different segments of the arc. Depth of penetration in general increases from Andaman arc in the north to Java arc towards southeast. In the Andaman arc and part of Sumatran arc

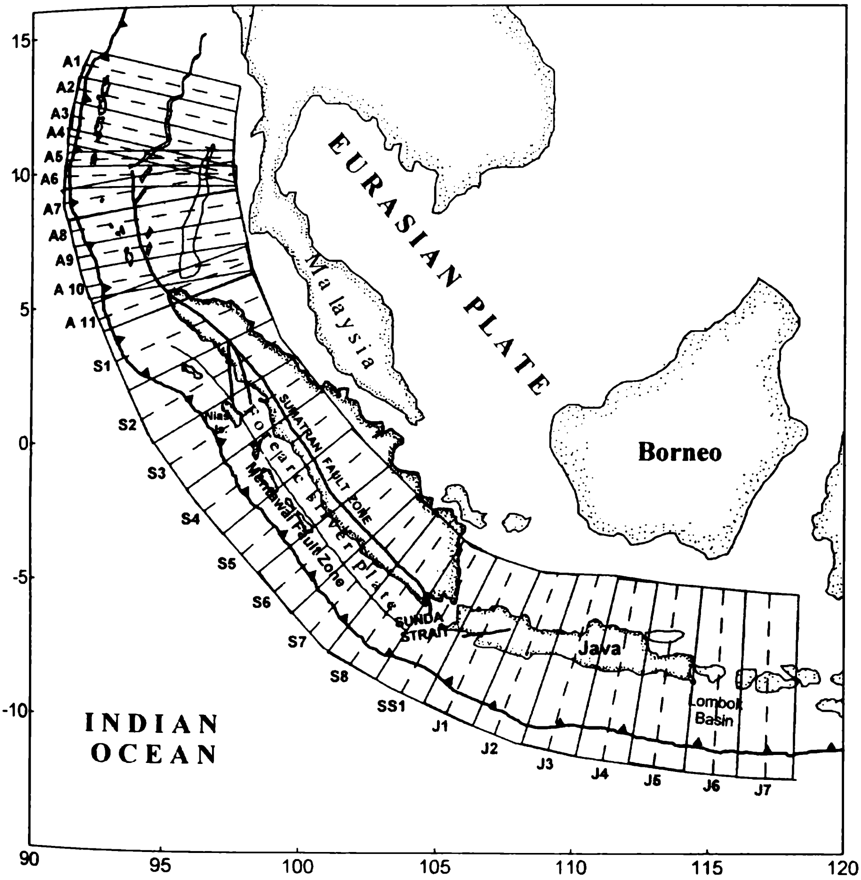

Figure 3.3. Location 27 blocks / rectangles in the Andaman (A1-A11), Sumatra (S1-S8) and Java (SS-1, J1-J7) arc region. The dashed lines in the center of each block is the location of seismic depth section on to which earthquakes and mechanisms have been projected.

in the north (between A1 – S3), the depth of WBZ varies from 150 km in the north to 250 km in the south. In southern Sumatra (S4 – S8), the depth extent of WBZ varies between 250 – 350 km. Deep seismicity has not been observed anywhere below Andaman as well as Sumatran arcs. Deep earthquakes start to appear beyond 105° between Sunda Strait and Java arc region where earthquakes in the WBZ occur at a depth of 600 to 650 km. Kirby et al. (1996) explain this increase in maximum hypocentral depth as being due to increasing age and subduction velocity from north towards southeast. However, a gap in seismic activity at intermediate depths is noticed in the Java arc region. The depth range over which this gap extends is seen to vary for different sections of the arc, but, generally in the range of 300-550 km. Estimates of slab length, depth and horizontal extent may be biased by the presence of such gaps in seismicity at intermediate depths.

An analysis of all 27 depth sections suggests that the seismic activity appears continuous up to a depth of 300 km within the upper part of the subduction zone. However, a closer look of seismic activity within the top 300 km revealed the presence of an aseismic gap in the WBZ along the Sumatran subduction zone at variable depths of 90 – 220 km having variable thicknesses (Hanus et al., 1996) and such aseismic gap has been observed for a section along the Andaman subduction zone at a depth range of 90 – 110 km (Dasgupta and Mukhopadhyay, 1997). Probing of such aseismic gaps in the WBZ of major subduction zones world over confirmed their spatial correlation with volcanic activity and occur below or in the near vicinity of active volcanoes (Hanus and Vanek, 1976, 1978, 1985; Hanus et al., 1996; Dasgupta and Mukhopadhyay, 1997; Spicak et al., 2004). The presence of such aseismic gaps has been interpreted by them as due to the presence of partial melt domain in the WBZ where the conditions for generating strong earthquakes are not

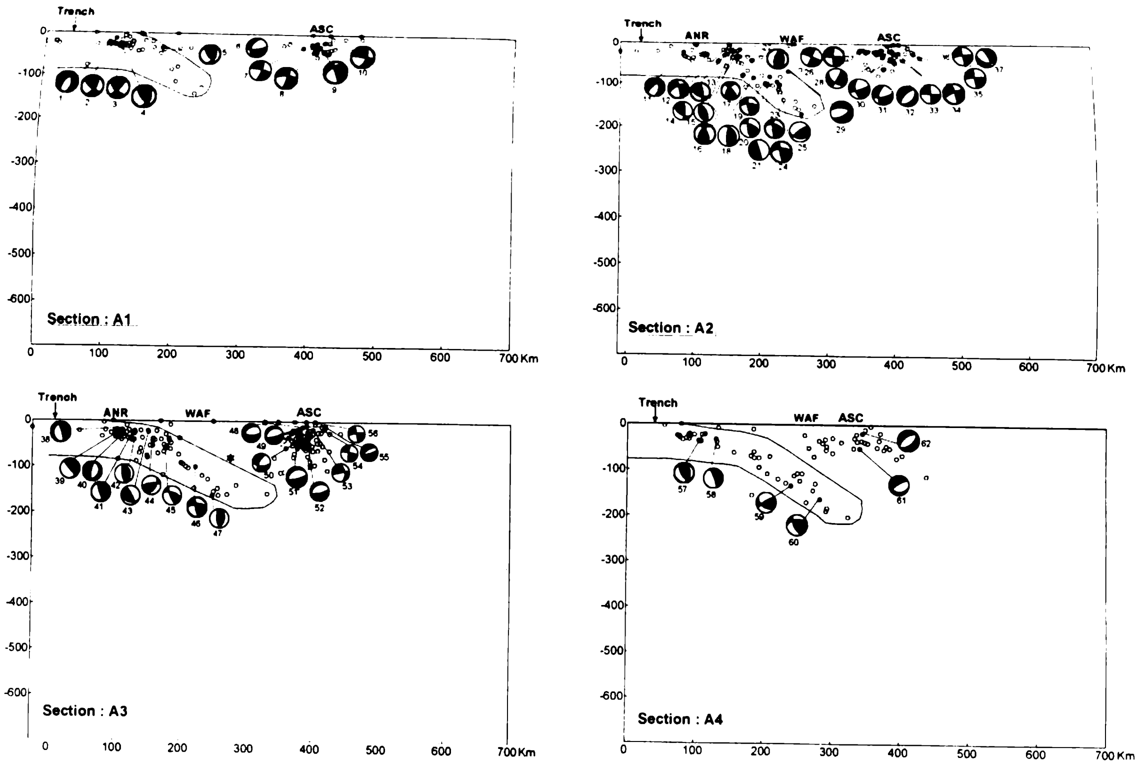

Figure 3.4.Configuration of the Wadati-Benioff Zone and the focal mechanism solutions for each of the 27 blocks considered perpendicular to the Sunda arc region (A1-A11; S1-S8; SS1; J1-J7). Dark circles are events with mechanisms available. The events within each block have been projected on to a line in the center of the block. Details are discussed in the text.

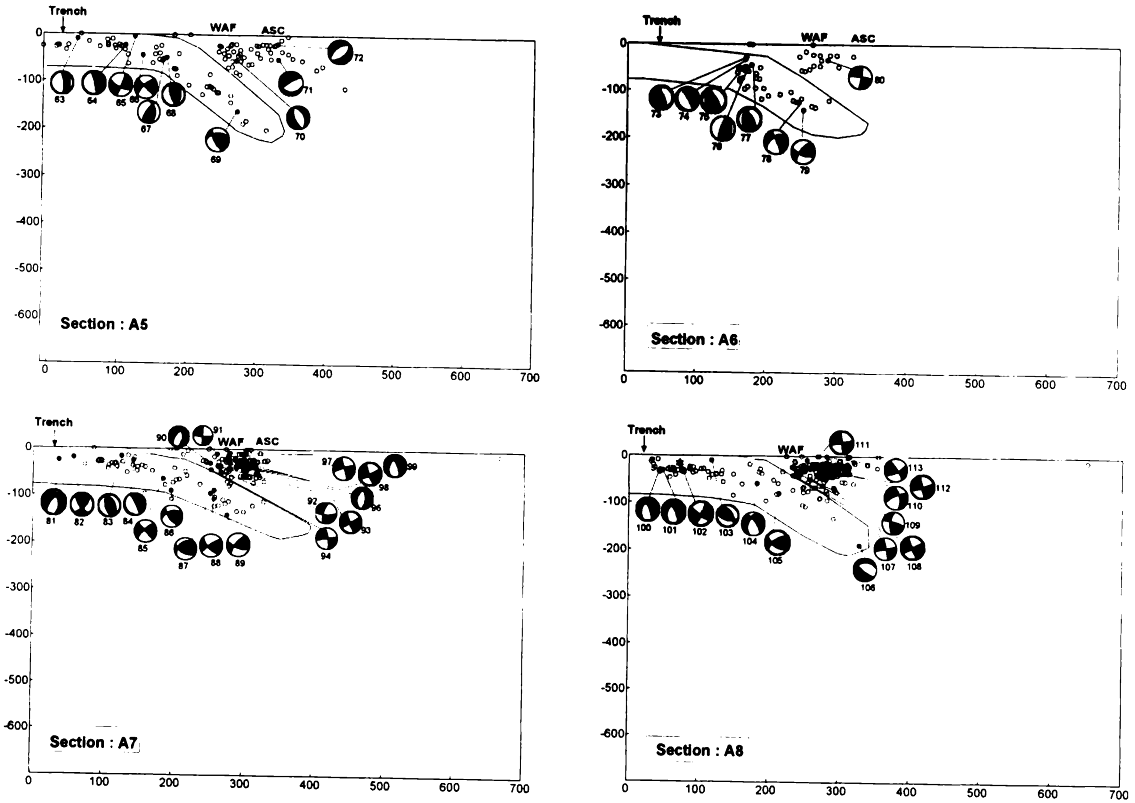
Trench
WAF
ASC
Section : A5
Section : A6
Section : A7
Section : A8
0
-100
-200
-300
-400
-500
-600
0
100
200
300
400
500
600
700

(Fig 3.4… Contd…)

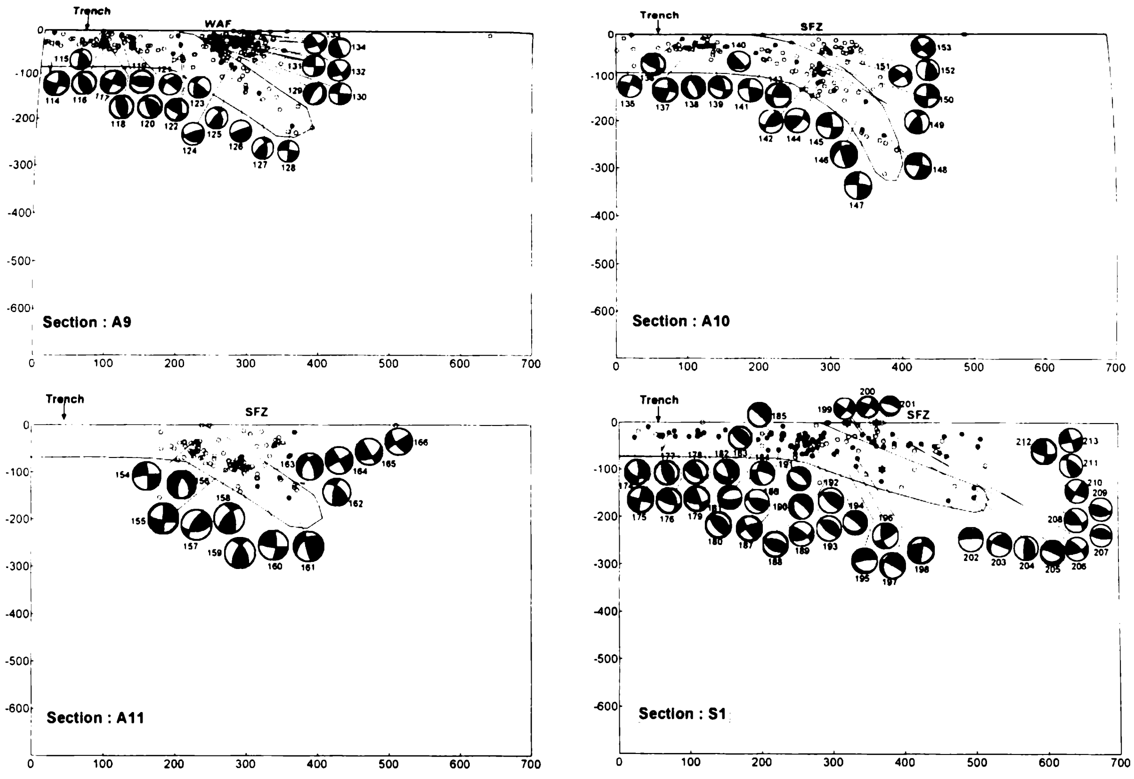
Section : A9
Section : A10
Section : A11
Section : S1
Trench
WAF
SFZ

(Fig 3.4… Contd…)

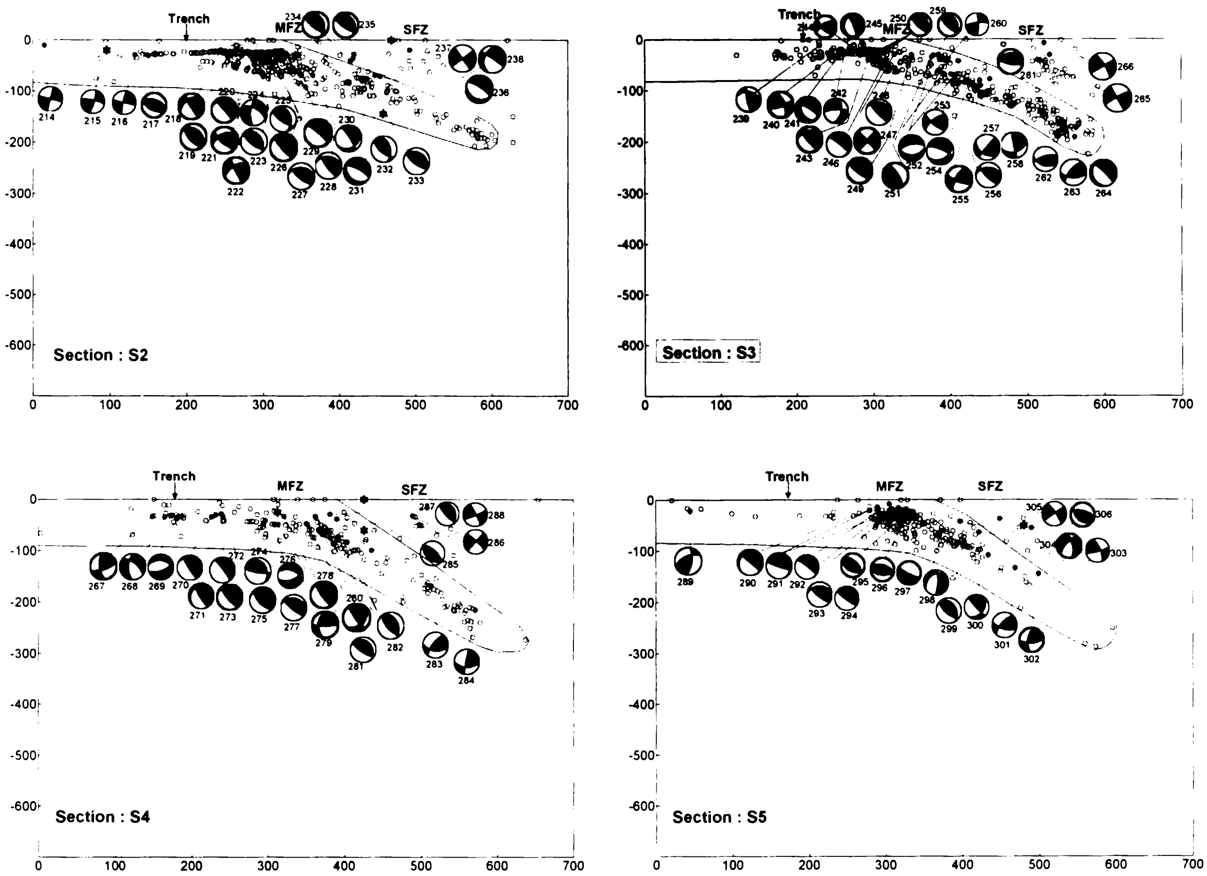

(Fig 3.4… Contd…)

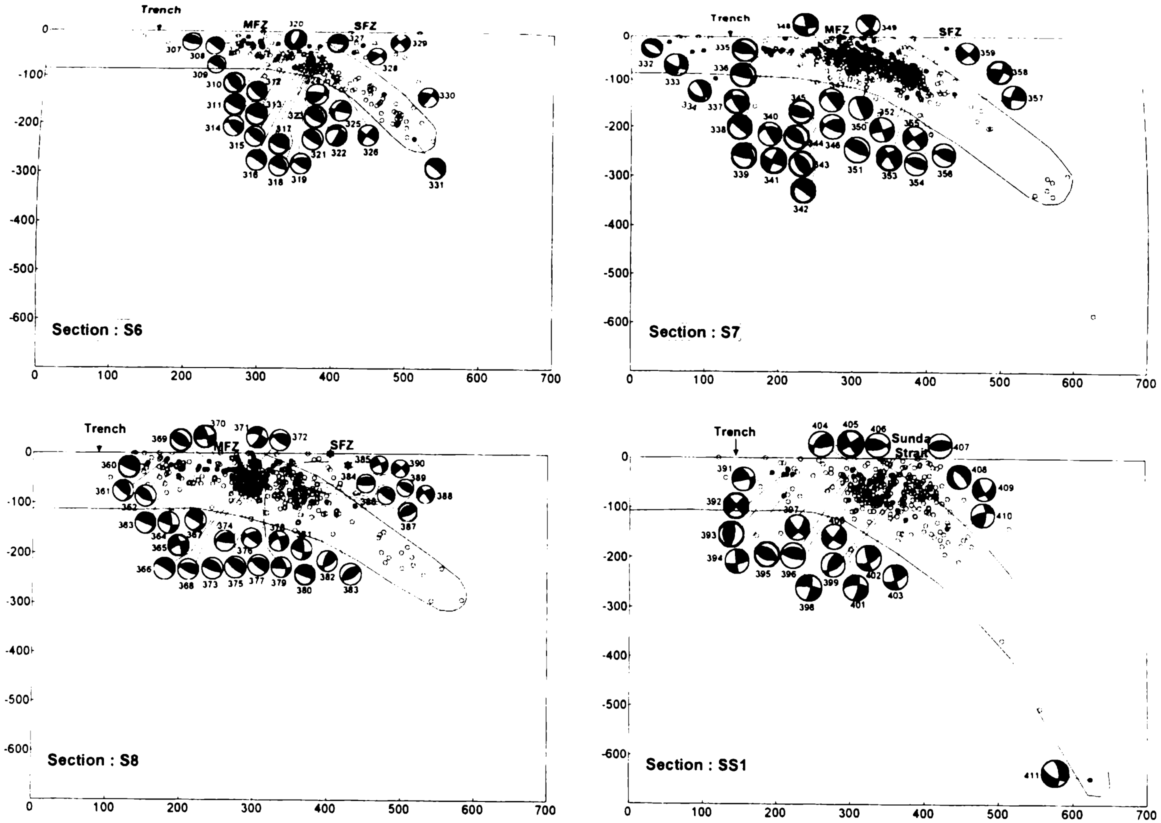
Section : S6
Section : S7
Section : S8
Section : SS1
Trench
MFZ
SFZ
Sunda Strait

(Fig 3.4… Contd…)

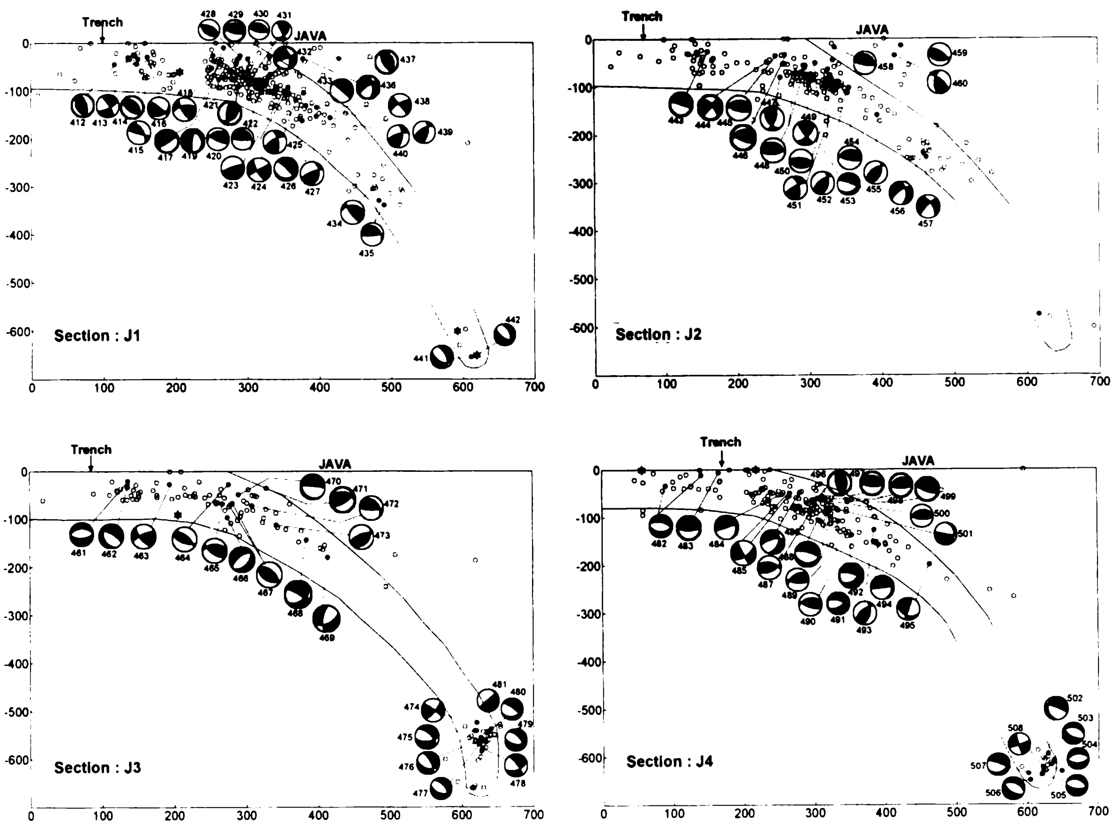

(Fig 3.4… Contd…)

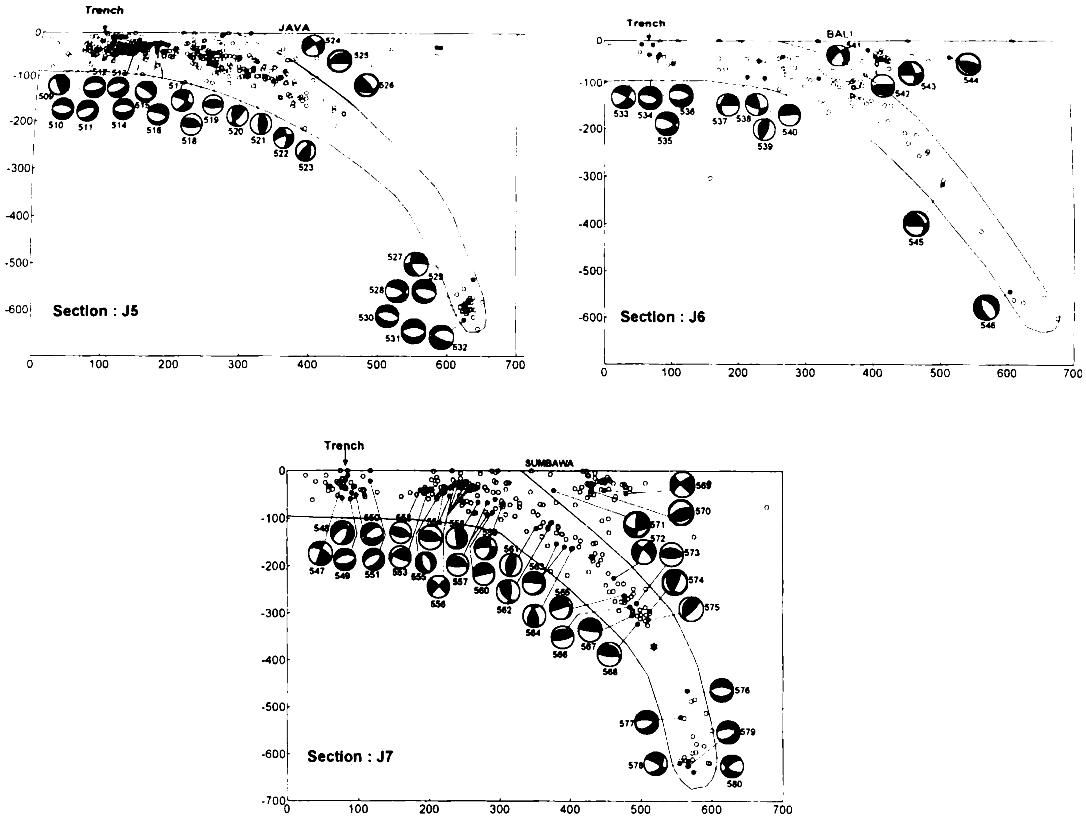

(Figure 3.4....Contd...)

fulfilled or in a way indicate loss of brittle character of the slab at the respective depth. Spicak et al. (2002) observed seismically active column below active cal-alkaline Krakatau volcano located above the WBZ. The presence of both aseismic gap in the WBZ as well as an active seismic column below an active volcano located in the continental wedge above the gap has been observed at many subduction zones by Spicak et al.(2004). They further observed that the fault plane solutions of earthquakes occurring in the down going slab and the overlying continental wedge are different suggesting different stress conditions in these two regions.

The dip of the WBZ varies considerably, but not systematically, all along the Sunda arc. In general smaller dip of the Benioff zone is usually accompanied with shallow penetration depth, but there are some exceptions also. In the northern Andaman (A1 – A3), the Benioff zone dip varies between 43^{O} to 53^{O}, while, in south Andaman- north Sumatra (blocks A4- A11), the dip is in the range 38°-50°. Along the Sumatran arc, the dip of the Benioff zone ranges between 40° to 50°. In the Java arc region, the dip of the Benioff zone is around 50° in the upper part.

It is useful to inspect the subduction zone geometry through three-dimensional perspective imaging so that the Benioff zone upper surface could be presented on a plan view. Bevis and Isacks (1984) adopted the hypocentral trend surface analysis through least-square fitting to infer Benioff zone geometry. This method gives mid-surface of the subducting lithospheric slab and will be very useful when precise knowledge on slab thickness as well as hypocentral locations of earthquakes are available from local network stations in the region. In the absence of such data, a simpler method is to trace the upper surface of the Benioff zone, by utilizing shallowest depth events. Using all 27 depth sections and top surface of the

WBZ, a contour map of geometry of the subducting Indo-Australian slab has been prepared as shown in Figure 3.5.

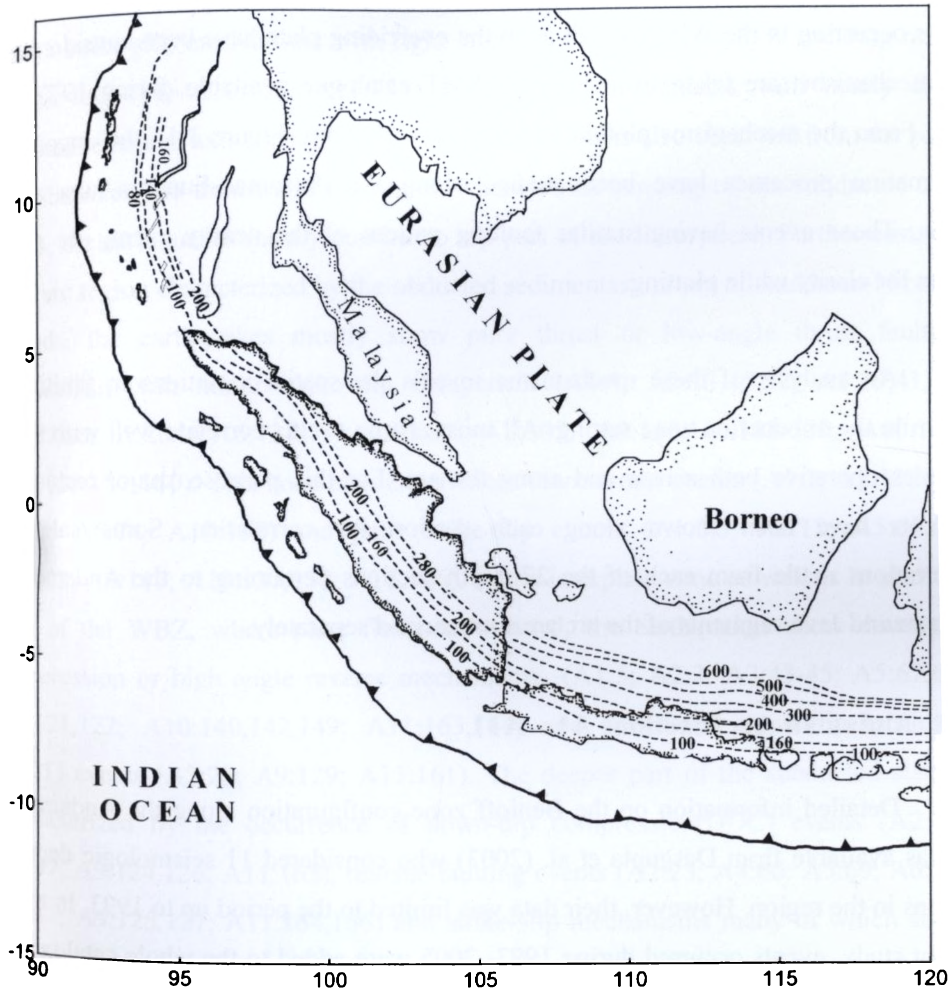

Figure 3.5. Surface projection of the three-dimensional geometry of the Subducting Indo-Australian plate. Lines with number show the top surface of the WBZ obtained through manually drawing the WBZ from the slab seismicity.

3.6. Deformation in the WBZ and the overriding plate

A large number of focal mechanism solutions of events covered by all 27 blocks occurring in the WBZ as well as in the overriding plate have been considered. The mechanisms are taken from Harvard CMT catalogue available during 1977 – 2005. From the mechanisms plotted as a function of depth (Figure 3.4), the ongoing deformation processes have been studied along the Andaman-Sumatra-Java arc region. Those events having similar faulting pattern of the nearby event, are not shown for clarity while plotting.

An analysis of these mechanisms reveals the spatial variations in faulting pattern in the subduction zone setting. All most all the events correlate well with the tectonics operative both across and along the arc. For this purpose, major tectonic elements have been shown along each section for correlation. Some salient observations made from each of the 27 depth sections pertaining to the Andaman, Sumatra and Java segments of the arc are summarized separately.

3.6.1. Andaman Arc: Sections A1 – A11

Detailed information on the Benioff zone configuration along the Andaman arc was available from Dasgupta et al. (2003) who considered 11 seismologic depth sections in the region. However, their data was limited to the period up to 1993. In the present study, events occurred during 1993- 2005 were added to the whole catalogue and with this additional database of hypocentral as well as the focal mechanism solutions, detailed geometry and deformation pattern in the WBZ has been studied.

An analysis of all 11 seismic sections reveals distinct seismic character of the arc. The results have been arranged from west to east across the arc. It is known that the trench is an important tectonic element in the subduction zone environment. The earthquake activity appears to be continuous starting from the trench location particularly in the southern Andaman arc (A5, A7-A11). The events near to the trench shows strike-slip mechanisms with right lateral shear motion on E-W trending nodal planes (A9:114, A10:135, A11:154) and normal mechanisms with nearly E-W oriented tensional axis (A5:63, A7:81, A8:100,101). It is also observed from the plots that, between the trench and the region where down-bending of the subducted slab starts, the earthquakes mostly confine to top part of the lithosphere. Further east, the fore arc region characterized by the obducted sedimentary prism of Andaman-Nicobar islands, the earthquakes mostly show pure thrust or low-angle thrust faulting mechanism with minor strike-slip component (A1:4; A2:13-15,22; A3:39,41,42; A4:57,58; A5:64; A6:73-77; A7:83,84; A8:103; A9:115,116,118-120; A10:136; A11:155,157-160). This zone also experiences few normal events (A1:1; A2:11; A3: 38,40; A6:74; A10:138) and pure strike-slip events (A1:2,3; A2:12; A5:65,66; A8:102; A9:117; A10:137,139; A11:156). In the interplate zone as well as in shallow part of the WBZ, where plate flexes downward, the earthquakes show down-dip compression or high angle reverse mechanisms (A1:5; A2:2; A3:43-45; A5:67,68; A9:121,122; A10:140,142,149; A11:163,164) and occasional down-dip tensional (DDT) events (A2:29; A9:129; A11:161). The deeper part of the subducted slab is characterized by the occurrence of down-dip compression(DDC) events (A2:25; A3:47; A9:124,126; A11:165), reverse faulting events (A2:23; A4:60; A5:69; A6:78; A7:87; A9:125,127; A11:164,166) and strike-slip mechanisms many of which show left-lateral motion on roughly E-W trending plane (A2:24; A3:46; A7:88,89; A9:128; A10:145-148; A11:167). Further east, considerable seismic activity is noticed in the overriding Burma platelet sandwiched between the Indian and Eurasian plates. An observation of sections show that the back arc spreading ridge is characterized by several normal faulting events with NE-SW trending nodal planes (A1:6; A2:31,32;

A3:48,49,51,52,55; A4:61,62; A5:71,72) and strike-slip events with left-lateral faulting on E-W trending nodal plane (A1:7-10; A2:27,30,33-36; A3:53,54,56). The normal faulting event with NW-SE trending nodal planes (A2:37) over the Andaman Spreading Ridge could be due to the geometrical complexity near the ridge transform intersections. In the southern Andaman arc, the Andaman Spreading Ridge meets the West Andaman Fault (WAF). Along section A7, two normal faulting events 96 and 99 relate to minor spreading segment in this region. Further south of this section, the mechanisms indicate mostly right-lateral shear motion along N-S trending nodal plane along the WAF.

3.6.2 Sumatra Arc: Sections S1-S8

The Sumatran Fault Zone (SFZ) is a major right-lateral fault zone that separates the Eurasian plate from the fore arc sliver plate which is a 300 km wide strip of the lithosphere covering most of the offshore Sumatra (Hamilton, 1979). The sliver plate is bounded on the west by the Sumatran deformation front that marks the location of the Sumatran trench where present day subduction of the Indo-Australian plate is taking place. The configuration of the WBZ has been delineated and analyzed in detail by Hanus et al. (1996) mainly to identify the aseismic gap within 100 – 200 km depth level all along the Sumatran arc and its relation to the volcanism in the overriding continental wedge. Here, considering all available events from the catalogue of earthquakes up to 2005 and good number of focal mechanisms, the WBZ is delineated along 8 sections to study the spatial variations in deformation process both along and across the Sumatran arc. These sections were drawn from southwest of the trench axis to northeast of the back-arc region sufficiently long enough to image entire seismic part of the lithosphere in the region.

It can be seen from the sections that the post mega thrust seismic activity has been spread over a wider area from the trench region towards the fore arc in the northern Sumatra. The events near or ocean ward of trench show either strike-slip mechanisms with consistent right-lateral motion (S1:174,175; S2:214-216; S4:267; S5:289; S7:333) and few thrust (S1:177-179; S2:217) or normal (S4:267-269; S7:332-334) mechanism events. The fore arc lithospheric sliver plate between the trench and the Sumatran fault in the offshore Sumatra is seismically the most active part of the entire arc as revealed by the historical and recent catalogue of earthquakes. This entire stretch forms part of the shallow WBZ and the interplate region characterized by the occurrence of predominantly thrust events mostly of low-angle thrust mechanisms (S1:183,185,186,188; S2:219,220,223,225,226,227,229; S3:243, 246,248,249,250; S4:270-275,277,278; S5:290-297; S6:307-312; S7:335,336,338,339,342-345; S8:360-363,366-369,372-375,377). Several strike-slip events with right-lateral shear motion on N-S or NNW-SSE trending nodal planes and reverse faulting mechanisms occurred in the Sumatran offshore (S1:187,189; S2:221,222; S3:242,247,253,260; S4:279; S7:346,347; S8:364,365,370,371,376,379). The mechanisms in the dipping subducted slab shows complex and varied pattern of events. These can be classified as: the thrust mechanisms within which, down-dip compression (DDC) (S2:232; S3:262,263; S7:350; S8:382,383,387), thrust events with nodal planes parallel to the orientation of slab (S2:228,233; S3:259,261; S4: 281,282,285,287; S5:299; S6: 315-318, 321,323; S7: 351,354; S8: 380, 384,386,389), normal faulting events; down-dip tension (DDT) events (S1:194,195; S2:230; S5:298; S6:320,327; with nodal planes parallel to the orientation of the slab (S1: 201,205; S2:231,236; S4:276), and strike-slip events (S1:196,203; S3: 253,255,260; S4:279,283,284; S5:301,302,303; S6:325,326,330; S7:352,353,355,357,358; S8:378, 379,381,388). In the continental Sumatra back-arc region, the SFZ is a regionally continuous but segmented locally active fault zone show consistently right-lateral fault mechanisms all along the Sumatran arc (S1:210-

213; S2:237; S3:265,266; S4:286,288; S5:305; S6:328,329; S7:359; S8:390). Hanus et al. (1996) observed a major transverse structure across the northern segment of the Sumatra with a left lateral sense of shear. The strike-slip solutions with left-lateral motion on NE-SW trending nodal plane (S1:199,200) are related to this transverse structure.

3.6.3. Java Arc: SS-1, J1 – J7

Further southeast of Sumatran arc, beyond 105°, from Sunda Strait onwards, the subducted slab penetrates to much deeper depths up to 600 – 650 km. The Sunda Strait is a consequence of the northwestward motion of the southwestern part of the Sumatran block along the central Sumatran fault. The extension zone widens southwestward and changes in to a composite zone of strike-slip as well as normal faulting (Huchon and Le Pichon, 1984).The section SS-1 across the Sunda strait shows that seismicity is diffuse and widespread in the upper part of the plate and earthquakes continuously occur all along the WBZ up to a depth of 250 km. Beyond his depth, the WBZ is defined by very few events and maximum depth of occurrence is at 650 km. The focal mechanism solutions along the section indicate dominantly strike-slip mechanisms (391,392,394,397,398,401,402,403,405,409,410) and few thrust faulting events in the shallow fore arc and interplate region (393,395, 396,399,404,406,407). A normal faulting mechanism (408) is observed below the Sunda Strait at the top part of the WBZ. The deepest earthquake in the WBZ at 650 km depth is another normal faulting event (411) with both nodal planes parallel to the WBZ orientation.

The sections (J1 –J7) across the Java arc reveal seismic activity all along the upper part of subduction zone right from trench onwards, sometimes even further southwest of trench (J4, J5). On the Java mainland, which is characterized by chain of volcanoes in the back-arc, the seismic incidence in the upper plate can be seen only along J1 and J2. However, further east, the seismic activity continues well into the back-arc in the Lombok and Sumbawa island region (J6, J7). The earthquake focal mechanisms indicate that near to the trench, the events show dominantly normal faulting on more or less E-W trending nodal planes (J3:461,462; J4:482; J5:509-516; J6:533-536; J7:548-551), few thrust (J1:412,414-416; J2:443; J4:483) and strike-slip (J1:413; J6:533; J7:547) mechanisms. In the fore arc as well as the shallow interplate region, most of the events show thrust faulting; some of them are of pure / low-angle thrust events some of them showing down-dip compression(J1:414-417,420,428-431; J2:445-448,450,452,454; J3:464,465,467,470-472; J4:483,484,487,489,490,496-501; J5:518-521,523,525,526; J6:539,540; J7:553,554,557,558,560). In this region, few down-dip tension mechanisms have also been noticed (J2:453; J3:466; J4:488,491,492). In the down-going slab, many of the WBZ events show either down-dip compression (J1:423,427,439; J2:455; J3:473; J4:493; J6:545; J7: 561,562,566,568, 573,575) or down-dip tension (J2:456; J3:468,469). Further deep, below 500 km depth, cluster of events observed almost in all sections through out Java, show consistently normal faulting mechanisms. The nodal planes of many of the events align parallel / slightly oblique to the trend of the slab (J1:441,442; J3:475-477,479; J4:502,503,506; J6:546) or along the dip of the WBZ (J3:480; J4:505,507,508; J5:528-532; J7:576-579). Another observation is that the strike-slip mechanisms are fewer in Java arc when compared to rest of the arc segment (J1:424,432,438; J2:451; J3:474; J4:504; J5:522,524,527; J6:538; J7:556,559, 572, 578). This could be due to increasingly oblique nature of the arc towards Sumatra and Andaman region. Further east, the shallow seismic events in the overriding plate occur in two regions of the arc, one is below western Java (J1,J2) and the other near Bali and Sumbawa islands (J6, J7). From the sections, it can be seen that the events in the western Java show mostly low-angle thrust / reverse faulting mechanisms (J1:437;

J2:458-460) and one strike-slip mechanism (J1:436). In the Bali and Sumbawa region, the earthquake mechanisms show both low-angle thrust faulting (J6:542,544; J7:570) and right-lateral shaer faulting on E-W to NNW-SSE nodal planes (J6:541,543; J7:569, 571).

3.7. Discussion and conclusions

The geometry of the WBZ and the variations in deformation pattern both along and across the Andaman-Sumatra-Java arc reveal the characteristics of active subduction in the region. The deformation field suggests that a pure normal subduction dominated by thrust faulting in the Java region, becomes progressively oblique towards Sumatra and the Andaman arc, characterized by thrust faulting and right-lateral shear motions in Sumatra region, and dominantly strike-slip and normal faulting in the Andaman region.

In the Andaman arc, the deformation pattern has been significantly changed due to the presence of back arc spreading in the Andaman Sea. The dominant compressional deformation in the Sumatran fore arc becomes progressively more oblique with respect to trench in the Andaman fore arc region. Many thrust faulting events along the Andaman-Nicobar islands in the upper plate occur on NNW-SSE nodal planes suggesting orientation of their P-axes in NW-SE i.e., in the direction of convergence between the Indo-Australian and SE Asian plates. Several N-S oriented faults have been identified over the Andaman-Nicobar islands and the adjacent offshore areas. Most significant among them are the Jarwa thrust on the main islands and the West Andaman Fault (WAF) in the east of islands. Some of these faults and thrusts are seismically active (Mukhopadhyay, 1984). Based on stress model, Biswas et al.(1992) inferred N-S oriented shear stresses along the Andaman arc and NW-SE trending tension in the Andaman Sea. On the basis of deformation velocities in the

Andaman arc-sea region, Radhakrishna and Sanu (2002) concluded that the oblique convergence, partial subduction of the ninetyeast ridge below the Andaman trench and the back arc spreading in the Andaman Sea all together contribute to the present day stress field in the region. For better understanding of seismotectonics of the region, it is essential to carry out a detailed study of lithospheric structure of Andaman arc and the adjoining areas and some of these aspects are presented in a subsequent chapter.

In the Sumatra arc, the oblique convergence characterizes the subduction which brings substantial arc parallel shear motion in the form of strike-slip earthquakes. Strike-slip faults oriented parallel to the arc play an important role in the tectonics of the overriding plate by acting as a boundary for detachment of a sliver between it and the subduction boundary. This aspect is very relevant and important in the case of Sumatra arc because of the presence of regionally extensive Sumatra Fault Zone (SFZ) and the 300 km wide lithospheric sliver plate between the Sumatra deformation front at the trench and the SFZ in the back arc region. The question is whether strike-slip motion or oblique slip motion along the arc is partially accommodated by any other faults within the sliver plate or entire slip is being taken up along the SFZ alone. Based on variations in the slip vector azimuth along the trench, McCaffrey et al.(1991) inferred arc parallel stretching of the fore arc. Bellier and Sebrier (1995) suggested significant right-lateral transpressional deformation across the arc that include the fore arc edge, Mentawai fault zone (MFZ) and the back arc. McCaffrey et al.(2000) observed that the additional slip required may not be accommodated along the MFZ due to absent of significant motion from GPS network. Further, the MFZ at the location of Nias island region shows as a reverse fault (Samuel and Harbury, 1996) which represents a compressive deviatoric stress regime (Mukhopadhyay, 1984). However, focal mechanisms of post-tsunami earthquakes in Sumatra – Andaman region show several right-lateral strike-slip events along the

MFZ. Subsequent chapters on deformation will throw light on the nature of faulting and oblique motion in the Sumatra region. Hanus et al. (1996) identified active transverse structure with left-lateral shear motion in the northern part of the Sumatra which extends far interior of the Indian plate. Stein and Okal (1978) interpreted such left-lateral shearing on N-S trending nodal planes within the Indian plate due to resistance to the collision of India with Asia.Guzman-Speziale and Ni (1996) also interpreted the shallow strike-slip events in the subducted slab along the arc as a result of collision of India with Asia.

Subduction of large bathymetric ridges causes compression in the upper plate along the convergent plate boundaries. Presently, the Wharton Ridge and Investigator Fracture Zone in the northern–central Sumatra (Whittakar et al, 2007) and the Roo Rise in the Java (Kopp et al., 2005) are subducting below the Sunda arc, thereby causing broadly distributed deformation in the fore arc region in he respective segments.

In the Java arc region, the deeper part of the slab geometry has been differently suggested as a southward bending slab ~ 15° from the vertical (Schoffel and Das, 1999), and as a northward bending slab (Widiyantoro and van der Hilst, 1996). While, the observation made by Schoffel and Das (1999) was based on precise hypocentral locations of deep earthquakes and bending stresses, Widiyantoro and van der Hilst (1996) observed it based on longer wavelength tomographic images which may provide only regional picture. The sections in the present study also show that the slab penetrates at an angle of 40° – 50° up to a depth of 300 – 350 km, beyond which the slab penetrates almost vertically and the deepest part of the slab appear slightly bending southward. This displacement of the seismic zone in the lowest part has been inferred due to shear flow in the mantle by Schoffel and Das (1999). Based on the analysis of state of stress at different depth levels of WBZ, Slancova et al.(2000) observed that in Java, maximum compression is perpendicular to the trench at shallow depths (0-165 km) and is parallel to the trench at the depth range of 25-225 km with no distinct boundary separating these two stress patterns. However, they observed clear stress variation in the deeper levels showing slab-dip-parallel extension at 225-315 km depth and slab-dip-parallel compression in the region deeper than 400 km. The focal mechanism solutions show normal faulting along the trench and thrust earthquakes in the back arc region. The seismic activity in the WBZ shows an aseismic gap in the depth range of 300-550 km. In spite of such large gap, many previous workers agreed that the slab is continuous and penetrate in to the lower mantle (e.g., Isacks and Molnar, 1971; Newcomb and McCann, 1987; Puspito and Shimazaki, 1995; among others). Isacks and Molnar (1971) suggested that the gap could have been caused by change in the down dip stress rather than a break in the slab. The global pattern of mantle seismicity shows such a gap with fewer and smaller earthquakes at these depths (Kirby et al., 1996). Hanus et al. (1996) interpreted that the earthquakes occurring in the depth range 500 – 650 km within the WBZ under southern Sumatra and Java as a manifestation of still seismically active lowest part of the Tertiary subduction zone buried in the upper mantle. They arrived at this conclusion based on the southwestward disposition of Oligocene volcanism in relation to the Quaternary volcanic chain in Sumatra (Katili, 1975).

CHAPTER 4

ACTIVE CRUSTAL DEFORMATION IN THE ANDAMAN-SUMATRA-JAVA TRENCH-ARC REGION

4.1 Introduction

The highly devastating and Tsunamigenic Sumatran earthquake of 26 December 2004 of M_w 9.3 and the continuing events since then have brought to fore, the seismicity of the Indonesian arc system and its extension into the Andaman Nicobar region. The Island arc system constitutes a major subduction zone in the eastern Indian Ocean extending over a distance of 5600 km and separates the Indian and Australian plates from the Eurasian plate. The occurrence of a mega thrust earthquake of such enormous dimension requires a detailed analysis of shallow earthquakes and quantification of deformation pattern in shallow regions of the entire arc system.

It can be seen that the fore arc geometry systematically varies from west to east as the sediment thickness on the subducted plate decreases (Newcomb and McCann, 1987). The ridge-transform motion in the Andaman Sea is believed to be connected further north into the Burma and meets the Shan-Sagaing fault. Therefore, the region of Andaman arc together with the Burmese arc forms an important transitional tectonic link between the Eastern Himalayas in the north and Indonesian arc in the south. The back-arc spreading center near the Andaman Islands continue southward to join the long trench parallel Sumatran fault Zone (SFZ) that runs along the entire length of Sumatra (Curray et al., 1979). The trend of the arc remains southeast offshore Sumatra and becomes nearly east west at about 105° between the islands of Sumatra and Java (Chandra,1984). The Sunda strait located in this region is viewed as a tectonic as well as physiographic break in the arc and it is a transition zone between two steady state tectonic regimes; a normal subduction in front of Java with a well developed fore arc basin in the east and an oblique subduction in front of Sumatra with sliver plates and strike slip faults accommodating the lateral component of oblique subduction (Fitch 1972; Malod et al., 1995) in the west (See Figure 2.2). The normal subduction below the Java is characterized by the development of typical fore arc basins. The oblique subduction beneath Sumatra and Andaman region results in partitioning of the convergent motion into thrust and strike-slip faulting. Along the arc, the age and thickness of the lithosphere increases considerably from west to east; from 49-96 Ma below Sumatra to the west to 96-134 Ma below Java (Veevers et al., 1991).

The 1900 km long trench parallel Sumatran fault Zone (SFZ) accommodates a significant amount of the right lateral component of oblique convergence from 10°N to 7° S (Sieh and Natawidjaja, 2000). It is suggested that it is probably the world's clearest example of this type of major shear fault system adjacent to a convergent margin and the right lateral component of the oblique convergence is the cause for the right lateral Sumatran fault zone or the Semangko fault (Fitch, 1972). About 20 separate en echelon segments constitute this fault system (Tjia, 1978). No such shear faulting of regional extent has been observed in Java, though Western Java is characterized by the presence of a fault called Cimanderi fault. The onshore Java is identified as a single tectonic belt called the Java fault zone (JFZ) (Slancova et al., 2000). The shape and location of the Sumatran fault, the presence of active volcanic arc and the fore arc structures are well correlated with the shape and character of the underlying subducting oceanic lithosphere (Sieh and Natawidjaja, 2000). According to them. Batee fault is a major right lateral strike–slip fault that diverges from the Sumatran fault at about 4.5° N (Figure 2.2) and except very locally, the Batee fault does not appear to be active on the mainland of Sumatra.

A 300 km wide strip of the lithosphere exists as a fore arc sliver plate between the Sumatran fault and the Sumatran deformation front. Seismic reflection data in this region reveals a 600 km long strike- slip fault parallel to the Sumatran fault Zone called the Mentawai Fault zone (MFZ) just east of Mentawai islands (Diament et al., 1992). They inferred that the MFZ is a zone of weakness that separates the oceanic and continental crust. According to them, the Sumatran sliver plate appears to be composed of several strips that move towards the northwest to accommodate the oblique subduction.

Subsequent part of this chapter deals with the estimation of active crustal deformation undergoing along this arc-trench system in the eastern Indian Ocean. For this purpose, available hypocentral data of all shallow earthquakes spanning over a century and large number of focal mechanism solutions have been used. For calculating crustal deformation rates, the entire region is divided into a number of seismogenic sources through the approach of seismotectonic regionalisation. The details on methodology adopted in the computation of crustal deformation rates, data set utilized, the basis for regionalisation and the results obtained are presented below.

4.2. Methodology adopted for estimation of crustal deformation

The relative movement of plates gives rise to earthquakes. The slip on the fault that generates the earthquake is determined by the direction of relative plate motion, and the average displacement rate is controlled by relative plate velocity. The magnitude of the slip can, in principle, be determined from the scalar seismic moment Mo, of the earthquake (Brune, 1968), which can be obtained as

$$\mathrm{Mo} = \mu \mathrm{AS} \longrightarrow (1)$$

Where μ is the shear modulus, A the area of the surface that slips and S is average amount of slip. This procedure has been known and used for several years. However, in tectonically active areas, when the deformation is distributed, the equation (1) has to be further modified.

4.2.1. Seismic Moment Tensor

The scalar seismic moment M_o can be combined with information derived from the fault-plane solution to form the moment tensor M as

$$M = Mo^n (\bar{u}.\bar{n} + \bar{n}.\bar{u}) = Mo^n F^n \longrightarrow (2)$$

Where $\bar{n}$, is a unit vector normal to the fault plane and $\bar{u}$ is a unit vector in the direction of slip (Aki and Richards, 1980). M_o can be computed either directly from the seismograms or using an empirical moment-magnitude relation. The only ambiguity involved here is that the determination of fault plane from the two nodal planes of source mechanism.

4.2.2. Moment tensors and distributed strain

If all the deformation that occurs within a volume V is seismic, Kostrov (1974) showed that there is a relationship between the average strain ε_{ij} of the volume and the sum of the moment tensors of all earthquakes within it:

$$\bar{\varepsilon}_{ij} = \frac{1}{2\mu v} \sum_{n=1}^{N} M_{ij}^{n} \longrightarrow (3)$$

The strain rate ε_{ij} during time τ is

$$\dot{\varepsilon}_{ij} = \frac{1}{2\mu v\tau} \sum_{n=1}^{N} M_{ij}^{n} \longrightarrow (4)$$

For a seismic zone of Volume v with known dimensions (length l_1, width l_2 and depth extent l_3), and by choosing a co-ordinate system with axes x_1 and x_2 parallel and normal to the trend of the zone respectively and the vertical axis x_3 +ve downwards, the elements of velocity tensor or the active crustal deformation rate can be calculated as given by Jackson and McKenzie (1988):

$$\left.\begin{aligned} U_{ii} &= \frac{1}{2\mu\tau l_k l_j}\sum M_{ii}^{n} \quad i=1,2,3 \quad k\neq j, i\neq k, j\neq i \\ U_{12} &= \frac{1}{\mu\tau l_1 l_3}\sum M_{12}^{n} \\ U_{i3} &= \frac{1}{\mu\tau l_1 l_2}\sum M_{i3}^{n} \quad i=1,2 \end{aligned}\right\} \longrightarrow (5)$$

This method of calculation requires knowledge of both the fault plane solutions and the seismic moment for each earthquake complete over a certain magnitude threshold. This actually restricts the method to be applicable for the most recent data, as such information would not be available for older (historic) events. The historic events can also be used, by assuming fault parameters for individual events. Jackson and McKenzie (1988) observed that the historic data being available for large devastating earthquakes only, they influence the calculations. To eliminate some of these drawbacks, Papazachos and Kiratzi (1992) proposed a method, which allows the use of all available data including historic earthquakes as explained below:

The equation (2) above consists of two parts: M_o^n, which represents the size of the earthquake and F^n, which is a shape tensor that represents the geometrical features of the earthquake. The equation can be rewritten using the annual moment rate tensor $\dot{M}$ and the scalar annual moment rate $\dot{Mo}$ for calculating $\overline{F}$.

$$\dot{M} = \dot{Mo}\overline{F} \longrightarrow (6)$$

Where

$$\overline{F} = \frac{\dot{M}}{\dot{Mo}} = \frac{\sum_{n=1}^{N} \frac{M^n}{T}}{\sum_{n=1}^{N} \frac{Mo^n}{T}} = \frac{\sum_{n=1}^{N} M^n}{\sum_{n=1}^{N} Mo} = \frac{\sum Mo^n F^n}{\sum Mo^n} \longrightarrow (7)$$

where T is the time period

Thus $\overline{F}$ represents an average shape tensor or in other words a representative focal mechanism tensor. The above method of calculation of F_{ij} gives a moment-normalized tensor i.e., a moment weighted average of F_{ij} tensors. In practical, for areas, where the numbers of focal mechanisms are limited, a single large event will influence the calculation of $\overline{F}$ because of its large moment. Alternatively, Kiratzi and Papazachos (1995) proposed a simple averaging of F^n_{ij} as $\sum_{n=1}^{N} \frac{F^n_{ij}}{N}$ where N is number of focal mechanisms in the deforming zone. This approach gives equal importance to all focal mechanisms. So, the calculation of deformation velocities involve two major steps such as

(1) Estimation of scalar moment release rate that give rise to magnitude of deformation
(2) Calculation of representative focal mechanism tensor, which controls the shape of deformation.

4.2.3. Calculation of Moment Rate

The size factor $\dot{M}$, which is the moment release rate, can be calculated by simple averaging of the scalar seismic moments of earthquakes over a magnitude threshold for a long enough period of time T. However, for such simple averaging of moments, it is necessary to have a complete record of seismicity of all earthquakes over Ms 6.0 for a time period considerably longer than the repeat times of large earthquakes. Alternatively, Molnar (1979) proposed a method, which utilizes the complete record of seismicity including historical events. The method is as discussed below:

The relative number of events with seismic moment greater or equal to M_0 is given by the relation:

$$N(Mo) = A \cdot Mo^{-B} \longrightarrow (8)$$

Where,

$$A = 10^{(a + \frac{bd}{c})} \quad \text{and} \quad B = \frac{b}{c}$$

Where, a and b are constants of Gutenberg-Richter relation,

$$\log N = a - bM \longrightarrow (9)$$

and c, d are constants of the empirical moment-magnitude relation,

$$\log Mo = cMs + d \longrightarrow (10)$$

The rate of recurrence of seismic moment $\dot{M}$ is then given by the relation,

$$\dot{M} = \frac{A}{1-B} M_{o,\max}^{(1-B)} \longrightarrow (11)$$

Where $M_{o,\max}$, is the seismic moment released by the maximum earthquake in the region.

The **a** and **b** values estimation is very critical because of its sensitivity to errors due to data gaps and incompleteness of data which is primarily attributed to detection capabilities of networks existed during the past. Milne and Davenport (1969) proposed a method called 'mean value method' for calculating **a** and **b** values in order to evaluate seismic risk and this method was suitably adopted by Papazachos (1990) which takes into consideration of both recent as well as historical data and at the same time normalizing the variations in network detection capability. The method of calculation is as given below.

4.2.3.1. *Estimation of a and b values: Milne-Davenport Method*

According to the statistical relation of Gutenberg-Richter (1944), the number N of earthquakes with magnitude M or larger which occurs in a certain region and in a certain time period is given by equation 9 as, $\log N = a - bM$, where **a** is the intercept and **b** is the slope of the least square fit, when log N is plotted against each increment (say 0.1) of magnitudes. The values of **a** and **b** depend on seismicity and other seismotectonic properties, while **a** value depends mainly on the time interval considered and also on the area under consideration. For accurate determination of these parameters, data should be available for a long time period and also the entire range of magnitudes occurring in the area. However, the availability of complete data concerning large and small earthquakes is restricted to only recent years. For the period prior to this, information is only available for large destructive earthquakes. From an analysis of seismicity worldwide, we can find relatively good number of lower magnitude events after 1964, which marks the inception of World Wide Standardized Seismograph Network (WWSSN). Since then the detection capability of networks considerably enhanced to sense even smaller magnitudes of 4.5. Prior to this we can find different periods of distinct levels of detection threshold for which reliable data are available. Because of this it is not possible to use the entire available data straight away for the calculation of <u>a</u> and <u>b</u> values as they can give erroneous values. For eliminating this problem Milne and Davenport (1969) suggested the 'mean value method'.

For applying the mean value method, we have to separate the whole interval of data into subintervals for which the data is complete and reliable down to a minimum magnitude. Thus say if 1900 (say t_1) to 1995 (say t_0) is the whole period for which data is complete for magnitude ≥ 6.5 (say M_1), we can have subintervals for which the data is complete for magnitude ≥ 5.5 (say M_2) ranging from 1950 to 1995 ($t_2 \sim t_0$) and for magnitudes ≥ 4.5 (say M_3) from 1964 to 1995 ($t_3 \sim t_0$). The number of events for each magnitude increment of $M \geq M_1$ for whole period ($t_1 \sim t_0$) is given by

$$N(M) = N_1(M_1) \longrightarrow (12)$$

and for subinterval $t_2 \sim t_0$ with magnitudes between M_1 and M_2 ($M_1 > M \geq M_2$) it is

$$N(M)=\frac{N_2(M_2)\times \text{no. of years in total period } (t_0-t_1)}{\text{no. of years in subinterval } (t_0-t_2)} \longrightarrow (13)$$

For the second subinterval $t_3 \sim t_0$ with magnitudes $M_2 > M \geq M_3$ it is

$$N(M)=\frac{N_3(M_3)\times (t_0-t_1)}{\text{no. of years in subinterval } t_0 \sim t_3} \longrightarrow (14)$$

Here number of events each subinterval are normalized and brought to the level of the whole time period ($t_0 \sim t_1$). Having got the number of events of each magnitude for whole time period, the cumulative frequency for each magnitude is calculated as follows.

	Magnitude	Number of events.
Subinterval 1	$M \geq M_1$	$N = N_1$
Subinterval 2	$M_1 > M \geq M_2$	$N = N_2 + N_1$
Subinterval 3	$M_2 > M \geq M_3$	$N = N_3 + N_2 + N_1$

Finally the number of events against each event is divided by number of years in the whole period ($t_0 \sim t_1$) leading to annual rates of occurrences. Using this, log N values are plotted against each magnitude increment and a and b values are calculated by least square fit method. The standard deviation is also calculated to estimate uncertainties in a and b values.

4.2.3.2. *Moment – Magnitude Relation*

The moment-magnitude relation given in equation 10 above is evaluated based on the seismic moments and surface wave magnitudes available for the whole region of analysis. The seismic moments for many large to moderate earthquakes have been obtained from the Harvard CMT solutions, reported in Physics of the Earth and Planetary Interior by Dziewonski and his co-workers are available for post 1977 events only. The slope and intercept of the least square fitting line to the data of log Mo against Ms gives **c** and **d** values. The slope c is very sensitive to the insufficient data and local trends or bias in moment values. Kanamori and Anderson (1975) estimated moment – magnitude relation for global data set and obtained a value of 1.5 for the slope **c**. We used this slope value (1.5) for **c** and determined the intercept **d** value by fitting least square line to the Ms – Mo scattered data.

Having estimated the **a**, **b**, **c** and **d** values, another parameter in evaluating equation 11 for calculating moment release rate is $M_{o,max}$, the largest ever moment occurred in that seismic zone. As this value may not be always available, it can be calculated by converting $M_{s,max}$, the magnitude of largest event occurred in the zone into its equivalent seismic moment using the moment-magnitude relation discussed above.

4.2.4. Calculation of Focal Mechanism Tensor ($\overline{F}$)

The focal mechanism tensor influences the direction of deformation. In order to calculate $\overline{F}$, all the focal mechanisms of events occurring in a given seismogenic source have to be considered for summation. Therefore, the seismogenic zone identified should have homogeneous faulting pattern. The strike φ, dip δ and rake λ values of the individual focal mechanisms are utilized to calculate the components of focal mechanism tensor based on the formulations of Aki and Richards (1980). The $\overline{F}$ can be calculated either as a moment weighted averaging method given in equation 7 or from simple averaging of individual focal mechanism tensors suggested by Kiratzi and Papazachos (1995). We used the later method of simple averaging of focal mechanism tensors. In case, more than one seismogenic zone falls in a single seismic belt, the mechanisms falling in the whole belt are utilized to obtain a single focal mechanism tensor $\overline{F}$ for the belt.

4.2.5. Strain rates and Deformation Velocities

After determining the quantities a, b, c, d, Mo,max and representative focal mechanism tensor $\overline{F}$ as outlined above, the strain rates and deformation velocities for each seismogenic zone can be calculated. The equations 4 and 5 can be transformed accordingly to calculate the strain rates and deformation velocities using the following relations.

$$\dot{\varepsilon} = \frac{1}{2\,\mu v}\dot{M}\overline{F}_{ij} \quad i,j=1,2,3 \longrightarrow (15)$$

$$\left.\begin{aligned} U_{ii} &= \frac{1}{2\mu l_k l_j}\Sigma \dot{M}\overline{F}_{ii} \quad i=1,2,3 \quad k \neq j, i \neq k, j \neq i \\ U_{12} &= \frac{1}{\mu l_1 l_3}\Sigma \dot{M}\overline{F}_{12} \\ U_{i3} &= \frac{1}{\mu l_1 l_2}\Sigma \dot{M}\overline{F}_{i3} \quad i=1,2 \end{aligned}\right\} \longrightarrow (16)$$

Reference co-ordinate system x_1, x_2, x_3 for these equations is along the length (l_1), width (l_2) and thickness (l_3) respectively of the seismic source. The rigidity modulus μ is considered as $\mu = 3\times10^{11}$ dyne/sq.cm. As $\overline{F}$, the focal mechanism tensor is defined in the North (x_1), East (x_2) and down (x_3) reference system, a rotation in $\overline{F}$

tensor is done for bringing it to the co-ordinate system of the source. The angle of rotation (θ) being the azimuth of the source i.e., angle made by the length (l_1) segment of the source with the North. Using this rotated $\overline{F}$ tensor, the deformation velocities are calculated. For the purpose of correlation and analysis of deformation in different sources, a single reference system should be used. Therefore, the velocity tensor is rotated back by the same angle (θ) for each source into the North (x_1), East (x_2) and down (x_3) reference system. Having calculated the velocity tensor, the eigen values and the respective eigen vectors define the deformation pattern along the three principal components. The eigen values give rise to magnitude. From the eigen vectors, the azimuth and plunge of respective component of deformation is obtained. For the horizontal components (U_{11} and U_{22}), -ve eigen values signify compressional component and +ve values signify extension. A +ve vertical component in U_{33} represents crustal thickening and –ve value refer to crustal thinning.

4.2.6. Error Analysis – Monte Carlo Method

In order to derive confidence limits for the estimated deformation velocities, a detailed error analysis is done. The analysis has to take into account all possible random errors of the parameters used in the calculation. Papazachos and Kiratzi (1992) proposed a Monte-Carlo method for the analysis. The errors are considered to have Gaussian probability density and analysis is based on the transmission of small fluctuations of the input parameters through the model to the output results.

Equation 16 suggests that the errors in estimated deformation velocities are due to errors in Mo and $\overline{F}$. While errors on Mo influence the magnitude of velocities, the errors in $\overline{F}$ affect the direction of velocity tensor. As standard errors for focal mechanism data set are generally difficult to estimate, also, we are primarily interested in estimating magnitude of deformation field, we attempted to evaluate only the errors in Mo, in the present study. From equations 8 and 11, it is seen that errors in Mo propagate mainly due to errors in **a**, **b**, **c**, **d** and $M_{s,max}$. If we assume that we have random errors in these parameters with known medians and standard deviations, we can introduce Gaussian deviation in them and estimate new value for Mo. Since the input parameters are correlated, the covariance matrix V of the parameter vector P = (a, b, c, d, $M_{s,max}$) is not diagonal. P is calculated from

$$P = Cz + m \longrightarrow (17)$$

Where m is the mean values of the parameters, C is the lower triangular matrix of the covariance matrix of parameter vector V such that $V = C \times C^T$ and z is the standard Gaussian random vector. The Gaussian random vector is generated using the polar Box-Muller transform for each of the standard errors in the mean values of parameters. Standard deviations and covariances are derived during the least square analysis while finding **a**, **b**, **c**, **d** values, variance being the square of the standard error. The r.m.s error in the least square fit of M_s–M_o relation is assigned as the standard error in **d** value. The covariance of **c** and **d** values $\sigma^2_{cd} = r_{cd}.\sigma_a.\sigma_b$, where $r_{cd} = -0.95$ is the correlation coefficient of **c** and **d**. The lower triangular matrix C for the above covariance matrix V is obtained by subjecting matrix V to Cholsky decomposition. The diagonal values in the covariance matrix V is replaced by the diagonal values of Cholsky decomposition and all upper diagonal values are made zero.

The equation 17 is repeatedly computed by introducing the generated Gaussian deviates and the velocity rates are computed in each step. The mean standard deviation for computed deformation velocities give rise to uncertainty in estimated velocities.

4.2.7. Classification of mechanisms -- Mean Slip Angle method

The focal mechanism solutions compiled for the Burmese – Andaman – west Sunda arc region indicate varied faulting pattern in terms of thrust, normal and strike-slip solutions. Such variation in faulting could be observed in general from the fore arc regions towards the back-arc areas in shallow subduction zones. A proper classification of the focal mechanism solutions in these regions would allow identification of various seismotectonic domains. However, the mechanisms pertaining to a seismogenic source may slightly vary due to geometrical complexities, local stress variations etc. Ravikumar et al. (1996) proposed a method called 'mean slip angle' for classification of focal mechanism solutions into thrust, normal and strike-slip faulting. Slip angle is the most basic and distinct quantity used to classify a fault as thrust, normal or strike-slip. When the slip vector coincides with the strike, it is a pure left-lateral strike-slip fault and if 180° opposite to the strike, it is a right lateral strike-slip fault. A slip angle of 90° or –90° corresponds to pure thrust and pure normal respectively. The method defines a quantity, 'modified slip angle' which is obtained by mapping lower half (>90°) into upper half (Figure. 4.1(I) and Figure. 4.1(II)). Using this modified slip angle, it is possible to classify the fault following the definitions given below (Figure. 4.1(III)).

+90°	–	+45°	Thrust
+45°	–	-45°	Strike-slip
-45°	–	-90°	Normal

However this classification is possible only when the actual fault plane is known. In

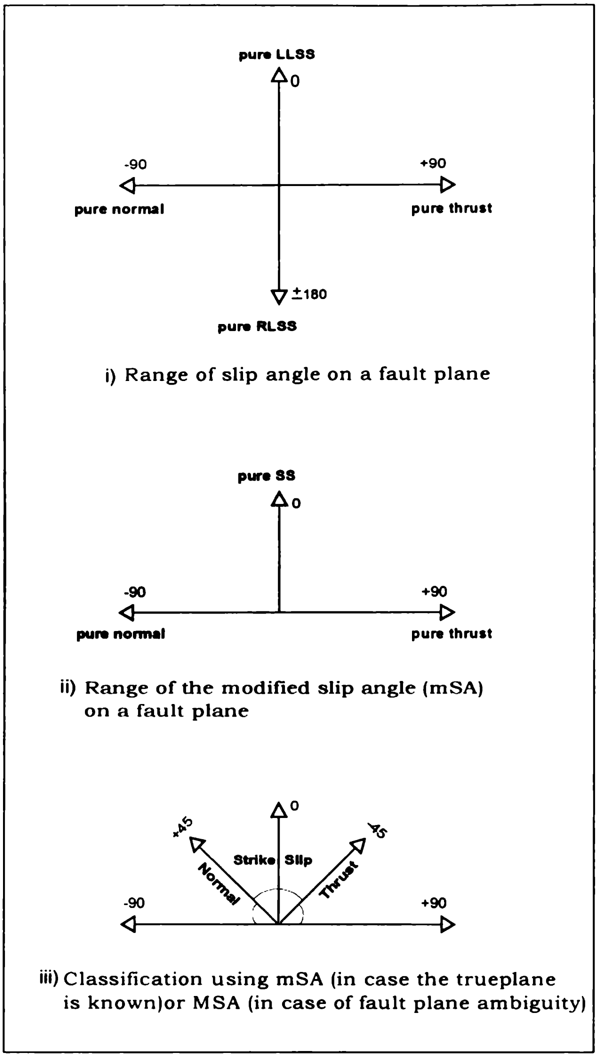

Figure 4.1. Classification of focal mechanisms based on 'mean slip angle method, given by Ravikumar et al (1996).

case of ambiguity in fault planes the method proposes a parameter called 'mean slip angle' (MSA), which is the average of the modified slip angles of twoauxiliary planes. This is only reliable if the slip discrepancy, i.e., the difference of modified slip angles is low. Slip discrepancy implies that the type of faulting on the two auxiliary planes is consistent and also the average (MSA) is close to each other. In the present study, the method of mean slip angle has been used to classify the focal mechanism solutions compiled for the region.

4.3. Data

The method described above requires two sets of data. i) Seismicity data for the estimation of the seismic moment rate. ii) Focal mechanism data for determining the shape of deformation.

For compilation of both historical and recent events in the region, we have noticed the hypocentral data from NOAA epicentral listing. The listing shows few significant earthquakes that occurred in the region prior to 1900. However, the magnitude and depth information for most of these events was not available, whereas, events later to 1900 such information is known. The most significant events from the historical earthquake records are 1833 and 1861 events. Though, Newcomb and McCann (1987) estimated the probable magnitude range for these two events, due to large uncertainities in the magnitude estimates and lack of depth information for uniform long term moment release calculations, we included events only after 1900. Also, as precise hypocentral parameters of recent sequence of events are not yet publicly available, we prepared an earthquake data set of all shallow earthquakes ($h \leq 70$ km) during 1900 – 2005 for the present analysis. Events before 1964 have been compiled from Rothe (1969) and Gutenberg-Richter (1954). For the period between 1953-1965, magnitudes from Rothe listing have been recalculated by Newcomb and McCann (1987). Similarly Engdahl et al. (1998) precisely determined hypo central parameters from ISC listing for the period 1964-1995. We considered these revised magnitudes with events Ms $\geq$4.5 for the present analysis. For events where Ms value is not available, it is obtained from Mb using Mb-Ms relation derived for the region. The magnitudes estimated by Gutenberg and Richter (1954) and Rothe (1969) are equivalent to 20-s Ms (Geller and Kanamori, 1977). The seismicity map of the region is shown in Figure 4.2. The seismicity map shown is for a period little more than a

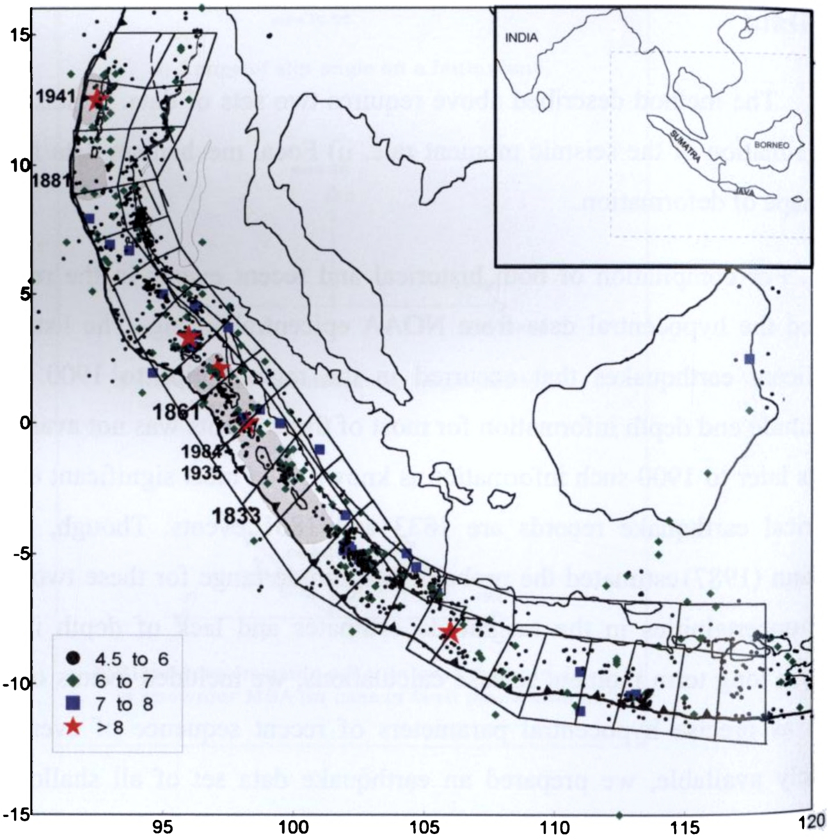

Figure 4.2. Seismicity map of the Andaman-Sumatra-Java arc and adjacent regions prepared from all shallow vents (h $\leq$ 70.0 km) during 1900-2004. The moving window configuration selected for regionalization is also shown on the map.

century during 1900-2005, which include all revised estimates of magnitudes and moments by previous workers. The post-Tsunami seismic events (after 26 December 2004) were compiled from the PDE listings and mechanisms from the Harvard CMT catalogue.

For the preparation of the second data set, about 678 focal mechanism solutions have been compiled from the region **(See Appendix I1)**. The mechanisms have been considered from Harvard CMT listings. For clarity we have shown about 100 events (from about 200 events of Ms>5.5) and plotted in Figure 4.3.

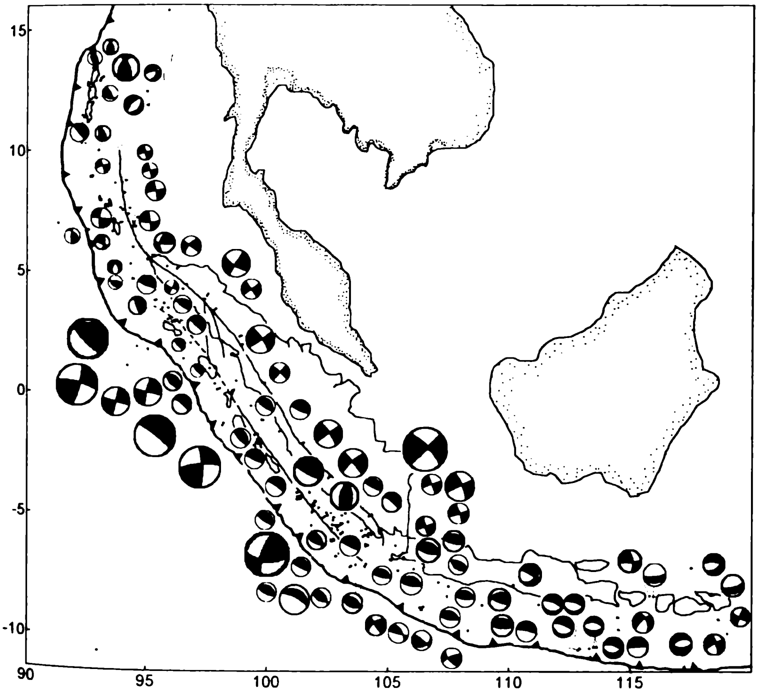

Figure 4.3. Map showing focal mechanism solutions (from Harvard CMT solutions) of shallow earthquakes (h ≤ 70 km). Note that only earthquakes of Ms > 5.5 are shown for clarity of the map.

To classify the focal mechanism solutions into thrust, normal and strike-slip faulting, the method of mean slip angle proposed by Ravikumar et al (1996) has been used. An analysis of faulting pattern from the focal mechanisms map suggests that thrust faulting events along low angle nodal planes are mostly observed all along the fore arc sedimentary complex. For most of the events, one of the nodal planes strike N–S around 10° N in the middle part of the arc, which changes to NE orientation towards northern part and to NW orientation towards southern part of the arc in conformity to the arcuate trend of the fore arc subduction complex. In the northern Sumatra region, the strike-slip events with right lateral slip correlate well with the Semangko fault zone. Between 6° and 7° N the events along the transverse seismic zone in the Andaman trench have been correlated with a wide ridge/upper trench slope and show left lateral shear along E–W fault. In south Andaman Sea, events located west and south of Sewell seamount and to the east of Nicobar deep indicate dextral slip along NNW–NW steeply dipping nodal planes and correlate with the west Andaman fault. The active back-arc spreading region in the Andaman Sea is highly conspicuous from the occurrence of large number of shallow focus earthquakes with focal mechanisms indicating normal faulting along NNE striking nodal planes. Also, few strike-slip events with right lateral slip correlate with the short transform segments that offset the spreading ridge. It can be seen from the seismicity map that several large earthquakes display distinct correlation with the SFZ as well as Sumatran offshore region. While focal mechanisms of earthquakes along the SFZ show mainly the right lateral faulting, in the Sumatran fore arc they show mostly thrust faulting. Sunda strait is the extension zone that widens southwestward and changes into a composite zone of strike slip as well as normal faulting (Huchon and LePichon, 1984). The Java onshore region is low in seismic activity whereas, the offshore Java shows considerable seismicity and the earthquake focal mechanisms show mainly thrust faulting with few normal faulting events.

4.4. Seismotectonic regionalisation

Previous studies on seismicity in relation to overall tectonics of the region gave valuable information on the geodynamics of the region. A first order segmentation of the Burmese-Indonesian arc has been presented by Chandra (1984). Based on change in the trend and offset in arc, bathymetry, faulting, trend of the line of volcanoes, spatial distribution of earthquakes and change in dip of the Benioff zone, he suggested two transverse boundary zones, the north Andaman Boundary zone and the Sunda Boundary zone. Based on seismicity and focal mechanism solutions, Rajendran and Gupta (1989) identified three tectonic units in the Andaman arc region such as the Sumatra trench region characterized by strike-slip and thrust faulting, the Andaman spreading ridge characterized by normal and strike-slip faulting and the Andaman–Nicobar ridge where faulting is mostly thrust type. Dasgupta (1992) suggested variable stress regime along and across the Andaman arc and the relatively aseismic nature in the fore arc and back-arc domain in north and south Andaman sea respectively. Dasgupta and Mukhopadhyay (1993) observed significant variation in seismicity pattern related to the subducting slab from north to south in the Andaman arc region. Based on the morpho-tectonic setting, gravity anomaly trends and seismicity pattern, they divided the region into four broad sectors from north to south. The seismic activity in these sectors is discernible into fore arc and back-arc seismic zones. Dasgupta (1992) and Dasgupta and Mukhopadhyay (1993) observed that several structural/tectonic features such as the Andaman–Nicobar–Nias fore arc ridge, the back-arc spreading ridge and the west Andaman fault in the Andaman sea and the Semangko fault zone in northern Sumatra show active and well developed seismicity pattern. According to Newcomb and McCann (1987), the occurrence of large and great earthquakes will be affected by plate tectonic parameters that vary significantly from arc to arc. Various segments of the Sunda arc are characterized in terms of typical size of gap-filling earthquakes, average repeat times for large shocks, mode of subduction (seismic versus aseismic) and seismic potential. They observed that the entire length of Sumatra has the potential to produce great thrust earthquakes whereas the plate interface near Java and Lesser Sunda islands can be considered to have low seismic potential. Slancova et al. (2000) identified seismically active boundaries within the overriding plates in the Sumatran Fault Zone (SFZ) and Java Fault Zone (JFZ) based on the criteria that (1) azimuths and dips of P and T axes should be similar for the majority of events in the particular domain (2) azimuths and dips of P and T axes in each domain should be clearly distinguishable from those in the neighboring domains (3) the hypocenters of events should be closer to each other in a particular domain. Assuming uniform stress in such domains, they inferred that the state of stress in the continental lithosphere overriding the subducting plate is represented by the state of stress in domains SFZ and JFZ.

Based on these previous studies and seismicity pattern, we identified several broad distinct seismogenic belts/sources. These are 1) the outer arc region consisting of Andaman-Nicobar islands 2) the back-arc Andaman Sea.3) The Sumatran fault zone (SFZ) 4) Java onshore region termed as Java Fault Zone (JFZ) 5) Sumatran fore arc sliver plate consisting of Mentawai fault (MFZ) 6) The offshore Java fore arc region 7) The Sunda Strait region. For belts 3 and 4, the boundaries have been defined by Slancova et al. (2000). The offshore belts 5 and 6 have been extended up to the deformation front below the Sumatra-Java trench. For each of these four belts, we need to identify seismogenic sources. As the seismicity is variable, it is difficult to demarcate individual seismogenic sources. Hence, we employed a moving window method having a window length of 3–4° and with 50% overlapping starting from one end to the other. The advantage in this method is that we obtain a continuous variation in deformation pattern along the length of active seismic belts and also selecting a different window length does not alter the deformation pattern significantly. We succeeded in defining 4 sources each in the Andaman fore arc and

Back arc region, 9 such sources (moving windows) in the Sumatran Fault zone (SFZ), 9 sources in the offshore SFZ region and 7 sources in the offshore Java region. Because of the low seismicity along JFZ, it is separated into three seismogenic sources namely West Java, Central Java and East Java. The Sunda strait is considered as a single seismogenic source. Each window representing the seismogenic source along the arc has been numbered as shown in the Figure 4.4.

4.5. Moment release rate

Seismic moment release rate for each seismogenic source can be estimated by using equation 2. The advantage of this formula is that the full record of seismicity can be used in any given region. An important parameter in the calculation of moment release is $M_{0,}max$. The seismic moment is related to the maximum magnitude event in a given source. $M_{0}max$ can be directly estimated from $M_{s,}max$ using the appropriate Ms-Mo relation. The seismic moments of all shallow earthquakes of depth $\leq$50 km and Ms $\geq$ 5.5 have been considered for deriving the moment-magnitude relation. The slope 'c' of the Ms-Mo relation is very sensitive to errors in Ms values. So by considering c=1.5, as defined by Kanamori and Anderson (1975), we calculated d value intercept from the observed data. The magnitude–moment relation shown in Figure 4.5 gives a value of d = 16.164 with an rms error of 0.26 with the observed data. Since the relation satisfactorily explains the observed data, we used it for converting M_{s},max to $M_{0,}max$.

Other important parameters in the calculation of $\dot{M}$ are the 'a' and 'b' values of the Gutenberg –Richter relation and estimated using Milne and Davenport method. The moment release rates and 'b' values for each seismogenic source (window) have been shown in the Table 4.1-Table 4.3.

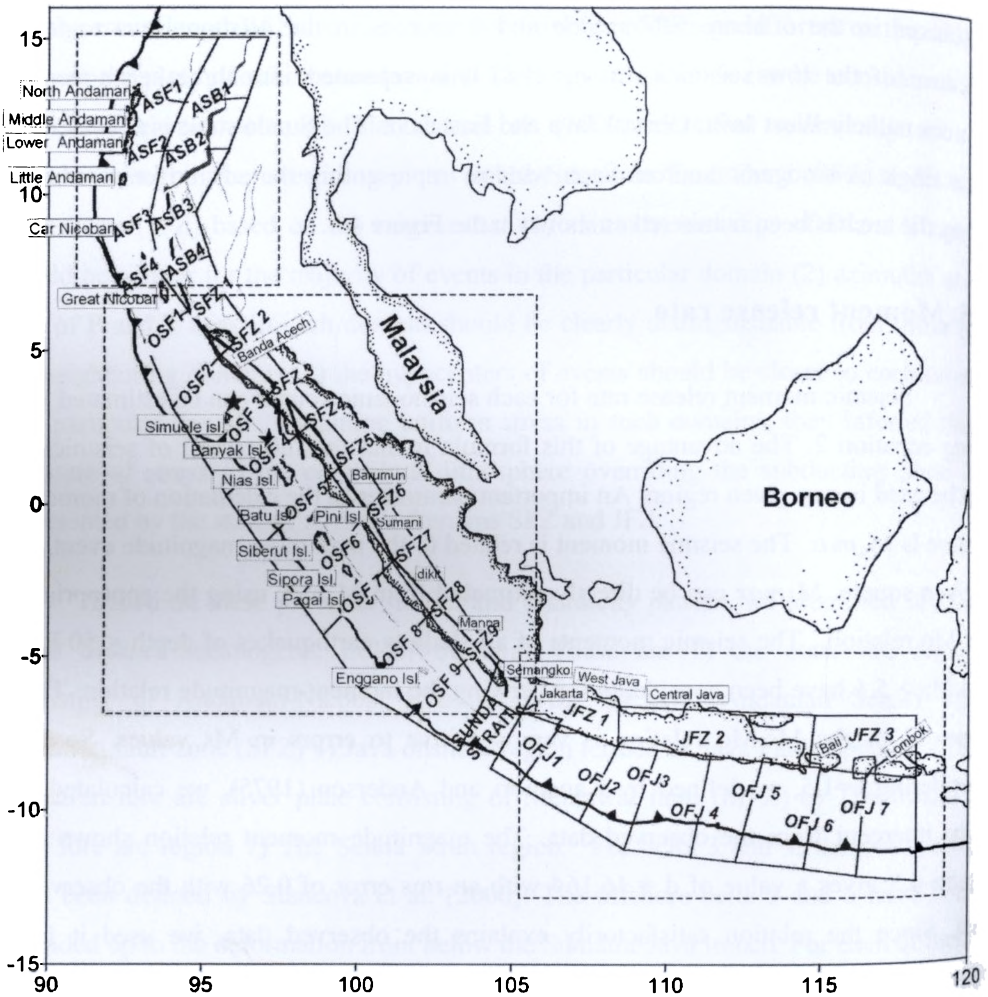

Figure 4.4. Map showing the moving window configuration of the seismogenic sources in the Andaman-Sumatra-Java trench- arc region. The rectangles 1–3 are: 1-Andaman arc; 2-Sumatra arc; 3-Java arc. The deformation results for each of these blocks are shown separately.

550 34
LAS

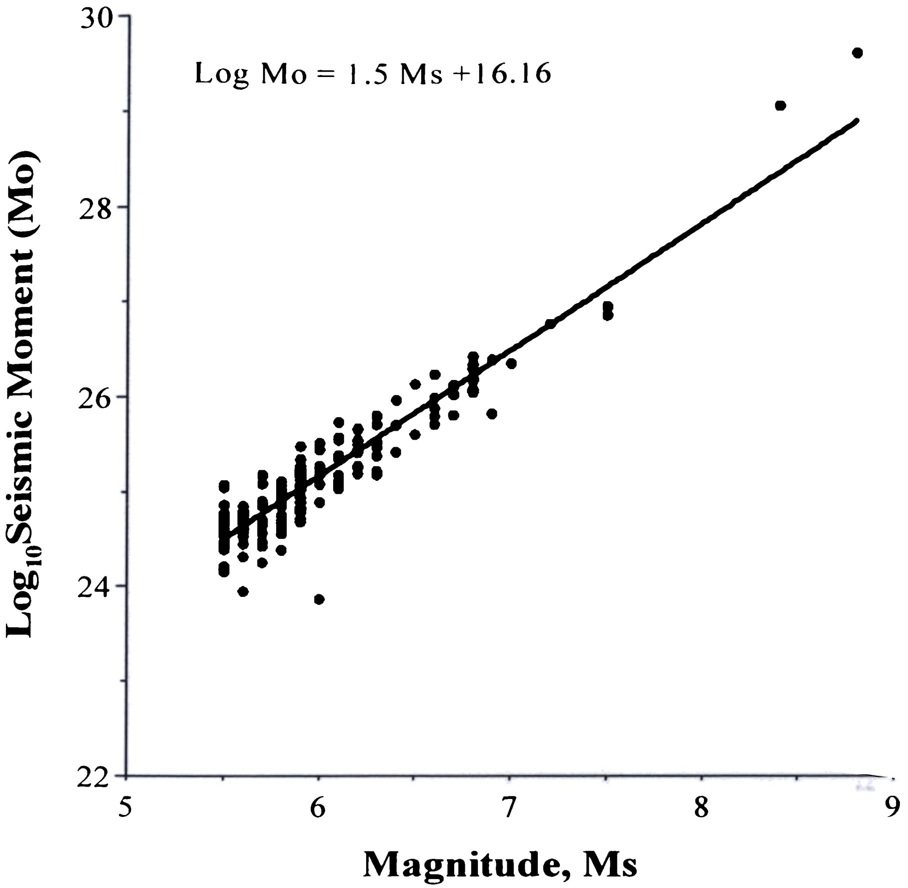

Figure 4.5. Plot of the logarithm of seismic moment (M_o) versus surface wave magnitude for large shallow earthquakes in the Andaman-Sumatra –Java trench- arc region.

The 'b' values in general, range between 0.50 - 1.0. In the Andaman back arc region, the $\dot{M}$ values are lower due to lack of large magnitude earthquakes. But in the fore arc of Andaman, higher values of moment rate have been observed in the northern part when compared to the southern part. Along the SFZ, the moment release is high in the southern part compared to the north.In the offshore Sumatra, along the MFZ the moment release rate is high towards south. In the JFZ region, the moment release rate is very low. Along the offshore Java, the moment release in general increases towards west with westernmost two sources showing several orders higher.

4.6. Crustal deformation Rates (1900 – 2004)

The velocity tensor for each seismogenic source can be calculated from equations (1) and (2). While magnitudes of velocities are controlled by errors in $\dot{M}$, their directions are mainly influenced by errors in $\overline{F}$. The uncertainties in the magnitude of observed velocities for each source are estimated through errors in $\dot{M}$ using Monte-Carlo simulation method. The errors in $\dot{M}$ are contributed from errors in **a**, **b**, **c**, **d** and Ms_{max}. For this purpose, the standard errors in **a** and **b** values are utilized. A value of 0.35 is assigned to the standard error in Ms_{max}. The error in c value is 0.05 and the rms error of 0.33 in the fit of Ms-Mo relation is assigned to the standard error in 'd' (Papazachos and Kiratzi, 1992).

Table 4.4-Table 4.6 shows the components of velocity tensor and the eigen system of velocity tensor with errors in eigen values for each of the seismogenic sources (window) in each region. The value of l_3, i.e., the depth extent of the seismogenic layer was taken to be 30 km for all zones of shallow seismicity. Positive or negative plunge means that the eigen vector is directed into or out of the solid earth.

Table 4.1. a, b and Mo values calculated for Andaman fore arc and back arc region

Source No.	*L1* (Km)	*L2* (Km)	t	M_{min}	Azimuth (° N)	a	b	Total No. of Events	Ms_{Max}	Mo x 10^{24} dyne cm/yr
ASF1	439.1	237.0	1941	5.8	22	2.32 $\pm$0.097	0.52 $\pm$0.038	120	8.7	1566.30
			1964	4.5						
ASF2	450.3	216.0	1915	6.0	11	2.82 $\pm$0.102	0.61 $\pm$0.04	157	8.7	898.88
			1931	5.5						
			1966	4.5						
ASF3	466.0	165.0	1915	6.0	177	3.13 $\pm$0.094	0.71 $\pm$0.039	86	6.8	8.79
			1931	5.5						
			1966	4.5						
ASF4	388.5	151.0	1935	5.6	157	2.07 $\pm$0.087	0.53 $\pm$0.035	38	7.3	31.94
			1964	4.5						
ASB1	431.9	214.7	1922	6.0	22	5.25 $\pm$0.072	1.08 $\pm$0.03	155	6.7	6.04
			1971	4.5						
ASB2	413.6	216.0	1922	6.2	20	6.37 $\pm$0.19	1.32 $\pm$0.08	301	6.3	3.88
			1964	4.5						
ASB3	413.0	165.0	1932	5.6	5	5.05 $\pm$0.078	1.03 $\pm$0.033	297	6.3	4.78
			1965	4.5						
ASB4	334.0	184.0	1939	5.6	154	4.33 $\pm$0.062	0.88 $\pm$0.026	238	6.3	6.08
			1964	4.5						

Table 4.2. a, b and Mo values calculated for **SFZ and** offshore Sumatra region

Source No.	L1 (Km)	L2 (Km)	t	M_{min}	Azimuth (° N)	a		b		Total no of Events	$Ms_{,max}$	Mo X10^{24} dyne cm/yr
SFZ1	300.0	143.0	1956 1966	5.8 4.5	149	4.09	±0.055	0.86	±0.023	135	6.3	4.53
SFZ2	362.0	139.0	1935 1963	6.8 4.5	141	3.05	±0.079	0.68	±0.032	76	7	16.50
SFZ3	430.2	104.2	1928 1963	6.0 4.5	140	2.91	±0.075	0.63	±0.03	44	7.2	37.50
SFZ4	367.8	105.3	1928 1965	6.0 4.5	140	2.55	±0.068	0.6	±0.027	27	7.2	26.10
SFZ5	361.8	109.7	1965	4.5	146	1.96	±0.077	0.54	±0.032	16	6.6	4.51
SFZ6	381.8	124.5	1943 1977	7.4 4.5	146	0.83	±0.097	0.33	±0.036	8	7.6	98.60
SFZ7	432.0	118.6	1909 1972	6.8 4.5	145	1.02	±0.101	0.36	±0.036	12	7.7	119.45
SFZ8	451.4	118.3	1909 1966	6.2 4.5	145	2.27	±0.132	0.56	±0.052	33	7.7	74.29

Table 4.2 continued

SFZ9	*327.2*	*123.6*	*1933* *1956* *1965*	*6.2* *5.0* *4.5*	*145*	3.33 ±0.079	0.71 ±0.032	76	7.5	49.37
OSF1	365.9	186.6	1929 1964	5.6 4.5	151	2.53 ±0.057	0.59 ±0.023	45	7.3	35.8
OSF2	435.5	278.1	1929 1964	5.6 4.5	148	3.93 ±0.054	0.77 ±0.021	156	7.5	76.20
OSF3	411.6	322.0	1931 1964	5.6 4.5	146	3.85 ±0.058	0.75 ±0.023	161	7.7	123.00
OSF4	373.8	341.4	1921 1963	5.5 4.5	146	2.95 ±0.051	0.62 ±0.02	99	8.1	298.00
OSF5	413.0	351.5	1921 1963	5.5 4.5	146	3.04 ±0.048	0.62 ±0.019	116	8.1	366.00
OSF6	383.9	355.5	1918 1965	5.6 4.5	145	3.48 ±0.036	0.68 ±0.014	127	8.1	353.00
OSF7	401.0	357.0	1918 1965	5.6 4.5	145	4.56 ±0.093	0.88 ±0.038	145	7	28.00
OSF8	437.8	346.2	1926 1964	5.6 4.5	140	4.46 ±0.042	0.79 ±0.016	368	7.9	361.00
OSF9	369.2	279.6	1931 1956 1964	5.9 5.2 4.5	130	4.62 ±0.036	0.82 ±0.014	392	7.9	316.00

Table 4.3. a, b and Mo values calculated for Sunda strait , Java and offshore Java region

Source No.	L1 (Km)	L2 (Km)	t	M_{min}	Azimuth (° N)	a	b	Total no of Events	$Ms_{,max}$	Mo X10^{24} dyne cm/yr
S.ST.	147.7	140.3	1933	7.0	117	3.34 $\pm$0.076	0.7 $\pm$0.03	92	7.5	59.84
			1954	5.5						
			1965	4.5						
JFZ1	320.2	114.7	1927	6.2	110	2.69 $\pm$0.079	0.66 $\pm$0.032	30	7.1	11.744
			1963	4.5						
JFZ2	694.2	174.2	1929	5.6	95	3.05 $\pm$0.162	0.81 $\pm$0.07	11	6.2	0.68
			1967	4.5						
JFZ3	367.4	241.1	1930	5.6	94	4.39 $\pm$0.067	0.93 $\pm$0.028	60	6.75	6.63
			1963	4.5						
OFJ1	412.5	269.3	1903	8.1	117	3.35 $\pm$0.137	0.7 $\pm$0.055	93	8.1	185.00
			1933	5.6						
			1964	4.5						

Table 4.3 contd.........

OFJ2	394.5	318.4	1903	8.1	115	3.44 $\pm$0.071	0.7 $\pm$0.028	104	8.1	228.00
			1933	5.6						
			1964	4.5						
OFJ3	376.1	335.4	1937	5.9	105	3.86 $\pm$0.057	0.79 $\pm$0.023	81	7.2	28.90
			1966	4.5						
OFJ4	374.9	369.5	1921	7.5	98	3.82 $\pm$0.085	0.78 $\pm$0.034	93	7.5	50.40
			1937	5.6						
			1967	4.5						
OFJ5	394.9	347.2	1921	7.5	96	4.66 $\pm$0.107	0.9 $\pm$0.043	245	7.5	52.70
			1939	5.5						
			1965	4.5						
OFJ6	398.6	364.2	1925	6.0	96	5.46 $\pm$0.112	1.05 $\pm$0.046	231	7.1	22.00
			1965	4.5						
OFJ7	372.1	372.2	1925	5.6	140	6.89 $\pm$0.157	1.34 $\pm$0.066	218	6.8	13.10
			1965	4.5						

The deformation pattern obtained for each seismogenic source (window) is presented diagrammatically in Figure 4.6-Figure 4.8. For a better understanding of the horizontal plate velocities, only those eigen vectors with a plunge less than 25° are shown in this figure. The deformation velocities pertaining to each seismogenic belt are discussed below.

4.6.1. Andaman Fore arc (ASF1- ASF4)

The focal mechanisms of earthquakes occurring in the Andaman fore arc sedimentary complex region suggest dominantly thrust faulting events along low angle nodal planes.

For sources ASF1 and ASF2, the compressional deformation takes place along a mean direction of N 70^0 and the extensional deformation along N 340°. The eigen system of velocity tensor suggests an average compression of 165.43 ± 21.09 mm/yr and an extension of 67.53 ± 8.61 mm/yr for ASF1. For Source ASF2, there is predominantly compression of 55.8 ± 6.74 mm/yr and extension is 13.23 ± 1.59. The values show that there is a higher compression rate in the Andaman fore arc region in the north. For source ASF3, the velocity deformation shows a compression of 0.321 ± 0.03 mm/yr in the N 317° direction. For source ASF4, the compressional deformation is 2.15 ± 0.26 mm/yr along N 16°.

4.6.2. Andaman back arc (ASB1-ASB4)

The active back-arc spreading region in the Andaman Sea is highly conspicuous from the occurrence of large number of shallow focus earthquakes with focal mechanisms indicating normal faulting along NNE striking nodal planes. Also, few strike-slip events with right lateral slip correlate with the short transform segments that offset the spreading ridge.

Table 4.4. Components of velocity tensor and eigen system of velocity tensor for Andaman Fore arc and Back arc.

	Elements of velocity tensor U (mm/yr).						**Eigen System of velocity tensor (mm/yr.)**								
	U_{11}	U_{12}	U_{13}	U_{22}	U_{23}	U_{33}	λ_1	Az°	Pl°	λ_2	Az°	Pl°	λ_3	Az°	Pl°
ASF1	40.287	-73.64	-7.666	-139.022	-0.34	10.4	67.536±8.61	340.4	-7.1	-165.436±21.09	70.3	0.9	9.564±1.22	332.7	82.8
ASF2	5.353	-21.424	-3.017	-47.901	-3.89	5.576	13.231±1.59	341.4	-12	-55.806±6.74	70.5	4.4	5.603±0.67	320.8	77.3
ASF3	-0.188	0.139	0.009	-0.142	-0.1	0.036	-0.321±0.03	316.8	-11.8	-0.064±0.007	40	29.7	0.092±0.01	246	57.6
ASF4	-1.881	-0.55	0.416	0.399	0.697	0.156	-2.151±0.26	16.1	-14.4	0.994±0.12	94.4	38.4	-0.169±0.02	302.7	48
ASB1	0.237	-0.582	0.01	-0.091	0.02	-0.035	0.677±0.054	322.9	-0.3	-0.532±0.042	52.9	-2.5	-0.034±0.0	45.9	87.5
ASB2	0.285	-0.262	-0.015	-0.024	0.008	-0.031	0.435±0.048	330.3	-2.1	-0.174±0.019	60.3	0.2	-0.031±0.0	325.5	87.9
ASB3	0.167	-0.512	-0.033	0.075	0.001	-0.036	0.636±0.053	317.6	-2.2	-0.394±0.033	47.5	3.4	-0.035±0.0	259.9	86
ASB4	-0.872	-0.946	0.007	0.95	-0.01	0.004	-1.274±0.11	23	-0.1	1.352±0.125	113	-0.5	0.004±0	100.5	89.5

Table 4.5. Components of velocity tensor and eigen system of velocity tensors along Sumatran Fault zone and offshore Sumatra

	Elements of velocity tensor U (mm/yr).						**Eigen System of Velocity tensor (mm/yr.)**								
	U_{11}	U_{12}	U_{13}	U_{22}	U_{23}	U_{33}	λ_1	Az°	Pl°	λ_2	Az°	Pl°	λ_3	Az°	Pl°
SFZ1	-0.856	-0.576	-0.005	0.865	-0.016	0.01	-1.031±0.097	16.9	0.5	1.04±0.098	106.9	-0.7	0.01±0.001	141.1	89.1
SFZ2	-3.864	1.176	-0.222	1.658	-0.052	0.1	-4.114±0.453	348.5	2.8	1.903±0.209	78.4	-3	0.105±0.012	121.2	85.9
SFZ3	-7.447	1.643	-0.169	3.02	-0.166	0.24	-7.701±0.879	351.3	1	3.284±0.375	81.2	-3.6	0.231±0.026	97.3	86.3
SFZ4	-3.64	-2.275	0.303	4.898	-0.089	0.074	-4.225±0.491	14	-3.6	5.471±0.636	104.1	-1.7	0.087±0.01	39.1	86
SFZ5	-1.29	-0.4	0.054	1.171	-0.037	0.004	-1.355±0.165	9	-2	1.236±0.151	99	-2.1	0.004±0	55.5	87.1
SFZ6	-23.875	-6.896	-0.505	15.963	-0.671	1.091	-25.049±3.588	9.6	1.3	17.144±2.455	99.5	-2.1	1.084±0.155	132.4	87.5
SFZ7	-16.909	-1.846	0.078	8.269	-0.849	0.921	-28.844±4.063	4.2	-0.1	14.384±2.026	94.2	-6.4	1.396±0.197	93.7	83.6
SFZ8	-1.244	-0.131	0.117	0.532	0.043	0.08	-14.052±1.859	4.3	-5.1	6.047±0.8	93.9	4.3	0.981±0.13	324.2	83.4
SFZ9	-2.486	-1.497	0.493	1.927	0.191	0.192	-9.746±1.051	17	-9.3	7.668±0.827	106.9	1	0.887±0.096	10.9	80.7

Table 4.5 contd ....

OSF1	-2.553	-1.116	0.281	1.531	0.241	0.113	-2.875±0.33	14.6	-6.3	1.832±0.21	103.9	5.5	0.134±0.016	333.2	81.6
OSF2	-5.206	-0.115	0.39	1.861	0.414	0.239	-5.237±0.53	1.2	-4.2	1.96±0.199	90.2	13.5	0.17±0.017	287.9	75.9
OSF3	-6.94	-1.422	0.686	1.889	0.784	0.413	-7.247±0.75	9.4	-6	2.351±0.24	97.2	19.6	0.258±0.027	295.6	69.4
OSF4	-11.889	-11.52	3.799	-6.788	3.794	1.644	-22.323±2.55	39.1	-12.6	2.048±0.23	138	-34.8	3.242±0.371	112.3	52.4
OSF5	-8.361	-8.603	3.492	-8.136	3.926	1.404	-18.251±2.08	44.9	-14.9	0.312±0.036	136.8	-7.2	2.846±0.325	71.8	73.3
OSF6	-12.494	-8.397	4.34	-0.89	3.704	1.125	-18.484±2.01	28.6	-15.9	4.395±0.479	107.4	34.4	1.829±0.199	319.3	51.1
OSF7	-1.992	-1.165	0.392	0.413	0.255	0.132	-2.542±0.24	22.3	-9.7	0.896±0.086	111	7.3	0.199±0.019	344.9	77.8
OSF8	-22.553	-6.819	3.79	4.03	2.561	1.517	-24.897±2.48	14.1	-9.2	6.291±0.63	100.5	21	1.601±0.16	306.5	66.9
OSF9	-20.055	-6.409	4.601	2.432	2.887	1.876	-22.845±2.22	15.6	-11.9	5.232±0.51	97.4	34.1	1.867±0.182	302	53.3

Table 4.6. Components of velocity tensor and eigen system of velocity tensor for Sunda strait, onland Java and offshore Java.

	Elements of velocity tensor U (mm/yr).						Eigen System of Velocity tensor (mm/yr.)								
	U_{11}	U_{12}	U_{13}	U_{22}	U_{23}	U_{33}	λ_1	Az°	Pl°	λ_2	Az°	Pl°	λ_3	Az°	Pl°
S.ST	-14.011	-1.19	3.561	7.775	0.817	1.38	-14.874±1.619	3.5	-12.5	7.905±0.86	92.1	6	2.113±0.23	337.1	76.1
JFZ1	-0.892	-0.906	0.33	0.581	0.101	0.248	-1.394±0.156	25.2	-11.8	1.016±0.114	116	-4	0.315±0.035	44.7	77.6
JFZ2	-0.008	-0.037	-0.012	-0.087	-0.001	0.006	0.017±0.002	341	-44.8	-0.102±0.013	68.2	2.8	-0.004±0.001	335.4	45
JFZ3	-0.419	0.023	-0.078	0.012	0.011	0.051	-0.433±0.039	356.8	9.2	0.012±0.001	85.6	-7.7	0.065±0.006	136.2	78
OFJ1	-13.941	2.316	1.902	4.062	0.161	1.042	-14.459±1.82	352.9	-6.9	4.405±0.55	82.1	7.1	1.217±0.153	306.4	80.1
OFJ2	-16.448	3.106	2.298	0.676	0.604	1.399	-17.245±1.88	350.4	-6.6	0.427±0.046	85.7	-38.5	2.445±0.266	72.2	50.7
OFJ3	-2.057	0.004	0.345	0.102	0.038	0.174	-2.109±0.21	0	-8.6	0.091±0.009	92.5	-15.6	0.237±0.024	62.1	72.1
OFJ4	-2.796	-0.952	0.447	0.258	-0.1	0.207	-3.118±0.32	15.6	-6.9	0.65±0.067	109.4	-28.6	0.136±0.014	93.2	60.4
OFJ5	2.077	-1.357	0.338	0.247	0.01	-0.195	2.827±0.28	332.3	5.6	-0.558±0.055	59.5	-26.4	-0.14±0.014	73.3	62.9
OFJ6	1.589	-0.646	0.079	-0.162	0.013	-0.118	1.804±0.16	341.8	2.1	-0.38±0.034	71.5	-8.2	-0.115±0.01	86.2	81.5
OFJ7	0.15	-0.39	0.026	0.326	-0.006	-0.038	-0.164±0.01	38.4	-7.5	0.638±0.058	128.7	-1.8	-0.037±0.003	51.9	82.3

For sources ASB1, the compressional deformation takes place along a direction of N 53^0 and the extensional deformation along N 323°. The eigen system of velocity tensor suggests an average compression of 0.53 ± 0.04 mm/yr and an extension of 0.677 ± 0.05 mm/yr for source ASB1. For Source ASB2, there is compression of 0.174 ± 0.019 mm/yr in the N 60° direction and an extension of 0.435 ± 0.05 mm/yr in the N 330° direction. For source ASB3, the velocity deformation shows a compression of 0.394 ± 0.033 mm/yr in the N 47° direction and an extension of 0.636 ± 0.053 mm/yr in the N 317° direction. For source ASB4, the compressional deformation is 1.274 ± 0.118 mm/yr along N 23° and an extension of 1.352 ± 0.125 along N 113°.

The deformation rate of the Andaman fore arc and back arc is shown in Figure 4.6.

4.6.3. Sumatran Fault Zone (SFZ1-SFZ 9)

Most of the focal mechanism solutions along the SFZ show pure right lateral strike-slip faulting, which agrees well with the geological observations. All along its length, the deformation velocities suggest N-S compression and E-W extension. In the northwestern part of the Sumatran fault, north of Sumatran main land (source SFZ1 in the figure) shows a compression of 1.03 ± 0.09 mm/yr. along N16.9° and an extension of 1.04 ± 0.098 mm/yr along N107°.

In the onshore Sumatra region, the deformation rate increases to 4.11 ± 0.45 mm/yr (compression) and 1.9 ± 0.21mm/yr (extension) in SFZ2. For source SFZ3, the deformation further increases to a compression rate of 7.7 ± 0.88 mm/yr and extension rate of 3.28 ± 0.37 mm/yr. Batee fault start from this Batee fault start from this region and continue into the offshore. For both the sources SFZ2 and SFZ3, the compressional deformation and extensional deformation takes place along

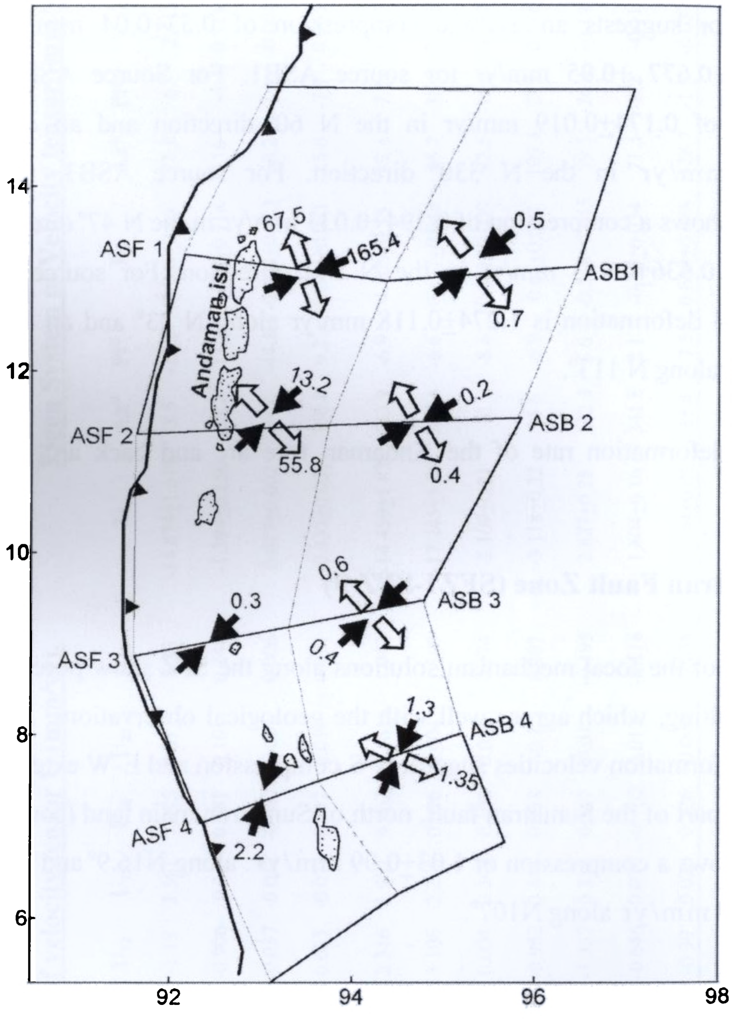

Figure 4.6. Distribution of deformation velocities (centered on each source) calculated for the overlapping seismogenic sources in the Andaman fore arc (ASF1-4) and back arc (ASB1-4) region.

a mean direction N349° and N80° respectively. The deformation velocities for source SFZ4 suggest compression of 4.22±0.49 mm/ yr along a direction of N14° and extension of 5.47±0.64 mm/yr in the N104° direction. The eigen system of velocity tensor suggest that for sources SFZ5 and SFZ6, the compressional deformation takes place along a mean direction of N9° and the extensional deformation along N99°. The velocities show a compression of 1.35±0.16 mm/yr and the extension of 1.23±0.15 mm/yr for source SFZ5. The deformation rate drastically increases further in sources SFZ6 and SFZ7 which show the compression of 25.05±3.59 mm/yr and the extension of 17.14±2.45 mm/yr in source SFZ6. For sources SFZ7 and SFZ8, the compressional deformation takes place along a mean direction of N4° and the extensional deformation along N94°. The compression is 28.84±4.06 mm/yr and extension of 14.38±2.03 mm/yr in source SFZ7. Further south, the deformation rate decreases to compression of 14.05±1.86 mm/yr and extension of 6.05±0.8 mm/yr for source SFZ8 and compression of 9.75±1.05 mm/yr (along N17°) and an extension of 7.67±0.83 mm/yr (along N 107°) for source SFZ9.

4.6.4. Sumatran Fore arc (OSF1-OSF9)

The Sumatran fore arc region constitutes Mentawai islands and Mentawai fault zone (MFZ). The majority of strong earthquakes in both historic and instrumental catalogs of Sunda arc locate in this region. A close examination of the deformation pattern shows that compressive stresses dominate here. The focal mechanism solutions show mainly thrust faulting events.

The eigen system of velocity tensor suggests a compression of 2.88± 0.33 mm/yr along N 15° and an extension of 1.832±0.21 mm/yr along N 104° for source OSF1. For source OSF2, the focal mechanism solutions show both strike-slip and thrust faulting. Deformation velocities suggest a compression of 5.24±0.53 mm/yr along N 1.2° and an extension of 1.96 ±0.2mm/yr along N 90°. Both strike-slip and thrust faulting events are seen in the source OSF3 with deformation suggesting dominantly compression of 7.25±0.75 mm/yr along N 9° and extension of 2.35±0.24 mm/yr along N 97°. The area of the sources OSF4, OSF5 and OSF6 seems to be very active. For source OSF4, dominantly thrust faulting events give rise to compressional deformation of 22.32±2.55 mm/yr along N 39°. Source OSF5 shows dominantly compression with compression velocity of 18.25± 2.08 mm/yr along N 45° and an extension of 0.312 ±0.036 mm/yr along N 317°. In source OSF6, the deformation velocities suggest compression of 18.48± 2.01 mm/yr along N 28°. Further south, the deformation velocities are low with compression velocities of 2.54± 0.24 mm/yr along N 22° and extensional velocities of 0.896± 0.086 mm/yr along N 111° in source OSF7. In source OSF8, the compression velocities are of 24.897± 2.48 mm/yr along N 14° and extensional velocities 6.29± 0.63 mm/yr along N 100°. The source OSF9 suggests a compression of 22.84± 2.22 along N 15°.

The deformation rate in the SFZ and Sumatra fore arc is shown in Figure 4.7.

4.6.5. Sunda Strait

The Sunda strait is a consequence of the northwestward motion of the southwestern part of the Sumatran block along the Central Sumatran fault. The extension zone widens southwestward and changes into a composite zone of strike slip as well as normal faulting (Huchon and Le Pichon, 1984). They further observed that the area is subjected to NW-SE extension because of the motion along Sumatran Fault and to NE-SW compression because of the subduction. It is comparatively a quiet zone with a cluster of moderate and large earthquakes immediately adjacent to the west coast of Java. Some studies indicate southward extension of SFZ in the

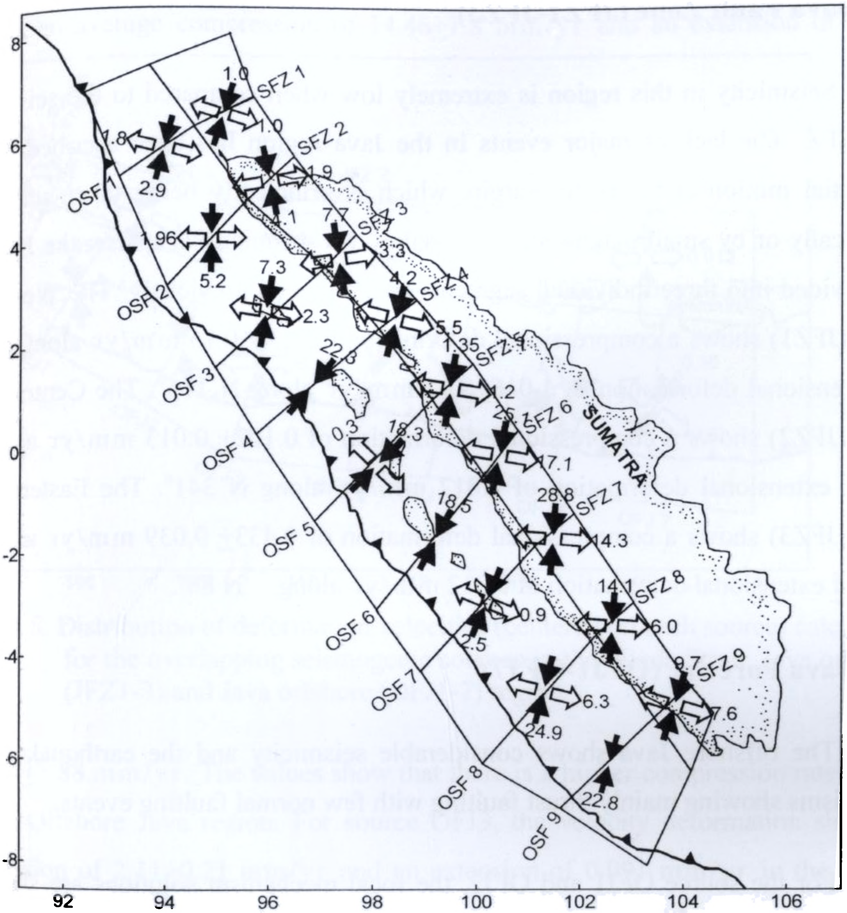

Figure 4.7. Distribution of deformation velocities (centered on each source) calculated for the overlapping seismogenic sources in the SFZ and Off Sumatra region (OSF).

Sunda Strait (Sieh and Natawidjaja, 2000; Pramumijoyo and Sebrier, 1991). The region shows a compressional deformation of 14.87$\pm$ 1.62 mm/yr along North 3.5° direction and extensional deformation of 7.9$\pm$ 0.86 mm/yr along N 92°.

4.6.6. Java Fault Zone (JFZ1-JFZ3)

Seismicity in this region is extremely low when compared to the seismicity along SFZ. The lack of major events in the Java region has been ascribed to the differential motion at the plate margin, which is principally being taken up either aseismically or by small magnitude earthquakes. As seismicity is sparse, the JFZ has been divided into three individual segments as mentioned previously. The West Java region (JFZ1) shows a compressional deformation of 1.39$\pm$0.15 mm/yr along N 25° and extensional deformation of 1.016$\pm$0.11 mm/yr along N 116°. The Central Java region (JFZ2) shows a compressional deformation of 0.102$\pm$ 0.013 mm/yr along N 68° and extensional deformation of 0.017 mm/yr along N 341°. The Eastern Java region (JFZ3) shows a compressional deformation of 0.433$\pm$ 0.039 mm/yr along N 357° and extensional deformation of 0.012 mm/yr along N 86°.

4.6.7. Java Fore arc (OFJ1-OFJ7)

The offshore Java shows considerable seismicity and the earthquake focal mechanisms showing mainly thrust faulting with few normal faulting events.

For the source OFJ1 and OFJ2, the focal mechanism solutions are showing mainly thrust faulting and some strike-slip events. The strike slip events may be accounting for the presence of Cimanderi fault in the Western Java. For sources OFJ1 and OFJ2, the compressional deformation takes place along a mean direction of N 351° and the extensional deformation along N 84°. The eigen system of velocity tensor $\pm$0.55 mm/yr for source OFJ1. For Source OFJ2, there is predominantly compression suggests an average compression of 14.46±1.8 mm/yr and an extension of 4.405

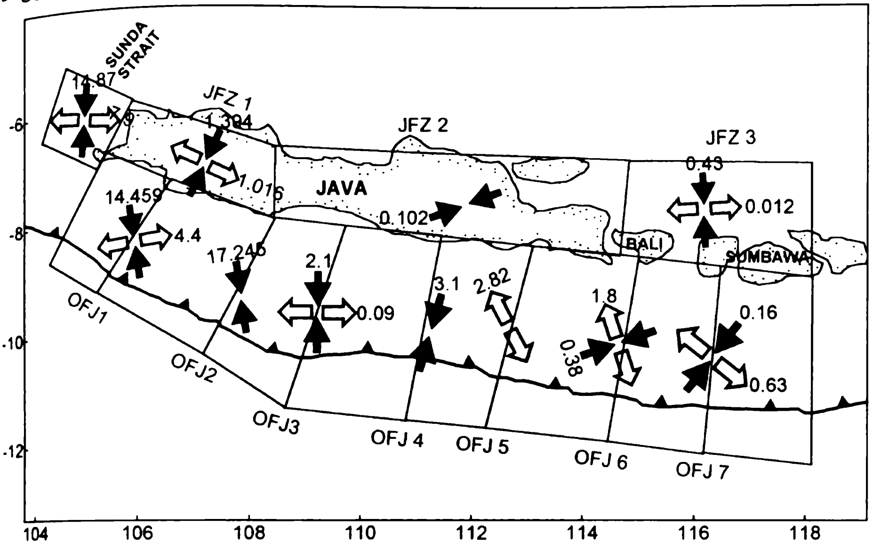

Figure 4.8. Distribution of deformation velocities (centered on each source) calculated for the overlapping seismogenic sources in the Sunda Strait, Java onshore (JFZ1-3) and Java offshore (OFJ1-7) region.

of 17.24±1.88 mm/yr. The values show that there is a higher compression rate in the western Offshore Java region. For source OFJ3, the velocity deformation shows a compression of 2.11±0.21 mm/yr and an extension of 0.091 mm/yr in the N 92° direction. For source OFJ4, the compressional deformation is 3.12±0.32 mm/yr along N 15°. The sources OFJ5 and OFJ6 are dominant in normal faulting. The velocity deformation shows an extension of 2.827±0.28 in the N 332° direction for source OFJ5 and for source OFJ6, the velocity deformation shows a compression of 0.38±0.034 mm/yr in the N 71° direction and an extension of 1.804 ±0.16 along N 342°. For source OFJ7, the compressional deformation is 0.164±0.01 mm/yr along N 38° and extensional deformation is 0.638 ±0.058 mm/yr. along N 129°.

The deformation rates in the Sunda strait, onshore and offshore Java region is as shown in Figure 4.8.

4.7. Discussion and conclusions

Estimation of the moment release pattern and crustal deformation rates based on 104 years of shallow seismicity in comparison with the previous studies bring out some significant results for the Andaman-Sumatra-Java arc region.

The results of the deformation studies in the Andaman – Sumatra – Java arc region are consistent with the overall tectonics of the region. The deformation pattern indicates the dominance of compressive stresses in the fore arc region with the direction of maximum compression in almost NNE – SSW. While, it is almost normal to the trench in the Sumatran fore arc near Nias island region, the compression takes more oblique trend with respect to the trench towards north near Andaman Islands. Biswas et al. (1992) infer N-S shear stresses due to oblique subduction in the Andaman arc region. The compressional velocities decrease northward in the fore arc region characterized by deficiency of moment release and absence of large magnitude earthquakes north of 8°N. Geophysical data indicate that the Ninetyeast ridge partially subducts below the Andaman trench (Curray et al., 1982; Mukhopadhyay, 1988; Mukhopadhayay and Krishna, 1995; Gopala Rao et al., 1997). Further, Dasgupta and Mukhopadhyay (1993) observed a contorted Benioff zone east of the Nicobar Islands and inferred as due to the effect of ridge subduction. Such characteristic changes in the seismicity pattern have been interpreted as due to subduction of aseismic ridges (Vogt, 1973; Kelleher and McCann, 1976; Chung and Kanamori, 1978). The deformation studies shows a compression of 0.2-0.5 mm/ yr along a mean direction of N 55° and extension of 0.4-0.7 mm/yr along a mean direction of N 320° along and across the Andaman spreading ridge. The events along the back arc spreading region also include an earthquake swarm of July 8, 1984 with most of the mechanisms reported by Dziewonski et al. (1983) showing dominantly normal faulting. Such a faulting pattern for swarms along the slow-spreading ridges indicates extensional tectonic activity (Bergman and Solomon, 1990; Radha Krishna and Arora, 1998). The vertical component of velocities indicates crustal thinning in the Andaman Sea and crustal thickening all along the fore arc.

Subduction of large bathymetric ridge causes compression in the upper plate (Whittaker et al, 2007). At 70 Ma, the Wharton Ridge first subducts beneath eastern Java (Heine et al., 2004), which caused the Sunda land margin to rotate clockwise about a rotation pole close to the area at this time. At present, the Wharton Ridge and Investigator Fracture Zone IFZ subduct beneath northern–central Sumatra. It is a well known fact that the subduction of bathymetric features cause broadly distributed deformation in the fore arc (Gardner et al, 1992; Chung and Kanamori, 1978). Geodetic strain and rotation rates show that the northern Sumatran region currently endures a highly compressive regime (Michel at al, 2001).

Due to oblique subduction and extension in the north, Sumatra, and the Sumatran fore arc, is divided into a series of NW–SE striking slices that move towards the northwest, separated by right-lateral faults (Diament et al., 1992). Most displacement on these faults occurs in northwest Sumatra and dissipates towards the southeast (McCaffery, 1996). Geodetic observations from GPS data (Prawirodirdjo et al., 1997) reveal an interesting change in Sumatran fore arc motion centered around Batu Island. Southeast of Batu Island, the Sumatra fore arc moves northeast, roughly parallel with the motion of the Indian plate, while northwest of Batu Island the Sumatran fore arc moves to the northwest (Prawirodirdjo et al., 1997). This change in fore arc motion has been attributed to decoupling between the northern fore arc and mantle wedge due to increased pore pressures in the fore arc thrust fault due to subduction of thick Nicobar fan sediments (Prawirodirdjo et al., 1997). The Wharton

Ridge subducts beneath Nias Island where seismic deformation is highest and the IFZ subducts directly beneath Batu Island where the Sumatran fore arc begins to move in a northwest direction. Thus, subduction of the Wharton Ridge and IFZ is another mechanism causing the high seismic deformation rates, change in fore arc motion, and concentration of strike-slip motion that occurs in northern Sumatra. It is possible that present-day compression from subduction of the Wharton Ridge and Investigator Fracture Zone dominates over extension resulting from the retreating upper plate. It is likely that this domination of compressive strain related to bathymetric ridge subduction has dominated over upper plate motion related extension since 15 Ma. The Roo Rise is presently being subducting adjacent to Java. Subduction of this major bathymetric feature is currently causing deformation in the Javanese fore arc (Kopp et al., 2006). Roo Rise subduction is likely to be contributing to Javanese compression in addition to compression caused by upper plate advance since 15 Ma (Whittaker et al., 2007).

The slip rate along the SFZ should range between 30 and 50 mm/yr assuming that the fault is accommodating all the trench parallel component of convergence between Indo- Australian and Eurasian plates (Jarrard, 1986). Based on SPOT images and topographic maps, Bellier and Sebrier (1994) estimated slip rates along SFZ, which show a slip rate of about 23 mm/yr in the north that decreases to 6 mm/yr in the south. Combined analysis of historical triangulation and recent GPS measurements along SFZ indicate slip rates of 23 to 24 mm/yr (Prawirodirjo et al., 2000). There is a general northward increase in slip rate along the SFZ (Mc Caffrey, 1991; Bellier and Sebrier, 1995). It is suggested that no significant fore arc stretching occurs due to the slip rate variation along the SFZ and the oblique convergence may be accommodated by deformation of 500 km wide zone between the fore arc to the back- arc domains (Bellier and Sebrier, 1995). The estimated velocity values along the SFZ seismic belt indicate variation in seismically active deformation with maximum dextral shear motion (seismic slip) of 29 mm/yr in the central part to 1 and 8 mm/yr both southward and northward respectively along the SFZ. Except between 0°-2°S, the estimated velocities are significantly less than the geologically estimated slip rates as well as geodetically measured slip rates which suggest that considerable amount of slip along the fault may be taking up aseismically. The Sumatran fore arc perhaps is the most active deformation belt in the region characterized by the occurrence of large historical, recent and most recent seismic events. The arc parallel shear in the Sumatran fore arc may be taken up on more than one strike–slip fault or shear zone (Diament et al., 1992). However, McCaffrey et al (2000) observed that this additional strike-slip required may not be accommodated along the MFZ as GPS network along the northern part of MFZ do not indicate such large transverse motions. Samuel and Harbury (1996) interpreted the trace of the MFZ on the Nias Island to be a reverse fault. Also there is a significant component of dip slip in Pliocene along MFZ (Sieh and Natawidjaja, 2000). The focal mechanism solutions obtained from Harvard CMT Catalogue since 1977 in this region and the large 1935 and 1984 events show thrust faulting mechanisms in the offshore Sumatra (Rivera et al, 2002). The deformation velocities estimated for the offshore Sumatra fore arc region indicate dominantly compression with higher compressional velocities of 22 mm/yr along N 40° near the equator. The deformation pattern further indicates that a portion of the motion is taken up by strike-slip or oblique slip, which means that the MFZ partly accommodates motion due to oblique subduction. The higher deformation velocities near equator may imply the effect of local interaction of the Investigator Fracture Zone. However, north of 3° N, the low deformation values in the offshore indicate lack of significant events during the period of study. The deformation velocities for the Sunda Strait show compression of 14.8±1.6 mm/yr along N-S and extension of 7.9±0.82 mm/yr along E-W direction. The eigen system of velocity tensor for the JFZ indicates dominance of compressional deformation. While western Java shows compression of

1.4±0.15 mm/yr along N 25° and extension of 1±0.11 mm/yr along N116° direction, the deformation in the central and eastern Java is negligible due to absence of large earthquakes within the upper plate. In the offshore Java fore arc region, the deformation velocities indicate dominance of compression (average 16 mm/yr) in the western part, which gradually changes to extension (average 2.5 mm/yr) towards eastern part. The deformation pattern further indicates that the Java segment of the arc is seismically less active than the Sumatran segment during the period of investigation.

CHAPTER 5

CHANGES IN THE LONG-ERM DEFORMATION PATTERN IN THE ANDAMAN-SUMATRA TRENCH-ARC REGION AFTER THE 26TH DECEMBER 2004 MEGATHRUST EARTHQUAKE

5.1. Introduction

On 26th December 2004, a subduction zone earthquake of magnitude Mw ~ 9.3 struck off the coast of northern Sumatra. The rupture propagated unilaterally to the north for over 1200 km to the Andaman Islands (Ishii et al., 2005). A second thrust event of Mw ~ 8.7 occurred on 28th March 2005, about 300 km to the east south east of the previous earthquake. These earthquakes occurred as a result of the subduction of Indo-Australian plate beneath Sumatra in an approximately NE direction at a rate of 60 mm/yr at an oblique angle to the Java trench. Oblique, but predominantly thrust motion occurs in the Andaman trench with a convergence rate of about 14 mm/yr (Figure 5.1). The width of the rupture zone of the 26 December 2004 event is approximately 100 km and maximum slip is approximately 20 m. The movement of the seafloor all along the rupture zone and the vertical uplift displaced a huge volume of water, which caused the tsunami. But the rupture of this event didn't progress further to the S-SE despite high rapid slip at the beginning of the rupture, which indicates that the rupture front hit a barrier in this direction that broke three months later on 28th March 2005 (Kruger et al., 2005).

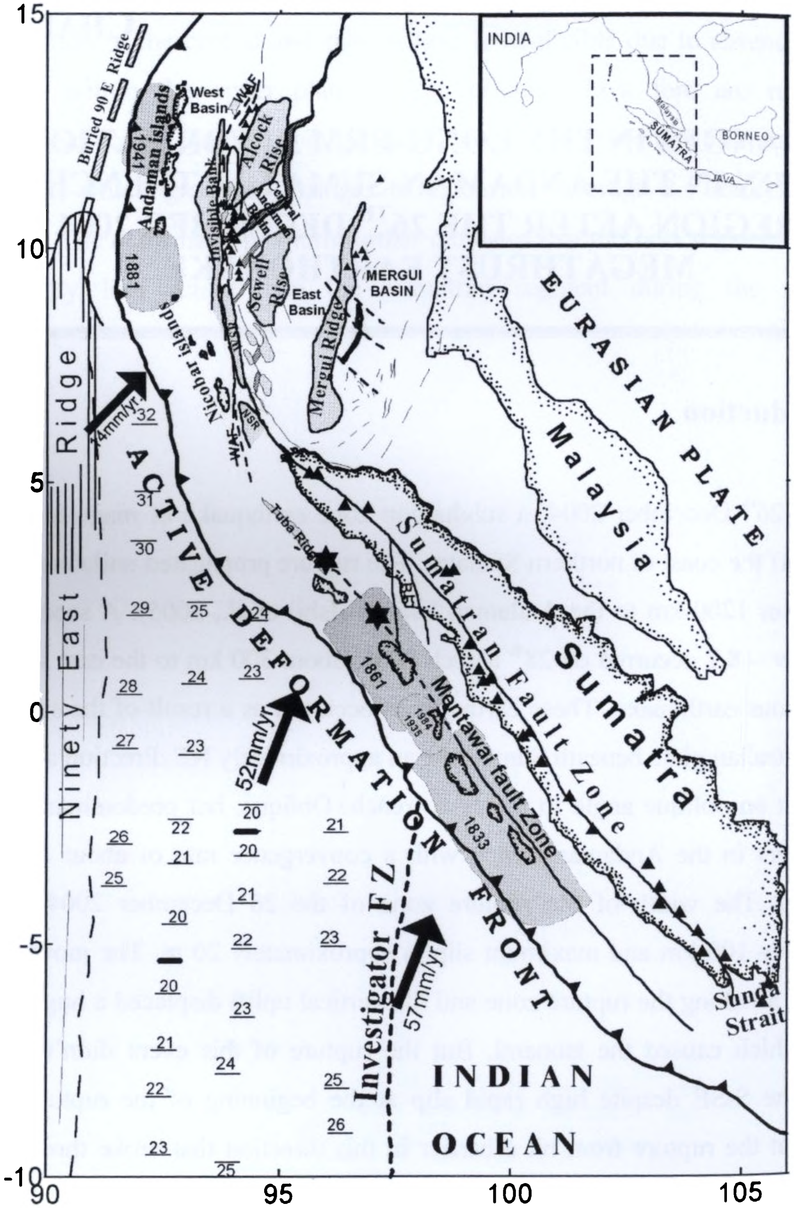

Figure5.1. Detailed tectonic map of Andaman-Sumatra arc and adjoining region

Historic great earthquakes along this plate boundary occurred in 1797 (~ 8.4), 1833 (~ 9), 1861 (~ 8.5) and1907 (~ 7.8). The 28th march 2005 event ruptured the same region as the 1861 and 1907 events. It is reported that the 1861 earthquake also did not cause a major tsunami, while the 1833 event caused a major tsunami (Gahalaut and Catherine, 2006). Nicobar Island in 1881 (~ 7.9) and near Andaman Islands in 1941 (~ 7.9) also presumed to involve thrusting motions (Lay et al., 2005). Bilham et al. (2005) observed that large thrust earthquakes in 1847 (~7.5), 1881 and 1941 occurred on intermediate regions of the down-dip boundary areas that have been surrounded and probably incorporated into the 2004 rupture. Numerous earthquakes occurred near the 2004 epicenter in recent years most notable among them is the Mw 7.2 event in 2002. Bilham et al. (2005) conclude that cross sections through the Andaman normal to the trend of the trench are consistent with the notion that the 100 km region on the upper surface of the descending Indian plate east of the trench axis was largely aseismic prior to the 2004 earthquake, and that the 1847, 1881, and 1941 earthquakes probably ruptured less than one third of the width of the plate boundary that slipped in December 2004. The recurrence time of 1881 type events is estimated to be 114-200 years on the basis of GPS convergence rates (Ortiz and Bilham, 2003). All these observations are consistent with long term strain accumulation in the eventual rupture zone and stress concentration in the vicinity of the main shock hypocenter.

Based on probabilistic hazard analysis using peak ground accelerations, Petersen et al. (2004) concluded that the largest contribution to hazard is from the Sumatran fault. Gahalaut and Catherine (2006) based on the GPS measurements undertaken between 1989 and 1994 in the region west of Sumatra suggested that the entire subduction interface under the islands experienced strain accumulation corresponding to a rate of 50 mm/yr. McCaffrey (2002) suggested that locking is strong everywhere in the subduction zone except in the equatorial region where the coupling is low. The region of low coupling coincided with the region where Investigator fracture zone subducts. The study of Mignan et al. (2006) based on accelerating moment release effect (AMR) also suggest that the 2004 December and 2005 March events showed clear evidence that they were approaching failure prior to the two events.

The velocity field obtained from GPS surveys shows abrupt rotation of the fore arc vector azimuths at about 0.5° S, near the Batu islands. South of 0.5° S, the fore arc vectors are roughly parallel to the convergence direction of the Indian Ocean and Eurasia. In the north, the vectors are more parallel to the Sumatra fault. This pattern suggests strong coupling of the fore arc to the subducted plate in the south and weaker coupling in the north. The change occurs where the Investigator fracture zone is subducting, but the coupling difference persists far from it, suggesting that the difference is due to properties of the interface rather than a mechanical barrier, as one might expect from a subducted ridge or seamount (Kelleher and McCann, 1976). Because, sites on the fore arc near 98° E, directly above IFZ show uncoupled behaviour, and the coupling difference persists far from the IFZ. Here, Prawirodirdjo et al. (1997) suggest that high fluid pore pressures due to sediment subduction cause weaker coupling in the north, although this observation alone is insufficient to explain this contrast in coupling. The great earthquakes (1833, 1861) as well as the smaller events (1907, 1908, 1914, and 1921) appeared not to cross the 0.5° S boundary. This suggest that asperities on the Sumatra subduction zone may remain stationary through more than one earthquake cycle instead of behaving dynamically as rate-dependent features of the fault zone.

These observations point towards the significance of understanding the long-term strain release pattern as well as the kinematics of interplate coupling in the shallow subduction zone for understanding future seismic hazard and potential in the region. In this chapter, a detailed analysis of changes in long-term seismic deformation (pre and post-tsunami) has been carried out along the Andaman-Sumatra arc mainly for two reasons, i) to study the changes that were brought out in the deformation due to intense post-tsunami seismic activity along various segments of the arc, ii) to update the long-term deformation pattern which will be useful to identify areas of increased future seismic hazard along and across the arc.

5.2. Data and Analysis

The region encountered a large number of earthquakes along the whole length of rupture zone following the mega thrust earthquake of 26th December 2004. The intense seismic activity continued more than a year. Here, all these events belonging to the period 2004-2005, (referred as post-tsunami) along with good number of focal mechanisms for some of these events during 2004-2005 were compiled and an augmented data set has been prepared for the period 1900-2005. Nearly 180 focal mechanisms have been compiled for the Andaman-Sumatra region from the post-tsunami sequence of earthquakes. The earthquakes compiled from NOAA epicentral listing for bath pre- and post-tsunami periods mentioned above are shown in Figure 5.2 and the focal mechanisms of events Ms>5.5 are shown in Figure 5.3. The long-term deformation has been calculated using the method described in chapter 4 for the augmented period (1900-2005), so as to compare with the pre-tsunami seismic deformation (1900-2004).

The analysis was made only along the Andaman-Sumatra arc as the post-tsunami seismic activity did not take place in the Java arc region and hence no changes in post-tsunami seismic deformation pattern anticipated. The post-tsunami seismic catalogue includes nearly 1000 small/moderate to large earthquakes (see Figure 5.2). The parameters required to calculate the deformation velocities have been

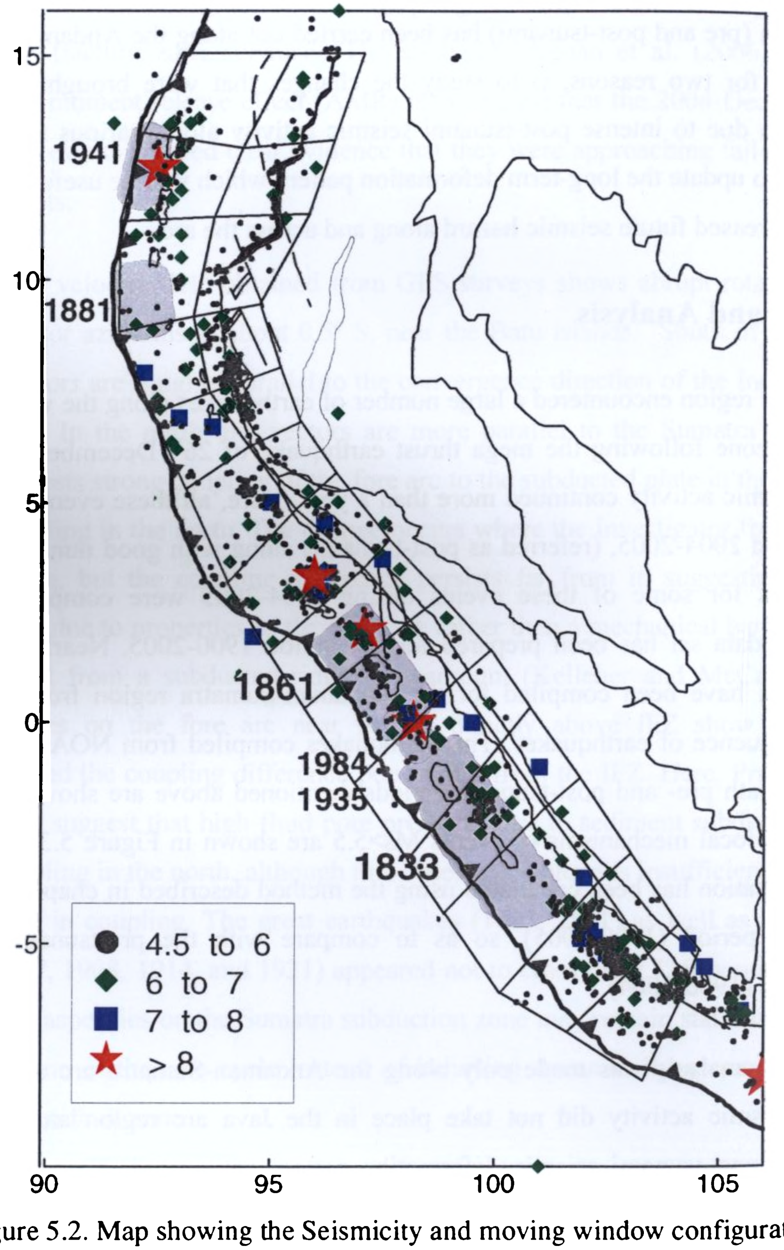

Figure 5.2. Map showing the Seismicity and moving window configuration of the sources in the Andaman-Sumatra trench-arc region.

re-estimated after including the post-tsunami events ie., for the augmented data of 1900-2005. As explained in chapter 4, the deformation velocities based on moment tensor summation require both moment rate and focal mechanism tensor. It can be seen that the moment estimation depends on 'a', 'b', 'c', 'd' and Mo, max values. It is observed that the c and d values which are constants of the magnitude-moment relation and depend on seismic moments of larger earthquakes as the moment contribution for smaller events is very low. Obviously, the Mo, max, which is the converted value or maximum magnitude using the above relation also depends on largest magnitude event during the whole time period. However, the 'a' and 'b' values which are constants of Gutenberg-Richter relation change significantly depending on the number of smaller events in each source. As the post-tsunami events contain large number of smaller events, the b-values were heavily skewed towards higher values in the estimation of a and b values with the augmented data set (1900-2005). It must be noted that smaller events will have greater errors in their magnitude estimation and therefore affect the b-values significantly in case of many such events. In view of this fact and also the insignificant contribution of low magnitude events for total moment release, from the post-tsunami events, only earthquakes of magnitude Ms > 5.5 were considered in the estimation of moment rate and deformation velocities. It can be seen from Figure 5.3 that the post-tsunami events are mostly characterized by dominantly thrust faulting events in offshore Sumatra, between Andaman trench and the fore arc ridge, and along the west Andaman fault and few normal faulting events in the Andaman back arc spreading region.

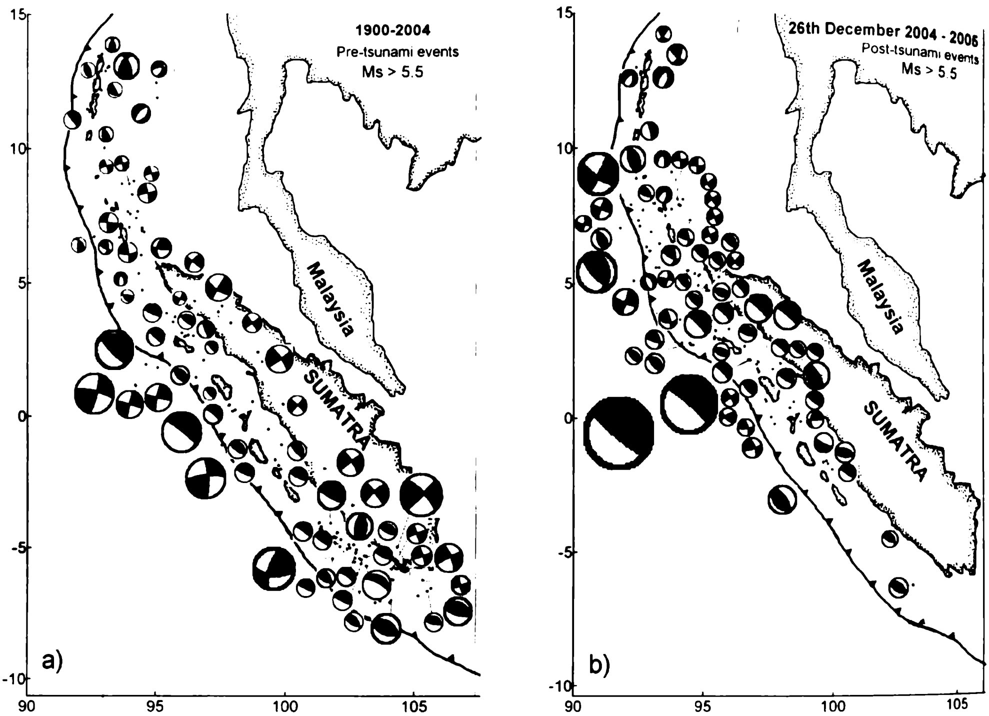

Figure 5.3. Map showing the events for which focal mechanism solutions are available from the Harvard CMT catalogue. Size of the solutions are based on the magnitude of the earthquake

5.3. Results

The long-term seismic deformation after including the post-tsunami earthquakes in the Andaman- Sumatra region for the period (1900-2005) has been estimated as discussed previously. The results of deformation are shown in Tables 5.1 and Table 5.2 which show the components of velocity tensor and the eigen system of velocity tensor with errors in eigen values for each of the seismogenic sources (window) in each region. The changes in moment rate after the mega thrust earthquake are shown in Figure 5.4 and Figure 5.5 for Andaman and Sumatra arc respectively. Similarly, the deformation pattern obtained for each seismogenic source (window) is presented diagrammatically in Figure 5.6 and Figure 5.7.

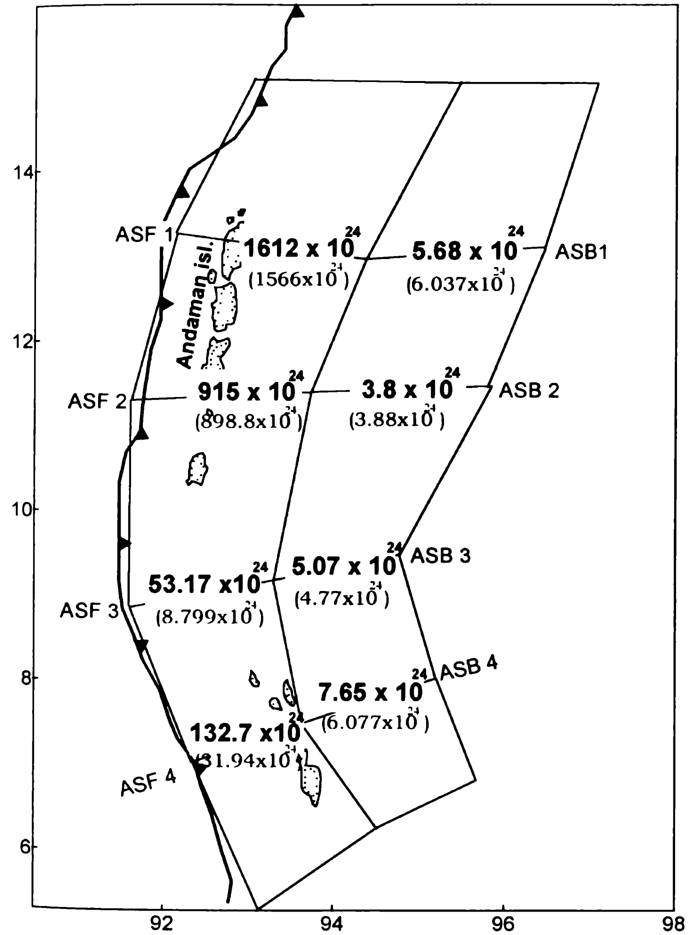

Figure 5.4. Map showing the difference in moment rate before and after tsunami in the Andaman region. The values given in bracket below the numbers in bold are pre-tsunami events.

Table 5.1: Components of velocity tensor and eigen system of velocity tensor in the Andaman fore arc and back arc region

	Elements of velocity tensor U (mm/yr).						**Eigen System of Velocity tensor (mm/yr.)**								
	U_{11}	U_{12}	U_{13}	U_{22}	U_{23}	U_{33}	λ1	Az°	Pl°	λ2	Az°	Pl°	λ3	Az°	Pl°
ASF1	56.034	-79.788	-2.213	-127.01	-1.177	7.523	85.965±10.672	339.5	-1.2	-156.93±19.481	69.5	0.7	7.509±0.932	311.1	88.6
ASF2	4.656	-23.924	-2.068	-44.439	-2.779	5.085	14.468±1.729	338.1	-5.4	-54.359±6.496	67.8	3.2	5.192±0.62	307	83.7
ASF3	-2.927	0.082	0.106	-0.515	-0.182	0.282	-2.934±0.33	357.9	-2	-0.551±0.062	87.5	12	0.324±0.036	277.2	77.8
ASF4	-8.467	-3.046	1.232	0.572	0.966	0.974	-9.599±1.248	17.4	-7.9	1.922±0.25	101.5	36.5	0.757±0.098	297.8	52.4
ASB1	0.176	-0.557	0.003	-0.091	0.017	-0.029	0.616±0.05	321.7	-0.7	-0.531±0.043	51.8	-1.7	-0.03±0.002	28.4	88.2
ASB2	0.265	-0.243	-0.022	-0.023	0.006	-0.029	0.404±0.039	330.3	-2.9	-0.161±0.016	60.2	2.4	-0.03±0.003	290.3	86.2
ASB3	0.066	-0.574	-0.03	0.109	0.004	-0.036	-0.487±0.04	43.9	2.4	0.663±0.054	134	1.9	-0.04±0.003	262.8	86.9
ASB4	-1.116	-1.231	0.009	1.252	-0.007	0	-1.64±0.155	23.1	-0.2	1.776±0.168	113.1	-0.3	0	83.2	89.6

Table 5.2: Components of velocity tensor and eigen system of velocity tensor along Sumatra fault zone and offshore Sumatra arc region

	Elements of velocity tensor U (mm/yr).						**Eigen System of Velocity tensor (mm/yr.)**								
	U_{11}	U_{12}	U_{13}	U_{22}	U_{23}	U_{33}	λ1	Az°	Pl°	λ2	Az°	Pl°	λ3	Az°	Pl°
SFZ1	-1.038	-0.667	-0.011	1.042	-0.014	0.01	-1.233±0.121	16.3	0.7	1.238±0.122	106.3	-0.5	0.01±0.00	158.7	89.2
SFZ2	-3.817	1.048	-0.219	1.797	-0.035	0.088	-4.017±0.439	349.8	2.9	1.989±0.217	79.7	-2.2	0.096±0.01	132.7	86.3
SFZ3	-6.988	1.437	-0.187	3.058	-0.119	0.204	-7.193±0.818	352	1.3	3.266±0.371	82	-2.7	0.201±0.02	107.9	87
SFZ4	-3.476	-2.172	0.29	4.677	-0.085	0.071	-4.035±0.471	14	-3.6	5.224±0.61	104.1	-1.7	0.083±0.01	39.1	86
SFZ5	-1.26	-0.391	0.053	1.145	-0.036	0.004	-1.324±0.162	9	-2	1.208±0.148	99	-2.1	0.004±0.00	55.5	87.1
SFZ6	-24.965	-6.692	0.55	21.768	-1.156	0.097	-25.91±3.722	8	-0.8	22.773±3.272	98	-3.1	0.037±0.005	82.6	86.8
SFZ7	-35.044	-1.651	1.818	21.7	-2.565	0.655	-35.177±4.988	1.5	-2.8	22.069±3.13	91.9	-7	0.42±0.059	69.9	82.5
SFZ8	-15.71	-1.792	1.087	8.435	-0.378	0.707	-15.91±2.053	4.2	-3.6	8.594±1.109	94.4	-3.3	0.747±0.096	46.7	85.1
SFZ9	-9.899	-4.598	1.879	6.648	0.608	0.769	-11.41±1.249	14.6	-9.2	7.842±0.858	104.4	1	1.086±0.119	8.4	80.8
OSF1	-5.363	-3.824	1.219	-0.197	0.813	0.823	-7.646±0.859	28.1	-9.8	1.861±0.209	116.4	10.2	1.047±0.118	340.9	75.8
OSF2	-136.22	44.376	14.985	12.565	13.918	11.212	-150.49±16.83	15.8	-6.4	30.039±3.361	102.2	29	3.011±0.896	297.1	60.1
OSF3	-217.85	89.621	28.604	20.564	28.465	17.158	-252.64±29.74	18.9	-7.7	59.047±6.951	105.3	25.5	3.469±1.586	304.4	63.3
OSF4	-60.586	48.867	15.339	-5.5	13.169	5.822	-93.139±11.09	30.7	-11.4	23.953±2.853	117.8	13.9	3.922±1.063	338.6	71.9
OSF5	-14.259	11.189	3.963	-3.507	3.77	1.51	-22.496±2.539	32.7	-12.6	4.253±0.48	114.2	33.5	1.986±0.224	320.4	53.6
OSF6	-14.095	-8.024	3.777	-1.124	3.076	1.27	-19.034±2.082	26.2	-13.2	3.673±0.402	105.1	39.6	1.412±0.154	311	47.4
OSF7	-2.303	-1.324	0.398	0.416	0.257	0.157	-2.912±0.291	22.3	-8.6	0.964±0.096	111.3	6.7	0.217±0.022	344	79.1
OSF8	-20.799	-6.374	3.467	3.786	2.326	1.395	-22.985±2.304	14.2	-9.2	5.867±0.588	100.8	20.1	1.5±0.15	307.4	67.8
OSF9	-18.435	-6.027	4.16	2.257	2.59	1.726	-21.033±2.057	15.8	-11.7	4.8±0.469	98.2	32.7	1.781±0.174	302.8	54.8

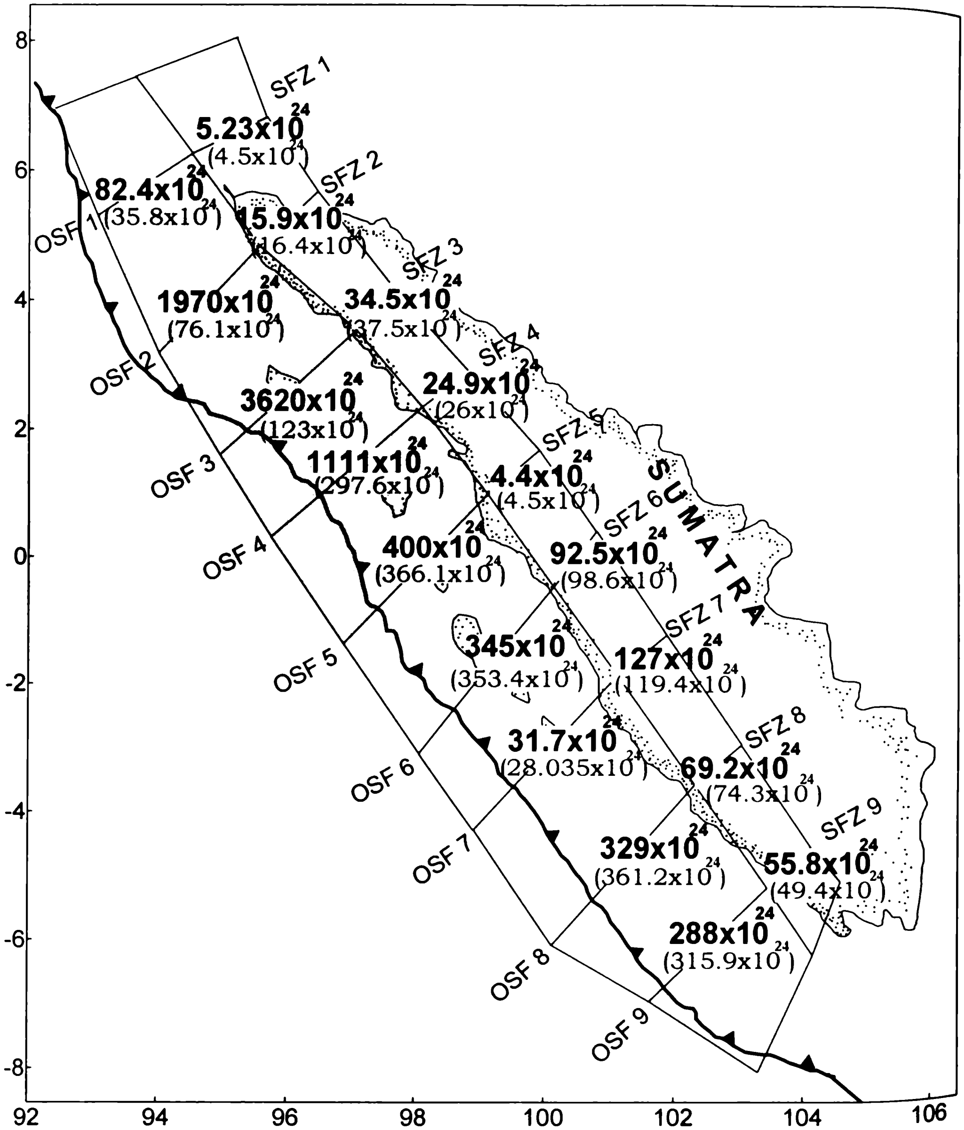

Figure 5.5. Map showing the difference in moment rate before and after tsunami in the Sumatra region. Values given in bracket are for pre-tsunami events. The light grey shaded region shows significantly large differences in moment rate.

A close examination of the moment release rates of both periods gives an idea on level of seismic activity in each of the source (window) regions. Those sources where significantly large earthquakes occurred in the post-tsunami period show large moment rate values, whereas the sources in which post-tsunami activity is negligible, the moment rate is reduced because of averaging over a long period. In the Andaman region, the fore arc region shows considerable moment release variation, whereas in the back arc region, the moment release rate is not very significant. Though several normal faulting events occurred along the Andaman spreading ridge after the mega thrust earthquake, their moment contribution is low. In the Sumatran region, where both 26th December 2004 and 28th March 2005 events were located, very high moment release rate has been observed in the offshore Sumatra between 2° S–5° N. Along the Sumatran Fault Zone, the moment release rate is significant in the southern part, while southern most and northern parts of the SFZ remained less affected by large scale deformation in the fore arc region.

5.3.1. Crustal deformation Rates (1900 – 2005)

The results on crustal deformation rates estimated in the Andaman-Sumatra region after the mega thrust earthquake show drastic change in the long-term deformation rate in the northern part of the Sumatra offshore. The deformation rates are discussed for different segments of the arc below:

5.3.1.1. *Andaman arc*

All along the fore arc region the deformation is predominantly compressional. For sources ASF1 and ASF2, the compressional deformation takes place along a mean direction of N 69° and the extensional deformation along N 339°. The eigen system of velocity tensor suggests an average compression of 156.93$\pm$19.481 mm/yr and an extensional deformation remain constant as 1.9 mm/yr after the tsunami. Shear velocity increased from 2.3 mm/yr to 4.2 mm/yr. In sources OSF2, OSF3 and OSF4, where the mega thrust earthquakes of 26th December 2004 and 28th March 2005 earthquake are located, the deformation rate as well as the shear velocity increased very significantly. Deformation velocities suggest a compression of 150.49±16.83 mm/yr along N 16°and an extension of 30.04±3.36 mm/yr along N 102°. In source OSF2, the compressional deformation rate increased from 5.2 mm/yr to 150 mm/yr. The shear velocity increased from 3 mm/yr to 86 mm/yr.

Both strike-slip and thrust faulting events are seen in the source OSF3 with deformation suggesting dominantly compression of 252.64± 29.74 mm/yr along N 19° and extension of 59.047±6.95mm/yr along N105°. Here, the compressional deformation rate increased from 7.3 mm/yr to 252 mm/yr after the tsunami. The shear velocity also increased from 4.6 mm/yr to 144 mm/yr. For source OSF4, dominantly thrust-faulting events give rise to compressional deformation of 93.14±11.09 mm/yr along N 31° and an extension of 23.95±2.85 mm/yr along N117°. Here, the variation is from 22mm/yr to 93 mm/yr. The shear velocity increases from 6.7 mm/yr to 44 mm/yr.

Source OSF5 shows dominantly compression with compression velocity of 22.49±2.53 mm/yr along N 33°. In this source, the variation in compressional deformation is from 18.3 to 22.5mm/yr. The shear velocity increased from 3.3 mm/yr to 9 mm/yr. In the Southern part of offshore Sumatra region (sources OSF6, OSF7, OSF8, OSF9), no significant changes took place in the magnitude of deformation after the tsunami. In source OSF6, the deformation velocities suggest compression of 19.03±2.08 mm/yr along N 26° shear velocity is 8.5 mm/yr. Further south, the deformation velocities are low with compression velocities of 2.91± 0.29 mm/yr along N 22° and extensional velocities of 0.964±0.096 mm/yr along N 111° in source OSF7.

Here shear velocity is 1.6 mm/yr. In source OSF8, the compression velocities are of 22.98$\pm$2.304 mm/yr along N14° and extensional velocities 5.867$\pm$ 0.59 mm/yr along N101° and the shear velocity shows a value of 14 mm/yr. The source OSF9 suggests a compression of 21.03$\pm$2.06 along N 16° and the shear velocity 9 mm/yr. The extensional deformation is negligible in almost all the cases.

Along the SFZ region, the right lateral strike slip motion prevails and deformation rate also remained almost constant due to lack of any major events after the tsunami in the region except in source SFZ7, where the compressional deformation increased from 29 mm/yr to 35mm/yr and extensional deformation increased from 14 mm/yr to 22 mm/yr.

In the northwestern part of the Sumatran fault, north of Sumatran main land (source SFZ1 in the figure) shows a compression of 1.233$\pm$0.121 mm/yr. along N16.3° and an extension of 1.238$\pm$0.122 mm/yr along N 106°. When entering into the onshore Sumatra region, the deformation rate increases to 4.01$\pm$0.44 mm/yr (compression) and 1.99$\pm$0.21mm/yr (extension) in source SFZ 2. For source SFZ3, the deformation further increases to a compression rate of 7.19$\pm$0.82 mm/yr and extension rate of 3.266 $\pm$ 0.37 mm/yr. Batee fault starts from this region and continue into the offshore. For both the sources SFZ2 and SFZ3, the compressional deformation and extensional deformation takes place along a mean direction N351° and N81° respectively. The deformation velocities for source SFZ4 suggest compression of 4.03$\pm$0.47 mm/ yr along a direction of N14° and extension of 5.22$\pm$0.61 mm/yr in the N104° direction. The eigen system of velocity tensor suggest that for sources SFZ5 and SFZ6, the compressional deformation takes place along a mean direction of N9° and the extensional deformation along N99°. The velocities show a compression of 1.324$\pm$0.16 mm/yr and the extension of 1.208$\pm$0.15 mm/yr for source SFZ5.

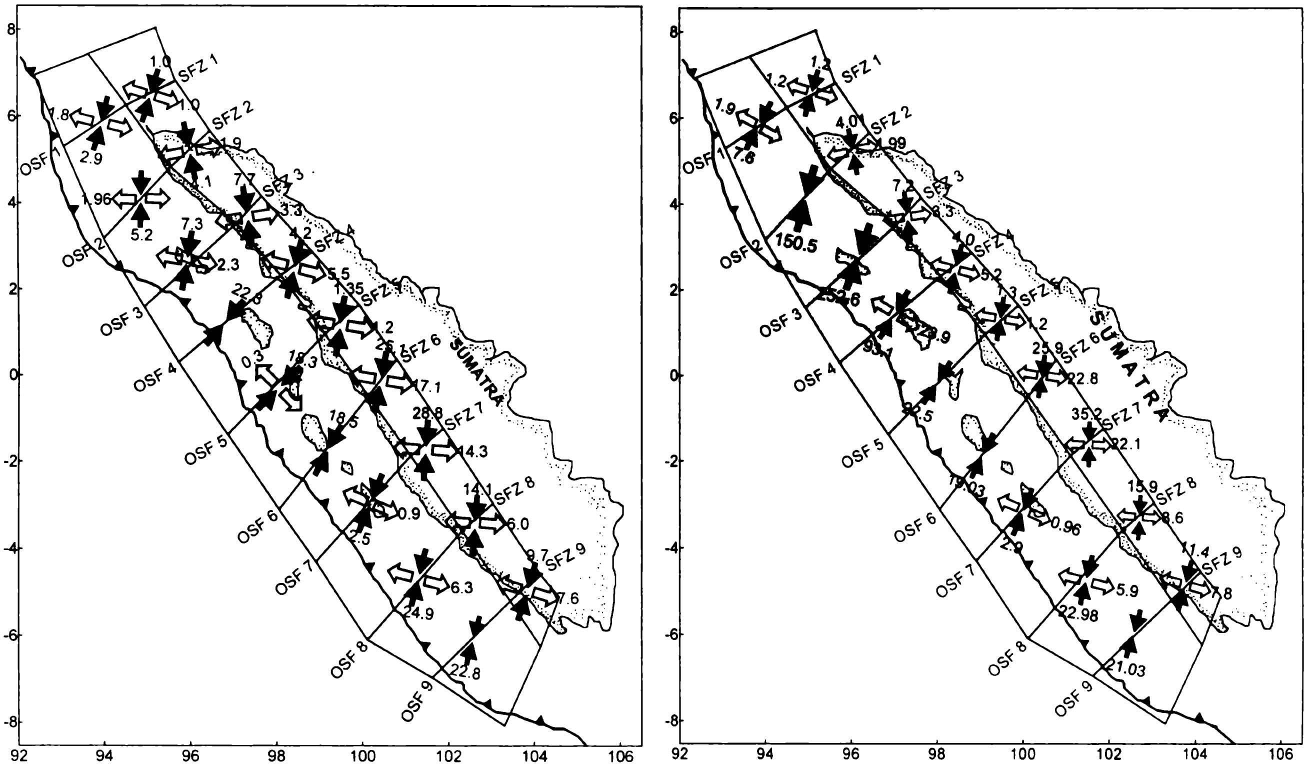

Figure 5.7. Map showing the difference in deformation velocities before and after tsunami in the Sumatra region.

The deformation rate increases further in sources SFZ6 and SFZ7. The source SFZ6 show the compression of 25.91±3.72 mm/yr and the extension of 22.77±3.27 mm/yr. For sources SFZ7 and SFZ8, the compressional deformation takes place along a direction of N1.5° and 4.2° respectively and the extensional deformation along N93°. The compression is 35.17±4.98 mm/yr and extension of 22.07±3.13 mm/yr in source SFZ7. Further south, the deformation rate decreases to compression of 15.91±2.05 mm/yr and extension of 8.59±1.1 mm/yr for source SFZ8 and compression of 11.41±1.25 mm/yr (along N15°) and an extension of 7.84±0.85 mm/yr (along N104°) for source SFZ9.

5. 4. Discussion and Conclusions

Comparison of long-term deformation pattern before and after the tsunami suggest that there is a drastic increase in the deformation in an around the region where the doublet events have occurred. In SFZ and Andaman back arc region, except at few locations, the deformation remains almost constant before and after the events.

The change in deformation before and after the earthquake is very significant in the region between 0° to 4° in the Sumatran offshore. For the sources OSF2 and OSF3, the extensional deformation rate becomes negligible after the major events. In the source OSF2, where the 26th December 2004 event was located, the compressional deformation rate increases from 5.2 mm/yr to 150.5 mm/yr. In the next overlapping window OSF3, where both the 2004 December and 2005 March events occurred, the compressional deformation rate changes from 7.3 mm/yr to 252.6 mm/yr. In the next source OSF4, where only the 28th March 2005 was located, the compression rate changes from 22.3 mm/yr to 93.1 mm/yr. From this it can be suggested that the partial compression with a component of strike-slip faulting had transformed into a completely compressional environment due to the post-tsunami seismic deformation in the Sumatran offshore.

Song and Simons (2003) predicted using the Trench Parallel Gravity Anomalies (TPGA) that the seismic potential is larger for the Andaman–Sumatra trench and lower for the Java trench with a negative and positive TPGA, respectively, as the shear stress will be higher where a negative TPGA occurs and lower where a positive TPGA is observed. Mignan et al. (2006) observed through estimation of Accelarated Moment Release (AMR) estimation that the region of Sumatra subduction system where 26 December 2004 and 28 March 2005 events occurred had been stressed and approaching failure prior to these earthquakes. Based on long-term catalogue of earthquakes before the mega thrust event, the deformation velocities estimated in the present study also gave rise to low-deformation rates in the region between 1° to 5° N in the offshore Sumatra. These independent estimates considering basically the moment release pattern confirm that the concept of seismic gaps could be applied in the active seismic belts for understanding/assessing the seismic hazard in seismically active belts.

Further north, in the Andaman arc region, pre- and post-tsunami GPS measurements indicated W-SW or SW oriented residual co-seismic displacements (Sridevi et al., 2005). According to Bilham et al. (2005), the reverse slip in the Nicobar islands (7° N) was more than twice as much as the slip in the Andaman islands (12°N) after the mega thrust earthquake. The unusual compression deformation near the Nicobar Islands region (ASF3) observed in the post-tsunami period in the present study could be an indication of such reverse slip.

The historic record of large mega thrust earthquakes suggests that the potential for great destructive events is much larger for Sumatra than Java. Grevemeyer and Tiwari (2006) made the observation that Bouguer gravity anomalies correlate well with the occurrence of large mega thrust earthquakes in the Sunda subduction zone; negative anomalies mark segments characterized by larger earthquakes while positive anomalies indicate lower seismic potential. With respect to Java, oblique subduction of young oceanic crust shifts the seismogenic coupling zone roughly 40 km trenchward. A prominent positive gravity anomaly offshore of Java is caused by a shallow mantle wedge underlying the fore arc basin. Based on their study, they suggested that the next great earthquake is likely to hit Sumatra in the area of the 1833 event, while a shallow and hydrated mantle wedge might be limiting the violence of earthquakes in Java.

Lay et al (2005) also suggested that the logical regions for concern about the future large earthquakes are the Sumatran fault zone and southeast of the 2005 rupture, the adjacent region failed in 1833 which likely to have accumulated substantial strain. But in contrast, Mignan et al (2006), based on the study of accelerated Moment release (AMR), are under the opinion that the section of the subduction zone where the 1833 earthquake occurred shows no reliable evidence of accelerating activity at present. However, they identified a region of accelerating seismic activity along a 750 km stretch of the mapped plate boundary along southeastern Sumatra and western Java and suggested that this region may be approaching failure.

The low deformation rate observed in the present study due to the absence of large/mega earthquakes during the period of observation, it can be inferred that the western Java region could be a probable future hazard. These various results need a detailed analysis and a study involving rigorous modeling using multiple geological and geophysical parameters would be very useful.

CHAPTER 6

GRAVITY ANOMALIES, SEISMICITY AND LITHOSPHERIC STRUCTURE BELOW THE ANDAMAN ARC REGION AND THE TECTONIC IMPLICATIONS

6.1. Introduction

The mega thrust earthquake of 26 December 2004 (~ Mw 9.3) and the large series of after shock events since then have ruptured nearly 1300 km long portion of the plate boundary along the Andaman and Sumatra trench-arc region (Ishii et al., 2005). This abnormally high recent seismic activity has brought to fore, the seismicity of the Indonesia arc system and its extension into the Andaman-Nicobar region. The segment of Andaman-Sumatra arc is characterized by oblique motion between the Indo-Australia and Burma – Sunda plates with predominantly thrust motion in the trench/fore arc region and strike slip motion in the back arc region. The strike-slip motion in the back arc region is mainly taken up through ridge-transform system in the Andaman Sea and along the Great Sumatran fault in the mainland Sumatra. The ridge-transform motion in the Andaman Sea is believed to be connected further north into the Burma and meets the Shan-Sagaing fault. Therefore, the region of Andaman arc together with the Burmese arc forms an important transitional tectonic link between the Eastern Himalayas in the north and Indonesian arc in the south.

Most of the large magnitude earthquakes (both historical and recent) in the Andaman arc region are related to the subduction zone at intermediate depths (Bilham et al., 2005) and no earthquake M$\geq$ 8.0 have been reported from this region. Characteristics of the rupture zone due to the 2004 mega thrust event have been studied in detail from far field GPS observations (Banerjee et al., 2005; Catherine et al., 2005) and co-seismic displacements of GPS sites on the islands before and after the event (Sridevi et al., 2005; Gahalaut et al., 2006) which suggest considerable variation in the rupture pattern along the arc from north to south. It is very well documented through multi- wave speed tomography by Kennet and Cummins (2005) that the changes in the geometrical configuration of the slab, physical properties and barriers related to variations in the nature of the slab controlled the rupture propagation of 2004 mega thrust earthquake. Previous investigations on seismicity in the subducting plate as well as the overriding plate suggest variations in the interplate coupling from north to south along the Andaman arc (Dasgupta and Mukhopadhyay, 1993). Song and Simons (2003) demonstrated that the topographic and gravity variations in the subduction zones have a strong correlation with the seismogenic behaviour. In the present chapter, we carry out a systematic and detailed gravity interpretation constrained by seismicity and seismic data in the Andaman arc and the Andaman Sea region in order to delineate the crustal structure and density heterogeneities along and across the arc and its correlation with the seismogenic behaviour.

6.2. Regional Tectonic Setting and evolution of the Andaman Arc–Sea Region

The Andaman arc in the northeastern Indian Ocean defines nearly 1100 km long active plate with the Burma plate (Curray et al., 1979; 1982). The arc is characterized by the presence of east dipping Benioff zone down to 200 km depth (Mukhopadhyay, 1984). The Andaman –Nicobar sedimentary islands evolved during Oligo-Miocene times (Rodolfo, 1969) form part of the fore arc sedimentary complex and west of these islands in the Andaman trench, the sediments of Bengal fan are filled and deformed (Curray et al., 1979). Detailed analysis of seismicity by Dasgupta and Mukhopadhyay (1993) suggest that the dip of the Benioff zone below the Andaman arc vary between 45°-55°. Along a section across the Andaman islands, Dasgupta and Mukhopadhyay (1997) observed a gap in the Benioff zone at a depth of 90-110 km and inferred due to partial melt zone related to the Barren island volcanism.

The Andaman basin that forms the back arc Andaman Sea lies between Burma and Sumatra with an average width of 650 km from the Malay Peninsula to the Andaman Nicobar islands. The sub aerial expression of the islands separates the basin from the Bay of Bengal. The Andaman and Nicobar islands together with the back arc basin is a part of the arc- trench system of the Andaman arc. A detailed tectonic map showing various tectonic elements related to the subduction of the Indian plate and opening of the Andaman Sea is shown in Figure 6.1.

The oblique subduction of the Indian plate in this region resulted in strike-slip faulting parallel to the trench; back arc extension and basin formation in the Andaman Sea (Curray et al., 1979). Uyeda and Kanamori (1979) related back arc spreading in the Andaman Sea to leaky transform tectonics. Based on multi channel seismic reflection data, Curray et al (1982) noticed partial subduction of ninety East Ridge below the Andaman trench. Eguchi et al (1979) inferred collision of this ridge with the Andaman trench in the middle or late Miocene. According to them, the ridge-trench collision transmitted compressional stresses in the back arc area and collision of India with Eurasia exerted a drag in the back arc region that caused opening of the Andaman Sea and age of this opening as inferred from magnetic anomaly identifications by Curray et al (1982) is about 13m.y or in the middle Miocene.

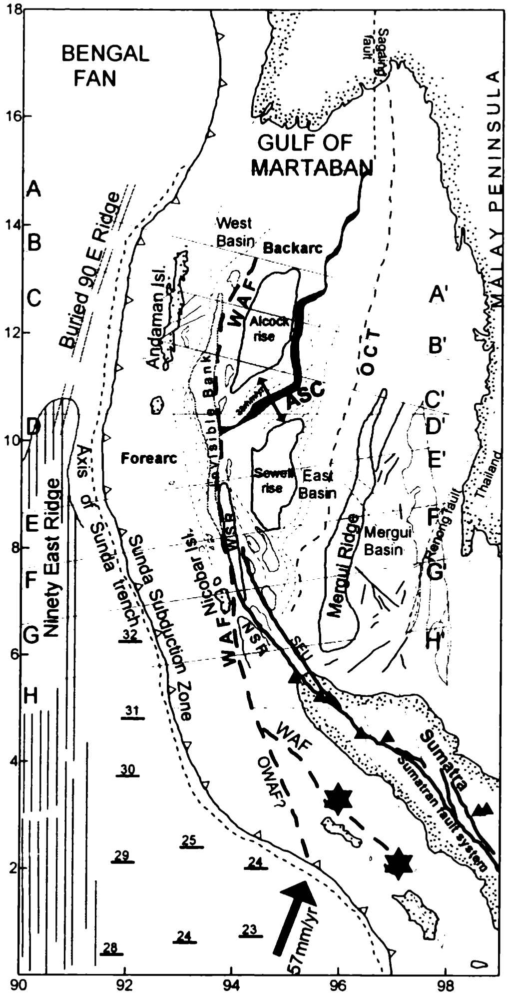

Figure 6.1. Detailed tectonic map showing various tectonic elements related to the subduction of the Indian plate and opening of the Andaman Sea (after Curray, 2005). OCT- Ocean- Continent transition, WAF- West Andaman Fault, NSR- North Sumatra ridge, WSR- West Sewell Rise, ASC- Andaman Spreading Center, SEU- Seuliman Fault. Filled triangle indicate location of volcanoes; Bold stars are the location of recent mega thrust earthquakes (26 December 2004 and 28 March 2005) in offshore Sumatra.The study area is shown as dashed rectangle. Profiles AA' to HH' are gravity traverses used for delineating lithospheric structure in the region.

Based on high resolution swath bathymetry, seismic and magnetic data, Raju et al. (2004) suggested that seafloor spreading started in the Andaman back arc basin 4 m.y ago as a consequence of extrusion tectonics which prompted extension and rifting along the plane joining the Sagaing and Semangko fault systems. The reconstruction of Benioff zone depth-dip angle trajectory in the Andaman arc region by Khan and Chakraborty (2005) revealed a two phase opening history of the Andaman Sea, while the first phase is related to the stretching and rifting in the southern part in 11 m.y, the second phase is related to the initiation of spreading in the Andaman sea during 4-5 m.y. Kamesh Raju et al. (2006) on the other hand proposed three phase evolution of the Andaman Sea, which include a late Oligocene spreading center jump, rifting and extension during middle Miocene to early Pliocene followed by seafloor spreading for the last 4 m.y. By exhaustive compilation of the published information, geological and seismic data, and re-interpretation of magnetic anomalies, Curray (2005) presented an excellent account of the tectonic history of the Andaman sea region in the overall realm of the geodynamics of the SE Asia. According to him, the late Paleocene collision of greater India and Asia with approximately normal convergence started clockwise rotation and bending of the northern and western Sunda arc. The initial sliver fault, which probably started in the Eocene, extended through outer arc ridge offshore from Sumatra, through the present region of the Andaman Sea into the Sagaing fault. With more oblique convergence due to rotation, the rate of strike-slip motion increased and a series of extensional basins opened obliquely by the combination of back arc extension and strike-slip motion . These basins in sequence are the Mergui baisn at ~ 32 m.y , conjoined Alcock and Sewell rises at 23 m.y, East basin at ~15m.y and separation of Alcock and Sewell seamounts and formation of the Central Andaman basin at 4m.y and shifting of the fault onshore from the Mentawai fault to the Sumatra fault system.

6.3. Data and analysis

For the purpose of present work, we compiled the hypocentral location parameters of all earthquakes (M≥4.5) in the Andaman arc region between 0°-16°N and 90°-100°E longitudes from the ISC catalogue and PDE listings during the period 1900-2005. From the catalogue, we selectively eliminated those events whose hypocentral parameters are poorly determined i.e., reported by few stations, and events whose focal depths are not available. Events before 1964 have been compiled from Rothe (1969) and Gutenberg and Richter (1954). For the period between 1953 and 1965, magnitudes from Rothe (1969) listings have been recalculated by Newcomb and McCann (1987). Similarly, precisely determined hypocentral parameters from the ISC listing for the period 1964-1995 by Engdahl et al (1998) have also been considered here. We also considered all available CMT solutions in the Andaman arc region for studying the stress distribution and faulting pattern in the Benioff zone as well as the overriding plate. The derived Benioff zone structure has also been used to calculate the gravity effect of three-dimensional geometry of the slab. The GEOSAT gravity anomaly values (2' x 2' resolution grid) and the GEBCO bathymetry (1'x 1' resolution grid) have been used to delineate the deep structure. A large amount of seismic reflection, refraction and other published information on sediment thickness, nature of basement and tectonics have been utilized to aid the interpretation of gravity anomalies.

6.3.1. Seismicity and Benioff zone

The compiled events for the Andaman arc-Sea region have been plotted as 3D wire frame diagram as shown in Figure 6.2. Based on all available earthquake data up to 1993, Dasgupta et al (2003) considered nearly 29 depth sections in several blocks, each section, projected on to center plane of the block of 1° width set perpendicular to

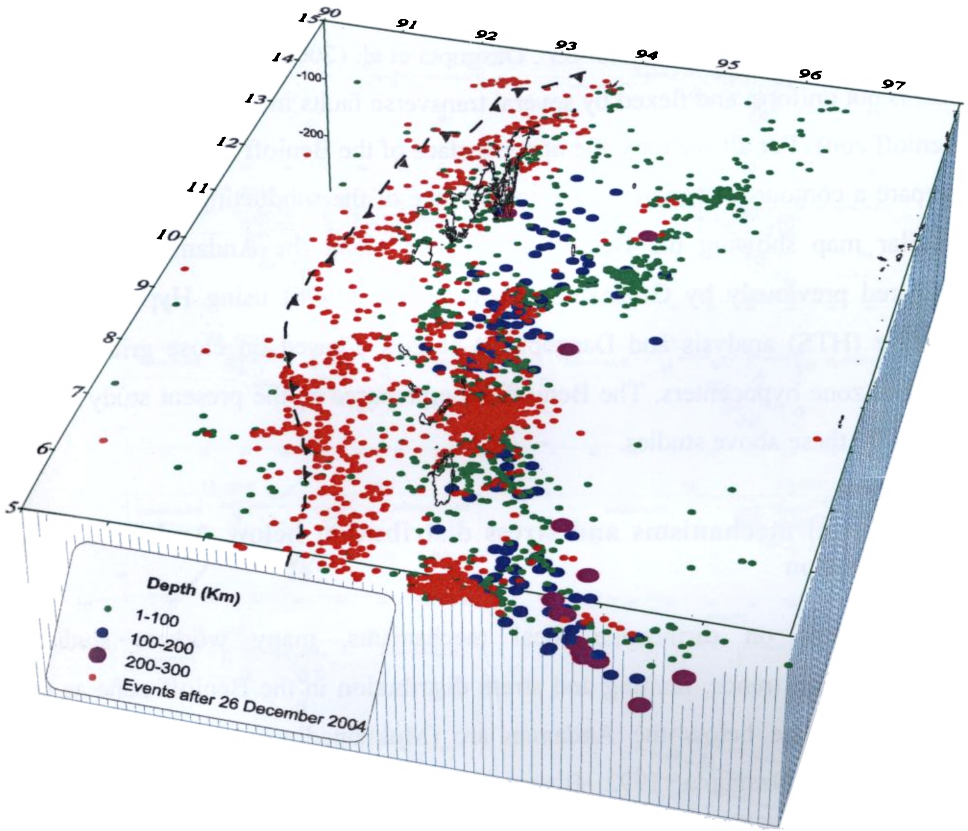

Figure 6.2. 3D wire frame plot of earthquakes in the Andaman Arc-Sea region

the local tectonic trend of the Burmese- Andaman and northern Sumatra arc region. Of these, 11 depth sections belong to the Andaman arc region. Using our updated data set from ISC catalogue up to 2001, we reconstructed all 10 sections in the region. Slight adjustments have been done to the Benioff zone configuration drawn by them in different sections to satisfy the additional data. The Benioff zone defined along these 11 depth sections is shown in Figure 6.3. Those events for which focal mechanisms are available have been shown in the depth sections. The dip of the Benioff zone varies between 40°-55°. Dasgupta et al. (2003) observed that the dipping slab is not uniform and flexed by several transverse faults indicating contortions in the Benioff zone. For all sections, the upper surface of the Benioff zone is marked so as to prepare a contour map representing top surface of the subducting Indian lithosphere. Similar map showing the Benioff zone trend along the Andaman arc had been prepared previously by Guzman-Speziale and Ni (1996) using Hypocentral Trend Surface (HTS) analysis and Dasgupta et al.(2003) based on close grid of shallow Benioff zone hypocenters. The Benioff zone prepared in the present study compares well with these above studies.

6.3.2. Focal mechanisms and stress distribution below Andaman arc-Sea region

Based on earthquake focal mechanisms, many workers studied the seismotectonic trends, faulting and stress distribution in the Benioff zone as well as overriding plate below the Andaman arc (Mukhopadhyay, 1984; Rajendran and Gupta, 1989; Dasgupta, 1992; Biswas et al, 1992; Dasgupta and Mukhopadhyay, 1993; Ravikumar et al, 1996; Radhakrishna and Sanu, 2002; Dasgupta et al, 2003; among others). In the present study, we utilize nearly 173 focal mechanism solutions by compiling all available events reported in previous studies (25) as well as the Harvard CMT solutions (148) up to 2004. We used the mean slip angle method (Ravikumar et al, 1996) to categorize all 173 mechanisms. Based on this classification, 32 mechanisms show normal faulting, 104 mechanisms strike- slip faulting and 37 events thrust faulting. In order to understand their spatial disposition in the subduction environment, we plotted the mechanisms in the depth sections shown in Figure 6.3. For clarity, we avoided plotting events that show similar faulting pattern and close by particularly in the back arc region. A preliminary analysis of their locations indicates that most of the normal faulting events occur in the back arc, while

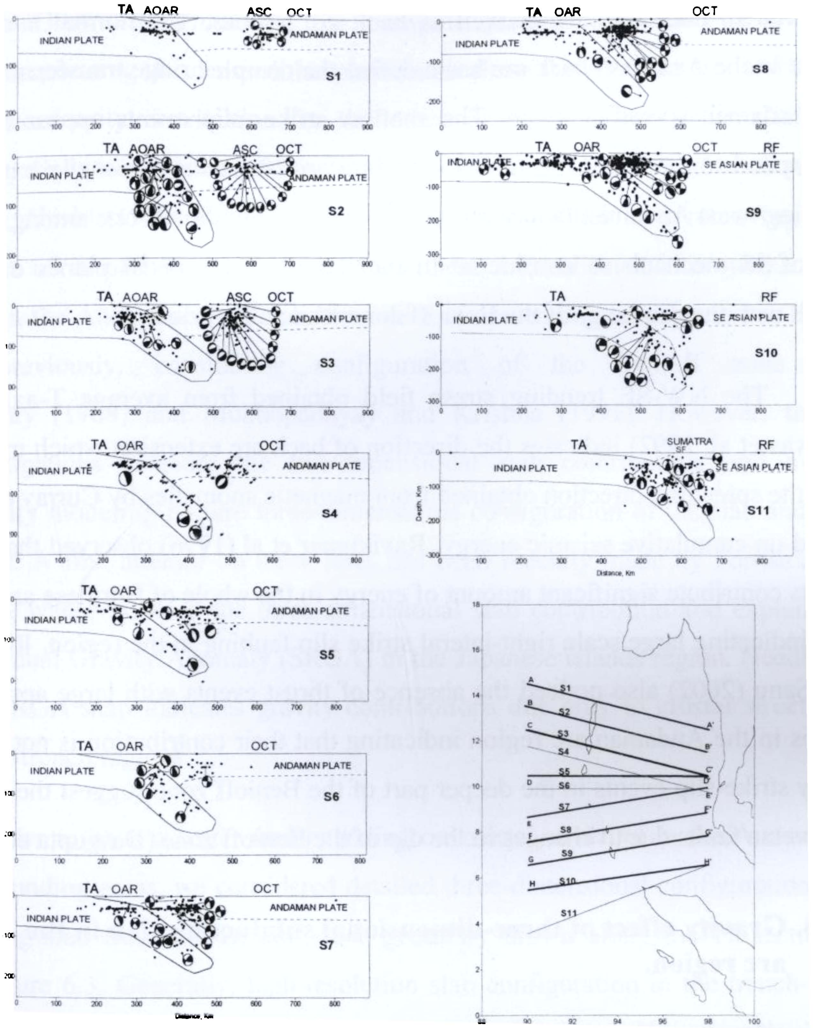

Figure 6.3. Sections showing the Benioff zone configuration and faulting pattern based on seismic incidence and focal mechanisms (Harvard CMT catalogue) across the Andaman arc region (modified after Dasgupta et al., 2003).Inset shows location of these sections (S1 – S11). Bold lines shown in the inset AA' to HH' are location of profiles used for gravity modeling.

thrust faulting events mainly confine to the fore arc area. The strike-slip events are observed in both fore arc as well as back arc regions. The normal and strike-slip events in the Andaman back arc basin define the complex ridge transform structure of the Andaman spreading ridge. The shallow strike- slip events appear off the slab correspond to the transform fault in the fore arc basin, the regionally extensive N-S trending west Andaman fault with right lateral shear motion is one among such faults. Out of 48 mechanisms considered in the Benioff zone, nodal planes of 26 events match with the geometry of the Benioff zone while others do not.

The NW-SE trending stress field obtained from average T-axis azimuths (Biswas et al, 1992) indicates the direction of back arc extension which matches well with the spreading direction obtained from magnetic anomalies by Curray et al (1979). Based on cumulative seismic energy, Ravikumar et al (1996) observed that strike-slip events contribute significant amount of energy in the whole of Burmese and Andaman arcs indicating large scale right-lateral strike slip faulting in the region. Radhakrishna and Sanu (2002) also noticed the absence of thrust events with large apparent stress values in the Andaman arc region indicating that their contribution is not significant. Many strike-slip events in the deeper part of the Benioff zone suggest the presence of transverse faults due to changes in the dip of the Benioff zone (Dasgupta et al., 2003).

6.3.3. Gravity effect of three-dimensional subducting slab in the Andaman arc region.

A general practice in the forward modeling of gravity is to remove contributions from known sources/structures. It is a well-established fact that the gravity modeling and crustal structure investigations in the island arc-trench areas must consider the geometry of the subducting lithosphere slab as it induces large-scale mass transfer in the region. They produce substantial long wavelength gravity anomalies at the surface as the descending slab is thermally colder (Minear and

Toksoz, 1970), seismically denser (Utsu, 1971) and penetrates into the lighter asthenosphere. Grow (1973) made the first attempt to quantitatively model the gravity anomalies incorporating the denser lithospheric slab along the Aleutian arc, and with more complex density distribution for the descending lithosphere under Chilean trench later by Grow and Bowin (1975). Along few reliable crustal seismic sections in Japan region, Yoshi (1973) obtained residual gravity anomalies after removing the gravity effect of crustal layers and explained these anomalies due to subducting lithosphere. In the Andaman arc region, the effect of descending lithosphere has been estimated previously, considering configuration of the Benioff zone by Mukhopadhyay (1988) and Mukhopadhyay and Krishna (1991). However, these above investigations consider the two-dimensional slab contribution, and more realistic gravity modeling require three-dimensional configuration of the slab and its gravity effect. A first attempt on these lines has been recently made by Furuse and Kono (2003), who computed the three-dimensional slab contribution and explained the Slab Residual Gravity Anomaly (SRGA) in the Japanese islands region. Needless to say, the SRGA map indicates gravity contributions due only to crustal structure below the arc-trench regions.

In order to have a better understanding on crustal structure in the Andaman arc and surrounding areas, we considered detailed three-dimensional configuration of the subducting slab from the Benioff zone geometry drawn along the 11 sections shown in Figure 6.3. Generally, high-resolution slab configuration in the trench-arc regions is possible through micro earthquake investigations or other seismological studies. Such data are absent for Andaman arc region due to linear disposition of Andaman and Nicobar islands along the arc and non-availability of azimuthally covered seismic stations data from the surrounding continents. Therefore, the hypocentral distribution of earthquakes provide, as a first approximation, the three dimensional configuration of the subducting lithosphere in the region. The isodepth contour map of top surface of the subducting slab (Figure 6.4) indicates that the depth of the slab varies from 80-220 km with maximum penetration depth in the south Andaman Sea. We used the method of Talwani and Ewing (1960) to calculate the gravity anomaly of the three- dimensional Subducting slab. For this purpose, we divided the slab into several horizontal cross-sections defined by the depth contours. The gravity effects of these horizontal laminae or cross-sections are calculated and numerically integrated over depths from top to the deepest point. We considered the 5km x 5km gridded points covering the study area for calculating the total gravity effect of the slab. The density contrast between the lithospheric slab and the asthenosphere is considered as 0.065gm/cm^3. A similar density contrast has been adopted by Furuse and Kono (2003) based on seismic velocity distribution studied by Yoshi (1973). The lithospheric plate thickness in the Andaman arc region is considered as 80 Km from the surface wave dispersion studies in the northeastern Indian Ocean (Singh, 1990). Furuse and Kono (2003) demonstrated that computed slab anomaly depends on the choice of various parameters such as the density contrast, subducting plate thickness, slab thinning and phase transitions within the slab, out of which, the density contrast and plate thickness have dominant effect. A density contrast of 0.05 gm/cm^3 was assumed by Grow (1973). In order to evaluate the effect of this parameter, we also calculated the slab contribution for a density contrast of 0.05 gm/cm^3. A comparison of the slab contribution from the two-density contrasts show similar anomaly pattern but the amplitude of the gravity high differs nearly by 20 mGal. Here, we finally chose a density contrast of 0.065gm/cm3 as it was constrained by seismic velocity distribution. However, it should be kept in mind that adopting a higher value would give rise to an upper bound to the crustal thickness that will be discussed in the next section. The effect of phase transitions in the slab may not be significant in the study region as the maximum penetration depth is only 220 km below the arc. In the absence of any knowledge on the detailed seismic structure of the descending slab, some trade off between the choices of these parameters definitely required and can be concluded that slab gravity anomaly is important in delineating realistic crustal models in arc-trench regions. The slab gravity anomaly map computed for the Andaman arc region (Figure 6.4) reveal a smooth, long wavelength and symmetric gravity high of maximum 85 mGal centered just east of Nicobar islands region. The trends of the gravity high contours align along the Nicobar deep in the east of Andaman- Nicobar islands. The slab contribution is ~ 20 mGal in the trench region and 5-10mGal in the Malayan margin far east of the Andaman arc.

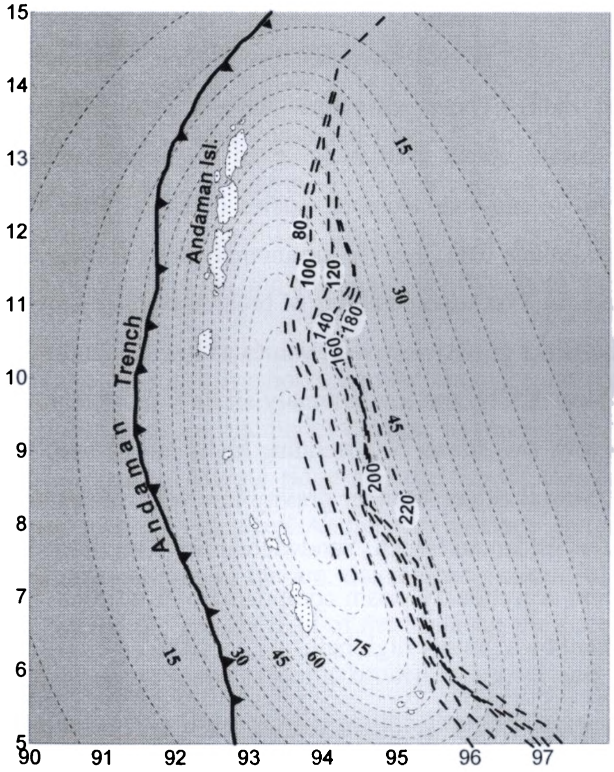

Figure 6.4. Depth contour map (thick dashed line in km) representing top surface of the three-dimensional geometry of subducting Indian lithosphere along the Andaman arc. Thin dashed contours (in mGal) represent the gravity effect of the three-dimensional geometry of the Benioff zone.

6.3.4. Gravity anomaly maps

6.3.4.1. *Free air anomaly map*

The gravity field of the Andaman arc-sea region was earlier described by Peter et al (1966), Mukhopadhyay (1988) and Mukhopadhyay and Krishna (1991), based on the available ship track gravity data in the region. Though they were able to highlight major structural features, large gaps in our understanding gravity picture still exist due to sparse and limited ship-track gravity data in the region. It is now known that satellite derived GEOSAT gravity anomalies (Sandwell and Smith, 1997) are very useful to study gravity field in such areas because of their fairly uniform coverage of (2-minutes gridded data). These anomalies have a resolution down to 23 km wavelength and accurate up to 5-10 mGal even in rough bathymetric areas and therefore very useful in regional tectonic studies (Marks, 1996; Radhakrishna and Searle, 2006). Based on this data, the free air anomaly map of the Andaman arc sea is presented in Figure 6.5a. The superpositions of broad tectonic elements onto this map reveal a broad and distinct gravity low with values as low as –200mGal coincide with the Andaman arc. Near 8.5°N, the low anomaly shifts towards east into the Nicobar deep. Hugging this low, two strong N-S trending highs can be seen over the invisible bank and the West Sewell ridge. Another gravity low with values around -40 to -60 mGal occur along the Andaman trench. Sandwiched between these two gravity lows, the outer arc sediment accretionary prism comprising of Andaman, Nicobar and Nias islands is characterized by a gravity high belt.

The ninety East Ridge is characterized by a positive gravity field with maximum gravity values of around +60mGal. The strong gravity field can be seen up to 10°N, where the ridge is exposed on the surface and further north, the gravity field becomes subdued as the ridge extends in the subsurface (Curray et al., 1982). Near 8°N, the trend of the gravity low associated with the trench is seen disrupted by the positive gravity field of the ridge suggesting partial subduction of the ridge below Andaman trench. East of the arc, in the Andaman basin, the gravity values ranging –20 to 20mGal coincide with the Andaman spreading ridge, whereas, both Alcock and Sewell seamounts complex display strong gravity highs of around 60 mGal. In the east basin, the Mergui ridge give rise to a strong gravity high of 50mGal. The shelf edge positive gravity field can be seen all along the Malayan shelf.

6.3.4.2. *Slab Residual Gravity Anomaly (SRGA) map*

The computed slab anomaly shown in Figure 4 has been subtracted from the free air anomaly map presented in Figure 5a in order to obtain the SRGA map. For this purpose both the data sets were converted into a 5km x 5km grid. The resultant SRGA map is shown in Figure 6.5b. As the slab contribution is mainly from below 80 km depth in the asthenosphere, the SRGA map should be attributed mainly to mass anomalies within the lithosphere i.e., the crust and the lithospheric mantle.

The SRGA map essentially shows similar anomaly pattern as the free air anomaly map but the range of the anomalies change. In some cases, amplitude of the anomalies diminished such as Mergui ridge and the Sewell seamount whereas, the amplitudes of the arc anomaly enhances. As the slab anomaly computed here effects only the immediate surroundings of the arc, the regions seaward of the trench along the Ninety East Ridge and the gravity field of the Malayan shelf are not significantly affected. This map has been considered for modeling crustal and sub crustal mass anomalies along a number of profiles, which will be discussed in the next section.

6.3.4.3. *Mantle Bouguer Anomaly (MBA) map*

The free air anomaly map is dominated in general by the gravity attraction of the density contrast at the seafloor. The subsurface density structure can be investigated by applying mantle Bouguer correction following the method of Prince and Forsyth (1988). The predicted gravity signal of the seafloor-water interface and crust-mantle interface assuming a constant thickness crustal layer of 6 km is obtained using the Fourier transform method of Parker (1972). This gravity effect when subtracted from the free-air gravity will give rise to Mantle Bouguer anomalies (MBA), a useful tool to decipher crustal thickness variations. The bathymetry data required for this purpose is considered from ~1-2 km interval digitized GEBCO database which is a compilation of accumulated ship track data from many sources. Recently, Subrahmanyam et al. (2005) made a comparison of GEBCO bathymetry with the ship track bathymetry and found good correspondence between them. Similarly, Marks (1996) observed that satellite derived GEOSAT gravity database compare well with shipboard measurements and resolve all wavelengths down to 23 km. The excellent correlation of free air anomaly map with various morpho tectonic features in the Andaman arc region further supports our intention to compute mantle Bouguer anomalies. However, we refrain ourselves from subjecting this map for any quantitative interpretation.

The gravity and bathymetry data sets were interpolated onto 4 km grid interval and very shallow shelf as well as land positions has been eliminated in the computation. The density values for water layer (1.03gm/cc), crust (2.73gm/cc) and mantle (3.33gm/cc) have been considered. Though seismic reflection records in the region compiled by Curray (2005) gives sufficient knowledge of the basement in many areas, it is not possible derive the sediment –basement information down to 4 km-interpolated grid, hence this layer was not considered in the computation. The MBA was then computed by removing the net mantle Bouguer correction from the free-air anomaly at the respective grid points. The deeper slab effect was also subtracted at these grid points, so that, the slab residual mantle Bouguer anomalies

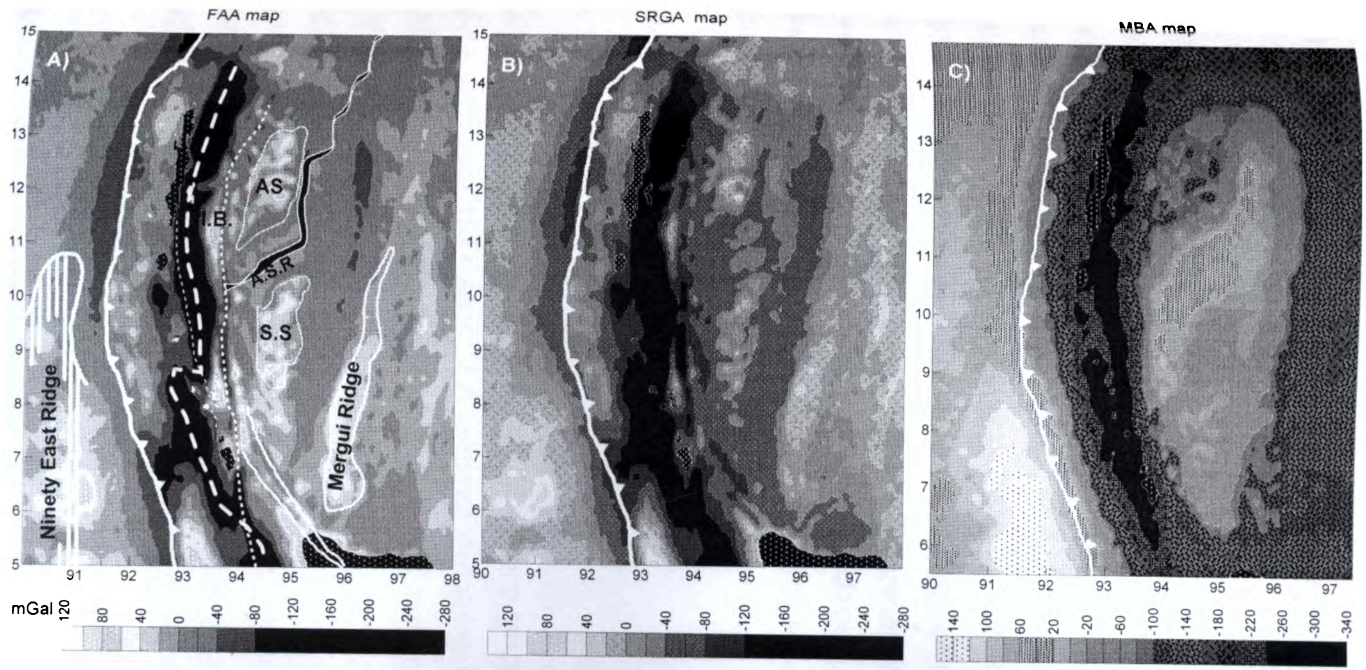

Figure 6.5 Gravity anomaly maps along Andaman arc and the Andaman Sea region used in the analysis / interpretation for delineating lithosphere structure. A) Free-air anomaly map (GEOSAT 2'x2' gravity) B) Slab Residual Gravity Anomaly (SRGA) deduced by subtracting the slab effect from the Free-air map C) Mantle Bouguer Anomaly (MBA) map. Details are discussed in text.

essentially reflect the crustal thickness variations or density heterogeneities. The MBA map of the region is shown in Figure 6.5c.

The MBA map shows a high anomaly coinciding with the ninetyeast Ridge, a broad and continuous gravity low zone between the trench and the arc, a gravity high over the Andaman spreading ridge flanked by minor negative anomalies over the Alcock and Sewell rises, and large negative anomalies in the eastern part of study region over the Malayan shelf. While, low MBA areas reflect the crustal thickening or presence of low-density crustal material, the positive MBA values indicate crustal thinning or densification of the crust. It should also be noted that more rigorous interpretation of the MBA is possible after removing the gravity effect of thermal flow models in any region (Kuo and Forsyth, 1988). However, in the present study, we utilize the observed MBA map to help further the seismically derived gravity modeling in the region.

6.4. Gravity Models

In order to delineate the crustal and lithospheric mantle configuration along and across the arc, eight regional gravity traverses, AA' through HH' (See Figures 6.1 and 6.3 for location) starting from Ninety East ridge in the west and ending at the Malayan shelf towards east have been considered. Figures 6.6 - 6.13 illustrates the changes in slab residual free-air and mantle Bouguer anomalies along these profiles. The SRGA values along with the bathymetry constrained by tectonic and sediment thickness details along these profiles were in terms of 2D-lithosphere structure in the region. A comparison of the SRGA and MBA along these profiles indicate that the double peaked SRGA associated with the Andaman trench-arc system shows up as a broad (250-300 km wide) MBA low.

6.4.1 Sediment thickness and nature of basement

For the delineation of deeper structure, it is important to consider the sediment thickness data in the region. While deriving this information, we focused mainly to obtain maximum number of control points on sediment thickness as well as nature of basement (oceanic / volcanics) along the profiles AA` to HH'. In the region west of Andaman islands consisting of the Andaman trench and the adjoining Bengal Fan, the sediment thickness and velocity structure was mainly from Curray et al.(1982) and in the deepest part of the trench, the values have been projected from the NGDC sediment thickness grid. In the Andaman Sea, excellent review as well as data on sediment thickness and basement information is available from Curray (2005). A compilation of all these information gave reasonable picture on basement structure along these profiles.

6.4.2. Interpreted Gravity Models

The 2D-forward gravity modeling has been carried out to delineate the lithospheric structure below the Andaman arc-sea region. Wherever seismic control is very high along these profiles, model parameters in that region are held fixed to infer structure in the surrounding areas. The modeling is carried out using the USGS SAKI program. Mukhopadhyay and Krishna (1991) obtained densities from seismic velocities for the whole NE Indian Ocean. Their values suggest densities of 2.4 gm/cc and 2.6 gm/cc for upper and lower parts of the sediments where sediment thickness exceed by 5.0 km. We adopted here the similar density structure for modeling. The densities for other rock types in the region are: volcanics (2.6 gm/cc), oceanic crust (2.9 gm/cc), and continental / transitional crust below Malayan shelf (2.85 gm/cc). Mukhopadhyay and Krishna (1991) also inferred a 60 km wide low density column below the volcanic arc / spreading ridge. We adopted a density of 3.29 gm/cc for this column below spreading ridge, with lithosphere and asthenosphere having densities of 3.3 gm/cc and 3.235 gm/cc.

Some salient observations on structure and gravity anomalies for each of the eight profiles is described below:

6.4.2.1. *Profile AA'*

This profile starts from Bay of Bengal in the west up to the Mergui terrace in the east passing over the buried Ninety East Ridge (NER), Andaman trench, Andaman-Nicobar Ridge (ANR), Barren - Narcondam basin, part of Alcock Rise, Andaman spreading center (ASC). The SRGA values show a low of around -200 mGal over the Andaman arc and the Benioff zone. It can be seen from the profiles that the MBA closely follows the shape of the oceanic crust with broad low of around -290 mGal over the Benioff zone. Futher east, over the Mergui terrace, which is the continental crust, the MBA values are largely negative of the order of -155 mGal. The NER is buried under the sediments north of 10° N. The sediment thickness on the western part of the profile is around 3-3.5 km, but on the top of the buried 90°E ridge it is around 1.5 km and below the trench, the sediment thickness again increases. In the Barren Narcondam Basin, in ASC and over the Mergui terrace, the sediment thickness is around 3-4 km.

The Mergui terrace is considered to be of transitional / rifted continental crust (Curray et al., 1982; Mukhopadhyay and Krishna, 1991) having a thickness of 18 km. Below ANR, the crust is maximum thickness of around 30-40 km. The NER, which is believed to be the Kerguelen hotspot trace, has a volcanic emplacement (underplated) below it. The crust below NER is thicker (9-10 km) than the adjacent regions (5 km). The thickness of the crust goes 9-10 km in that region, where the adjacent crust has a

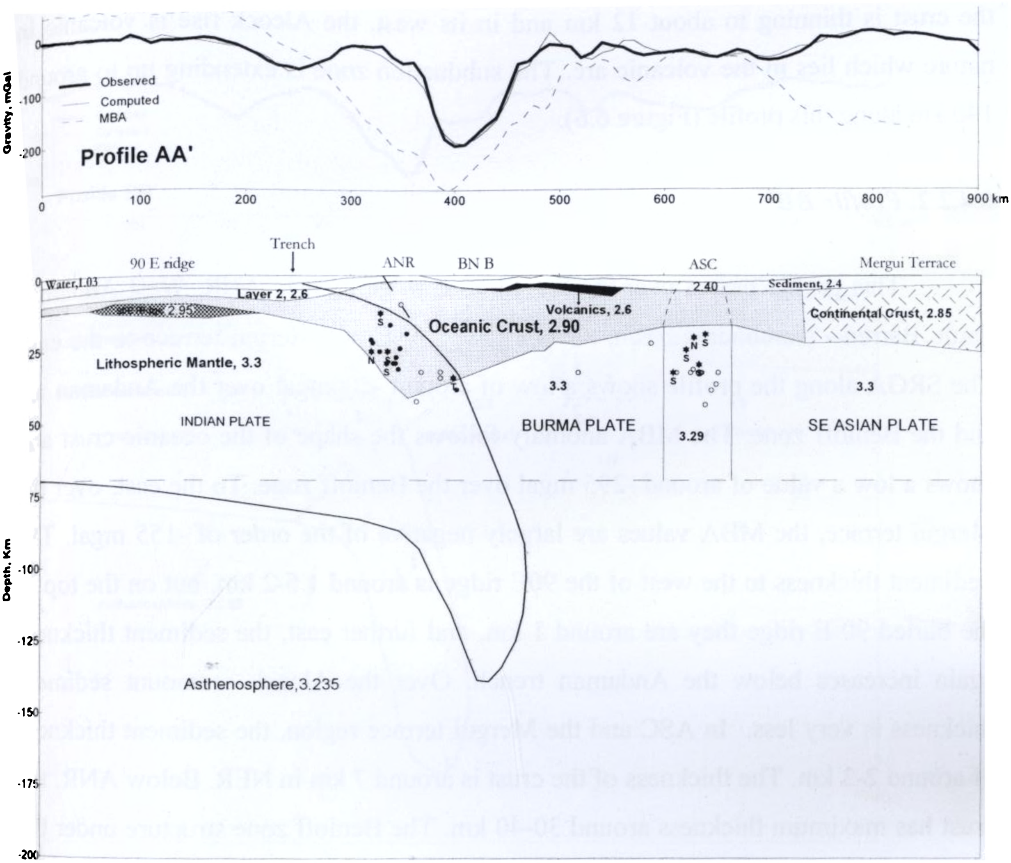

Figure 6.6- Gravity derived crustal models along the profiles AA' in the Andaman arc region. The post-tsunami earthquakes are projected on to the crustal section to understand the relation of crustal structure and seismogenic behaviour. Open circles are events without any mechanisms, filled circles have focal mechanisms and stars are >5.5 magnitude events with type of faulting shown Thrust (T), Normal (N),Strike-slip (S)

thickness of around 5 km. To its east, below the Andaman trench, nearly 9 – 10 km of thick sediments have been observed. In the ASC, which is a back arc spreading ridge, the crust is thinning to about 12 km and in its west, the Alcock rise is volcanic in nature which lies in the volcanic arc. The subduction zone is extending up to around 140 km along this profile (Figure 6.6).

6.4.2.2. *Profile BB'*

This profile passes over the buried 90 E ridge, trench, ANR, West Andaman Fault, Barren - Narcondam basin, Alcock Rise , ASC and Mergui terrace to the east. The SRGA along the profile shows a low of around -200mgal over the Andaman arc and the Benioff zone. The MBA anomaly follows the shape of the oceanic crust and shows a low a value of around -295 mgal over the Benioff zone. To the east, over the Mergui terrace, the MBA values are largely negative of the order of -155 mgal. The Sediment thickness to the west of the 90E ridge is around 1.5-2 km, but on the top of the buried 90 E ridge they are around 1 km, and further east, the sediment thickness again increases below the Andaman trench. Over the Alcock seamount sediment thickness is very less. In ASC and the Mergui terrace region, the sediment thickness of around 2-3 km. The thickness of the crust is around 7 km in NER. Below ANR, the crust has maximum thickness around 30-40 km. The Benioff zone structure under the ANR extends up to 175 km. The post-tsunami seismic activity is seen to be more confined to the subducting Indian plate with strike slip and thrust faulting events in the deep Benioff zone. Seismic activity is seen along the WAF region which suggest that the after shock events propagated through the WAF. To the east of WAF, the Alcock rise is volcanic in nature and lies within the volcanic arc of the subduction zone. In the ASC, the crust is thinning to about 6-7 km while the crust surrounding has thickness of 13-16 km. In ASC, seismic events are more of normal and strike slip mechanisms. Under the Mergui terrace, the continental crust is having a thickness of around 18-19 km (Figure 6.7).

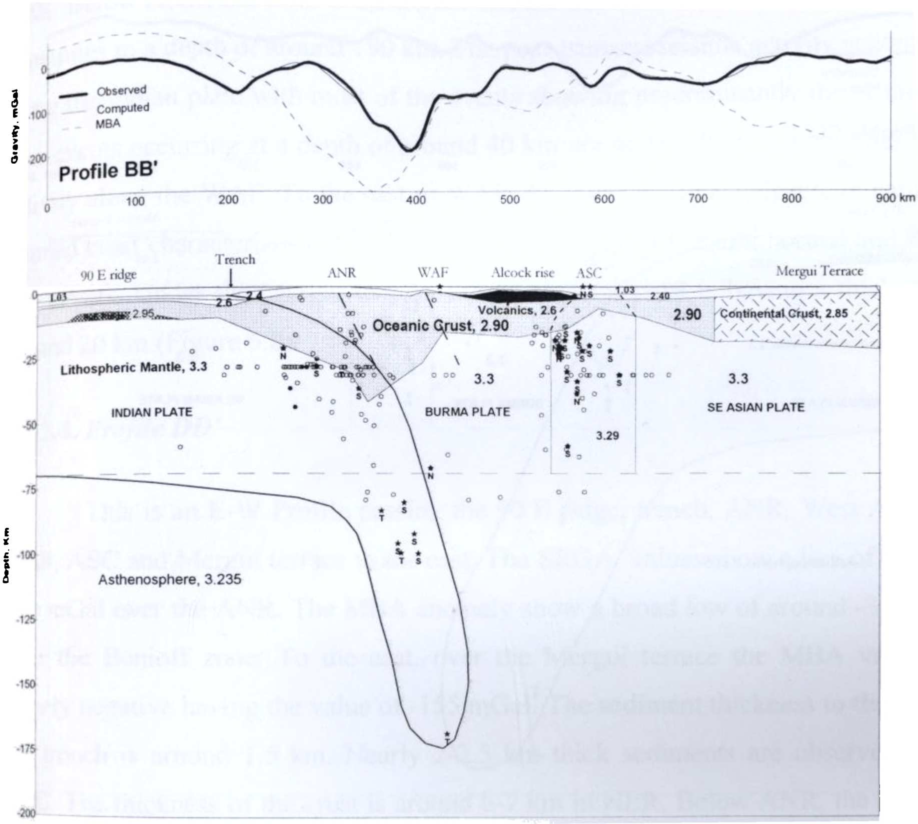

Figure 6.7. Gravity derived crustal models along the profiles BB' in the Andaman arc region. The post-tsunami earthquakes are projected on to the crustal section to understand the relation of crustal structure and seismogenic behaviour. Open circles are events without any mechanisms, filled circles have focal mechanisms and stars are >5.5 magnitude events with type of faulting shown Thrust (T), Normal (N),Strike-slip (S)

6.4.2.3. *Profile CC'*

This profile passes over the buried 90 E ridge, trench, ANR, West Andaman Fault, ASC and Mergui terrace to the east. The SRGA shows a low of around -150

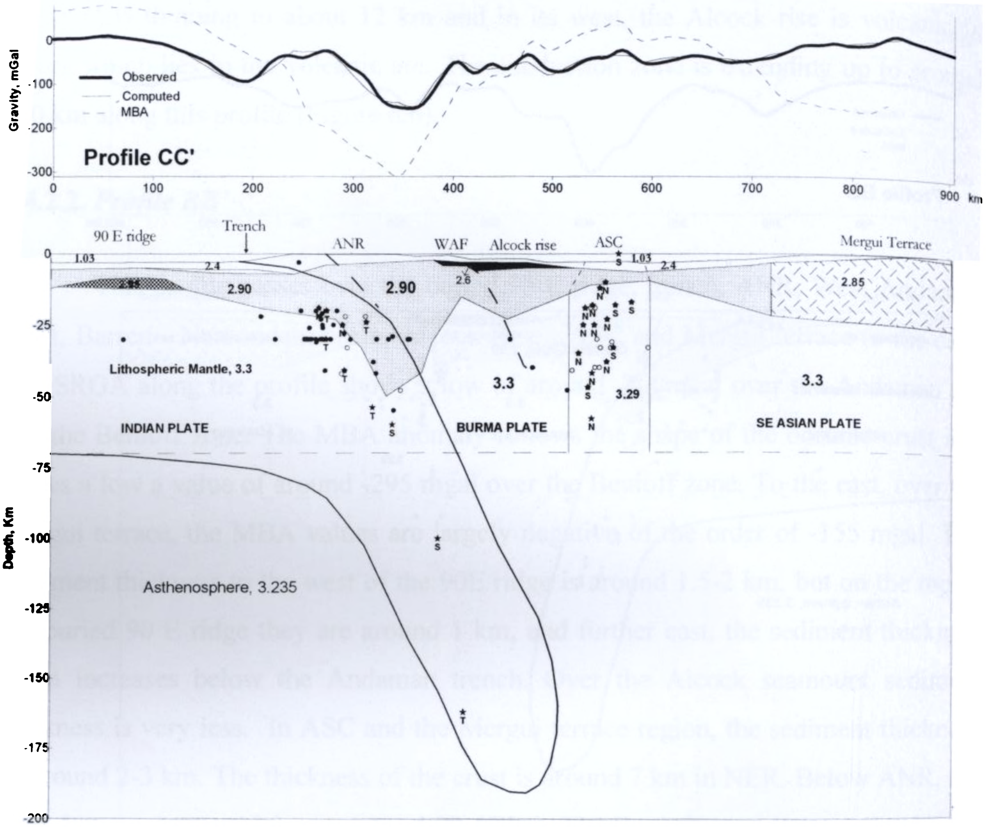

Figure 6.8. Gravity derived crustal models along the profiles CC' in the Andaman arc region. Open circles are events without any mechanisms, filled circles have focal mechanisms and stars are >5.5 magnitude events with type of faulting shown Thrust (T), Normal (N),Strike-slip (S)

mGal over the ANR. The MBA anomaly follows the shape of the oceanic crust and show a low a value of around -315 mGal over the Benioff zone. To the east, over the Mergui terrace the MBA values are largely negative of the order of -155 mGal. The Sediment thickness to the west of the trench region shows 2-3 km. Over the Alcock seamount sediment thickness is very less to the order of 1-1.5km. In ASC, the sediment thickness is around 3.5- 4 km. The thickness of the crust is around 7 km in

NER. Below ANR, the crust is maximum and around 40-47 km. The subducting plate penetrates to a depth of around 190 km. The post-tsunami seismic activity is confining along the Indian plate with most of the events showing predominantly thrust faulting. Few events occurring at a depth of around 40 km are seen to be related to after shock activity along the WAF. To the east of WAF, the Alcock rise is volcanic in nature. A thinned crust characterizes the ASC and shows many post-tsunami normal and strike-slip events. Under the Mergui terrace, the continental crust is having a thickness of around 20 km (Figure 6.8).

6.4.2.4. *Profile DD'*

This is an E-W Profile passing the 90 E ridge, trench, ANR, West Andaman Fault, ASC and Mergui terrace to the east. The SRGA values show a low of around -240 mGal over the ANR. The MBA anomaly show a broad low of around -315 mGal over the Benioff zone. To the east, over the Mergui terrace the MBA values are largely negative having the value of -155 mGal. The sediment thickness to the west of the trench is around 1.5 km. Nearly 2-2.5 km thick sediments are observed below ASC. The thickness of the crust is around 6-7 km in NER. Below ANR, the crust has a thickness of around 45 km. The WBZ is seen extending to a depth of 220 km. The post-tsunami earthquakes occur mainly in to the upper part of the Benioff zone as well as plate interior up to the location of trench. Most of the events are either thrust or strike-slip faulting. Good number of events occurs at a depth of around 30 km in the downward projection of WAF. In ASC, seismic activity is seen with most of the events showing normal mechanisms. Under the Mergui terrace, the continental crust is having a thickness of around 19- 20 km (Figure 6.9).

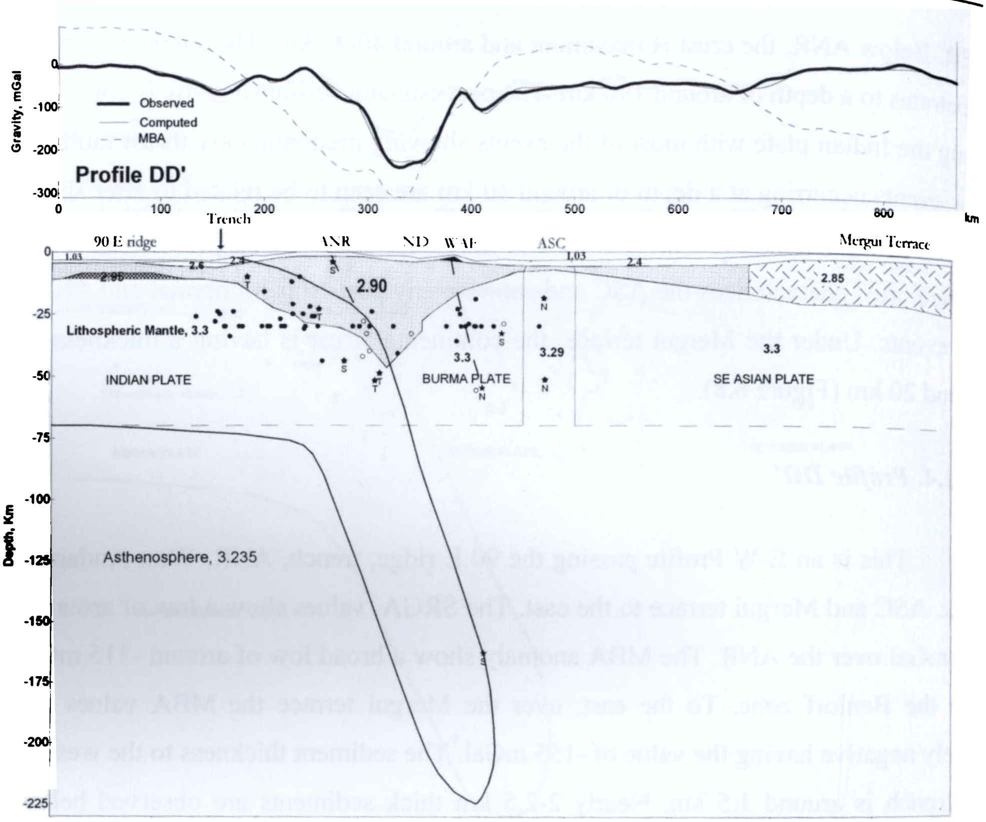

Figure 6.9. Gravity derived crustal models along the profiles DD' in the Andaman arc region. Open circles are events without any mechanisms, filled circles have focal mechanisms and stars are >5.5 magnitude events with type of faulting shown Thrust (T), Normal (N),Strike-slip (S)

6.4.2.5. *Profile EE'*

This profile passes over the 90 E ridge, trench, ANR, West Andaman Fault, Sewell Seamount, East Basin and Mergui terrace to the east. The gravity anomalies show a SRGA low of around -218 mGal over the ANR and a wider MBA low of -287 mGal over the Benioff zone. To the east, over the Mergui terrace the MBA values are

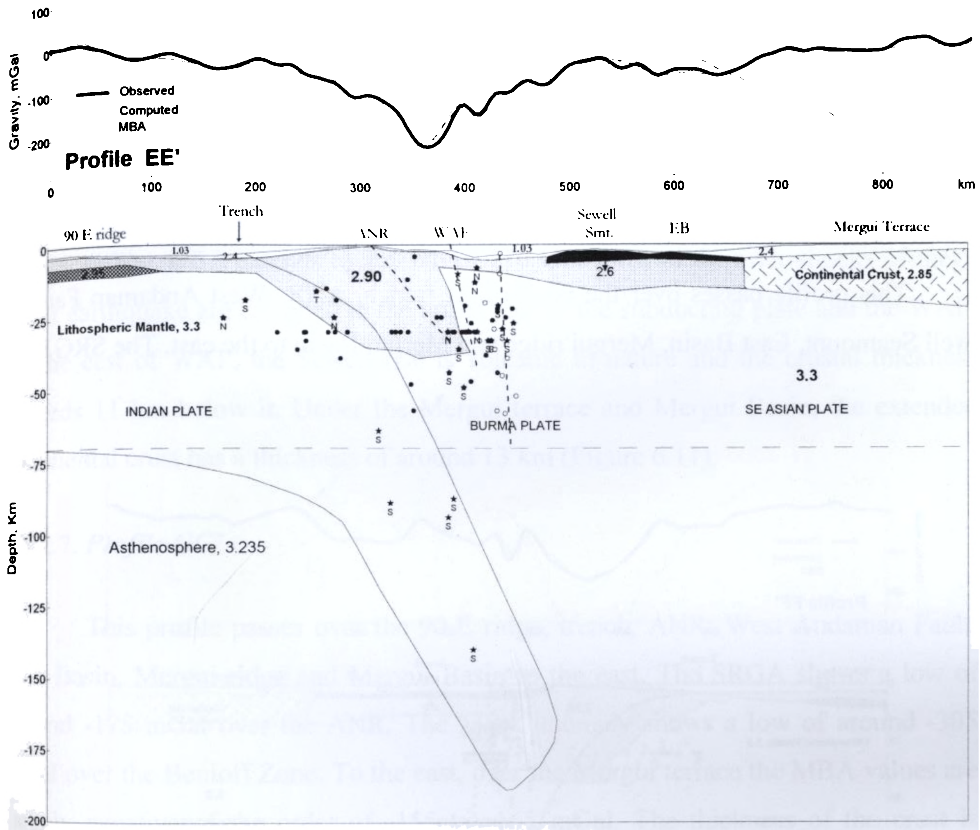

Figure 6.10. Gravity derived crustal models along the profiles EE' in the Andaman arc region. Open circles are events without any mechanisms, filled circles have focal mechanisms and stars are >5.5 magnitude events with type of faulting shown Thrust (T), Normal (N),Strike-slip (S)

largely negative of the order of -155 to -160mGal. Very thin sediments are observed over the NER. The thickness of the crust is around 7 km below NER. Below ANR, the crust is of 33-37 km thick. The post-tsunami events are characterized by predominantly strike slip events. The seismicity in the overriding plate shows that apart from WAF, the fault located below ANR also might be responsible for the seismic activity. To the east of WAF, the Sewell rise is volcanic in nature and the crustal thickness below it exceeds 15 km. Under the Mergui terrace, the continental crust is having a thickness of around 16 km (Figure 6.10).

6.4.2.6. *Profile FF'*

This profile passes over the 90 E ridge, trench, ANR, West Andaman Fault, Sewell Seamount, East Basin, Mergui ridge and Mergui Basin to the east. The SRGA

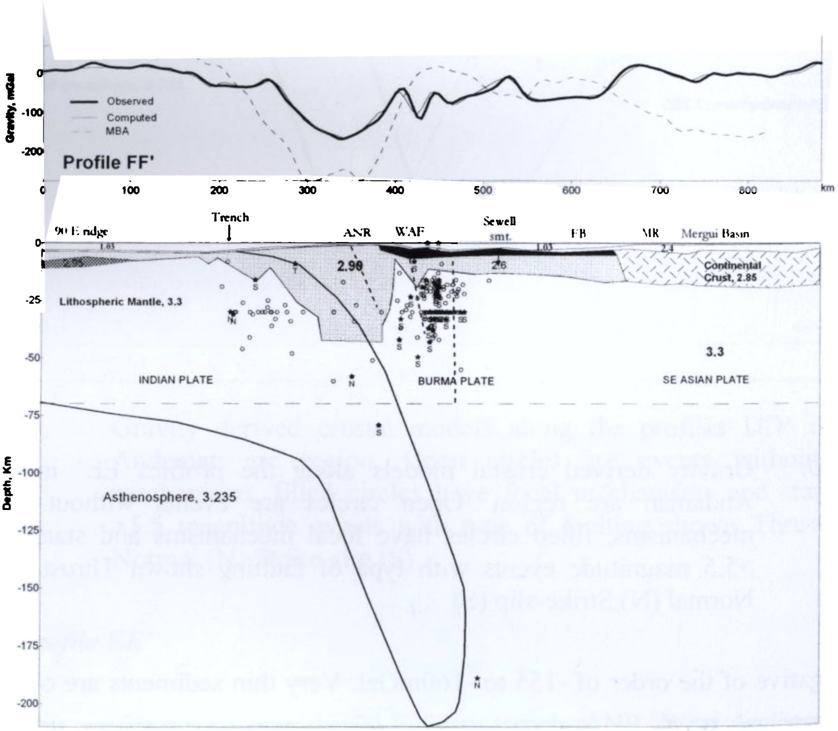

Figure 6.11. Gravity derived crustal models along the profiles FF' in the Andaman arc region. Open circles are events without any mechanisms, filled circles have focal mechanisms and stars are >5.5 magnitude events with type of faulting shown Thrust (T), Normal (N),Strike-slip (S)

shows a low of around -165mGal over the ANR. The MBA anomaly show a low of around -250 mGal over the Benioff zone. To the east, over the Mergui terrace the MBA values are largely negative of the order of -155 to -165 mGal. Over the NER, the sediments are practically absent. In the Mergui basin around 3 km thick sediments are present. The thickness of the crust is 7 km in NER. Below ANR, the crust is of 40 km thick. The WBZ extends to a depth of 210 km. Most of the after shocks of mega thrust earthquake are confined to the upper part of the subducting plate and the WAF. To the east of WAF, the Sewell rise is volcanic in nature and the crustal thickness exceeds 11 km below it. Under the Mergui terrace and Mergui Basin, the extended continental crust has a thickness of around 13 km (Figure 6.11).

6.4.2.7. *Profile GG'*

This profile passes over the 90 E ridge, trench, ANR, West Andaman Fault, East Basin, Mergui ridge and Mergui Basin to the east. The SRGA shows a low of around -175 mGal over the ANR. The MBA anomaly shows a low of around -305 mGal over the Benioff Zone. To the east, over the Mergui terrace the MBA values are largely negative of the order of -155 to -165 mGal. The thickness of the crust is around 10 km in NER. Below ANR, the crust has maximum thickness of around 40 km. The Benioff zone extends up to a depth of 240 km. The post-tsunami events in the region are characterized by thrust and strike-slip in the WBZ as well as in the plate interior. Strong seismicity is seen along the WAF region and suggest that the after shock events propagated through the WAF. The crustal thickness under the East basin is around 10 km. Under the Mergui terrace and Mergui Basin, the continental crust has a thickness of around 16 km (Figure 6.12).

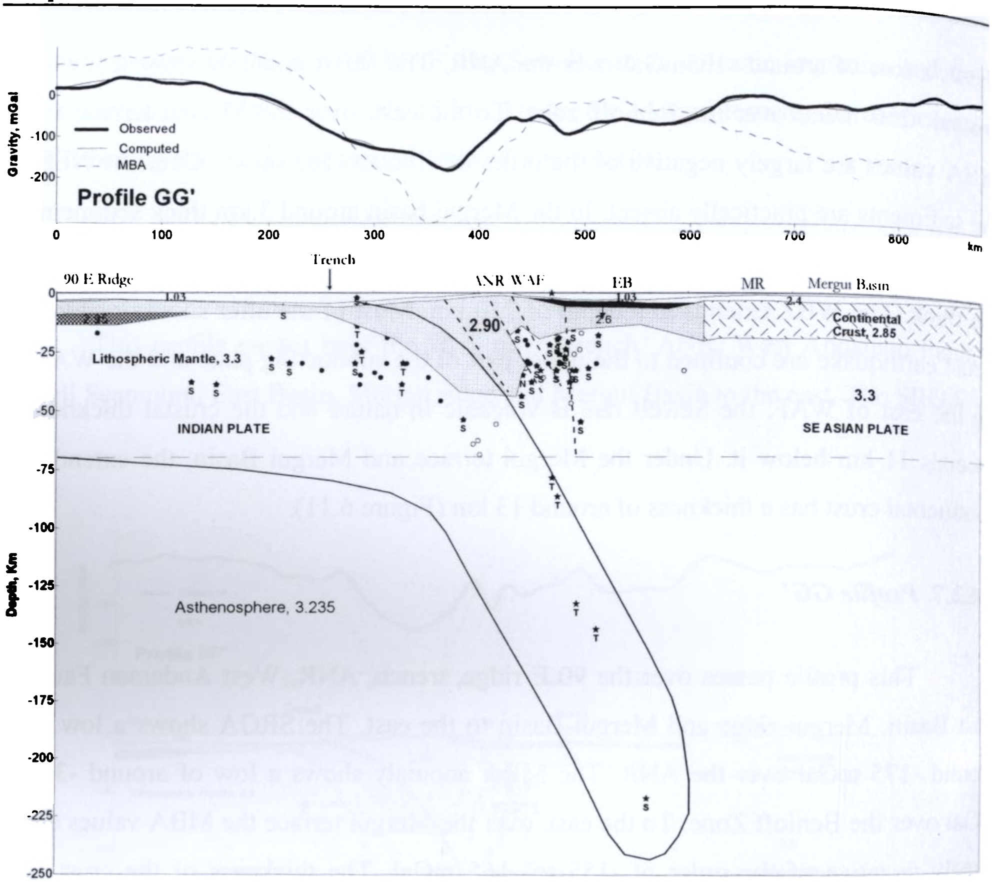

Figure 6.12. Gravity derived crustal models along the profiles GG' in the Andaman arc region. Open circles are events without any mechanisms, filled circles have focal mechanisms and stars are >5.5 magnitude events with type of faulting shown Thrust (T), Normal (N),Strike-slip (S)

6.4.2.8. *Profile HH'*

This profile passes over the 90 E ridge, trench, ANR, West Andaman Fault, North Sumatra Ridge, SFS, East Basin, Mergui ridge and Mergui Basin to the east. The SRGA shows a low of around -175 mGal over the ANR. The MBA anomaly show a low of around -270 mGal over the Benioff zone. To the east, over the Mergui

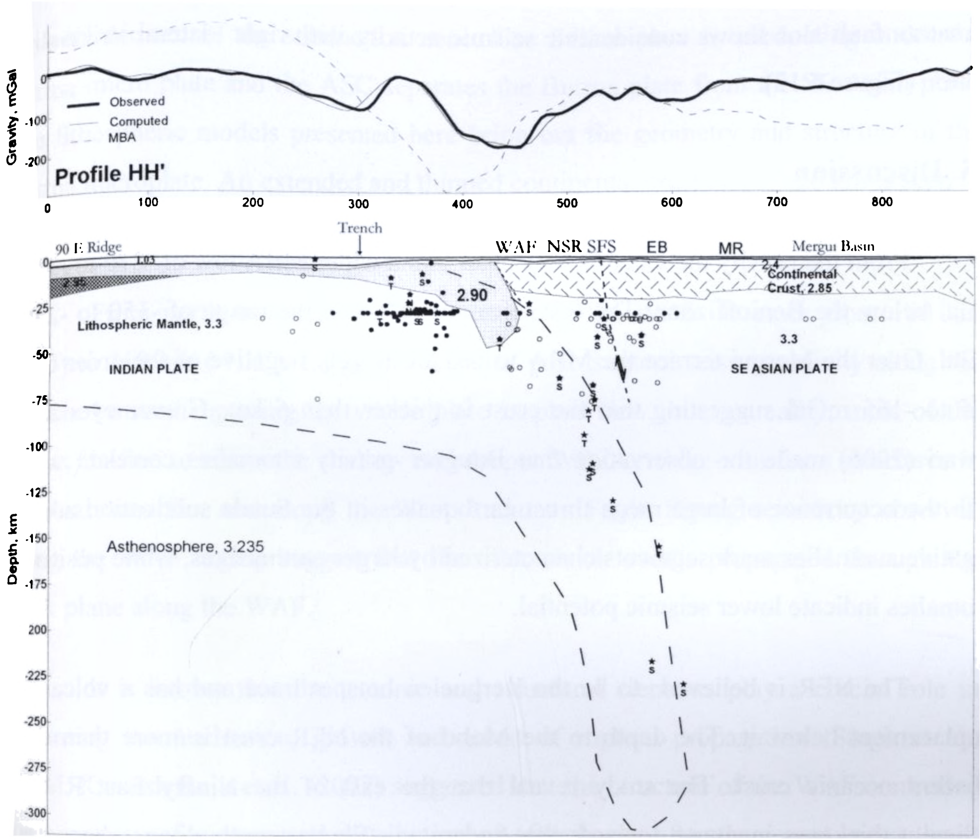

Figure 6.13. Gravity derived crustal models along the profiles GG' in the Andaman arc region. Open circles are events without any mechanisms, filled circles have focal mechanisms and stars are >5.5 magnitude events with type of faulting shown Thrust (T), Normal (N),Strike-slip (S)

terrace, the MBA values are largely negative of the order of -155 to -165 mGal. The thickness of the crust is around 16 km in NER. Below ANR, the crust has maximum thickness of around 43 km. The WBZ below ANR extends up to 310 km. Many strike slip and thrust faulting events are seen within the WBZ and plate interior. The

Sumatran fault alos shows considerable seismic activity with right –lateral strike-slip motion (Figure 6.13).

6.5. Discussion

From the gravity models it is very clear that a wider MBA low of -270 to -315 mGal below the Benioff zone. The SRGA are also low in the range of -150 to -240 mGal. Over the Mergui terrace the MBA values are largely negative of the order of -155 to -165 mGal suggesting that the crust is thicker than 6 km. Grevemeyer and Tiwari (2006) made the observation that Bouguer gravity anomalies correlate well with the occurrence of large mega thrust earthquakes in the Sunda subduction zone; negative anomalies mark segments characterized by larger earthquakes, while positive anomalies indicate lower seismic potential.

The NER is believed to be the Kerguelen hotspot trace and has a volcanic emplacement below it. The depth to the Moho of the NER crust is more than the adjacent oceanic crust. The study reveal that the east of the Ninety East Ridge sediment thickness increases towards the Andaman – Sunda trench slope, where the sediments are accreted and are much deformed, with thickness of the order of 9- 10 km as also observed by Curray et al. (1982) from seismic reflection and multi channel seismic data. The seismic refraction studies by Moore and Curray (1980) and Kieckefer et al. (1980) in the Sunda fore arc region indicate a thick crust of 40 km in the fore arc region which thins towards Sumatra main land to 25 km. From the models (AA' to HH'), it can be seen that the crust exceeds thickness of 40 km at few places under the ANR. Crustal thinning is observed below the back arc spreading ridge. This back arc spreading ridge bisects the Andaman volcanic arc in the Central Andaman Sea between Barren and Sewell seamounts and is characterized by normal and strike-slip events. The Sewell and Alcock seamounts are volcanic in origin as it is lying in the volcanic arc of the subduction zone. The Indian plate is subducting under the Burma micro plate and the ASC separates the Burma plate from the SE Asian plate. The lithospheric models presented here bring out the geometry and structure of the Burma microplate. An extended and thinned continental crust of 15 – 20 km is seen to be present below the Mergui terrace.

From north to south, the depth extent of the WBZ increases from 140 km (AA') to 310 km (HH'). Large incidence of post-tsunami seismic activity along the arc can be seen rupturing the whole plate in plan view, but, in reality, most of the events confine to either the shallow and deeper WBZ or ridge-transform structures in the Andaman Sea and along the West Andaman Fault. Strong seismicity observed along the WAF region suggest that the after shock events propagated through the weak plane along the WAF.

It is known that the tectonic and structural elements play a crucial role in governing the nucleation, growth and arrest of rupture propagation (Singh et al., 2005). Kamesh Raju et al. (2007) suggested that the structure of the WAF controlled the geometry of rupture and distribution of aftershocks after the recent mega thrust earthquake of 26 December 2004. Sieh and Natawadjaja (2000) pointed out that lithospheric boundaries in the upper plate play a key role in the size and nature of mega thrust earthquakes. The aftershock pattern in the Andaman region indicates the influence of lithospheric plate boundaries which was confirmed through the gravity models presented here and also by Kamesh Raju et al. (2007). However, more detailed marine geophysical studies and GPS measurements are necessary to understand the structure and tectonics of this highly complex segment of the convergent plate boundary.

CHAPTER 7

SUMMARY AND CONCLUSIONS

The Burmese- Indonesian arc system extends from the Eastern Himalayan syntaxis southward through Burma, Andaman-Nicobar, Sumatra and eastward through Java to at least Sumba. The eastern edge of the Indo-Australian plate is being subducted beneath the Burmese plate along the Sunda subduction zone. This region is a classical example of a subduction system, composed of the down going Indo-Australian slab along the Andaman-Sumatra-Java trench, an accretionary wedge, the outer arc ridge, the Bengkulu - Mentawai fore arc basin off Sumatra and Java fore arc basin in front of the volcanic arc. The Andaman – Burmese arc system serves as an important transitional link between the Himalayan collision zone to the north and the Sumatra – Java trench system in the south. The Andaman Sea is an extensional basin marking the edge between the China and Burma plates. The zone of active convergent margin along the Andaman – Sumatra-Java arc in the eastern Indian Ocean is geodynamically quite complex and interesting in view of wide variation in subduction geometry, morphology and stress field in both along and across the arc and the presence of active back arc spreading in the Andaman Sea.

Major tectonic features in the eastern Indian Ocean were inherited from the break-up of the eastern Gondwanaland and subsequent spreading of the Indian Ocean floor. Some of these features which are important in the evolutionary history of the region are: (1) the large sediment filled basin called the Bengal fan in the Bay of Bengal, 2) the ninety east ridge, a 4500 km long aseismic ridge trending N – S along the 90° E meridian (3) The fold mountain belt of Andaman and Indo-Burman ranges formed by eastward subduction and motion along the Shan-Sagaing transform and the Neogene back arc spreading in the Andaman Sea (4) the Sumatran fault Zone (SFZ), a northwest trending active strike-slip fault that cuts the entire length of Sumatra and Indonesia (5) Java onshore region termed as Java Fault Zone (JFZ) (6) Sumatran fore arc sliver plate consisting of Mentawai fault zone (MFZ) (7) The offshore Java fore arc region, which is characterized by typical fore arc basins and (8) The Sunda strait, which is considered as a transition zone between the normal subduction in front of Java to the east and oblique subduction to the west. Most of these features came into existence during the northward flight of India since the late Cretaceous.

The evolutionary history of the Indian Ocean can be described in different phases. The first phase of spreading started in northwest-southeast direction and resulted in India's movement away from Antarctica-Australia during early Cretaceous. This resulted in the formation of the Mesozoic basins along the western Australian margin, and the eastern Indian margin as evidenced by the Mesozoic anomaly sequences M11 through M0. During middle Cretaceous, the Indian plate rotated from its early NW-SE to N-S direction and moved at a slow spreading rate. During this period, the Cretaceous quiet/smooth zone (118-84 m.y) crust evolved in the distal Bengal Fan. Northward movement of Indian plate away from Antarctica took place during middle Cretaceous to middle Eocene. The first major reorganization of the plates took place during middle Cretaceous time, evidenced by the change in India's motion from northwest –southeast to north–south. The second phase of spreading started in the N-S direction and continued up to formation of anomaly 19 (about 24 m.y) in the Central Indian Ocean. During this period, India drifted in the N-S direction from Antarctica with a rapid speed of 11 to 7 cm/yr. The magnetic lineations 34 through 19 have evolved in the east-west direction with large lateral offsets, giving rise to the major fracture zones. During this phase of drifting, major parts of the Central Indian and Crozet basins have evolved. The initiation of seafloor spreading between Australia and Antarctica and the opening of Wharton basin also took place during this period. The second major plate reorganization occurred in the middle Eocene time when Indian and Australian plates merged and formed as a Single Indo-Australian plate (magnetic anomaly 20 to 18). The third phase of spreading initiated in northeast-southwest direction in the middle Eocene and appears to continue since then. The Australian and Antarctica basins were formed along the SE Indian ridge (SEIR) in the third phase.

The 2004 and 2005 witnessed two mega earthquakes that have ruptured the boundary between the Indo-Australian plate, which moves generally northward at 40-50mm/yr, and the southeastern portion of Eurasian plate, which is segmented into the Burma and Sunda sub plates. East of Himalayas, the plate boundary trends southward through Myanmar, continuing offshore as a subduction zone along the Andaman-Nicobar islands and further south to Sumatra, where it turns eastward along the Java trench. This zone of convergence is characterized by the occurrence of numerous earthquakes, both shallow and deep. The area is a classical example of a subduction system, composed of the down going indo-Australian slab along the Sumatra-Java trench, an accretionary wedge, the outer arc ridge forming the backstop, the Bengkulu- Mentawai fore arc basin off Sumatra and Java fore arc basin in front of the Volcanic arc. The Andaman – Sumatra- Java arc system has evolved through mainly subduction related processes responding kinematically to the plate reorganizations and other tectonic adjustments taking place during the evolution of the Indian Ocean as well as the Philippine Sea region.

The geometry of the subduction plate varies as it comes from Andaman to Java as the sediment thickness of the subducted plate decreases. Off Java, it is covered by only few hundred meters of sediments, whereas, off Sumatra it exceeds 1km and at the head of the Bay of Bengal the sediments are thicker by an average of

10 km. West of the Andaman arc, the Ninety East ridge continues subsurface below the Bay of Bengal sediments up to 17^{O} N. Geophysical studies indicate that the ridge could be a hot spot trace. Refraction data suggests that off southern Sumatra, in the arc region, the basement is continental whereas, off western Java it changes to oceanic. The outer high, which represents the fossil part of the accretionary wedge, is of Eocene-Oligocene age. The Andaman – Nicobar ridge is believed to have formed in Oligocene – Miocene times due to east – west compression of sediments derived from the Malayan shelf. The age and thickness of the subducted oceanic crust and the convergence rate increase from Andaman towards Java along the arc. The increasing dip and depth of penetration of the Benioff zone reflects this change as well as changes in slab geometry. Oblique, but predominantly thrust motion occurs in the Andaman trench with a convergence rate of about 1.4cm/yr. The Andaman back arc spreading ridge-transform system accommodates the remaining plate motion, joining with the Sumatra fault to the south. The subducting oceanic crust off Sumatra is 46-60 my old and has a present convergence rate of 6.81cm/yr, while the crust off Java with an age ranging from 70 to 100 m.y converges at a rate of 7.23 cm/yr. The slab configuration is ambiguous in the northern Sumatra, where as, in the south the observed dip is 40-50^{O}. West of Sunda strait, seismic activity does not extend below 300 km. But by Java, seismic activity extends from the surface to a depth of 650 km with a gap in seismicity between 300 and 500 km. As a result of highly oblique motion between the Indo-Australian plate and the Eurasian plate, a plate sliver, referred to as the Burma micro plate, has sheared off parallel to the subduction zone from Myanmar to Sumatra.

Though many of these previous geophysical investigations have brought out significant variations on the tectonics operative in different segments of the arc, a unified picture through detailed Seismotectonic regionalization to understand the upper plate deformation, geometry of the subducting lithosphere is required. The recent mega thrust earthquake of 26 December 2004 has devastated the region and strongly ruptured plate boundary over a length of 1300 km along the Andaman-Sumatra arc. This resulted in a need for reassessment of the long-term deformation pattern as well as understanding the crustal mass anomalies in this segment of the arc.

In the present study, detailed analysis of earthquake hypocentral parameters and source mechanisms of large number of seismic events have been carried out in order to understand the configuration of the Benioff zone and the deformation pattern varying with depth in various segments of the arc; Seismotectonic regionalization of the upper plate seismicity and the variations in deformation pattern both along and across the arc; crustal structure and density heterogeneities and its relation with seismogenic behaviour along the arc.

The occurrence of deep and intermediate depth earthquakes along a trench – arc system marking slab like geometry of the descending oceanic lithosphere essentially result from compressional / extensional stresses aligned parallel to the slab. This inclined seismic zone associated with all trench-arc systems world over is called as the Wadati-Benioff Zone (WBZ) and knowledge on state of stress in these zones is important in understanding the geodynamic processes along convergent margins in general, and ongoing tectonic deformation within the upper plate, in particular. The latter aspect is more significant due to the fact that the negative buoyancy of the dense rocks of the descending lithosphere results n a downward body force which gets transmitted to the surface plate. Earthquake focal mechanism solutions give valuable information on the state of stress and their spatial variations, in turn, help to identify contortions and disruptions in the descending lithosphere. The focal mechanisms in the WBZ in general show the following pattern: i) either P- or T- axes are parallel to the dip of the WBZ ii) slab-dip-parallel compression in the deepest parts of the WBZ iii) slab-dip-parallel compression or extension in the intermediate parts of the WBZ.

However, deviations from this general pattern have been observed in the WBZ of various arc systems.

As already stated the Sunda arc region is seismically active and characterized by the occurrence of shallow as well as deeper earthquakes. A compilation of both historical and recent events has been made from the NOAA epicentral listing during 1900-2005. As the events related to the upper plate mostly confine to depths < 70 km, they have been divided into shallow ($\leq$ 70 km) or deeper WBZ events (> 70 km) for the purpose of distinguishing between upper plate and subducted plate events. To study the spatial variations in deformation process in the overriding and subducting plates as a function of depth, the hypocenters and focal mechanisms have to be projected normal to the trench to have a side perspective. All the events of magnitude > 4.5 and located by at least 10 stations have been considered and the events have been projected on cross sections curving along the arc. The focal mechanism solutions have been shown on the sections by orienting parallel to the azimuth of the cross section. The region was divided into a number of rectangular shaped blocks based on the density and spread of seismic events. As far as possible, the blocks have been considered of uniform width. The 27 seismologic depth sections have been prepared (A1 – A11 in Andaman arc; S1 – S8 in Sumatra arc; SS1- in Sunda Strait; J1 – J7 in Java arc) by projecting all events as well as mechanisms pertaining to the block on to a line in the center of each block. The depth sections thus prepared are utilized to investigate, the average dip of the Benioff zone in the different parts of the arc; the penetration depth of the subducting lithosphere; and, the subduction zone geometry.

It can be seen from the sections that the WBZ is characterized by variable seismic incidence and depth of penetration in different segments of the arc. Depth of penetration in general increases from Andaman arc in the north to Java arc towards southeast. In the Andaman arc and part of Sumatran arc in the north (between A1 –

S3), the depth of WBZ varies from 150 km in the north to 250 km in the south. In southern Sumatra (S4 – S8), the depth extent of WBZ varies between 250 – 350 km. Deep seismicity has not been observed anywhere below Andaman as well as Sumatran arcs. Deep earthquakes start to appear beyond 105° between Sunda Strait and Java arc region where earthquakes in the WBZ occur at a depth of 600 to 650 km. However, a gap in seismic activity at intermediate depths is noticed in the Java arc region. The depth range over which this gap extends is seen to vary for different sections of the arc, but, generally in the range of 300-550 km. An analysis of all 27 depth sections suggests that the seismic activity appears continuous up to a depth of 300 km within the upper part of the subduction zone. However, a closer look of seismic activity within the top 300 km revealed the presence of an aseismic gap in the WBZ along the Sumatran subduction zone at variable depths of 90 – 220 km having variable thicknesses and such aseismic gap has been previously observed for a section along the Andaman subduction zone at a depth range of 90 – 110 km. Probing of such aseismic gaps in the WBZ of major subduction zones world over confirmed their spatial correlation with volcanic activity and occur below or in the near vicinity of active volcanoes. The presence of such aseismic gaps has been interpreted due to the presence of partial melt domain in the WBZ where the conditions for generating strong earthquakes are not fulfilled or in a way indicate loss of brittle character of the slab at the respective depth.

The dip of the WBZ varies considerably, but not systematically, all along the Sunda arc. In general smaller dip of the Benioff zone is usually accompanied with shallow penetration depth, but there are some exceptions also. In the northern Andaman (A1 – A3), the Benioff zone dip varies between 43° to 53°, while, in south Andaman- north Sumatra (blocks A4- A11), the dip is in the range 38°-50°. Along the Sumatran arc, the dip of the Benioff zone ranges between 40° to 50°. In the Java arc region, the dip of the Benioff zone is around 50° in the upper part.

The geometry of the WBZ and the variations in deformation pattern both along and across the Andaman-Sumatra-Java arc reveal the characteristics of active subduction in the region. The deformation field suggests that a pure normal subduction dominated by thrust faulting in the Java region, becomes progressively oblique towards Sumatra and the Andaman arc, characterized by thrust faulting and right-lateral shear motions in Sumatra region, and dominantly strike-slip and normal faulting in the Andaman region.

Based on the previous studies and seismicity pattern, several broad distinct seismogenic belts/sources have been identified to estimate the active crustal deformation for each of these sources based on method of summation of moment tensors. These are 1) the outer arc region consisting of Andaman-Nicobar islands 2) the back arc Andaman Sea 3) The Sumatran fault zone (SFZ) 4) Java onshore region termed as Java Fault Zone (JFZ) 5) Sumatran fore arc sliver plate consisting of Mentawai fault (MFZ) 6) The offshore Java fore arc region 7) The Sunda Strait region. For belts 3 and 4, the boundaries have been considered from previous studies. The offshore belts 5 and 6 have been extended up to the deformation front below the Sumatra-Java trench. For each of these four belts, we need to identify seismogenic sources. As the seismicity is variable, it is difficult to demarcate individual seismogenic sources. Hence, we employed a moving window method having a window length of 3 - 4^0 and with 50% overlapping starting from one end to the other. The advantage in this method is that we obtain a continuous variation in deformation pattern along the length of active seismic belts and also selecting a different window length does not alter the deformation pattern significantly. We succeeded in defining 4 sources each in the Andaman fore arc and Back arc region, 9 such sources (moving windows) in the Sumatran Fault zone (SFZ), 9 sources in the offshore SFZ region and 7 sources in the offshore Java region. Because of the low seismicity along JFZ, it is separated into three seismogenic sources namely West Java, Central Java and East Java. The Sunda strait is considered as a single seismogenic source.

The results of the deformation studies in the Andaman – Sumatra – Java arc region are consistent with the overall tectonics of the region. The deformation pattern indicates the dominance of compressive stresses in the fore arc region with the direction of maximum compression in almost NNE – SSW. While, it is almost normal to the trench in the Sumatran fore arc near Nias island region, the compression takes more oblique trend with respect to the trench towards north near Andaman Islands. The deformation studies shows a compression of 0.2 – 0.5 mm/ yr along a mean direction of N55° and extension of 0.4 - 0.7 mm/yr along a mean direction of N320° along and across the Andaman spreading ridge.

Due to oblique subduction and extension in the north, Sumatra, and the Sumatran fore arc, is divided into a series of NW–SE striking slices that move towards the northwest, separated by right-lateral faults. Most displacement on these faults occurs in northwest Sumatra and dissipates towards the southeast. Geodetic observations from GPS data reveal an interesting change in Sumatran fore arc motion centered on Batu Island. Southeast of Batu Island, the Sumatra fore arc moves northeast, roughly parallel with the motion of the Indian plate, while northwest of Batu Island the Sumatran fore arc moves to the northwest. This change in fore arc motion has been attributed to decoupling between the northern fore arc and mantle wedge due to increased pore pressures in the fore arc thrust fault due to subduction of thick Nicobar fan sediments. The Wharton Ridge subducts beneath Nias Island where seismic deformation is highest and the IFZ subducts directly beneath Batu Island where the Sumatran fore arc begins to move in a northwest direction. Thus, subduction of the Wharton Ridge and IFZ is another mechanism causing the high seismic deformation rates, change in fore arc motion, and concentration of strike-slip motion that occurs in northern Sumatra. It is possible that present-day compression from subduction of the Wharton Ridge and Investigator Fracture Zone dominates over extension resulting from the retreating upper plate. It is likely that this domination of compressive strain related to bathymetric ridge subduction has dominated over upper plate motion related extension since 15 Ma. The Roo Rise is presently being subducting adjacent to Java. Subduction of this major bathymetric feature is currently causing deforming the Javanese fore arc (Kopp et al., 2006). Roo Rise subduction is likely to be contributing to Javanese compression in addition to compression caused by upper plate advance since 15 Ma (Whittaker et al, 2007).

On 26 December 2004, a subduction zone earthquake of magnitude Mw ~ 9.3 struck off the coast of northern Sumatra. The rupture propagated unilaterally to the north for over 1200 km to the Andaman Islands. A second thrust event of Mw ~ 8.7 occurred on 28 March 2005, about 300 km to the east south east of the previous earthquake. These earthquakes occurred as a result of the subduction of Indo-Australian plate beneath Sumatra in an approximately NE direction at a rate of 60 mm/yr at an oblique angle to the Java trench. Oblique, but predominantly thrust motion occurs in the Andaman trench with a convergence rate of about 14 mm/yr. The width of the rupture zone of the 26 December 2004 event is approximately 100 km and maximum slip is approximately 20m. The movement of the seafloor all along the rupture zone and the vertical uplift displaced a huge volume of water, which caused the tsunami. But the rupture of this event didn't progress further to the S-SE despite high rapid slip at the beginning of the rupture, which indicates that the rupture front hit a barrier in this direction that broke three months later on 28 March 2005. a detailed analysis of changes in long-term seismic deformation (pre- and post-tsunami) has been carried out along the Andaman-Sumatra arc mainly for two reasons, i) to study the changes that were brought out in the deformation due to intense post-tsunami seismic activity along various segments of the arc, ii) to update the long-term deformation pattern which will be useful to identify areas of increased future seismic hazard along and across the arc.

A close examination of the moment release rates of both periods gives an idea on level of seismic activity in each of the source (window) regions. Those sources where significantly large earthquakes occurred in the post-tsunami period show large moment rate values, whereas the sources in which post-tsunami activity is negligible, the moment rate is reduced because of averaging over a long period. In the Andaman region, the fore arc region shows considerable moment release variation, whereas in the back arc region, the moment release rate is not very significant. Though several normal faulting events occurred along the Andaman spreading ridge after the mega thrust earthquake, their moment contribution is low. In the Sumatran region, where both 26 December 2004 and 28 March 2005 events were located, very high moment release rate has been observed in the offshore Sumatra between 2°S – 5°N. Along the Sumatran Fault Zone, the moment release rate is significant in the southern part, while southern most and northern parts of the SFZ remained less affected by large scale deformation in the fore arc region.

In order to have a better understanding on crustal structure in the Andaman arc and surrounding areas, we considered detailed three-dimensional configuration of the subducting slab from the Benioff zone geometry drawn along the 11 sections. Generally, high-resolution slab configuration in the trench-arc regions is possible through micro earthquake investigations or other seismological studies. Such data are absent for Andaman arc region due to linear disposition of Andaman and Nicobar islands along the arc and non-availability of azimuthally covered seismic stations data from the surrounding continents. Therefore, the hypocentral distribution of earthquakes provide, as a first approximation, the three dimensional configuration of the subducting lithosphere in the region. The isodepth contour map of top surface of the subducting slab indicates that the depth of the slab varies from 80-220 km with maximum penetration depth in the south Andaman Sea. We calculated the gravity anomaly of the three- dimensional Subducting slab. For this purpose, we divided the slab into several horizontal cross-sections defined by the depth contours. The gravity effects of these horizontal laminae or cross-sections are calculated and numerically integrated over depths from top to the deepest point. We considered the 5km x 5km gridded points covering the study area for calculating the total gravity effect of the slab. The density contrast between the lithospheric slab and the asthenosphere is considered as 0.065gm/cm^3. The lithospheric plate thickness in the Andaman arc region is considered as 80 km from the surface wave dispersion studies in the northeastern Indian Ocean. The computed slab anomaly depends on the choice of various parameters such as the density contrast, subducting plate thickness, slab thinning and phase transitions within the slab, out of which, the density contrast and plate thickness have dominant effect. The slab gravity anomaly map computed for the Andaman arc region reveal a smooth, long wavelength and symmetric gravity high of maximum 85 mGal centered just east of Nicobar islands region. The trends of the gravity high contours align along the Nicobar deep in the east of Andaman- Nicobar islands. The slab contribution is ~ 20 mGal in the trench region and 5-10mGal in the Malayan margin far east of the Andaman arc.

The free air anomaly map is dominated in general by the gravity attraction of the density contrast at the seafloor. The subsurface density structure can be investigated by applying mantle Bouguer correction. The predicted gravity signal of the seafloor-water interface and crust-mantle interface assuming a constant thickness crustal layer of 6 km is obtained using the Fourier transform method of PARKER. This gravity effect when subtracted from the free-air gravity will give rise to Mantle Bouguer anomalies (MBA), a useful tool to decipher crustal thickness variations. The MBA map shows a high anomaly coinciding with the Ninety East Ridge, a broad and continuous gravity low zone between the trench and the arc, a gravity high over the Andaman spreading ridge flanked by minor negative anomalies over the Alcock and Sewell rises, and large negative anomalies in the eastern part of study region over the Malayan shelf. While, low MBA areas reflect the crustal thickening or presence of low-density crustal material, the positive MBA values indicate crustal thinning or densification of the crust.

From the gravity models it is very clear that the MBA anomaly closely follows the shape of the oceanic crust with a value which is too low as -270 to -315 mgal over the Benioff zone. Here, the free air anomaly values are also low in the range of -150 to -240 mgal. Over the 90°E ridge, the MBA values are positive which shows larger values than the free air gravity values. Over the Mergui terrace the MBA values are largely negative of the order of -155 to -165 mgal. It is known that Bouguer gravity anomalies correlate well with the occurrence of large mega thrust earthquakes in the Sunda subduction zone; negative anomalies mark segments characterized by larger earthquakes while positive anomalies indicate lower seismic potential. The Indian plate is subducting under the Burma micro plate and the ASC separates the Burma plate from the SE Asian plate. The lithospheric models presented here bring out the geometry and structure of the Burma microplate. An extended and thinned continental crust of 15 – 20 km is seen to be present below the Mergui terrace. It is known that the tectonic and structural elements play a crucial role in governing the nucleation, growth and arrest of rupture propagation. The aftershock pattern in the Andaman region indicates the influence of lithospheric plate boundaries which was confirmed through the gravity models presented in the thesis.

REFERENCES

Aki, K., and Richards, P., 1980. Quantitative Seismology, Theory and methods. Freeman, San Francisco, C.A. 557.

Apperson, K. D., and Frohlich, C., 1987. The relationship between Wadati-Benioff zone geometry and the P, T and B axes of intermediate and deep focus earthquakes, J. Geophys. Res., 92 (B13), 13821-13831.

Argus, D. F., and Gordon, R. G., 1991. No-Net-Rotation Model of Current Plate Velocities Incorporating Plate Motion Model Nuvel-1, Geophys. Res. Lett., 18, 2038-2042.

Arifin L., Tamaki K., Kisimoto K., Yokokuraf T., Okuda Y., 1987. Seismic reflection of the Sunda trench in Western Java. CCOP Technical Bulletin, 19, 13-23.

Banerjee, P., Pollitz, F. F. and Burgmann, R., 2005. The size and duration of the Sumatra-Andaman earthquake from far-field static offsets. Science, 308, 1769-1771.

Baroux, E., Avouc,J-P., Bellier O., and Sebrier M., 1998. Slip partitioning and forearc deformation at the Sunda trench, Indonesia. Terra nova, 10 (3), 139-144

Beaudry, D., and Moore, G., 1981. Seismic-stratigraphic framework of the forearc basin off central Sumatra, Sunda Arc, Earth planet. Sci.Lett., 54, 17–28.

Beaudry, D., & Moore, G., 1985. Seismic stratigraphy and Cenozoic evolution of West Sumatra forearc basin, Am. Assoc. Petrol. Geol. Bull., 69, 742–759.

Bellier, O., Sebrier,M., 1994. Relationship between tectonism and volcanism along the Great Sumatran Fault zone deduced by SPOT image analyses. Tectonophysics, 233, 215-231.

Bellier, O., Sebrier,M., 1995. Is the slip rate variation on the Great Sumatran Fault accommodated by fore-arc stretching?. Geophysical research letters, 22, 1969-1972.

Bergman, E. A., and Solomon, S. C., 1990. Earthquake Swarms on the Mid-Atlantic Ridge: Products of Magmatism or Extensional Tectonics? J. Geophys. Res. 95, 4943–4965.

Bevis, M., and Isacks, B., 1984. Hypocentral trend surface analysis: Probing the geometry of Benioff Zones. Journal of Geophysical Research 89(B7): doi: 10.1029/0JGREA0000890000 B7006153000001. issn: 0148-0227.

Bilham R., Engdahl, E. R., Feldl, N., and Satyabala S. P., 2005. Partial and Complete Rupture of the Indo-Andaman plate boundary 1847-2004. Seism. Res. Lett.

Bilham, R., 2005. A Flying Start, Then a Slow Slip. Science. 308, 1126-1127.

Bina, C. R., and Okal, E.A., 1998. Investigating the depth of the deepest deep earthquakes. Abstracts of the Sixth Symposium of Study of the Earth's Deep Interior (SEDI), Tours, France, 119.

Biswas, S., Majumdar, R.K., and Dasgupta, A., 1992. Distribution of stress axes orientation in the Andaman-Nicobar island region, a possible stress model and its significance for extensional tectonics of the Andaman Sea. Phys. Earth Planet. Inter: 70, 57-63.

Brune, J. N., 1968. Seismic moment, seismicity, and rate of slip along major fault zones, J. geophys. Res., 73, 777-784.

Brune, J.N., Brown, S., Johnson, E A., 1993. Rupture mechanism and interface separation in foam rubber models of earthquakes: a possible solution to the heat flow paradox and the paradoxof large overthrusts. Tectonophysics 218, 59-67.

Cande, S.C., and Mutter, J.C., 1982. A Revised Interpretation of Seafloor Spreading Magnetic Anomalies between Australia and Antarctica, Earth and Planet. Sci. Lett., 58, 151-160.

Catherine, J. K., Gahalaut, V. K. and Sahu, V. K., 2005. Constraints on rupture of the 26 December 2004, Sumatra arthquake from farfield GPS observations. Earth Planet. Sci. Lett., 237, 673-679.

Chandra, U., 1984. Tectonic segmentation of the Burmese Indonasian arc. Tectonophys, 105, 279-289.

Chatterjee, P.K., 1967. Geology of the main Islands of the Andaman area. Proc. Symp. Upper mantle project, Hyderabad, India, 348 - 362.

Chung, W.-Y., and Kanamori, H., 1978a. A mechanical model for plate deformation associated with aseismic ridge subduction in the New Hebrides arc: Tectonophysics, 50, 29-40.

Chung, W.-Y., and Kanamori, H., 1978b. Subduction process of a fracture zone and aseismic ridges -- the focal mechanism and source characteristics of the New Hebrides earthquake of January 19, 1969 and some related events: Geophys. J. Roy. Astron. Soc., 54, 221-240.

Cloos, M., 1992. Thrust-type subduction-zone earthquakes and seamount asperities - A physical model for seismic rupture, Geology, 20, 601-604.

Curray, J. R., Moore, D. G., Lawver, L. A., Emmel, F. J., Raitt, R. W., Henry, M., & Kieckheffer, R., 1978. Tectonics of the Andaman Sea and Burma. In: Geological and Geophysical Investigations of Continental Margins (edited by Watkins, J. S., Montaderi, L. & Dickenson, P. W.). Memoir 29. American Association of Petroleum Geologists, Tulsa, 189-198.

Curray, J.R., 1987. The Sunda arc, A model for oblique plate convergence. In: Proc. Symp. Snellius-II expedition, Eds. : Van Hinte, Tj., van Weering, C.E. and Fortruin, A.R. Jakarta, Nov. 23- 28, 1987. Vol. 1 Geology and Geophysics of the Banda arc and adjacent areas, Neth. J. Sea Res.

Curray, J.R., 2005. Tectonics and history of the Andaman Sea region. J. Asian Earth Sci. 25, 187-232.

Curray, J.R., Emmel, F.J., Moore, D.G., and Raitt, R.W., 1982. Structure, tectonics and geological history of the northeastern Indian Ocean. In: The Ocean Basins and

Margins, (Eds) A.E.M Nairn and F.G. Stehli, Vol. 6. Plenum, New York N.Y., 399 - 450.

Curray, J.R., Moore, D.G., Lawver, L., Emmel, E., Raith, R., Henry, M., and Kieckhefer, R., 1979. Tectonics of the Andaman sea and Burma. Am. Assoc. Pet. Geol. Mem. 29, 189 - 198.

Curray, J.R., Shor, G.G., Raitt, R.W., & Henry, M., 1977. Seismic refraction and reflection studies of crustal structure of the eastern Sunda and western Banda Arcs, J. Geophys. Res., 82, 2479–2489.

Dardji N., Villemin T., Rampnoux J.P., 1994. Paleo stress and strike slip movement : The Cimandiri Fault Zone, West Java, Indonesia. J.SE Asian Earth Sci.9, 12311.

Dasgupta, S., 1992. Seismotectonics and stress distribution in the Andaman plate. Mem. Geol. Soc. Ind. 23, 319 - 334.

Dasgupta, S., and Mukhopadhyay, M., 1993. Seismicity and plate deformation below the Andaman arc, northeastern Indian Ocean, Tectonophys, 225, 529 - 542.

Dasgupta, S. and Mukhopadhyay, M. 1997. Aseismicity of the Andaman subduction zone and recent volcanism. J. Geol. Soc. India 49, 513 - 521.

Dasgupta, S., Mukhopadhyay, M., Bhattacharya, A., and Tapan K. Jana., 2003. The geometry of the Burmese-Andaman subducting lithosphere. J. of Seismology, 7, 155–174.

DeMets, C., Gordon, R.G., Argus, D.F., and Stein, S., 1994. Effect of recent revisions to the geomagnetic reversal time scale on estimates of current plate motions. Geophysical Research Letters 21, 2191-2194.

DeMets, C., Gordon, R.G., Argus, D.F. & Stein, S., 1990. Current plate motions, Geophys. J. Int., 101, 425–478.

Deng,Q., Chang, Y., Hsu, K. and Fan,F., 1979. On the tectonic stress field in China and its relation to plate movement. Phys. Earth Planet. Inter., 18, 257-273.

Diament,M., Harjono, H., Karta, C., Deplus, C., Gerard,M., Malod, J., 1992. Mentawai fault zone off Sumatra: A new key to the geodynamics of the western Indonesia. Geology, 20, 259-262.

Dickinson, W.R., 1995. Fore arc basins, in Tectonics of sedimentary Basins. Edited by C.J.Busby and R.V Ingersoll. 579. Blackwell Sci., Malden.Mass.

Duncan R, A., 1978. Geochronology Of Basalts From The Ninetyeast Ridge And Continental Dispersion In The Eastern Indian-Ocean.Journal of Volcanology and Geothermal Research 4 (3-4), 283-305.

Dziewonski, A.M., Friedman, A., Giardini, D., and Woodhouse, J.H., 1983. Global seismicity of 1982, Centroid moment tensor solutions for 308 earthquakes. Phys. Earth Planet. Inter: 33, 76 - 90.

Eguchi, T., Uyeda, S., and Maki, T., 1979. Seismotectonics and tectonic history of the Andaman sea. Tectonophys. 57, 35 - 51.

Engdahl, E.R., van der Hilst, R.D. and Buland, R., 1998. Global teleseismic earthquake relocation with improved travel times and procedures for depth determination. Bull. Seis. Soc. Am., 88, 722-743.

Eramenko, N.A., and Sastri, V.V., 1977. On the petroleum geology of Andaman Islands. Bull. ONGC. India. 14, 1 - 13.

Eva, C., Cattaneo, M., and Merlanti, F., 1988. Seismotectonics of the central segment of the Indonesian arc. Tectonophysics, 1446, 241-259.

Fitch, T.J., 1970. Earthquake mechanisms in the Himalaya, Burmese and Andaman regions and Continental tectonics in Central Asia. J. Geophys. Res. 75, 2699 - 2709.

Fitch, T.J., 1972. Plate convergence, transcurrent faults and internal deformation adjacent to Southeast Asia and the western Pacific. J. Geophys. Res. 77, 4432 - 4460.

Frolich, C., and Apperson, K.D., 1992. Earthquake focal mechanisms, moment tensors, and the consistency of seismic activity near plate boundaries, Tectonics, 11, 279-296.

Furuse, N., and Kono, Y., 2003. Slab residual gravity anomaly: gravity reduction due to subducting plates beneath the Japanese Islands. J. of Geodynamics 36, 497-514.

Gahalaut, V. K., and Catherine, J. K., 2006. Rupture characteristics of 28 March 2005 Sumatra earthquake from GPS measurements and its implication for tsunami generation.EPSL. doi:10.1016/j.epsl.2006.07.015.

Gardner, T.W., Verdonck, D., Pinter, N.M., Slingerland, R., Furlong, K.P., Bullard, T.F., and Wells, S.G., 1992,Quaternary uplift astride the aseismic Cocos Ridge, Pacific coast, Costa Rica: Geological Society of America Bulletin, 104, 219-232.

Geller, R.J., and Kanamori, H., 1977. Magnitudes of great shallow earthquakes from 1902 to 1952. Bull. Seis. Soc. Am. 67, 587- 598.

Genrich, J.F., Bock,Y., Mc Caffrey, R., Prawirodirdjo,L., Stevans, C.W., Puntodewo, S.S.O., Subarya, C., Wdowinski, S. J., 2000. Geophys. Res. 105, 28327 - 28341.

Ghose , R., Yoshika, S., and Oike, K., 1990. Three dimensional numerical simulations of the sedimentary dynamics in the Sunda rac region, Southeast Asia. Tectonophysics, 181, 223-255.

Giardini, D., and Woodhouse, J. H., 1986. Horizontal shear flow in the mantle beneath the Tonga arc, Nature, 319, 551-555.

Gill, J. B., 1981. Orogenic andesites and plate tectonics, Springer, 1390.

Gopala Rao, D., Krishna, K.S., and Sar, D., 1997. Crustal evolution and sedimentation history of the Bay of Bengal since the Cretaceous, J. Geophys. Res. 102 (B8), 17,747- 17, 768.

Grevemeyer, I., Tiwari, V.M., 2006. Overriding plate controls spatial distribution of megathrust earthquakes in the Sunda-Andaman subduction zone Earth and Planetary Science Letters , 251 (3-4), 199-208

Grow, J.A., Bowin, C.O., 1975. Evidence for high density crust and mantle beneath Chile Trench due to the descending lithosphere. J. Geophys. Res. 80, 1449–1498.

Grow, J. A., 1973. Crustal and upper mantle structure of the central Aleutian arc *Bull. geol. Soc. Am.*, 84, 2169–2192.

Gutenberg, B., and Richter, C.F., 1944. Seismicity of the earth. Geol. Soc. Am. Sp. Paper. 34, 1 - 133.

Gutenberg, G., and Richter, C.F., 1954. Seismicity of the Earth and its Associated Phenomena. Princeton University Press, Princeton, NJ, 310.

Guzman-Speziale, M., and Ni, J.F., 1996. Seismicity and active tectonics of the Western Sunda Arc.: in The Tectonic Evolution of Asia, edited by An Yin and T. Mark Harrison, 63-84.

Hamilton, W., 1979. Tectonics of the Indonesian region. U.S.G.S Prof. Paper 1078, p. 345.

Hamilton, W., 1988. Plate tectonics and island arcs, Geol. Soc. Am.Bull., 100, 1503-1527.

Hanuš, V., and Vaněk, J., 1976. Intermediate aseismicity of the Andean subduction zone and recent andesitic volcanism. J. Geophys. 42, 219 -223.

Hanuš, V., and Vaněk, J., 1978. Morphology of the Andean Wadati-Benioff zone, andesitic volcanism, and tectonic features of the Nazca plate. Tectonophysics, 44, 65–77.

Hanuš, V., and Vaněk, J., 1985. Structure of Wadati-Benioff zones and volcanism produced by the process of subduction. Tectonophysics, 112, 51-67.

Hanuš, V., and Vaněk, J., 1988. Deep structure, volcanism and Wadati-Benioff zone of the northwestern Pacific convergent margin. J. Geodynamics 10, 25–41.

Hanuš, V., Špičák, A., and Vaněk, J., 1996. Sumatran segment of the Indonesian subduction zone: morphology of the Wadati-Benioff zone and seismotectonic pattern of the continental wedge. J. Southeast Asian Earth Sci. 13, 39–60.

Harjono, H., Diament, M., Dubois, J., Larue, M., 1991. Seismicity of the Sunda Strait: Evidence for crustal extension and Vocanologic implications. Tectonics, 10, 17-30.

Heine, C.,Müller,R.D.,Gaina,C., 2004.Reconstructing the Lost Eastern Tethys Ocean Basin: convergence history of the SE Asianmargin and marine gateways. In: P.C., et al. (Ed.), Continent-Ocean Interactions in Southeast Asia, AGU Geophysical Monograph, . 37–54.

Hlo Maung, 1987. Transcurrent movements in the Burma-Andaman Sea Region. Geology. 15, 911-912.

Huchon, P., Le Pichon, X., 1984. Sunda Strait and Central Sumatra fault. Geology.12, 668-672.

Hyndman, R. D., and Wang, K. J., 1993. Thermal constraints on the zone of major thrust earthquake failure: The Cascadia subduction zone, J. Geophys. Res., 98, 2039-2060.

Isacks, B., and Molnar, P., 1971. Distribution of stress in the descending lithosphere from a global survey of focal-mechanism solutions of mantle earthquakes, Rev. Geophys. Space Phys. 9, 103–174.

Isacks, B., Oliver, J and Sykes, L.R., 1969. Seismology and the new global tectonics, J. Geophys. Res. 73, 5855–5899.

Ishii, M., Shearer, P.M., Houston, H., and Vidale, J. E., 2005. Extent, duration and speed of the 2004 Sumatra -Andaman earthquake imaged by Hi-Net array. Nature, 435, 933-936.

Izart, A., Mustafa Kemal, B. and Malod, J.A., 1994. Seismic stratigraphy and subsidence evolution of the northwest Sumatra fore-arc basin, Mar. Geol., 122, 109–124.

Jackson, J., and McKenzie, D.P., 1988. The relationship between plate motion and seismic moment tensors, and the rates of active deformation in the Mediterranean and Middle East. Geophys. J. 93, 45 - 73.

Jarrard, R.D., 1986. Relations among subduction parameters. Rev. Geophys., 24, 217-284.

Johnson, B.D., Powell, C.McA. and Veevers, J.J., 1976. Spreading history of the eastern Indian Ocean and Greater India's northward flight from Antarctica and Australia. Geol. Soc. Am. Bull. 87, 1560 - 1566.

Kamesh Raju, K. A., Murty, G. P. S., Dileep Amarnath, Mohan Kumar, M. L., 2007. The west Andaman fault and its influence on the aftershock pattern of the recent megathrust earthquakes in the Andaman-Sumatra region. Geophysical Research Letters 34, 3, L03305.

Kanamori, H., and Anderson, D., 1975. Theoretical basis of empirical relations in seismology. Bull. Seis. Soc. Am. 65, 1073 - 1095.

Kanamori, H., 1983. Global Seismicity, in Earthquakes: Observation, theory and interpretation, edited by H. Kanamori and E. Bosch, North Holland, New York. p. 597

Karig, D. E., Suparka, S. Moore, G. F. & Hehanussa, P. 1979. Structure and Cenozoic evolution of the Sunda Arc in the central Sumatra region. *Mem. Am. Assoc. Petrol. Geol.*, **29**, 223–237.

Karig, D. E., 1971. Origin and development of marginal basins in the Western Pacific *J.* geophys. Res., *76*, 2542–2561.

Karig,D.F., Moore, G.F., Curray, J.R., and Lawrence, M.B., 1980. Morphology and shallow structure of the lower trench slope off Nias Island, Sunda arc. In: The Tectonic and Geologic Evolution of Southeast Asian seas and islands, Geophys. Monogr. Ser. Vol.23, edited by D.E. Hayes. AGU, Washington D.C. 179-208.

Katili, J.A., 1975. Volcanism and plate tectonics in the Indonesian island arcs. Tectonophysics, 26, 3-4

Katili, J.A., 1962. On the age of the granitic rocks in relation to the structural features of Sumatra, In: The crust of the Pacific basin, (Eds.) G.A. Macdonald and H. Kuno, Washington, Am. Geophy. Union. Mono. 6, 116 - 121.

Kuo, B.Y., Forsyth, D.W., 1988. Gravity anomalies of the ridge-transform system in the South Atlantic between 31 and 34.5° S: Upwelling centers and variations in crustal thickness. Marine Geophysical Researches, 10(3-4), 205-232.

Kawakatsu, H., 1986a. Double seismic zones: Kinematics. J. Geophys. Res., 91fB5): 4811-4825.

Kawakatsu, H., 1986b. Downdip tensional earthquakes beneath the Tonga arc: A double seismic zone. J. Geophys. Res., 91fB6): 6432-6440.

Kelleher, J., and McCann, W., 1976. Buoyant zones, great earthquakes, and unstable boundaries of subduction. J. Geophys. Res. 81, 4885 - 4896.

Khan, P. K., and Chakraborty, P. P., 2005. Two-phase opening of Andaman Sea: a new seismotectonic insight. Earth Planet. Sci. Lett., 229, 259–271.

Kieckhefer, R.M., Shor, G.G. Jr. and Curray, J.R., 1980. Seismic refraction studies of the Sunda trench and fore arc basin, J. Geophys. Res. 85, 863 - 889.

Kiratzi, A. and Papazachos, C.B. 1995. Active crustal deformation from the Azores triple junction to the Middle East. Tectonophys. 243, 1 - 24.

Kirby, S. H., Stein, S., Okal, E. A., and Rubie, D. C., 1996. Meta stable mantle phase transformations and deep earthquakes in subducting oceanic lithosphere. Rev. Geophys., **34**, 261–306.

Klootwijk, C.T., Gec, J.S., Peirce, J.W., Smith, G.M., McFadden, P.L.,1992. An early India–Asia contact: Paleomagnetic constraints fromNinetyeast Ridge, ODP Leg 121. Geology 20, 395–398.

Kopp, H., Flueh, E.R., Klaeschen,D., Jo¨rg Bialas and Reichert, C., 2001. Crustal structure of the central Sunda margin at the onset of oblique Subduction. Geophys. J. Int. 147, 449–474.

Kopp, H., Kukowski, N., 2002. Backstop geometry and accretionary mechanics of the Sunda margin TECTONICS, VOL. 22, NO. 6, 1072, doi:10.1029/2002TC001420, 2003

Kopp, H., Flueh, E.R., Petersen, C.J.,Weinrebe,W.,Wittwer, A.& Meramex Scientists, 2005. The Java margin revisited: evidence for subduction erosion off Java, Earth planet. Sci. Lett., 242, 130–142.

Kostrov, V. V., 1974. Seismic moment and energy of earthquakes and seismic flow of rocks. Lzv. Acad. Sci., USSR. Phys. Solid Earth. 1, 23 - 44.

Krishna, K.S., Gopala Rao, D.,Ramana, M.V., Subrahmanyam, V. and Sarma, K.V.L.N.S. Pilipenko, A.I., Shcherbakov, V.S., Murthy,I.V.R. 1995. Tectonic model for the evolution of the oceanic crust in the northeastern Indian Ocean from the Late Cretaceous to the early Tertiary. J. Geophy. Res. 100, 20011 - 20024.

Kruger, F., and Ohrnberger, M., 2005. Tracking the rupture of the Mw 9.3 Sumatra earthquake over 1,150 km at teleseismic distance. Nature , 435, 937-939.

Larson, R.L.L, Mutter, J. C., Diebold, J. B., Carpenter, G. B., and Symonds, P., 1979. Cuvier Basin: a product of ocean crust formation by Early Cretaceous rifting off western Australia. Earth Panet.Sci.Lett., 45: 105-114.

Lassal ,O., Huchon, P., and Harjono, H., 1989. Extension crustale dan le detroit de la Sonde (Indonesie), donees de sismique reflexion (capagne KRAKATAU), c.r.Acad. Sci. Paris.Ser.II, 309, 205-212.

Lawver, L.A., and Curray, J.R., 1981. Evolution of the Andaman Sea (abs.), in EOS: Trans. Am. Geophys. Union, 62(45), 1044.

Lay, T., Kanamori, H., Ammon, C.J., Nettles, M., Ward, S.N., Aster, R.C., Beck, S.L., Bilek, S.L., Brudzinski, M.R., Butler, R., DeShon, H.R., Ekstrom, G., Satake, K and Sipkin, S. 2005. The great Sumatra-Andaman Earthquake of 26 December 2004. Science., 308, 1127-1133.

LeDain, A.Y., Tapponnier, P., Molnar, P., 1984. Active faulting and tectonics of Burma and surrounding regions. J, Geophys. Res. 89, 452 - 472.

Lee, T.T., Lawver, L.A., 1995. Cenozoic plate reconstruction of Southeast Asia. Tectonophysics 251, 85–138.

Liu, C.S., Curray, J.R., and McDonald, J.M. 1983. New constraints on the tectonic evolution of the Esatern Indian Ocean. Earth. Planet. Sci. Lett. 65, 331 - 342.

Liu, X., McNally, K.C., and Kang Shen, Z., 1995. Evidence for a role of the down going slab in earthquake slip partitioning at oblique subduction zones. J. Geophys. Res. 100, No. B8, 15351- 15372.

Longley, I.M., 1997. The tectono stratigraphic evolutionof SE Asia. In: Petroleum geology of south East asia, edited by A.J.Fraser, S.J. Matthews, and r.W.Murphy. Geol.soc. Spec. Publ., 126,311- 339.

Malod, J.A., Komar Karta, Beslier, M.O., and Zen Jr., M.T. 1995. From normal to oblique subduction: Tectonic relationships between Java and Sumatra. J. SE Asian Earth. Sci. 12, 85 - 93.

Malod, J-A., and Kemel,B. M., 1996. The Sumatra margin: Oblique subduction and lateral displacement of the accretionary prism. Geol.soc. Spec. Publ., 106, 19-28.

Markl, R.G., 1978. Further evidence for the Early Cretaceous breakup of Gondwanaland off Southwestern Australia, Earth and Planet. Sci. Letters, 39, 211-225.

Markl, R.G., 1974. Evidence for the breakup of eastern Gondwanaland by the Early Cretaceous. Nature 251, 196 - 200.

Marks, K.M., 1996. Resolution of the Scripps/NOAA marine gravity field from satellite altimetry, *Geophys. Res. Lett.*, **23**, 2069–2072.

Maung, H., 1987. Transcurrent movements in the Burma-Andaman Sea Region.Geology, .15, 911-912.

McCaffrey, R., 1992. Oblique plate convergence, slip vectors and forearc deformation. Journal of Geophysical Research 97(B6), 8905-8915.

McCaffrey, R., 1991. Slip vectors and stretching of the Sumatran fore arc. Geology, 19, 881-884.

McCaffrey, R., 1993. On the role of the upper plate in great subduction zone earthquakes, J. Geophys. Res., 98, 11953-11966.

McCaffrey, R., Zwick, P.C., Bock,Y., Prawirodirdjo,L., Genrich, J.F., Stevens, C.W., Puntodewo, S.S.O., Rais,J., Subarya, C., 2000. Strain partitioning during oblique plate convergence in northern Sumatra: Geodetic and seismologic constraints and numerical modeling. J. Geophy. Res., 105, No.B 12. 28363 - 28376.

McCaffrey, R., 2002. Block rotations and plate coupling, AGU volume on Plate Boundary Zones, S. Stein and J. Freymueller, editors, in press.

McCaffrey, R., 1994. Global variability in subduction thrust zone - forearc systems, Pure & Applied Geophysics 142(1), 173-224,.

McCaffrey, R., 1996. Estimates of modern arc-parallel strain rates in fore arcs, Geology 24, 27-30,

McCaffrey, R., 1996. Slip partitioning at convergent plate boundaries of SE Asia, in Tectonic Evolution of SE Asia Symposium, Geol. Soc. Special Publication No. 106, 3-18,

McKenzie, D.P., and Scalter, J.G., 1971. The evolution of the Indian Ocean since the late Cretaceous. Geophys. J. R. Astron. Soc. 25, 437 - 528.

Michel, G. W., Becker, M. Reigber, Ch, Tibi, R. Yu Y. Q., Zhu S. Y..2001. Regional GPS data confirm high strain accumulation prior to the 2000 June 4 M_w=7.8 earthquake at southeast Sumatra Geophysical Journal International.146(3),571-582. doi:10.1046/j.0956-540x.2001.01469.x

Mignan, A., King, G., Bowman,D., Lacassin,R., and Dmowska, R., 2006. Seismic activity in the Sumatra-Java region prior to the December26, 2004 (Mw=9.0-9.3) and March 28, 2005 (Mw=8.7) earthquakes. EPSL 244,639-654.

Milne, W., Davenport, A., 1969. Determination of earthquake risk in Canada. Bull. Seis. Soc. Am. 59, 729 - 754.

Minster, J.B., and T.H.Jordan., 1978. Present-day plate motion, J. Geophys. Res., 83, 5331-5354.

Minear, J., and Toks¨oz M. N., 1970. Thermal regime of a downgoing slab and new global tectonics, J. Geophys. Res., 75, 1379- 1419,

Molnar, P., 1979. Earthquake recurrence intervals and plate tectonics. Bull. Seis. Soc. Am. 69, 115 - 133.

Molnar, P., and Tapponnier, P., 1975. Cenozoic tectonics of Asia: effects of a continental collision. Science 159, 419 - 426.

Molnar, P., and Tapponnier, P., 1978. Active tectonics of Tibet: Journal of Geophysical Research B: Solid Earth, 83, 5361-5375.

Moore, G.F., and Curray, J.R., 1980. Structure of the Sunda trench lower slope off Sumatra from multi-channel seismic reflection data. Mar. Geophys. Res. 4, 319 - 340.

Mukhopadhayay, M., and Krishna, M.R., 1991. Gravity field and deep structure of the Bengal fan and its surrounding continental margins, northeast Indian Ocean. Tectonophys. 186, 365 - 386.

Mukhopadhyay, M., 1984. Seismotectonics of subduction and back arc rifting under the Andaman sea. Tectonophys. 108, 229 - 239.

Mukhopadhyay, M., 1988. Gravity anomalies and deep structure of the Andaman arc. Mar: Geophys. Res. 9, 197 - 210.

Mukhopadhyay, M., and Dasgupta, S., 1988. Deep structure and tectonics of the Burmese arc: constraints from earthquake and gravity data. Tectonophys. 149, 299 - 322.

Mukhopadhyay, M., and Krishna, M.R., 1995. Gravity anomalies and deep structure of the Ninety east Ridge north of the equator, eastern Indian Ocean - A hot spot trace model. Mar: Geophys. Res. 17, 201 - 216.

Natawidjaja, D.H., and Sieh, K., 1994. Slip rate along the Sumatra transcuurrent fault and its tectonic significance, paper presented at conference on Tectonic evolution of South East Asia, Geol.Soc.of London.

Newcomb,K.R., McCann,W.R., 1987. Seismic history and seismotectonics of the Sunda arc. J. Geophy. Res. 92, 421 - 439.

Ni, J.F., Guzman-Speziale, M., Bevis, M., Holt, W.E., Wallace, T.C., and Seager, W., 1989. Accretionary tectonics of Burma and three dimensional geometry of the Burma subduction zone. Geology 17, 68 - 71.

Nishimura, S.; Harjono, H.; Suparka, S. 1992. The Krakatau Island: the geotctonic setting. In: GeoJournal, 28 , S. 87-99

Nishimura, S., Nishida,J., Yokoyama,T., and Hehuwat, F., 1986. Neotectonics of the Strait of sSunda, Indonesia. J.Asain. Earth.Sci., 1, 81-91.

Norton, I.O., and Sclater, J.G., 1979. A model for the evolution of the Indian Ocean and the breakup of Gondwanaland. J. Geophys. Res. 84, 6803 - 6830.

Oliver, J.,and Isacks, B., 1967. Deep earthquake zones, anomalous structures in the upper mantle, and the lithosphere. J. Geophys. Res. 72, 4259-75.

Ortiz, M., and R. Bilham., 2003. Source area and rupture parameters of the 31 Dec. 1881Mw 7.9 Car Nicobar earthquake estimated from Tsunami recorded in the Bay of Bengal, J. Geophys. Res., 108 (B4) 23 April 2003 [2002J B001941RR 2003.

Packham, G. H., and Falvey, D. A., 1971. An hypothesis for the formation of marginal seas in the western PacificTectonophysics, **11**, 79.

Papazachos, B.C., 1990. Seismicity of the Aegean and surrounding area. Tectonophys. 178, 287 - 308.

Papazachos, C.B., and Kiratzi, A., 1992. A formulation for reliable estimation of active crustal deformation and its application to central Greece. Geophys. J. Int. III, 424 - 432.

Parker, R.L., 1972. The Rapid Calculation of Potential Anomalies. Geophysical Journal International 31 (4), 447–455. doi:10.1111/j.1365-246X.1973.tb06513.x

Peter,G., Weeks, L.A., Burns, R.E., 1966. A Reconnaissance geophysical survey in the Andaman Sea and across the Andaman-Nicobar island arc. J. Geophys. Res., 71, 495-509.

Petersen Mark D., James Dewey, Stephan Hartzell, Charles Mueller, Stephan Harmsen, Arthur D. Frankel, Ken Rukstales, 2004. Probabilistic seismic hazard analysis for Sumatra, Indonesia and across the Southern Malaysian Peninsula, Tectonophysics ,390 , 141- 158.

Platt, J.P., 1986. Dynamics of orogenic wedges and the uplift of high-pressure metamorphic rocks. Geological Society of America Bulletin, 97, 1037-1053.

Powell C. McA., Roots S. R., and Veevers J. J., 1988. Pre-breakup continental extension in East Gondwanaland and the early opening of the eastern Indian ocean. Tectonophysics, 155, 261-283.

Pramumijoyo, S., and Sebrier, M., 1991. Neogene and Quarternary fault kinematics around the Sunda strait area, Indonesia. J.SE Asian Earth Sci., 6, 137-145.

Prawirodirdjo, L., Bock,Y., McCaffrey, R., Genrich, J., Calais, E., Stevens, C., Puntodewo, S.S.O., Subarya, C., Rais, J., Zwick, P., and Fauzi. 1997. Geodetic observations of inter seismic segmentation at the Sumatra subduction zone. Geophy. Res lett., 24, 21, 2601 - 2604.

Prawirodirjo, L., Bock, Y., Genrich, J.F., Puntodewo, S.S.O., Rais, J., Subarya, C., Sutisna, S., 2000. One century of tectonic deformation along the Sumatran fault from triangulation and Global positioning system surveys. J. Geophy. Res. 105, No.B 12. 28343 - 28361.

Prince, R.A., and Forshyth, D.W., 1988. Horizontal extent of anomalously thin crust near the Vema fracture zone from the three-dimensional analysis of gravity anomalies. Journal of Geophysical Research, 93(B7), 8051-8063.

Pubellier , M., Rangin, C., Cadet, J-P., Tjashuri,I., Butterlin, J., and Mutter C. 1992. L'ile de Nias, un edifice polyphase sur la bordure interne de la fosse de la sonde (Archipel de Mentawai, Indonesie). C.R.Acad. Sci. Paris.Ser.II, 315, 1019-1026.

Purdy, G.M., and Detrick, R.S., 1978. A seismic refraction experiment in the central Banda Sea, J. Geophys. Res., 83, 2247-2257.

Puspito, N.T., and Shimazake, K., 1995. Mantle structure and seismotectonics of the Sunda and Banda arcs: Tectonophysics, 251, 215-228.

Radha Krishna and Arora, 1998. Space-time seismicity and earthquake swarms: Certain observations along the slow-spreading mid-Indian Ocean ridges, Earth and Planetary Sciences, 107, 161-173.

Radhakrishna, M., and Sanu T.D., 2002. Shallow seismicity,stress distributionand crustal deformation patternin the Andaman-West Sunda arc and Andaman Sea,Northeastern Indian Ocean. J.of Seismology 6, 25-41.

Radhakrishna, M., and Serale, R.C., 2006. Isostatic response of the Alula-Fartak and Owen transforms in the Eastern Gulf of Aden and the adjoining Arabian Sea. Geophysical Journal International, 165 (1), 62–72.

Rajendran, K., and Gupta, H.K., 1989. Seismicity and tectonic stress field of a part of the Burma-Andaman-Nicobar arc. Bull. Seis. Soc. Am. 79, 989 - 1005.

Raju, K.A.K., Ramprasad, T., Rao, P.S., Rao, B.R., Varghese, J., 2004. New insights into the tectonic evolution of the Andaman basin, northeast Indian Ocean. Earth and Planet.Sci. Lett, 221, 145–162.

Raju,K.A.K., 2005. Three-phase tectonic evolution of the Andaman backarc basin. Curr.Sci, Vol. 89, No. 11.1932-1937.

Raju,K.A.K.,. Murty, G. P. S ., Dileep Amarnath and. Mohan Kumar, M. L.2007. The west Andaman fault and its influence on the aftershock pattern of the recent Megathrust earthquakes in the Andaman-Sumatra region. Geophys. Res. Lett, 34, L03305, Doi:10.1029/2006gl028730.

Ramana , M.V., Subrahmanyan V., Sarma, K.V.L.N.S., Murty, G. P. S., Mittal, G. S. and Drolia, R. K., 1994a .Magnetic studies in the northern Bay of Bengal, Mar. Geophys. Res., 16, 237-242.

Ramana, M. V., Ramprasad, T., Desa, M., 2001. Seafloor spreading magnetic anomalies in the Enderby basin, East Antarctica, Earth Planet. Sci. Lett.191, 241-255.

Ramana, M.V., Subrahmanyam, V., Sarma, K.V.L.N.S., Desa, M., and Malleswara Rao, M.M., 1997a, Record of the Cretaceous Magnetic Quiet Zone: A precursor to the understanding of the evolutionary history of the Bay of Bengal, Current Science, 72,9,669-673

Ramana, M.V., et al., 1997. Mesozoic anomalies in the Bay of Bengal, Earth planet. Sci. Lett., 121, 469–475.

Ravikumar, M., Rao, N.P., and Chalam, S.V., 1996. A seismotectonic study of the Burma and Andaman arc regions using centroid moment tensor data, Tectonophys. 253, 155 - 165.

Ravikumar, M., Rao, N.P., and Chalam, S.V., 1996. A seismotectonic study of the Burma and Andaman arc regions using centroid moment tensor data, Tectonophys, 253, 155 - 165.

Rivera, L., Sieh, K., Helmberger, D., and Natawidjaja, D., 2002. A comparative study of the Sumatran subduction-zone earthquakes of 1935 and 1984. Bull. Seis. Soc. Am., 92, 1721 - 1736.

Rodolfo, K.S., 1969. Bathymetry and marine geology of the Andaman basin and its tectonic implications for SE Asia. Am. Assoc. Pet. Geol. Bull. 52, 2422 - 2437.

Rothe, J.P., 1969. The Seismicity of the Earth. UNESCO, Paris, .336.

Roy, T.K., 1983. Geology and hydrocarbon prospects of Andaman - Nicobar basin. Petrol. Asia J., Nov. 37 - 50.

Royer, J.Y., and Sandwell, D.T., 1989. Evolution of the Eastern Indian Ocean Since the Late Cretaceous: Constraints from Geosat Altimetry, J. Geophys. Res., 94(B10), 13,755-13,782.

Royer, J.-Y., Sclater, J.G., and Sandwell, D.T., 1989. A preliminary tectonic fabric chart of the Indian Ocean,Proceedings of the Indian Academy of Sciences (Earth and Planetary Sciences), 98(1), 7-24.

Ruff, L. J., 1989. Do trench sediments affect great earthquake occurrence in subduction zones?, 129, 263-282.

Samuel, M.A., and Harbury, N.A., 1996. The Mentawai Fault Zone and deformation of the Sumatra fore arc in the Nias area, in Tectonic Evolution of Southeast Asia edited by R.Hall and D.J.Blundell, Geol.Soc. sp.Publ., 106, 337-351.

Sandwell, D.T., & Smith, W.H.F., 1997. Marine gravity anomaly from Geosat and ERS1 satellite altimetry, J. geophys. Res., 102 (B5), 10 039–10 054.

Schlich, R., 1975. Structure et age de l'ocean Indien occidental. Mem. Hors-Ser. Soc. Geol. Fr., 6, 1-103.

Schlich, R., 1982, The Indian Ocean: Aseismic ridges, spreading centers and basins, in Nairn, A.E.M., and Stehli, F., The Indian Ocean, 6: 51-147.

Schluter, H.U., Gaedicke, C., Roeser,A., Schreckenberger, B., Meyer, H ., Reichert, C., Djajdihardja.Y., and Prexl, A., 2002. Tectonic features of the southern Sumatra-westren Java forearc of Indonesia. Tectonics. 21, no.5, 1047, II-1 -II-13, doi: 10.1029/2001TC901048

Schoffel H.J., and Das, S., 1999. Fine details of the Wadati-Benioff zone under Indonesia and its geodynamic implications. J. Geophy. Res., 104, No.B6, 13101 - 13114.

Scholz, C. H., and Campos, J., 1995. On the mechanism of seismic decoupling and back arc spreading at subduction zones, J. Geophys. Res., 100, 22103-22115.

Sclater, J.G., and Fisher, R.L., 1974. Evolution of the east central Indian Ocean with emphasis on the tectonic setting of the Ninetyeast ridge. Bull. Geol. Soc. Am. 86, 683 - 702.

Sclater, J.G., Luyendyk, B.P., and Meinke, L., 1976. Magnetic lineations in the southern part of the Central Indian Basin, GSA Bull., 87: 371-378.

Scotese, C. R., Gahagan, L. M., and Larson, R. L., 1988. Plate tectonic reconstruction of the Cretaceous and Cenozoic ocean basins. Tectonophysics, 155, 27–48.

Sieh, K., Natawidjaja, D., 2000. Neotectonics of the Sumatran fault, Indonesia. J. Geophy. Res. 105, No.B 12. 28295 - 28326.

Silver, E.A., Donald, R and McCaffrey, R. 1983. Back arc thrusting in the eastern Sunda arc, Indonesia:A convergence of arc-continent collision. J. Geophys. Res., 88, 7429 - 7448

Simandjuntak , T.O., and Barber, A.J., . 1996. Contrasting tectonic styles in the Neogene orogenic belts of Indonesia. In: Tectonic Evolution of Southeast Asia, edited by R. Hall and D. Blundell. Geol.Soc.Spec.Publ.106, 185-201.

Singh et al., 2005. Sumatra Earthquake research indicates why rupture propograted northward,Eos, Transactions American Geophysical Union, 86,497

Singh, D. D., 1990, Q-structure beneath the north and central Indian Ocean from the inversion of the observed Love and Rayleigh wave attenuation data, Phys. Earth Planet. Inter. 59, 243-258.

Slancova, A., Spicak, A., Hanus, V., and Vanek, J., 2000. How the state of stress varies in the Wadati-Benioff zone: indications from focal mechanisms in the Wadati-Benioff zone beneath Sumatra and Java. Geophys.J.Int 143, 909-930.

Song, T-R A., and Simons, M., 2003. Large Trench-Parallel Gravity Variations Predict Seismogenic Behavior in Subduction Zones *Science*, 301, 630-633 DOI:0.1126/science.1085557

Spicak, A., Hanu, V., and Vanek, J., 2004. Seismicity pattern: an indicator of source region of volcanism at convergent plate margins Physics of The Earth and Planetary Interiors 141(4), 303-326

Spicak, A., Hanu, V., and Vanek, J., 2002. Seismic activity around and under Krakatau volcano, Sunda Arc: constraints to the source region of island arc volcanics. Studia Geophysica et Geodaetica 46, 545-565.

Sridevi Jade, M. B. Ananda, P. Dileep Kumar and Souvik Banerjee, 2005. Co-seismic and post-seismic displacements in Andaman and Nicobar Islands from GPS measurements, Current Science, 88, (12), 1980-1984.

Stein, S., Okal, E. A., 1978. Seismicity and tectonics of the Ninetyeast Ridge area: Evidence for internal deformation of the Indian plate. Journal of Geophysical Research, 83(B5), 2233-2246

Subarya,C., Chlieh, M., Prawirodirdjo, L., Avouac, J., Bock, Y., Sieh, K., Meltzner A.J., Natawidjaja, D.H., . and McCaffrey, R., 2006. Plate-boundary deformation associated with thegreat Sumatra–Andaman earthquake, Nature, 440, 46–51.

Talwani, M., and Ewing.M., 1960. Rapid computation of gravitational attraction of three-dimensional bodies of arbitrary shape: Geophysics, 25 (1), 203-225.

Tapponnier, P., . and Molnar, P., 1979. Active faulting and Cenozoic tectonics of the Tien Shan, Mongolia and Baykal Regions. J. Geophys. Res., 84:3425-3459.

Tapponnier, P., and Molnar, P., 1977. Active Faulting and Tectonics in. China, J. Geophys. Res., 82, 2905-2930.

Taylor, B., and Karner, G.D., 1983. On the Evolution of Marginal Basins. Reviews of Geophysics and Space Physics, 21, 1727.

Tjia, H.D., 1978. Active faults in Indonesia. Geological Society of Malaysia, 10.73-92.

Turcotte, D.L., and Schubert, G., 2002. Geodynamics (2nd ed.), Cambridge University Press (2002) 456.

Turcotte, D.L. ; Schubert, G., 1982. Geodynamics applications of continuum physics to geological problems. Publisher: New York, NY (US) ;John Wiley and Sons, Inc. 459.

Utsu, T., 1971. Seismological evidence for anomalous structure of island arcs with special reference to the Japanese region. Rev. Geophys. Space Phys. 9, 839–890.

Uyeda, S., . and Kanamori, H., 1979. Back arc opening and the mode of subduction. J. Geophys. Res. 84, 1049 - 1061.

Van der Weff, W., 1996. Variation in forearc basin development along the Sunda arc, Indonesia, J. Asian Earth Sci.14, 331-349.

Veevers, J.J., 1986. Breakup of Australia and Antarctica estimated as mid-Cretaceous (95+5 Ma) from magnetic and seismic data at the continental margin, Earth Planet. Sci. Lett., 77, 91-99.

Veevers, J.J., Powell, C.M., and Roots, S.R., 1991. Review of seafloor around Australia, I, Synthesis of the patterns of s preading, Aust.J.Earth Sci., 38,373-389.

Veevers. J., Taytonj. W., Johnsonb. D., Hansenl. 1985b. Magnetic expression of the continent-ocean boundary between the western margin of Australia and the eastern Indian Ocean. J.Gephys., 56, 106-120.

Vogt, P. R. (1973), Subduction and aseismic ridges, Nature, 241, 189- 191.

Watts, A.B., and. Talwani, M., 1975. Gravity effect of downgoing lithospheric slabs beneath island arcs, Geol. Soc. Amer. Bull., 86, 1- 4.

Weeks, L.A., Harbison, R.A., and Peter, G., 1967. Island arc system in Andaman sea. Am. Assoc. Pet. Geol. Bull. 51,1803-1815.

Weissel, J. K., 1981. Magnetic Lineations in Marginal Basins of the Western Pacific. Philosophical Transactions of the Royal Society of London. Series A, Mathematical and Physical Sciences, 300(1454), 223-245.

Weissel, J.K., and Hayes, D.E., 1972. In: Antractic Oceanology II: The Australian- New Zealand sector, d.E.Hayes (Ed.), Antarctic res.Ser. ,19, AGU, Washington D.C., 165-196.

Whittaker A.C., Cowie. P.A., Attal. M., Tucker.G.E., and Roberts G.P., 2007. Bedrock channel adjustment to tectonic forcing: Implications for predicting river incision rates Geology, 35(2), 103-106.

Widiyantoro, S., and Rob van der Hilst. 1996. Structure and Evolution of Lithospheric Slab Beneath the SundaArc, Indonesia Science 271(5255), 1566-1570 DOI: 10.1126/science.271.5255.1566

Win Swe, 1972. . Strike-slip faulting in central belt of Burma. In: Regional Conference on the geology of southeast Asia. Ed. N.S. Haile, Geol. Soc. Malaysia, .59.

Wittwer, A., Flueh, E., Kopp, H., Rabbel, W., Wagner, D., and Barckhausen, U., 2006. Sundaarc subduction zone: new insights of the Central Java part. Geophysical Research Abstracts, Vol. 8, 04524.

Yoshii, T., 1973. Upper mantle structure beneath the north Paci.c and the marginal seas. J. Phys. Earth 21, 313–328.

Zen, M.T.,. 1983. Krakatau and the tectonic importance of Sunda strait. Bull. Jurusan Geol., 12, 9-22.

Appendix – I

Appendix 1: Details of the earthquake events plotted in the Benioff zone sections.

M. No	Year	M	D	Lat		Long		Depth	Mb	Ms		Str	Dp	Slp	Str	Dp	Slp
1	2004	12	26	13.46	N	92.74	E	-26	6.1	6	N	1	41	-116	215	54	-69
2	2004	12	26	13.53	N	92.84	E	-13	6.3	6.3	S	29	56	158	132	72	36
3	2004	12	26	13.59	N	92.91	E	-30	5.8	5.7	S	137	56	15	38	78	145
4	2004	12	26	13.71	N	92.95	E	-26	5.3	4.7	S	144	69	174	236	84	21
5	2005	2	6	13.85	N	93.58	E	-35	5.6	5.1	T	17	31	139	144	70	66
6	1983	12	17	12.75	N	95.46	E	-21	5.3	0	N	201	35	-145	82	71	-60
7	1994	11	22	13.54	N	95.47	E	-33	4.8	5.2	S	17	74	-164	283	75	-16
8	2002	11	3	13.35	N	95.54	E	-25.2	4.7	5.1	S	277	62	-14	14	78	-151
9	2003	1	13	12.87	N	95.53	E	-30.3	4.9	4.9	S	11	52	-180	281	90	-38
10	2003	1	26	12.95	N	95.61	E	-20	4.9	0	S	245	32	-6	340	87	-122
11	2004	12	27	12.98	N	92.39	E	-23	6	5.5	N	359	42	-132	229	60	-59
12	2003	3	26	12.55	N	92.61	E	-29.6	5.8	5.3	S	245	51	-20	348	74	-140
13	2005	1	29	13.10	N	93.00	E	-30	5.5	4.8	T	118	41	44	352	62	122
14	1978	2	7	12.81	N	93.00	E	-3	5.5	5.3	T	121	43	46	2	61	123
15	1978	2	7	12.89	N	93.04	E	-17	5.6	5.6	T	162	36	95	336	54	56
16	2002	9	13	13.01	N	93.11	E	-21	6.2	6.7	T	212	42	137	337	63	57
17	2004	3	6	12.96	N	93.14	E	-38	5.2	5.2	S	214	52	157	319	72	41
18	1986	9	20	13.02	N	93.39	E	-84	4.8	0	T	332	23	59	185	71	102
19	2001	8	5	12.22	N	93.35	E	-96.4	5.4	5.2	S	274	57	22	172	72	145
20	1983	1	24	12.91	N	93.59	E	-81	6.1	0	S	291	50	39	174	62	133
21	1984	3	22	12.93	N	93.56	E	-100	5	0	T	344	86	90	344	4	90
22	2004	5	3	13.09	N	93.19	E	-31	5.3	5	T	1	34	68	207	59	104
23	2001	5	2	12.28	N	93.53	E	-92.8	5.1	0	S	290	42	30	177	70	128
24	2003	8	11	12.12	N	93.53	E	-100.2	5.5	0	S	270	51	18	168	76	139
25	1991	7	10	12.59	N	93.94	E	-168.5	5	0	T	97	23	134	231	74	74

M. No	Year	M	D	Lat		Long		Depth	Mb	Ms		Str	Dp	Slp	Str	Dp	Slp
26	1990	11	10	12.19	N	93.76	E	0	5.3	0	S	293	87	-2	23	88	-177
27	2003	7	12	12.14	N	95.08	E	-3.4	4.8	4.6	S	83	73	-13	177	78	-162
28	1993	3	19	12.13	N	95.10	E	-17.1	5.3	5.1	N	192	52	-129	65	52	-51
29	1990	12	25	12.29	N	93.69	E	-68	4.9	4.9	N	277	46	-61	58	51	-117
30	1999	4	7	11.81	N	95.03	E	-35.4	4.9	4.6	S	171	48	-166	71	80	-42
31	1993	4	18	12.16	N	95.02	E	-59.7	5	4.8	S	194	48	-143	77	63	-48
32	1984	4	13	11.89	N	95.04	E	-40	5.3	6	N	223	31	-90	43	59	-90
33	1972	11	13	12.44	N	95.23	E	-24	5	0	S	346	86	-17	74	76	-176
34	2003	7	13	12.56	N	95.63	E	-33	5.1	4.2	S	247	72	-16	342	75	-162
35	1986	8	7	11.73	N	95.33	E	-24	5.2	0	S	173	82	172	265	82	8
36	1990	1	10	11.71	N	95.12	E	0	5.3	5.4	S	260	81	0	170	90	171
37	1982	11	1	12.39	N	95.23	E	0	4.2	0	N	108	35	-135	338	66	-54
38	2004	12	27	12.35	N	92.47	E	-19	5.8	5.3	N	191	19	-64	344	73	-98
39	1974	2	16	11.47	N	92.32	E	-20	5.2	6	T	10	10	41	320	84	98
40	2004	12	30	12.24	N	92.51	E	-30	5.8	5.2	T	29	13	138	160	81	80
41	2004	12	27	11.59	N	92.50	E	-25	5.5	5.1	N	22	20	-77	188	71	-95
42	1993	9	30	11.84	N	92.58	E	-41	5.3	4.8	T	344	25	82	173	65	94
43	1981	11	2	12.18	N	92.87	E	-24	5.7	5.5	T	109	21	50	331	74	104
44	1979	7	5	11.98	N	92.88	E	-54	5	0	T	30	38	42	83	64	118
45	1982	12	16	11.70	N	93.00	E	-60	5.4	0	S	286	52	30	158	67	138
46	2003	8	11	12.12	N	93.53	E	-100.2	5.5	0	S	270	51	18	168	76	139
47	1992	9	16	11.64	N	93.65	E	-162	5.2	0	T	11	32	104	175	60	81
48	1984	7	8	11.08	N	94.79	E	-12	5.2	0	N	231	31	-126	91	65	-71
49	1984	7	10	10.90	N	94.59	E	-25	5	0	N	234	17	-114	80	74	-83
50	1984	7	8	11.18	N	94.71	E	-47	5.1	5.1	S	94	52	-36	207	62	-139
51	1984	7	5	11.27	N	94.76	E	-58	5.4	0	N	239	30	-109	81	62	-79

M. No	Year	M	D	Lat		Long		Depth	Mb	Ms		Str	Dp	Slp	Str	Dp	Slp
52	1984	7	19	10.93	N	94.82	E	-38	5	4.3	N	86	47	-58	233	52	-120
53	1985	4	4	11.40	N	95.02	E	-18	5.1	4.7	S	349	40	179	79	89	50
54	1971	3	29	11.16	N	95.11	E	-17	5.1	0	S	8	81	14	280	79	174
55	1984	7	9	10.90	N	94.80	E	-10	5.2	0	N	236	50	-108	73	75	-85
56	1990	1	10	11.71	N	95.12	E	0	5.3	5.4	S	260	81	0	170	90	171
57	2005	10	11	10.89	N	92.30	E	-22	5.5	5.1	T	348	29	105	151	62	82
58	1998	11	6	11.06	N	92.49	E	-33	5.1	4.6	T	321	11	72	159	79	94
59	1988	2	28	11.07	N	93.53	E	-134	5	0	S	125	39	151	238	72	54
60	1980	6	1	10.70	N	93.83	E	-163	4.9	0	S	154	58	146	264	32	37
61	1994	8	9	10.67	N	94.36	E	-51.7	5.1	4.8	N	96	20	-55	239	74	-102
62	1994	8	10	10.49	N	94.35	E	-18.7	5.1	5	N	234	45	-87	49	45	-93
63	2005	1	4	10.56	N	91.73	E	-10	5.6	5.3	T	358	21	93	175	69	89
64	2005	1	4	10.67	N	92.36	E	-23	6	5.9	T	353	12	96	167	78	89
65	1972	2	22	10.42	N	92.48	E	-4	5.4	0	S	22	80	-28	296	64	-167
66	1973	7	9	10.67	N	92.59	E	-44	5.6	5.2	S	315	86	25	47	65	176
67	1976	4	21	10.29	N	92.86	E	-52	5.3	0	T	355	30	57	35	66	107
68	2005	7	13	10.35	N	92.90	E	-49	5.3	0	T	4	28	112	160	65	79
69	1980	6	1	10.70	N	93.83	E	-163	4.9	0	S	154	58	146	264	32	37
70	1994	11	7	10.29	N	93.81	E	-55.1	4.9	4.5	N	334	34	-94	158	56	-88
71	1994	8	9	10.67	N	94.36	E	-51.7	5.1	4.8	N	96	20	-55	239	74	-102
72	1994	8	10	10.49	N	94.35	E	-18.7	5.1	5	N	234	45	-87	49	45	-93
73	2000	11	5	9.88	N	92.92	E	-26.7	5.2	5.3	T	193	23	126	335	72	76
74	1970	5	6	9.81	N	92.91	E	-32	5.3	5.1	N	330	80	-89	330	10	-91
75	2000	10	12	9.98	N	92.86	E	-51.3	5.1	4.9	T	174	26	115	327	67	79
76	1971	11	5	10.11	N	92.93	E	-53	5.9	0	T	360	20	73	20	70	95
77	2000	10	9	10.01	N	92.99	E	-44.2	5.2	5.5	T	184	33	123	327	63	71

M. No	Year	M	D	Lat		Long		Depth	Mb	Ms		Str	Dp	Slp	Str	Dp	Slp
78	1968	10	6	9.98	N	93.61	E	-124	5	0	S	335	81	-50	54	42	-163
79	1998	1	12	9.48	N	93.67	E	-139.9	5	0	S	111	60	149	218	64	33
80	1998	5	15	10.19	N	93.98	E	-33	4.9	4.8	S	8	78	-174	277	84	-12
81	2005	7	26	8.37	N	91.64	E	-25	5.2	0	N	350	46	-128	218	56	-58
82	2005	5	4	9.29	N	91.69	E	-19	5.4	4.9	S	41	59	153	147	67	35
83	2004	12	26	8.88	N	92.38	E	-16	6	6.6	T	333	38	82	163	53	96
84	1971	6	5	9.38	N	92.46	E	-25	5.3	5.2	N	333	80	-89	333	10	-91
85	1992	3	17	9.13	N	92.89	E	-64	4.9	0	S	227	71	1	137	89	161
86	1964	9	15	8.90	N	93.03	E	-89	6.3	0	S	323	60	54	70	40	145
87	1986	6	2	9.12	N	93.51	E	-94	5.6	0	S	118	45	154	227	27	48
88	1992	12	8	9.27	N	93.53	E	-87.6	5.9	0	S	137	58	164	235	76	33
89	1998	1	12	9.48	N	93.67	E	-139.9	5	0	S	111	60	149	218	64	33
90	2005	1	7	8.77	N	93.56	E	-30	5.5	4.9	N	0	46	-114	214	49	-67
91	1997	1	11	8.84	N	93.64	E	-10.1	4.6	4.6	S	92	81	-4	182	86	-171
92	1995	7	27	8.88	N	93.68	E	-49.1	5	4.7	S	195	62	-156	93	69	-30
93	1968	7	19	8.68	N	93.67	E	-36	5.5	5.5	S	344	84	-11	72	80	-164
94	1967	7	2	8.65	N	93.59	E	-44	5.7	0	S	351	75	-180	81	90	-18
96	2004	12	28	9.45	N	93.71	E	-30	5.3	4.8	N	199	37	-74	0	55	-101
97	1986	1	28	8.78	N	94.14	E	-27	5.7	5.8	S	346	86	-178	256	88	-4
98	2002	12	13	8.84	N	94.07	E	-33	4.9	0	S	325	70	174	58	84	20
99	2004	12	29	9.11	N	93.76	E	-8	6	5.7	N	220	42	-46	347	61	-122
100	2005	9	13	8.07	N	91.91	E	-30	5.4	4.9	N	204	32	-48	337	67	-112
101	2005	7	25	8.12	N	91.93	E	-31	5.3	5.1	N	207	32	-43	335	69	-115
102	2005	7	24	7.92	N	92.19	E	-16	6.6	7.5	S	121	72	-173	29	83	-18
103	2004	12	27	7.71	N	92.64	E	-9	5.4	5.6	T	326	44	119	109	52	65
104	1983	9	17	7.94	N	93.21	E	-58	5.2	0	N	199	43	-43	324	62	-124

M. No	Year	M	D	Lat		Long		Depth	Mb	Ms		Str	Dp	Slp	Str	Dp	Slp
105	2002	8	6	8.34	N	93.43	E	-79.2	5.1	0	S	122	53	142	237	61	43
106	1986	6	19	7.81	N	94.56	E	-189	5.8	0	N	263	27	-132	128	70	-71
107	1985	4	25	8.55	N	93.61	E	-42	5.3	5.3	S	348	82	178	78	88	8
108	1999	8	29	8.43	N	93.82	E	-49.5	4.8	4.8	S	187	58	167	285	79	33
109	2005	1	26	7.75	N	93.75	E	-33	0	5.5	S	155	83	-177	65	87	-7
110	2005	1	27	8.02	N	94.00	E	-37	5.4	5.1	S	345	85	177	75	87	5
111	2005	2	16	8.11	N	93.97	E	0	5.6	5.7	S	352	86	178	82	88	4
112	2005	1	27	7.91	N	94.35	E	-30	5.2	5	S	185	79	-171	93	81	-11
113	1989	2	18	7.69	N	94.15	E	0	5.2	5	S	62	66	16	326	76	156
114	2005	1	6	6.94	N	91.91	E	-6	5.2	0	S	105	83	-176	15	86	-7
115	1980	2	19	6.73	N	92.58	E	-2	5.1	5.5	T	308	35	38	186	69	119
116	2004	12	31	7.12	N	92.53	E	-14	5.7	6.3	T	319	44	75	160	48	104
117	2005	1	24	7.33	N	92.48	E	-30	6.1	6.2	S	203	84	0	112	90	174
118	2005	2	9	6.80	N	92.62	E	-25	5.4	4.9	T	347	40	95	160	50	86
119	2004	12	28	6.82	N	92.81	E	-13	5.3	4.6	T	271	42	83	100	48	96
120	2005	1	1	7.19	N	92.76	E	-10	5.4	5.4	T	300	32	55	160	64	110
121	1991	3	8	7.27	N	93.45	E	-54.1	5.2	4.5	S	219	43	0	309	90	-133
122	2003	7	21	6.68	N	93.58	E	-12.2	5.2	5.5	S	5	49	148	117	67	46
123	1982	4	8	7.49	N	93.92	E	-44	5.1	4.9	S	305	75	54	16	40	154
124	1997	11	17	6.92	N	94.28	E	-79	4.8	0	T	117	25	135	250	73	72
125	1976	8	5	7.00	N	94.31	E	-87	5.7	0	T	340	40	36	40	70	115
126	1979	6	8	7.30	N	94.43	E	-133	5.1	0	T	55	13	77	249	77	93
127	1971	7	17	6.98	N	94.65	E	-144	5.6	0	T	350	48	41	50	62	130
128	1986	12	7	6.81	N	95.13	E	-217	5.3	0	S	274	79	-5	4	90	-169
129	1982	5	22	7.54	N	93.92	E	-35	5.5	5.3	N	19	21	-98	208	68	-86
130	1990	8	18	7.56	N	94.00	E	-38	5.5	6	S	185	73	180	275	90	17

M. No	Year	M	D	Lat		Long		Depth	Mb	Ms		Str	Dp	Slp	Str	Dp	Slp
131	1976	4	16	7.42	N	94.35	E	-38	5.3	0	T	134	20	91	314	70	89
132	1994	5	25	7.65	N	94.28	E	-24	5.6	5.6	S	148	85	177	238	87	5
133	1989	2	18	7.69	N	94.15	E	0	5.2	5	S	62	66	16	326	76	156
134	1976	12	11	7.65	N	93.90	E	-8	5.4	5.9	S	335	90	11	64	10	176
135	1989	2	10	6.25	N	92.24	E	-1	5.3	5.3	S	291	71	-176	200	87	-19
136	2004	12	31	6.20	N	92.91	E	-11	5.5	6.1	T	359	39	143	119	68	57
137	2005	5	18	5.59	N	93.27	E	-9	5.7	0	S	14	63	7	281	83	153
138	2005	1	6	5.59	N	93.15	E	-24.6	5.7	5.7	N	329	41	-99	161	50	-82
139	2004	12	27	6.48	N	93.28	E	-30	5.4	5.7	S	352	49	148	104	66	46
140	1973	11	9	5.98	N	93.90	E	-44	5.1	0	T	321	82	73	80	20	152
141	1978	6	7	6.29	N	94.11	E	-25	5.1	4.5	S	275	68	16	179	75	158
142	1983	7	2	5.71	N	94.68	E	-95	5.6	0	T	83	44	132	211	59	57
143	2002	10	24	6.03	N	94.42	E	-64.6	6.2	0	S	197	43	18	94	78	132
144	1993	8	28	6.50	N	94.65	E	-110.3	5.7	0	S	283	53	143	38	61	43
145	1991	1	5	5.94	N	94.90	E	-130.3	4.6	0	S	2	68	166	97	77	23
146	1984	8	11	6.05	N	95.29	E	-155	5.3	0	T	348	74	60	52	34	146
147	1986	12	7	6.81	N	95.13	E	-217	5.3	0	S	274	79	-5	4	90	-169
148	2000	9	9	6.42	N	95.46	E	-229.3	5.1	0	S	15	65	-168	280	79	-25
149	1983	4	4	5.71	N	94.72	E	-82	6.5	0	T	342	52	41	44	60	129
150	2000	8	17	5.77	N	94.75	E	-68.3	5.5	5.1	S	96	69	-175	5	86	-21
151	1991	8	26	6.69	N	94.66	E	-42.7	4.9	4.9	S	317	59	170	52	81	31
152	1996	9	21	5.89	N	95.16	E	-41.6	4.6	4.8	S	61	40	1	330	89	130
153	2001	8	12	6.32	N	94.77	E	-33	5.1	5.2	S	143	71	-179	52	89	-19
154	1999	6	22	4.85	N	94.48	E	-34.6	4.8	4.3	S	264	79	-11	356	79	-169
155	2000	8	17	5.77	N	94.75	E	-68.3	5.5	5.1	S	96	69	-175	5	86	-21
156	2001	10	31	5.34	N	94.34	E	-41.9	5.6	5.5	N	331	41	-126	195	58	-63

M. No	Year	M	D	Lat		Long		Depth	Mb	Ms		Str	Dp	Slp	Str	Dp	Slp
157	1983	4	4	5.71	N	94.72	E	-82	6.5	0	T	342	52	41	44	60	129
158	1983	7	2	5.71	N	94.68	E	-95	5.6	0	T	83	44	132	211	59	57
159	1982	2	13	5.75	N	94.77	E	-76	5.1	0	T	328	50	41	30	60	130
160	1991	1	5	5.94	N	94.90	E	-130.3	4.6	0	S	2	68	166	97	77	23
161	1984	8	11	6.05	N	95.29	E	-155	5.3	0	T	348	74	60	52	34	146
162	1981	9	10	5.50	N	95.37	E	-112	5.1	0	T	309	50	115	14	64	35
163	1983	1	30	5.47	N	94.96	E	-89	5.2	0	N	338	66	-121	34	40	-43
164	1964	4	2	5.75	N	95.42	E	-65	5.6	0	S	330	86	0	60	90	-174
165	1996	9	21	5.89	N	95.16	E	-41.6	4.6	4.8	S	61	40	1	330	89	130
166	1985	7	5	5.68	N	95.51	E	-15	4.9	5.2	S	145	61	176	237	86	29
174	2005	7	29	2.86	N	93.56	E	-32	5.8	5	S	112	44	-154	3	72	-49
175	2000	8	1	4.03	N	93.23	E	-9.7	5.2	5	S	192	86	4	102	86	176
176	2004	12	26	2.79	N	94.16	E	-30	5.5	6.2	T	342	34	139	108	68	63
177	2005	1	14	3.13	N	93.92	E	-22	5.4	5.1	T	312	42	85	139	48	95
178	2004	12	30	2.70	N	94.39	E	-30	5.3	4.6	T	334	45	118	117	51	64
179	2004	12	26	2.78	N	94.47	E	-30	5.5	5.9	T	307	35	83	136	56	95
180	2005	1	26	2.70	N	94.60	E	-22	5.6	6	T	306	31	78	140	60	97
181	2004	12	30	4.23	N	94.22	E	-16	5.5	4.9	N	144	31	-64	294	63	-105
182	2004	12	28	3.61	N	94.40	E	-30	5.2	4.7	N	99	36	-148	342	72	-59
184	1987	6	10	4.18	N	94.84	E	-59	5.5	5.3	S	176	46	-25	284	72	-133
185	2005	3	30	2.99	N	95.41	E	-22	5.9	6.2	T	305	7	82	132	83	91
186	1988	4	3	4.71	N	94.46	E	-36	5.8	5.7	T	141	36	130	275	63	65
187	2000	9	4	4.22	N	94.96	E	-58.2	4.8	4.7	S	147	69	158	245	69	22
188	2005	1	2	3.24	N	95.46	E	-8	5.6	5.9	T	119	41	100	285	50	81
189	1986	4	29	4.48	N	95.03	E	-49	5.2	4.9	S	61	43	29	308	71	129
191	1995	6	30	3.72	N	95.42	E	-66.3	5.1	0	N	120	38	-99	311	52	-83

M. No	Year	M	D	Lat		Long		Depth	Mb	Ms		Str	Dp	Slp	Str	Dp	Slp
192	1995	11	22	3.12	N	95.99	E	-52.5	5.5	5.7	T	285	25	63	135	68	102
193	1995	3	14	3.11	N	95.93	E	-57.2	5	5.2	T	299	27	79	131	64	95
194	1977	5	25	4.21	N	95.74	E	-67	5.7	0	N	78	19	-140	310	78	-76
195	1991	7	23	3.81	N	95.96	E	-60.9	5.8	0	N	132	13	-38	260	82	-100
196	1989	7	20	5.07	N	95.66	E	-93	5.8	0	S	169	54	28	62	68	141
197	1974	1	1	4.64	N	95.87	E	-76	5.1	0	S	299	86	-71	20	20	-167
198	2003	9	5	5.32	N	95.90	E	-124.8	5.7	0	S	274	40	175	8	87	50
199	1999	2	15	4.92	N	95.82	E	-25.9	5.1	5.2	S	34	67	0	304	90	157
200	1990	11	18	3.90	N	97.26	E	-50	5.7	0	T	87	29	66	294	64	103
200	2000	7	19	4.24	N	96.31	E	-50	4.8	4.8	S	296	71	165	31	75	19
201	1964	4	3	3.91	N	96.56	E	-51	5.8	0	N	290	70	-88	290	20	-92
202	1999	7	21	4.59	N	97.15	E	-165.5	5.8	0	T	275	13	98	87	77	88
203	1994	11	20	4.31	N	97.63	E	-159.5	5.6	0	S	217	29	15	113	83	119
204	1986	9	8	4.50	N	96.44	E	-44	5.1	5.1	S	118	68	166	214	77	22
205	2002	12	27	4.11	N	97.72	E	-138.5	5.7	0	N	71	12	-132	293	81	-82
207	1967	4	12	5.32	N	96.45	E	-45	5.4	0	T	278	28	92	278	62	87
208	1990	11	18	3.86	N	97.36	E	-64	5.1	0	S	85	51	41	326	59	132
210	1990	11	15	3.89	N	97.40	E	-29	6	6.8	S	122	67	178	212	88	23
211	1982	2	24	4.38	N	97.65	E	-50	5.4	5.4	T	300	49	51	171	54	126
212	2003	9	13	4.53	N	97.63	E	-34.5	5	5	S	103	62	25	1	68	150
213	1980	4	1	4.10	N	97.55	E	-24	5.5	5.9	S	72	80	5	341	85	170
214	1979	9	29	1.16	N	94.21	E	-10	6.2	6.8	S	284	88	-179	194	89	-2
215	1969	11	21	1.94	N	94.61	E	-20	6.4	7.7	S	282	74	163	15	76	18
216	1995	11	8	1.82	N	95.06	E	-29.2	6	6.8	S	192	77	0	102	90	167
217	2005	2	5	2.26	N	94.99	E	-30	5.4	5.8	T	290	44	86	116	46	94
218	2003	6	28	2.74	N	95.71	E	-19.5	5.1	4.8	S	239	29	1	148	89	119

M. No	Year	M	D	Lat		Long		Depth	Mb	Ms		Str	Dp	Slp	Str	Dp	Slp
219	2000	9	1	1.45	N	96.55	E	-31.3	5.5	6.1	T	308	33	83	137	57	95
220	2005	2	24	2.89	N	95.73	E	-30	5.6	5.5	T	292	7	63	139	84	93
221	2003	9	15	2.55	N	96.03	E	-21.6	5	4.7	T	247	40	36	128	68	124
222	2002	11	13	2.98	N	96.04	E	-31.8	5.2	5.4	T	297	18	81	127	72	93
223	1996	9	13	2.86	N	96.20	E	-66.1	4.9	0	T	324	29	105	127	62	82
224	1982	10	31	2.93	N	96.06	E	-48	5.5	0	S	299	51	-144	184	63	-46
225	1989	8	2	2.79	N	96.15	E	-41	5.2	4.9	T	345	28	126	125	67	72
226	2003	9	10	2.09	N	96.84	E	-38.8	5.3	5.5	T	305	14	78	138	77	93
227	1994	10	31	3.03	N	96.25	E	-46.2	5.6	6.2	T	276	24	59	129	69	103
228	1982	3	22	2.56	N	97.08	E	-69	5.1	5.3	T	281	22	51	143	73	104
229	2005	3	28	2.09	N	97.11	E	-30	7.2	8.4	T	329	7	109	130	83	88
230	1997	6	11	2.92	N	97.37	E	-84.2	5.1	0	N	59	19	-140	327	78	-76
231	1986	6	14	2.05	N	98.05	E	-76	5.3	0	T	345	38	120	129	58	69
232	1984	5	29	3.64	N	97.14	E	-77	5.7	0	N	130	21	-78	297	70	-75
233	1981	1	11	2.09	N	98.08	E	-75	5.6	0	T	301	23	86	126	67	92
234	2004	11	27	1.98	N	97.93	E	-41	5.3	4.6	T	335	28	114	128	65	78
235	2005	4	3	2.02	N	97.94	E	-36	6	5.9	T	326	23	110	125	68	82
236	1993	1	20	3.10	N	97.69	E	-71	6.1	0	N	115	19	-98	303	72	-87
237	1996	10	10	3.49	N	97.88	E	-19.7	5.5	6	S	54	88	-1	144	89	-178
238	1970	8	3	2.54	N	97.94	E	-69	5.7	0	S	304	82	-61	18	30	-159
239	1980	12	30	0.07	N	97.21	E	-11	5	5.4	T	286	27	31	168	77	113
240	2005	4	8	-0.22	S	97.73	E	-20	5.7	6.3	S	337	59	166	74	78	32
241	2005	4	25	0.36	N	97.28	E	-35	5.4	5.1	N	155	29	-58	300	66	-106
242	2005	9	6	0.03	N	97.60	E	-27	5.4	5.5	S	345	60	161	85	74	32
243	2001	3	7	0.33	N	97.73	E	-39.3	4.8	4.7	T	272	21	45	139	75	105
244	2005	4	7	0.61	N	97.42	E	-26	5.9	5.7	S	133	61	147	240	62	34

M. No	Year	M	D	Lat		Long		Depth	Mb	Ms		Str	Dp	Slp	Str	Dp	Slp
245	2005	4	17	0.31	N	97.66	E	-25	5.7	5.2	N	193	14	-57	339	78	-98
246	1984	11	17	0.22	N	98.05	E	-42	6.2	7.2	T	334	10	116	128	81	86
247	2005	4	1	0.32	N	98.11	E	-29	5.6	5	S	133	89	-179	43	89	-1
248	1997	7	7	1.04	N	97.63	E	-56.1	5.4	5.8	T	294	15	68	137	76	96
249	2005	4	3	0.37	N	98.32	E	-30	5.9	5.9	T	330	19	112	127	72	83
250	2004	5	11	0.41	N	97.82	E	-21	5.6	6.2	T	322	14	102	130	76	87
251	2005	4	16	1.81	N	97.66	E	-31	6	6.2	T	338	19	125	122	74	79
252	1995	2	26	1.31	N	97.94	E	-70.8	5.1	0	N	89	13	-130	310	80	-81
253	1979	4	28	0.56	N	98.77	E	-82	5.7	0	S	233	61	26	130	68	148
254	1985	6	29	1.38	N	98.46	E	-84	5.4	0	N	63	29	-135	292	70	-69
255	2001	5	11	0.88	N	98.94	E	-80.2	5	0	S	211	61	23	109	70	149
256	1993	11	1	2.06	N	98.16	E	-90.5	5.1	0	T	272	27	51	135	69	108
257	1984	7	8	1.02	N	98.87	E	-104	5.1	0	S	124	32	172	220	86	58
258	1988	1	14	0.94	N	99.13	E	-118	4.9	0	S	72	35	173	168	86	55
259	2005	4	4	1.61	N	97.87	E	-30	5.5	5.3	T	335	25	109	134	66	81
260	1971	2	4	0.53	N	98.72	E	-40	6.2	7.1	S	358	76	20	84	72	162
261	2002	1	4	1.95	N	97.92	E	-42.2	5.3	0	T	257	23	65	103	69	100
262	1985	1	2	1.68	N	98.83	E	-113	5.4	0	T	107	34	118	254	61	73
263	1977	1	12	1.57	N	99.82	E	-191	5.6	0	T	92	46	132	220	58	56
264	1995	7	15	2.67	N	99.10	E	-171.8	5.1	0	N	161	14	-63	314	78	-96
265	1984	8	27	1.87	N	99.10	E	-40	5.1	5.2	S	241	81	3	151	87	171
266	1987	4	25	2.38	N	98.92	E	-30	5.8	6.6	S	324	75	172	56	83	15
267	2001	6	15	-1.37	S	97.38	E	-33	5.1	0	S	176	57	30	69	65	144
268	1979	6	13	-0.98	S	97.26	E	-34	5.3	4.2	N	182	54	-45	309	55	-134
269	1994	7	23	-1.09	S	97.44	E	-31.5	5.1	4.7	N	279	36	-67	71	58	-106
270	1979	4	19	-1.25	S	98.17	E	-34	5.3	5	T	292	11	55	148	81	97

M. No	Year	M	D	Lat		Long		Depth	Mb	Ms		Str	Dp	Slp	Str	Dp	Slp
271	1979	4	19	-1.21	S	98.20	E	-30	5.5	5.6	T	210	13	72	149	77	94
272	1988	5	21	-1.12	S	98.22	E	-28	5.1	5.3	T	330	8	97	143	82	89
273	2000	5	8	-0.88	S	98.06	E	-33	5.4	5.3	T	306	16	78	139	74	94
274	1990	9	12	-0.46	S	98.34	E	-47	5.1	5	S	330	23	139	99	75	22
275	1979	5	8	-0.36	S	98.29	E	-41	5.4	4.8	T	268	5	43	136	56	94
276	1994	1	10	-0.65	S	98.65	E	-48.5	4.9	4.5	N	287	44	-64	73	52	-113
277	1994	1	7	-0.57	S	98.64	E	-48.8	5.6	5.4	T	285	19	67	129	73	98
278	2002	3	27	-0.50	S	98.68	E	-33	5.1	0	T	305	14	71	144	77	95
279	2005	2	14	-0.13	S	98.73	E	-47	6	5.9	S	190	35	15	88	82	124
280	2001	7	23	0.29	N	98.54	E	-33	5	0	S	44	30	165	146	83	60
281	1998	4	1	-0.50	S	99.32	E	-61.6	6.1	0	T	320	21	105	124	69	84
282	1986	4	17	-0.83	S	99.88	E	-83	5.4	0	T	333	32	103	138	59	82
283	1980	2	27	0.62	N	100.03	E	-168	5	0	T	97	42	141	218	65	55
284	1999	11	11	1.25	N	100.21	E	-214.6	6	0	S	92	44	168	190	82	46
285	1998	12	22	-0.21	S	99.25	E	-38.2	5	4.3	T	312	32	90	132	58	90
286	1986	8	12	0.12	N	100.24	E	-49	5.3	5.3	S	66	81	10	334	81	170
287	1991	7	2	-1.10	S	99.83	E	-28.7	5.9	6.1	T	336	20	108	137	71	84
288	1977	3	8	0.44	N	99.89	E	-32	5.5	6	S	312	80	179	42	89	10
289	1979	7	17	-4.44	S	98.74	E	-21	5.7	5.2	T	247	48	138	8	60	51
290	1997	12	18	-2.00	S	99.57	E	-13.8	5.3	5.4	S	219	11	-1	310	90	-101
291	1998	5	29	-2.20	S	99.61	E	-20.8	5.2	5.1	T	308	10	100	118	80	88
292	1994	5	17	-2.05	S	99.62	E	-22.5	5.2	5.5	T	254	11	29	135	84	100
293	1994	5	11	-2.06	S	99.70	E	-28	5.8	5.9	T	299	12	83	127	78	92
294	1994	5	9	-2.03	S	99.77	E	-31.1	5.9	5.5	T	271	22	54	129	72	103
295	1998	8	25	-1.64	S	99.63	E	-35.2	4.9	4.2	S	89	74	173	181	83	16
296	2005	4	14	-1.91	S	99.95	E	-33	5.8	5.6	T	325	14	111	124	77	85

M. No	Year	M	D	Lat		Long		Depth	Mb	Ms		Str	Dp	Slp	Str	Dp	Slp
297	2005	4	10	-1.59	S	99.72	E	-30	5.9	6.2	T	124	13	99	296	77	88
298	1977	6	24	-2.26	S	100.81	E	-61	5.5	0	N	228	24	-48	3	73	-107
299	1981	12	8	-1.52	S	100.51	E	-82	5.3	0	T	327	29	105	130	62	82
300	1988	8	9	-1.33	S	100.72	E	-108	5	0	S	39	28	169	138	85	62
301	1979	5	19	-1.10	S	100.95	E	-133	5.3	0	S	107	54	142	222	60	43
302	2003	7	14	-0.54	S	100.82	E	-144.2	5.4	0	S	191	58	30	84	65	144
303	1981	11	12	-0.97	S	100.26	E	-63	5.4	5.1	S	339	63	168	75	79	28
304	2004	2	22	-1.56	S	100.49	E	-42	6.3	5.7	N	224	54	-45	346	55	-134
305	1995	10	6	-2.01	S	101.50	E	-36.7	5.8	6.8	S	326	74	-177	235	87	-16
306	2004	2	16	-0.47	S	100.65	E	-55	5.2	4.5	T	133	38	113	285	56	73
307	1989	5	1	-4.22	S	101.36	E	-12	5.5	5.6	T	294	21	99	105	70	87
308	1989	4	28	-4.33	S	101.39	E	-21	5.4	5.8	T	277	6	61	127	85	93
309	1989	4	28	-4.30	S	101.33	E	-34	5.2	5.6	T	315	19	107	116	72	84
310	2001	1	16	-4.19	S	101.60	E	-57.7	5.6	0	T	325	32	96	139	58	86
311	2001	1	16	-4.07	S	101.74	E	-28	6.3	6.8	T	321	14	111	119	77	85
312	2001	1	18	-4.05	S	101.75	E	-55.4	5.5	5.3	T	311	19	87	135	71	91
313	2002	9	19	-3.25	S	101.38	E	-43.9	4.9	0	T	311	20	109	111	71	83
314	1983	1	4	-3.15	S	101.16	E	-50	5.6	5.2	T	279	32	53	141	65	110
315	1997	5	10	-3.19	S	101.53	E	-47.7	5.4	5.1	T	305	20	87	129	70	91
316	1994	8	5	-3.17	S	101.47	E	-68.2	5.4	0	T	267	10	55	122	82	96
317	2003	2	3	-2.79	S	101.19	E	-59.7	5.5	5.2	T	314	22	108	115	69	83
318	1980	7	23	-2.75	S	101.18	E	-65	5.5	5	T	325	19	120	113	74	80
319	1991	12	17	-3.63	S	101.97	E	-67.6	5.4	0	T	258	32	48	125	67	113
320	2002	1	22	-2.88	S	101.21	E	-33	5	0	N	164	33	-124	23	64	-70
321	1977	6	10	-3.11	S	101.52	E	-79	5.3	5.2	T	319	20	105	123	70	84
322	1992	8	5	-3.10	S	101.79	E	-76.2	5.3	0	T	37	36	35	278	71	121

M. No	Year	M	D	Lat		Long		Depth	Mb	Ms		Str	Dp	Slp	Str	Dp	Slp
323	2003	7	2	-3.64	S	102.06	E	-75.2	5.3	0	T	318	24	107	120	67	83
324	1999	12	2	-2.87	S	101.58	E	-78.5	4.8	0	S	280	27	-18	27	82	-116
325	1997	4	22	-3.38	S	102.10	E	-100.7	5.6	0	S	205	35	13	104	82	124
326	1988	6	15	-3.39	S	102.17	E	-109	5.1	0	S	217	75	7	125	83	165
327	2003	11	14	-3.61	S	102.04	E	-33	5.1	0	S	7	19	179	97	90	71
328	1999	2	18	-2.74	S	101.85	E	-46.3	5	4.5	S	305	56	158	48	72	36
329	1979	12	15	-3.41	S	102.58	E	-30	5.8	6.6	S	229	74	-4	320	86	-164
330	1992	6	12	-2.12	S	101.84	E	-138.2	5.1	0	S	295	49	164	35	78	42
331	2002	6	16	-2.34	S	102.56	E	-231.6	5.4	0	T	291	7	71	130	83	92
332	1979	6	17	-6.30	S	100.50	E	-13	5.3	4.6	N	128	40	-84	300	50	-95
333	1983	3	3	-6.13	S	100.73	E	-36	5.4	5.4	S	9	58	-25	113	69	-146
334	1982	11	11	-6.61	S	101.70	E	-96	6.1	6	N	108	35	-135	338	66	-64
335	2003	9	7	-5.71	S	102.02	E	-3.8	5.5	5.2	T	310	37	118	97	58	71
336	2002	5	24	-5.83	S	101.80	E	-33	5	5	S	264	41	25	154	74	128
337	2005	2	19	-5.64	S	101.61	E	-29	5.5	4.7	T	334	24	137	104	74	72
338	2000	6	11	-5.52	S	101.49	E	-33	5	5.3	T	242	11	21	131	86	100
339	2004	2	29	-6.13	S	102.22	E	-41	4.8	4.7	T	331	22	138	102	76	74
340	1999	6	12	-5.98	S	102.10	E	-33	4.9	5	S	261	29	22	151	80	117
341	2002	5	23	-5.84	S	102.08	E	-33	5.4	5.4	T	288	35	74	127	57	101
342	2003	8	29	-5.44	S	102.24	E	-26.9	5	4.6	N	202	12	-13	305	87	-101
343	2002	1	21	-5.63	S	102.34	E	-33	5	5.1	T	317	41	81	149	50	97
344	2003	12	24	-5.78	S	102.04	E	-29.3	5.4	5.3	T	95	41	76	294	50	102
345	2000	9	12	-5.43	S	101.82	E	-33	5.7	6.1	T	330	41	117	116	54	68
346	1991	6	11	-5.24	S	102.67	E	-82.1	5.2	0	T	241	38	41	117	66	121
347	1988	9	23	-4.90	S	101.90	E	-59	4.7	0	S	253	25	20	145	82	114
348	2000	7	16	-5.21	S	102.14	E	-18.8	4.9	5	S	90	60	-173	356	84	-30

M. No	Year	M	D	Lat		Long		Depth	Mb	Ms		Str	Dp	Slp	Str	Dp	Slp
349	1980	3	18	-4.24	S	102.03	E	-56	5.4	4.9	S	37	47	162	139	77	44
350	1989	11	14	-5.03	S	102.81	E	-78	4.8	4.8	T	317	11	68	160	79	94
351	1996	6	5	-4.54	S	101.99	E	-67.8	5	0	T	309	21	103	116	69	85
352	1991	7	18	-4.42	S	102.81	E	-132.7	4.6	0	S	73	81	1	342	89	177
353	2001	5	27	-4.33	S	102.84	E	-100	5.1	0	S	232	57	-12	328	80	-147
354	1986	12	31	-4.26	S	102.79	E	-91	5.1	0	T	280	30	72	115	61	78
355	1988	5	5	-4.44	S	102.99	E	-102	5.2	0	S	144	83	173	235	83	7
356	1991	11	8	-4.24	S	102.81	E	-93.5	5.6	0	T	265	34	57	123	62	110
357	1991	1	26	-3.47	S	102.64	E	-125.3	5.5	0	S	199	65	19	101	73	154
358	2003	3	3	-3.86	S	102.57	E	-75.7	5.1	0	S	284	67	157	23	69	25
359	1999	9	18	-4.06	S	103.20	E	-24.7	4.9	5.2	S	48	75	2	318	88	165
360	2004	11	10	-6.96	S	102.87	E	-20	5.2	4.8	T	322	16	117	114	76	83
361	1984	2	25	-7.09	S	103.48	E	-12	5.4	5.6	T	359	23	136	130	75	73
362	1983	1	22	-6.69	S	102.87	E	-15	5.6	6.1	T	325	41	113	116	53	71
363	1979	7	29	-6.30	S	102.42	E	-24	5.4	4.9	T	5	12	163	111	86	78
364	1983	1	22	-6.58	S	102.98	E	-46	5.2	5.5	S	2	56	156	106	70	36
365	2000	11	5	-6.08	S	102.68	E	-33	5.2	5.6	S	342	65	-164	245	75	-26
366	1992	8	5	-5.55	S	102.85	E	-52.9	5.5	5.3	T	333	6	121	122	85	87
367	1982	2	21	-6.03	S	102.63	E	-27	5.3	5.5	S	21	24	171	119	86	66
368	1998	7	8	-6.27	S	104.07	E	-59.6	5.3	4.9	T	271	27	67	117	65	101
369	2005	5	10	-6.23	S	103.14	E	-17	5.9	6.4	T	311	42	98	120	48	83
370	2000	6	20	-5.73	S	102.60	E	-33	4.7	5.2	S	342	69	162	78	73	22
371	1979	6	25	-5.96	S	103.57	E	-38	5.6	0	S	287	56	-25	32	70	-144
372	1999	2	1	-5.97	S	103.85	E	-18.4	5.1	4.8	T	261	26	46	128	71	109
373	1997	10	29	-6.30	S	104.15	E	-64.1	5.3	0	T	309	24	108	110	67	82
374	1992	12	25	-5.61	S	103.21	E	-71.7	5	0	T	232	22	45	99	75	106

M. No	Year	M	D	Lat		Long		Depth	Mb	Ms		Str	Dp	Slp	Str	Dp	Slp
375	1996	12	13	-6.21	S	104.08	E	-79.7	5.2	0	T	301	18	81	130	72	93
376	1991	6	6	-5.93	S	103.92	E	-50	5.2	5.2	S	236	37	19	130	79	126
377	1992	6	14	-6.18	S	104.29	E	-63.9	5.1	0	S	346	41	160	92	77	51
378	1993	12	25	-5.76	S	104.21	E	-80.8	5	0	S	242	57	-16	341	77	-146
379	1983	12	27	-6.16	S	104.15	E	-59	5.4	4.9	T	325	27	142	90	74	68
380	2002	11	6	-5.65	S	104.57	E	-98.1	4.9	0	T	339	13	137	111	81	81
381	1983	11	3	-5.77	S	104.54	E	-93	5.3	0	S	103	63	26	1	67	150
382	1994	1	21	-4.86	S	103.71	E	-96.5	6	0	T	66	46	128	197	56	57
383	1983	10	7	-4.61	S	103.56	E	-122	4.9	0	T	232	38	82	61	52	96
384	1995	9	23	-5.57	S	104.07	E	-50.7	5.9	5.6	T	262	20	83	90	70	93
385	1985	12	28	-5.80	S	104.30	E	-15	5.7	6	S	342	80	174	73	84	10
386	1987	2	7	-4.89	S	103.27	E	-70	5.3	0	S	234	56	-2	325	89	-146
387	2000	7	10	-4.47	S	103.76	E	-104.7	5.8	0	T	234	31	77	69	60	98
388	1998	12	11	-5.77	S	104.45	E	-69.3	5.1	0	T	287	17	72	126	74	95
389	1997	11	16	-4.92	S	103.20	E	-55.5	5.4	4.7	T	289	29	76	124	61	98
390	1994	2	15	-4.97	S	104.33	E	-23.1	5.9	7	S	315	71	176	46	86	19
391	1987	10	9	-7.88	S	105.25	E	-30	5.1	5.3	S	337	36	162	77	83	55
392	2002	8	13	-7.10	S	104.04	E	-33	5.4	5.9	S	317	87	-179	227	89	-3
393	2002	6	28	-7.01	S	103.98	E	-23.7	5.4	4.8	T	176	27	79	9	64	95
394	1993	2	10	-7.75	S	105.31	E	-75.9	5.5	0	S	80	66	173	173	83	24
395	2002	6	27	-7.00	S	104.09	E	-33	5.9	6.9	T	305	40	100	112	50	81
396	1999	2	1	-6.48	S	104.68	E	-23.5	5.2	4.5	T	271	24	76	106	67	96
397	1990	4	6	-6.85	S	105.14	E	-33	5.6	5.6	S	36	61	-20	136	72	-150
398	1998	5	24	-6.51	S	104.77	E	-36.1	5	5.1	S	12	70	-167	277	77	-20
399	1995	4	5	-6.29	S	105.23	E	-92.3	5	0	T	199	47	59	60	51	118
400	1991	10	23	-6.91	S	105.42	E	-83.5	5.2	0	S	129	70	-177	38	87	-20

M. No	Year	M	D	Lat		Long		Depth	Mb	Ms		Str	Dp	Slp	Str	Dp	Slp
401	1990	1	20	-6.59	S	105.98	E	-88	5.2	0	S	269	59	-24	12	69	-147
402	1999	8	14	-5.87	S	104.73	E	-105.2	6.2	0	S	65	52	265	164	78	39
403	1979	5	7	-6.39	S	105.93	E	-123	5.9	0	S	69	58	171	164	82	33
404	1984	3	15	-6.56	S	105.30	E	-66	5.4	0	S	216	42	47	88	60	22
405	2000	7	31	-6.73	S	105.48	E	-41.4	5	4.8	S	149	82	-177	58	87	-8
406	1990	8	2	-6.45	S	105.37	E	-26	5.4	5.2	T	295	46	120	74	52	63
407	1994	12	11	-5.87	S	104.62	E	-50.7	5.4	4.6	T	257	26	58	113	68	105
408	1996	12	13	-6.20	S	105.55	E	-51.2	4.7	4.9	N	168	35	-61	314	60	-109
409	1985	8	10	-5.98	S	105.33	E	-64	5.3	0	S	50	51	-18	151	76	-140
410	1992	3	3	-5.91	S	106.12	E	-140	5.1	0	S	4	62	30	259	64	148
411	1985	1	22	-5.88	S	104.54	E	-56	5.5	0	T	252	26	48	117	71	108
412	2001	4	25	-9.17	S	106.56	E	-44.3	5.4	5	T	151	33	81	342	57	96
413	1994	9	12	-8.94	S	106.48	E	-29.8	5.8	5.3	S	64	66	-165	327	76	-25
414	2004	1	13	-8.57	S	105.87	E	-25	5.1	4.7	T	318	38	102	124	53	81
415	1981	10	23	-8.79	S	106.46	E	-33	5.1	5.7	T	331	50	135	105	80	79
416	1990	1	5	-8.71	S	106.55	E	-29	5.4	5.8	T	64	26	27	309	78	113
417	2003	5	14	-8.00	S	107.21	E	-38	5.3	5.3	T	257	11	109	57	80	86
418	1991	12	19	-7.81	S	106.54	E	-52.3	4.8	0	S	258	54	30	150	66	140
419	2003	11	24	-7.50	S	106.24	E	-9.5	5.1	4.9	N	327	16	-130	188	78	-80
420	1992	10	30	-7.94	S	107.03	E	-75.7	5.1	0	T	247	23	44	115	74	107
421	2001	6	1	-7.74	S	107.21	E	-90.3	5.1	0	T	48	36	126	187	62	67
422	1995	1	12	-7.14	S	106.63	E	-84.3	4.9	0	T	315	17	133	91	78	78
423	1999	7	13	-7.08	S	107.14	E	-102.5	4.8	0	T	62	11	82	251	80	92
424	1986	12	12	-7.13	S	107.37	E	-92	5	0	S	151	69	178	242	86	21
425	1983	3	9	-7.18	S	107.70	E	-118	5.4	0	S	350	56	32	241	64	142
426	1980	9	22	-7.08	S	107.69	E	-161	5.2	0	N	91	16	-133	315	79	-79

M. No	Year	M	D	Lat		Long		Depth	Mb	Ms		Str	Dp	Slp	Str	Dp	Slp
427	1977	9	10	-6.61	S	107.09	E	-152	5.7	0	T	11	29	38	247	73	114
428	1988	8	17	-7.69	S	107.16	E	-27	6	5.8	T	128	41	100	295	49	82
429	1984	3	10	-7.58	S	106.98	E	-61	5.7	0	T	315	26	122	100	68	75
430	2000	6	5	-7.36	S	106.66	E	-33	4.9	4.2	T	259	23	65	105	70	100
431	1986	5	20	-7.26	S	106.54	E	-75	5.5	0	S	48	34	162	152	80	57
432	2002	10	21	-7.37	S	107.36	E	-65.5	4.9	0	S	343	49	-179	252	90	-41
433	1985	10	9	-6.76	S	107.04	E	-104	6	0	T	254	2	32	131	89	91
434	1992	3	24	-5.57	S	106.54	E	-303.8	4.5	0	T	272	30	43	143	70	113
435	1999	3	7	-5.86	S	107.50	E	-337.9	4.9	0	T	299	33	131	73	66	67
436	2000	7	12	-6.68	S	106.85	E	-33	5.2	5	S	350	42	-152	238	71	-51
437	2000	9	24	-6.65	S	107.88	E	-33	5	0	T	331	30	91	149	60	89
438	1964	11	24	-6.84	S	107.28	E	-130	5.5	0	S	140	90	23	240	70	180
439	1999	5	26	-6.26	S	106.35	E	-133.9	4.8	0	T	241	52	128	9	52	52
440	1998	10	17	-6.32	S	106.88	E	-155	4.9	0	S	5	51	34	252	64	136
441	, 1997	1	19	-5.05	S	108.38	E	-653.5	4.8	0	N	121	46	-117	337	50	-65
442	1963	12	15	-4.80	S	108.00	E	-650	0	7.1	N	125	57	-72	340	39	-118
443	2003	6	1	-9.55	S	108.37	E	-25.9	5.3	4.9	T	285	3	87	108	87	90
444	2004	12	12	-8.84	S	108.62	E	-48	4.9	4.5	S	314	62	-178	224	88	-28
445	1979	8	7	-8.78	S	108.78	E	-35	5.6	0	T	262	27	69	105	65	100
446	2001	1	7	-8.70	S	108.89	E	-33	5.5	5.1	T	252	29	52	114	68	109
447	1977	8	10	-8.28	S	107.67	E	-80	5.5	0	T	146	43	43	21	62	124
448	1990	11	8	-8.57	S	108.93	E	-70	5.2	0	T	288	26	109	85	56	77
449	1999	1	26	-8.24	S	108.61	E	-73.4	5.2	0	S	46	57	165	144	78	34
450	1984	12	12	-7.91	S	107.94	E	-50	5.5	0	T	276	29	90	96	61	90
451	1987	11	18	-8.07	S	108.79	E	-63	5.5	0	S	346	55	23	242	72	143
452	1985	4	25	-7.69	S	108.04	E	-91	5.1	0	T	260	16	71	100	75	95

M. No	Year	M	D	Lat		Long		Depth	Mb	Ms		Str	Dp	Slp	Str	Dp	Slp
453	1977	1	1	-7.90	S	109.00	E	-112	5.8	0	N	63	23	-130	285	73	-75
454	1994	7	1	-7.93	S	109.13	E	-101.5	4.8	0	T	255	25	66	102	67	101
455	1982	10	26	-7.39	S	108.71	E	-158	5.4	0	T	23	45	69	232	49	110
456	1989	9	1	-6.67	S	108.46	E	-237	5.2	0	N	357	44	-139	235	63	-53
457	1965	1	17	-6.85	S	109.01	E	-246	5.7	0	S	224	75	-44	328	50	-158
458	1990	5	21	-8.10	S	109.06	E	-17	5.5	5.2	T	303	19	113	98	72	82
459	1990	7	6	-6.81	S	108.09	E	-14	5.6	4.8	T	98	33	67	305	60	104
460	1992	2	4	-7.26	S	108.99	E	-34.6	4.9	4.5	T	186	46	138	308	61	52
461	1990	2	4	-10.24	S	110.29	E	-20	5.8	5.4	N	87	36	-89	267	54	-90
462	1999	5	24	-9.91	S	109.08	E	-33	4.8	4.3	N	153	26	-61	301	67	-103
463	1996	9	25	-9.26	S	108.73	E	-26.6	5.3	5.6	S	141	58	155	245	69	34
464	1989	9	12	-8.98	S	110.52	E	-27	5.2	0	T	310	55	106	111	57	79
465	1997	7	12	-9.06	S	110.51	E	-67.6	4.7	0	T	267	35	57	125	61	111
466	1999	2	4	-8.98	S	110.43	E	-96	5.3	0	N	41	35	-100	233	56	-83
467	1989	9	12	-8.97	S	110.55	E	-70	5.2	5.1	T	119	41	81	311	49	98
468	2001	5	25	-7.87	S	110.18	E	-143.1	5.8	0	S	49	32	-158	300	79	-60
469	1979	10	7	-7.74	S	110.71	E	-179	5.2	0	N	65	48	-43	187	60	-129
470	1981	3	13	-8.83	S	110.43	E	-48	5.5	0	N	139	11	-47	275	82	-98
471	1985	7	9	-8.44	S	110.33	E	-35	5.6	0	T	283	41	135	150	62	58
472	1992	11	21	-8.66	S	110.44	E	-71.1	5.2	0	T	321	26	137	91	73	71
473	1985	7	23	-8.42	S	110.74	E	-112	5.3	0	T	42	27	66	248	65	102
474	1965	4	29	-5.65	S	110.24	E	-524	5.7	0	S	40	70	169	126	80	22
475	1991	12	24	-5.66	S	110.24	E	-540.8	4.9	0	N	84	49	-127	313	53	-55
476	2000	9	21	-5.71	S	110.62	E	-560.9	5.3	0	N	96	37	-114	306	57	-73
477	1994	9	28	-5.77	S	110.42	E	-660.5	5.8	0	N	108	44	-113	319	50	-69
478	1997	7	11	-5.72	S	110.73	E	-577.5	5.4	0	S	69	46	-158	324	75	-46

M. No	Year	M	D	Lat		Long		Depth	Mb	Ms		Str	Dp	Slp	Str	Dp	Slp
479	1967	2	3	-5.65	S	110.42	E	-555	4.8	0	N	100	46	-65	134	49	-113
480	1984	7	9	-5.76	S	111.29	E	-537	5.8	0	N	74	23	-138	305	75	-73
481	1975	12	13	-5.62	S	110.55	E	-564	4.9	0	T	5	9	136	50	84	82
482	1982	7	23	-10.82	S	111.72	E	-33	5.1	0	N	91	37	-98	281	53	-84
483	2003	11	20	-10.01	S	111.12	E	-5.6	5.1	5.6	T	286	20	106	89	71	84
484	1990	8	26	-9.13	S	110.78	E	-52	5.3	4.7	S	338	15	176	72	89	75
485	1989	10	31	-9.24	S	111.94	E	-56	5.3	5.2	S	69	56	26	323	69	143
486	1980	12	24	-9.12	S	112.01	E	-48	5.5	0	N	23	40	-135	256	63	-59
487	1983	8	17	-8.77	S	111.16	E	-74	5.2	0	T	282	43	116	68	52	68
488	1995	5	5	-8.72	S	111.15	E	-105.7	5.7	0	N	93	22	-100	284	69	-86
489	1995	7	27	-8.66	S	111.32	E	-88.8	5	0	T	236	38	56	96	59	114
490	1984	5	3	-8.61	S	111.28	E	-81	5.6	0	T	258	33	64	109	61	106
491	2000	2	22	-8.70	S	112.44	E	-107.9	5	0	N	58	49	-128	288	54	-54
492	2000	9	5	-8.47	S	112.14	E	-136.9	4.9	0	N	55	35	-135	285	66	-64
493	1986	3	9	-8.10	S	111.72	E	-126	5.2	0	T	14	44	60	233	53	116
494	1998	9	28	-8.17	S	112.45	E	-157.2	6	0	S	358	13	-176	263	89	-77
495	1978	10	14	-7.48	S	112.27	E	-198	5.4	0	S	115	29	7	19	86	119
496	2005	6	11	-8.92	S	112.20	E	-60	5.4	0	T	0	31	102	166	59	83
497	2003	7	19	-8.68	S	111.23	E	-56.2	5.9	0	T	283	25	97	95	65	87
499	2000	1	29	-8.63	S	111.14	E	-60.7	5.4	4.6	T	244	29	67	90	64	102
499	2003	5	28	-8.58	S	112.50	E	-65.3	5.2	0	T	281	18	81	110	72	93
500	1983	8	13	-8.69	S	111.17	E	-64	5.9	0	T	260	36	78	94	55	98
501	1992	6	9	-8.48	S	111.12	E	-81.8	5.8	0	S	1	17	-11	101	87	-107
502	1987	2	27	-6.06	S	112.79	E	-594	5.2	0	N	172	20	-31	292	80	-107
503	1982	8	29	-5.97	S	112.79	E	-608	5.6	0	N	278	34	-105	117	57	-80
504	1984	11	5	-5.94	S	111.78	E	-622	5.4	0	S	163	80	-173	71	83	-10

M. No	Year	M	D	Lat		Long		Depth	Mb	Ms		Str	Dp	Slp	Str	Dp	Slp
505	1982	1	27	-6.11	S	111.68	E	-635	5.1	0	N	62	22	-136	290	75	-74
506	1981	11	8	-6.17	S	112.17	E	-649	5.7	0	N	291	39	-109	123	51	-82
507	1996	12	12	-6.04	S	112.94	E	-616.7	4.9	0	N	265	43	-92	87	47	-88
508	1992	9	2	-6.02	S	112.18	E	-637.6	5.9	0	N	291	34	-79	97	57	-97
509	2004	11	3	-10.71	S	112.68	E	-11	5.1	5	N	119	35	-82	290	55	-95
510	1994	6	4	-10.75	S	113.43	E	-11	6	6.3	N	88	41	-98	279	49	-83
511	1994	6	4	-10.81	S	113.31	E	-37	5.4	5.1	N	52	44	-121	272	53	-64
512	1997	7	10	-10.77	S	113.62	E	-31.1	5.1	4.7	S	55	64	-169	320	80	-26
513	1994	7	24	-10.62	S	113.35	E	-34.7	5.8	4.9	S	113	58	-25	217	69	-146
514	1994	6	2	-10.41	S	112.93	E	-38.9	5.7	7.1	T	278	7	89	99	83	90
515	1994	6	5	-10.32	S	113.50	E	-25.9	5.7	6.3	N	96	24	-111	299	68	-81
516	1994	6	18	-10.23	S	113.61	E	-44	5.5	5.1	N	88	11	-119	297	80	-85
517	1994	7	18	-9.62	S	112.99	E	-33	5.4	5.1	S	32	53	-165	292	78	-38
518	1984	1	26	-9.50	S	112.83	E	-48	5.1	5.1	T	294	34	109	90	58	78
519	1994	4	25	-9.37	S	113.03	E	-54.3	5.6	5.3	T	268	32	86	92	58	92
520	1985	4	13	-9.19	S	114.26	E	-88	6	0	T	167	35	36	44	70	119
521	1992	6	26	-8.87	S	112.54	E	-82.1	5.1	0	T	356	29	88	178	61	91
522	1989	12	3	-8.82	S	113.42	E	-101	5.7	0	S	358	59	-154	253	68	-34
523	2001	8	7	-8.61	S	113.83	E	-90.5	5.4	0	T	1	38	53	225	61	115
524	1989	10	10	-9.03	S	113.26	E	0	5.3	4.2	S	328	60	-169	233	81	-31
525	2000	1	16	-9.27	S	113.96	E	-58.5	5.1	0	T	233	29	53	94	67	109
526	2003	8	25	-8.91	S	113.18	E	-67.8	5.2	0	T	90	27	43	320	72	111
527	1978	6	10	-6.12	S	114.26	E	-535	5.5	0	S	165	48	-22	270	74	-136
528	1993	7	17	-6.07	S	113.13	E	-586.7	5.2	0	N	61	39	-137	296	65	-59
529	1987	10	10	-6.05	S	113.18	E	-584	5.5	0	N	120	29	-68	275	63	-102
530	1998	4	27	-6.09	S	113.14	E	-598.6	5.3	0	N	108	45	-82	276	46	-98

M. No	Year	M	D	Lat		Long		Depth	Mb	Ms		Str	Dp	Slp	Str	Dp	Slp
531	1985	8	8	-6.10	S	113.50	E	-604	5.7	0	N	91	37	-88	269	53	-91
532	1992	12	27	-6.10	S	113.11	E	-621.9	5.8	0	N	250	29	-131	115	68	-70
533	1983	11	15	-11.48	S	115.23	E	-34	5.3	0	S	42	59	-159	300	72	-33
534	2001	9	20	-11.42	S	115.04	E	-10	5.6	5.1	N	82	32	-113	288	61	-77
535	1983	9	29	-11.37	S	115.32	E	-40	5.6	0	N	70	44	-128	297	57	-60
536	1982	8	7	-11.16	S	115.42	E	-55	6.1	0	N	288	45	-65	75	50	-113
537	1990	10	15	-10.11	S	114.61	E	-85	5.7	0	S	195	26	14	92	84	116
538	1984	2	2	-9.96	S	115.02	E	-48	5.4	4.8	S	102	53	31	352	66	139
539	1999	8	31	-9.94	S	116.05	E	-87.3	5.1	0	T	187	34	78	22	57	98
540	1991	7	5	-9.60	S	114.64	E	-37.4	5.6	5.5	T	340	8	163	87	88	82
541	1987	12	17	-9.11	S	114.63	E	0	5.7	5.5	S	339	49	-148	227	67	-46
542	1979	12	17	-8.49	S	115.82	E	-22	5.6	0	T	106	15	111	264	76	85
543	2004	1	1	-8.31	S	115.79	E	-44	5.5	5.4	S	349	63	162	87	74	28
544	2003	2	24	-7.31	S	114.54	E	-38.8	5	4.8	T	135	24	121	282	69	77
545	2002	10	3	-7.53	S	115.66	E	-315.8	6	0	T	330	33	147	88	73	61
546	1984	1	16	-6.64	S	115.82	E	-543	5.2	0	N	311	39	-112	159	54	-73
547	1977	8	23	-11.52	S	117.62	E	-33	5.5	0	S	296	51	9	200	83	141
548	1980	10	5	-11.51	S	117.61	E	-57	5.5	0	N	13	46	-125	237	54	-60
549	1978	4	10	-11.39	S	116.68	E	-59	6.6	0	N	81	45	-87	256	45	-93
550	1981	2	1	-11.33	S	117.35	E	-51	5.5	0	N	91	47	-57	227	52	-121
551	1990	3	6	-11.15	S	117.48	E	-22	5.6	4.9	N	250	46	-73	45	46	-107
552	1978	5	4	-10.41	S	116.98	E	-43	5.4	0	T	230	25	32	110	77	111
553	1991	10	7	-10.50	S	117.20	E	-40.4	5.1	5	T	96	46	77	295	46	103
554	1992	10	18	-10.12	S	117.11	E	-52.8	5.4	5.1	T	296	37	111	90	56	75
555	1977	10	7	-10.20	S	117.45	E	-33	5.4	0	N	337	38	-94	162	52	-87
556	1977	10	16	-9.83	S	117.11	E	-39	5.5	0	S	314	82	178	44	88	8

M. No	Year	M	D	Lat		Long		Depth	Mb	Ms		Str	Dp	Slp	Str	Dp	Slp
557	1985	7	6	-9.65	S	117.74	E	-67	5.5	0	T	340	35	143	102	70	60
558	1996	10	6	-9.77	S	117.97	E	-65.8	4.9	0	T	58	14	156	172	84	77
559	1988	8	15	-9.44	S	117.40	E	-69	5	0	S	12	43	-160	267	77	-48
560	1991	12	24	-9.59	S	117.98	E	-88	5.2	0	T	333	6	167	76	89	84
561	1991	10	19	-9.01	S	117.17	E	-120.7	5.7	0	T	188	43	84	16	47	95
562	1988	4	8	-8.81	S	117.50	E	-108	5.7	0	T	136	39	48	5	62	118
563	1992	5	21	-8.76	S	117.61	E	-152.7	5.5	0	S	353	14	-173	256	88	-76
564	1983	8	20	-8.55	S	117.48	E	-162	5.3	0	T	211	40	135	338	63	59
565	1989	6	9	-7.88	S	117.51	E	-262	5.5	0	S	346	17	-175	252	89	-73
566	1997	2	15	-7.81	S	117.50	E	-286.4	5.4	0	T	267	20	99	78	70	87
567	1993	2	17	-7.78	S	117.43	E	-304.7	5.1	0	T	315	13	127	97	80	82
568	1984	1	17	-7.71	S	117.39	E	-322	5.5	0	T	314	20	127	95	74	77
569	1997	3	3	-7.86	S	117.61	E	-47.2	5	4.4	S	229	68	9	136	82	158
570	2005	5	16	-8.31	S	117.51	E	-41	5.5	0	T	77	28	98	247	63	86
571	2003	1	3	-8.79	S	117.77	E	-41.1	4.8	4.8	S	89	45	176	183	87	45
572	1995	3	20	-8.00	S	116.54	E	-224.9	5.2	0	S	212	64	-23	312	69	-152
573	1992	3	24	-7.73	S	117.46	E	-278.3	5.5	0	T	276	34	96	89	56	86
574	2001	10	23	-7.55	S	117.14	E	-294.6	4.9	0	T	154	29	44	24	70	112
575	1996	11	2	-7.57	S	117.33	E	-312.7	5.5	0	T	199	21	66	45	71	99
576	1978	12	11	-7.08	S	117.95	E	-465	5.8	0	N	87	34	-93	271	56	-88
577	2001	2	16	-7.16	S	117.49	E	-521	5.9	0	N	55	38	-124	276	59	-66
578	1983	8	2	-7.17	S	117.45	E	-619	5.4	0	S	40	38	-166	299	81	-52
579	1999	3	24	-7.05	S	117.08	E	-624.4	5.2	0	N	55	43	-119	272	53	-66
580	1984	9	16	-6.99	S	117.50	E	-638	5.3	0	S	120	51	-35	233	64	-136

Appendix – II

Appendix II: Details of the shallow (h≤ 70 km) earthquakes with magntitude ≥ 5.5 and focal mechanisms are available from Harvard CMT Catalogue.

Year	Month	Date	Latitude	Longitude	Depth	Mb	Ms	type	moment	str	dip	slp	str	dip	slp
1964	4	2	5.75	95.42	65	5.6	0	S	0	3	285	86	60	3	196
1964	4	3	3.91	96.56	51	5.8	0	N	0	26	20	0	290	65	200
1964	7	28	14.17	96.12	22	5.9	0	N	0	7	160	16	250	71	45
1967	2	14	13.75	96.47	13	5.6	0	N	0	10	150	0	60	80	330
1967	7	2	8.65	93.59	44	5.7	0	S	0	10	307	76	81	10	215
1967	8	21	3.72	95.74	40	6.1	0	T	0	57	23	0	293	33	203
1967	9	6	14.65	93.55	36	5.5	0	N	0	31	106	0	16	59	286
1968	7	19	8.68	93.67	36	5.5	5.5	S	0	2	120	78	15	14	211
1969	11	21	1.94	94.61	20	6.4	7.7	S	0	21	236	70	56	2	147
1970	8	3	2.54	97.94	69	5.7	0	S	0	30	60	30	308	45	184
1971	2	4	0.528	98.719	40	6.2	7.1	S	0	24	223	68	32	2	132
1971	11	5	10.109	92.93	53	5.9	0	T	0	64	120	7	19	25	284
1973	4	7	7.004	91.325	39	5.8	6.6	S	0	1	78	82	168	10	350
1973	7	9	10.665	92.586	44	5.6	5.2	S	0	22	86	63	305	12	182
1975	12	17	5.246	95.834	40	5.6	6.2	S	0	23	80	60	302	17	177
1976	11	3	4.219	95.19	54	5.5	5.2	S	0	37	198	39	344	17	90
1977	1	2	-10.155	119.034	19	5.7	0	T	3.07E+25	72	357	1	89	18	179
1977	3	8	0.438	99.893	32	5.5	6	S	1.85E+25	7	268	80	46	6	177
1977	5	20	-4.464	101.932	36	5.6	5.3	T	3.12E+24	65	28	3	124	25	216
1977	5	25	4.206	95.74	67	5.7	0	N	4.15E+25	32	28	14	127	54	237
1977	6	24	-2.257	100.809	61	5.5	0	N	5.43E+23	26	106	16	8	59	250
1977	8	14	-7.894	107.547	60	5.8	5.7	T	1.58E+25	67	353	6	98	22	190
1977	8	19	-11.206	118.432	54	5.8	0	N	5.24E+24	18	4	22	102	61	239
1977	8	19	-11.16	118.406	33	6.8	0	N	3.59E+28	21	157	7	64	67	317
1977	8	19	-10.961	119.169	42	5.6	0	N	8.23E+24	25	343	7	76	64	180

1977	8	19	-10.95	119.214	39	5.5	0	N	6.53E+24	12	354	17	88	69	230
1977	8	20	-11.189	119.144	33	5.7	0	N	3.40E+25	10	22	6	291	79	170
1977	8	20	-11.097	119.09	33	5.9	0	N	9.59E+25	28	2	4	93	61	190
1977	8	23	-11.523	117.616	33	5.5	0	S	1.98E+24	32	150	51	11	21	254
1977	8	25	-10.885	119.261	51	6	0	N	3.60E+25	12	327	11	60	73	191
1977	8	26	-10.922	119.3	33	5.5	0	S	1.29E+25	15	168	44	63	42	272
1977	9	5	-11.198	118.238	33	5.5	0	N	1.27E+24	8	183	30	278	59	80
1977	9	23	-11.291	118.096	34	5.8	0	N	5.50E+24	16	187	29	89	57	302
1977	10	5	-11.341	117.172	33	5.5	0	S	2.23E+24	0	185	63	95	27	275
1977	10	7	-10.068	117.346	30	5.6	0	S	1.32E+25	6	269	77	27	11	177
1977	10	7	-9.993	117.294	29	5.9	0	S	5.35E+25	22	262	68	68	5	170
1977	10	7	-9.916	117.3	27	5.6	0	S	1.22E+25	4	268	85	57	2	178
1977	10	7	-9.829	117.255	31	5.7	0	S	1.17E+25	16	260	71	115	10	353
1977	10	7	-10.005	117.29	34	5.5	0	S	3.33E+24	5	259	52	356	37	165
1977	10	7	-9.974	117.27	36	5.7	0	S	8.44E+24	5	256	72	2	17	165
1977	10	12	-11.233	119.374	37	5.6	0	N	1.40E+24	14	0	24	264	62	118
1977	10	16	-9.828	117.105	39	5.5	0	S	2.77E+25	7	269	82	55	5	178
1977	10	30	-10.38	118.779	51	5.6	0	S	3.31E+24	9	148	35	244	54	45
1977	11	18	-4.425	101.994	21	5.7	5.9	T	1.85E+25	66	42	4	303	23	211
1977	12	3	3.522	95.912	22	5.8	5.9	S	1.43E+25	24	47	50	170	30	302
1977	12	6	-11.339	118.225	43	5.5	0	S	1.11E+25	14	354	43	98	44	250
1978	2	7	12.807	92.997	3	5.5	5.3	T	3.05E+24	60	321	28	164	10	69
1978	2	7	12.888	93.044	17	5.6	5.6	T	4.51E+24	81	230	3	338	9	68
1978	2	25	-10	117.02	24	5.6	0	S	4.56E+24	22	84	61	309	19	181
1978	4	10	-11.391	116.684	59	6.6	0	N	9.06E+25	0	348	2	258	88	87
1978	4	29	-5.915	103.92	54	5.9	5.1	T	2.77E+24	62	356	18	122	21	219
1978	6	12	-5.151	102.716	51	5.6	5.3	T	2.06E+24	55	352	17	108	30	208
1978	6	24	-5.052	102.382	37	5.9	6.4	T	5.00E+25	54	23	2	117	36	208
1978	6	24	-5.072	102.327	0	5.9	0	T	0	54	23	2	117	36	208

1978	8	5	-4.034	102.391	66	5.7	5.3	T	3.16E+24	61	10	10	119	26	215
1979	1	11	-4.053	101.297	28	5.7	6.2	T	2.76E+25	52	30	5	125	38	219
1979	3	16	5.197	96.329	49	5.6	5.8	T	7.25E+24	61	229	21	86	19	349
1979	4	19	-1.208	98.204	30	5.5	5.6	T	6.19E+24	57	64	4	328	32	235
1979	5	21	-8.372	115.952	44	5.6	0	T	6.15E+24	58	175	2	82	32	351
1979	5	30	-8.322	115.921	40	6	5.8	T	0	63	176	3	85	37	354
1979	5	30	-8.322	115.921	40	6	0	T	2.39E+25	63	178	2	85	27	354
1979	6	25	-5.959	103.567	38	5.6	0	S	2.37E+24	8	157	49	57	40	254
1979	7	17	-4.439	98.737	21	5.7	5.2	T	3.82E+24	56	226	33	30	7	125
1979	7	24	-11.161	107.723	32	6.3	6.9	S	3.44E+26	29	29	46	154	29	280
1979	8	7	-8.784	108.777	35	5.6	0	T	1.47E+24	68	34	9	281	20	187
1979	9	29	1.158	94.205	10	6.2	6.8	S	2.21E+26	0	239	88	332	2	149
1979	10	10	-7.165	106.103	69	5.8	0	T	6.53E+24	70	358	6	104	19	196
1979	10	20	-8.396	115.827	37	5.9	0	T	4.87E+25	65	190	4	91	25	359
1979	11	13	-4.435	101.997	50	6	6.3	T	3.34E+25	69	26	6	126	30	219
1979	12	15	-3.407	102.585	30	5.8	6.6	S	7.56E+25	8	94	73	334	14	186
1979	12	17	-8.489	115.818	22	5.6	0	T	6.14E+25	58	166	5	265	31	358
1980	4	1	4.103	97.554	24	5.5	5.9	S	1.47E+25	10	295	79	136	4	27
1980	4	3	-5.587	103.152	41	5.7	5.2	S	4.02E+24	42	52	32	177	31	289
1980	6	20	-10.911	119.178	38	5.6	0	N	6.17E+24	8	326	16	234	72	82
1980	7	23	-2.751	101.182	65	5.5	5	T	3.86E+24	60	9	9	116	28	211
1980	10	5	-11.51	117.615	57	5.5	0	N	1.36E+24	5	307	24	39	66	206
1980	10	8	-5.342	103.124	44	5.8	6.3	T	5.09E+25	59	20	5	117	31	210
1980	12	24	-9.117	112.007	48	5.5	0	N	2.72E+24	13	324	27	61	59	212
1981	1	24	-5.376	102.951	41	5.6	5.2	T	2.04E+24	57	66	22	298	23	197
1981	2	1	-11.325	117.349	51	5.5	0	N	2.40E+24	3	338	24	247	66	74
1981	3	13	-8.829	110.431	48	5.5	0	N	8.99E+24	36	12	6	277	53	176
1981	11	2	12.176	92.871	24	5.7	5.5	T	4.47E+24	59	259	13	147	28	50
1982	1	20	7.058	93.952	16	5.5	6.3	S	2.90E+25	31	308	67	152	8	41

1982	1	20	7.151	93.879	25	5.6	0	S	1.91E+25	14	317	75	122	4	226
1982	3	11	-9.521	118.35	33	6	0	S	7.43E+25	5	54	62	314	28	147
1982	5	22	7.54	93.924	35	5.5	5.3	N	2.25E+24	23	296	3	27	67	125
1982	6	14	-4.699	103.038	59	5.9	0	T	4.01E+24	56	334	30	126	13	223
1982	8	7	-11.163	115.422	55	6.1	0	N	5.57E+25	3	181	17	90	72	279
1982	10	31	2.929	96.061	48	5.5	0	S	1.32E+24	7	244	38	340	51	145
1983	1	4	-3.153	101.163	50	5.6	5.2	T	1.75E+24	64	85	18	312	18	216
1983	1	22	-6.687	102.866	15	5.6	6.1	T	2.39E+25	74	330	15	128	6	219
1983	4	16	-10.193	110.837	11	5.8	0	N	5.65E+24	0	4	3	94	87	268
1983	4	23	-11.208	118.917	39	5.5	0	N	1.12E+24	3	199	4	108	85	329
1983	8	13	-8.69	111.174	64	5.9	0	T	6.86E+24	78	35	7	270	9	178
1983	9	17	4.76	95.052	67	5.7	0	S	1.47E+25	17	49	40	304	45	157
1983	9	29	-11.368	115.323	40	5.6	0	N	2.09E+24	7	6	25	99	64	261
1983	10	10	-5.805	103.204	31	5.6	5.1	S	2.06E+24	49	342	24	103	31	208
1983	10	31	-9.098	119.093	57	6	0	T	4.74E+25	50	213	16	323	35	64
1984	3	10	-7.576	106.984	61	5.7	0	T	9.52E+24	64	345	14	106	22	201
1984	6	8	-5.825	104.088	17	5.6	6.1	S	1.49E+25	1	155	88	4	2	205
1984	10	4	-9.97	118.729	0	5.7	6.1	T	3.65E+25	58	11	13	259	29	162
1984	11	17	0.219	98.051	42	6.2	7.2	T	5.83E+26	53	33	4	128	36	221
1984	12	12	-7.907	107.939	50	5.5	0	T	2.65E+24	74	6	0	96	16	186
1985	1	22	-5.877	104.54	56	5.5	0	T	9.79E+23	60	53	17	291	24	193
1985	3	22	-6.61	105.396	45	5.9	0	T	4.04E+25	60	348	8	92	28	186
1985	7	6	-9.648	117.739	67	5.5	0	T	1.95E+24	55	334	28	113	19	213
1985	7	9	-8.435	110.33	35	5.6	0	T	3.91E+24	59	273	28	66	12	162
1985	12	27	-5.755	104.182	25	5.9	6.6	S	6.18E+25	11	292	69	54	18	199
1985	12	28	-5.803	104.296	15	5.7	6	S	1.86E+25	11	298	78	102	3	207
1986	1	28	8.78	94.135	27	5.7	5.8	S	1.01E+25	2	301	86	55	4	211
1986	3	25	-6.235	104.161	22	5.6	5.7	T	5.03E+24	72	21	1	115	18	205
1987	4	25	2.379	98.921	30	5.8	6.6	S	5.08E+25	16	281	74	82	5	190

1987	4	28	2.025	99.082	7	5.6	5.6	S	4.99E+24	14	286	70	59	14	192
1987	6	4	-4.608	101.882	27	5.6	5.8	T	5.56E+24	59	9	7	110	30	204
1987	6	10	4.178	94.836	59	5.5	5.3	S	5.01E+24	16	44	41	300	45	150
1987	11	18	-8.074	108.787	63	5.5	0	S	1.74E+24	39	198	49	40	11	297
1987	12	17	-9.111	114.628	0	5.7	5.5	S	1.19E+25	11	287	40	26	48	185
1988	4	3	4.712	94.462	36	5.8	5.7	T	7.32E+24	63	143	22	287	14	23
1988	5	11	-11.127	116.302	0	5.5	4.8	N	2.08E+24	19	178	2	88	70	353
1988	8	17	-7.693	107.157	27	6	5.8	T	1.17E+25	83	153	6	300	4	31
1989	5	1	-4.219	101.365	12	5.5	5.6	T	4.07E+24	65	9	3	106	25	197
1990	1	22	3.919	96.128	53	6	5.8	T	2.53E+25	72	44	0	313	18	223
1990	2	4	-10.239	110.289	20	5.8	5.4	N	5.87E+24	9	357	0	267	81	175
1990	3	6	-11.147	117.479	22	5.6	4.9	N	2.11E+24	0	147	12	57	78	237
1990	4	6	-6.846	105.139	33	5.6	5.6	S	5.67E+24	7	264	55	163	34	359
1990	5	21	-8.095	109.062	17	5.5	5.2	T	3.06E+24	62	356	7	101	27	194
1990	7	6	-6.807	108.09	14	5.6	4.8	T	2.34E+24	71	248	12	118	14	25
1990	8	18	7.563	93.999	38	5.5	6	S	1.19E+25	12	141	73	275	11	48
1990	9	17	-5.925	103.792	25	5.7	0	S	6.43E+24	16	23	33	124	52	271
1990	11	15	3.894	97.405	29	6	6.8	S	1.19E+26	17	79	67	217	15	345
1990	11	18	3.899	97.264	50	5.7	0	T	2.04E+24	68	229	11	108	18	15
1990	12	29	8.281	94.067	16	5.6	6	S	1.50E+25	3	302	86	90	2	212
1991	1	6	0.592	98.617	66.9	5.7	0	T	1.34E+24	74	35	0	127	16	217
1991	6	21	-5.997	104.847	38.6	5.5	4.9	T	1.47E+24	86	51	3	265	2	175
1991	7	2	-1.098	99.828	28.7	5.9	6.1	T	3.47E+25	63	37	6	139	26	232
1991	7	5	-9.602	114.642	37.4	5.6	5.5	T	1.65E+25	47	349	8	87	42	185
1991	7	23	3.808	95.96	60.9	5.8	0	N	3.27E+24	36	359	10	261	52	158
1991	8	6	3.858	95.411	26.9	5.9	5.5	T	3.67E+24	87	277	3	123	2	33
1991	8	26	6.882	94.547	5.5	5.6	5.9	S	7.70E+24	5	281	67	24	22	189
1991	12	22	-4.881	103.172	58.9	5.7	4.8	T	1.40E+24	68	57	12	294	18	200

1992	2	6	-5.712	103.13	35	6	6.5	T	3.98E+25	67	26	0	117	23	207
1992	4	18	-5.458	102.94	25.8	5.6	6.4	T	9.16E+25	54	24	2	117	36	208
1992	6	24	-5.323	103.054	54.8	5.5	5.7	T	3.54E+24	60	58	11	307	28	211
1992	8	5	-5.554	102.851	52.9	5.5	5.3	T	4.07E+24	50	28	3	122	40	214
1992	8	31	-11.502	118.396	27.1	5.6	4.7	S	1.29E+24	5	13	36	107	54	277
1992	11	25	-4.053	102.198	62.4	5.8	0	S	2.85E+24	43	63	43	272	15	168
1993	2	8	-4.817	101.901	29.8	5.8	5.7	T	4.39E+24	59	14	5	113	31	206
1993	8	4	-1.66	99.596	15.4	5.8	6.3	T	5.05E+25	57	21	3	116	33	208
1993	9	1	2.989	96.138	36.1	5.8	6.2	T	3.09E+25	54	43	1	311	36	221
1993	9	20	-5.221	102.872	41.5	5.5	5.4	T	2.72E+24	65	41	8	292	23	198
1994	1	7	-0.565	98.643	48.8	5.6	5.4	T	2.90E+24	61	51	7	307	27	213
1994	2	15	-4.971	104.328	23.1	5.9	7	S	2.24E+26	16	272	71	58	10	179
1994	4	25	-9.372	113.03	54.3	5.6	5.3	T	4.77E+24	77	10	2	271	13	181
1994	5	2	-1.102	97.544	37.5	6.1	5.9	N	1.72E+25	2	56	1	146	88	260
1994	5	9	-2.031	99.77	31.1	5.9	5.5	T	3.41E+24	60	58	13	305	26	208
1994	5	11	-2.017	99.777	21.1	6	6.3	T	5.26E+25	53	40	1	308	37	218
1994	5	11	-2.059	99.702	28	5.8	5.9	T	1.64E+25	57	39	1	306	33	215
1994	5	17	-1.885	99.714	33	5.5	5.7	T	7.60E+24	51	47	9	306	37	209
1994	5	25	7.646	94.28	24	5.6	5.6	S	6.99E+24	6	103	84	272	1	13
1994	6	2	-10.413	112.926	38.9	5.7	7.1	T	5.34E+24	52	9	0	279	38	189
1994	6	3	-10.551	112.993	42.9	5.5	5.1	N	2.79E+24	4	183	12	92	77	292
1994	6	3	-10.427	112.9[illegible]9	25.9	6	6.4	N	8.81E+25	7	178	3	88	82	337
1994	6	4	-10.745	113.43	11	6	6.3	N	5.82E+25	4	4	5	94	83	236
1994	6	4	-10.748	113.655	34.1	5.7	5	N	7.87E+23	6	172	5	82	82	308
1994	6	4	-10.804	113.295	30.3	5.5	5.1	N	2.14E+24	3	352	10	262	79	100
1994	6	5	-10.319	113.504	25.9	5.7	6.3	N	1.42E+25	22	22	8	115	66	225
1994	6	7	-5.779	104.463	41.1	5.5	4.7	T	1.62E+24	57	58	17	299	27	200
1994	6	13	-10.273	113.548	23.5	5.6	5.6	N	3.16E+24	29	30	5	123	60	222
1994	6	15	-10.335	113.644	35.3	5.9	6	N	1.38E+25	23	16	6	109	66	211

1994	6	15	-10.197	113.757	28.8	5.6	5.9	N	1.50E+25	26	10	8	104	63	210
1994	6	18	-10.233	113.605	44	5.5	5.1	N	2.25E+24	35	22	5	116	54	213
1994	7	24	-10.618	113.349	34.7	5.8	4.9	S	1.49E+24	7	343	50	245	39	79
1994	9	12	-8.943	106.483	29.8	5.8	5.3	S	3.50E+24	7	17	62	121	27	284
1994	10	31	3.026	96.254	46.2	5.6	6.2	T	1.85E+25	64	59	12	304	23	209
1994	12	12	-9.8806	119.2371	27.8	5.7	5.1	T	2.60E+24	73	297	13	77	10	169
1995	5	5	-10.049	118.9972	33	5.7	5.4	T	3.63E+24	71	6	2	271	19	181
1995	9	23	-5.568	104.074	50.7	5.9	5.6	T	1.10E+25	65	5	2	269	25	178
1995	10	6	-2.01	101.502	36.7	5.8	6.8	S	1.47E+26	9	281	74	44	13	189
1995	11	5	-4.926	103.234	44.1	6.4	6.1	T	3.73E+25	67	20	4	118	23	210
1995	11	8	1.822	95.06	29.2	6	6.8	S	2.65E+26	9	56	77	280	9	147
1995	11	22	3.118	95.992	52.5	5.5	5.7	T	5.77E+24	65	65	11	310	22	216
1996	2	12	-11.075	118.7424	42.5	5.9	5.7	N	1.45E+25	4	348	18	257	71	91
1996	8	9	-2.033	99.674	33	5.6	5.5	T	5.35E+24	56	33	2	300	34	209
1996	10	10	3.485	97.877	19.7	5.5	6	S	2.73E+25	1	279	88	172	2	9
1996	12	9	-7.893	107.567	55.3	5.6	5.6	T	1.38E+25	71	349	8	103	17	195
1997	2	10	-9.5652	119.4972	3.3	5.5	5.4	T	8.80E+24	65	19	4	280	25	188
1997	3	17	-6.66	105.484	50.9	5.8	6.2	T	4.23E+25	69	1	6	105	20	197
1997	8	20	4.308	96.506	24.7	5.7	5.9	S	1.11E+25	8	250	74	129	13	342
1998	4	1	-0.502	99.322	61.6	6.1	0	T	3.33E+26	65	25	5	126	24	218
1998	7	17	-4.714	103.017	58.9	5.8	5.1	T	3.76E+24	67	12	5	115	22	207
1998	8	10	7.406	94.239	33	5.5	5.8	S	9.42E+24	5	102	84	326	4	192
1999	2	3	-6.202	104.079	14.9	5.5	5.6	T	6.22E+24	67	41	6	297	23	205
1999	2	4	4.054	95.279	55.2	5.8	5.3	S	6.20E+24	17	43	37	146	48	293
1999	3	27	-9.66	112.763	33	5.6	5	S	2.07E+24	26	70	10	165	62	275
2000	3	10	-8.792	106.319	24	5.5	5	S	8.09E+23	25	94	56	321	22	195
2000	6	4	-4.692	102.141	52.7	6.7	7.9	S	7.46E+27	42	60	47	225	7	323
2000	6	5	-5.615	102.93	21.6	5.5	5.5	S	5.73E+24	10	265	35	2	53	161
2000	6	5	-4.14	102.01	33	5.5	5.1	T	2.13E+24	64	45	7	299	25	206

2000	6	6	-5.086	102.75	49.3	5.9	6.1	T	2.19E+25	65	32	1	123	25	213
2000	6	7	-4.615	101.936	20.2	6.1	6.7	T	1.28E+26	76	128	7	9	12	277
2000	6	9	-5.55	102.68	33	5.8	5.8	N	9.11E+24	34	28	5	294	55	197
2000	7	8	-5.405	102.695	9.3	5.6	5.8	N	6.90E+24	3	137	27	46	63	233
2000	7	22	-4.07	102.37	69.1	5.8	0	T	4.05E+24	67	11	7	117	22	210
2000	8	17	5.77	94.75	68.3	5.5	5.1	S	3.61E+24	12	52	68	174	18	319
2000	8	24	-5.982	102.747	33	5.6	5.9	T	5.93E+24	90	262	0	119	0	29
2000	9	1	1.445	96.548	31.3	5.5	6.1	T	1.07E+25	77	62	4	314	12	223
2000	9	12	-5.43	101.82	33	5.7	6.1	T	1.28E+25	72	331	17	129	6	221
2000	9	22	-4.96	102.1	33	5.8	5.9	S	2.18E+25	15	56	72	204	9	324
2000	10	25	-6.55	105.63	38	6.3	6.6	T	1.72E+26	71	3	5	108	19	200
2000	10	30	-9.855	118.979	33.8	5.5	5.3	S	1.01E+25	7	294	63	38	26	201
2001	1	7	-8.7	108.89	33	5.5	5.1	T	1.53E+24	62	53	17	286	21	190
2001	1	16	-4.071	101.744	28	6.3	6.8	T	1.97E+26	58	22	5	120	32	213
2001	1	16	-4.19	101.6	57.7	5.6	0	T	4.23E+24	77	38	3	141	13	231
2001	1	18	-4.05	101.75	55.4	5.5	5.3	T	1.44E+24	64	46	1	314	26	224
2001	2	14	-5.16	102.49	33	5.5	5.3	T	3.14E+24	61	18	6	118	29	211
2001	2	21	-4.9	102.45	33	5.7	5.6	T	3.99E+24	59	350	15	107	27	205
2001	3	8	-5.36	102.19	33	5.6	5.3	T	1.15E+24	71	9	3	108	19	200
2001	3	12	-7.215	106.049	33	5.5	5.6	T	6.46E+24	68	7	3	105	22	197
2001	3	15	8.689	93.955	33	5.5	5.9	S	1.04E+25	5	303	81	65	8	213
2001	7	31	-5.28	10[illegible].34	33	5.5	5.3	S	3.48E+24	20	102	32	359	51	219
2001	9	20	-11.42	115.044	10	5.6	5.1	N	2.81E+24	15	8	12	101	71	228
2001	10	31	5.336	94.336	41.9	5.6	5.5	N	4.61E+24	9	266	23	0	65	156
2001	12	29	-6.034	102.762	33	5.6	5.8	S	2.40E+24	33	290	57	106	2	199
2002	1	15	-6.246	105.302	33	5.6	6.3	S	1.55E+25	1	119	81	216	9	29
2002	1	24	3.547	95.648	33	5.6	5.3	T	1.01E+24	85	283	4	123	1	33
2002	1	24	3.53	95.66	33	5.6	5.6	T	2.77E+24	88	114	2	302	0	212

2002	6	27	-7	104.088	33	5.9	6.9	T	6.58E+25	82	335	7	117	5	208
2002	7	24	-9.28	118.62	28.8	5.8	5.4	S	8.12E+24	13	72	77	237	3	341
2002	8	26	-6.732	105.648	46.9	5.7	5.3	T	5.04E+24	80	0	1	99	10	189
2002	9	13	13.005	93.105	21	6.2	6.7	T	6.35E+25	58	199	29	353	12	90
2002	9	14	13.06	93.16	33	5.7	5.6	T	4.70E+24	62	184	28	359	2	90
2002	10	6	-8.2232	118.3393	19.1	5.6	6	T	2.67E+25	66	168	0	78	24	348
2002	10	24	6.03	94.42	64.6	6.2	0	S	4.21E+24	42	43	41	263	21	153
2002	11	2	2.9794	96.1147	31	6.2	7.5	T	9.01E+26	60	52	5	314	30	221
2002	11	2	3.0059	96.4367	25.7	5.9	6.3	T	3.26E+25	55	77	7	336	34	241
2002	11	18	-4.2129	102.1445	36.8	5.6	5.2	T	1.40E+24	63	149	7	46	26	313
2002	12	1	-11.219	117.2331	50.4	5.6	5	N	2.14E+24	5	172	11	263	78	56
2003	1	9	0.5468	98.5986	36.8	5.8	4.9	T	2.33E+24	65	24	7	130	23	223
2003	1	10	0.1713	97.9514	28.3	5.5	5.5	T	3.91E+24	82	48	2	155	8	246
2003	2	3	-2.7871	101.1856	59.7	5.5	5.2	T	2.85E+24	65	13	7	117	24	210
2003	3	26	12.5454	92.6103	29.6	5.8	5.3	S	5.66E+24	15	111	47	5	39	214
2003	4	29	-7.0315	103.6683	33	5.6	5.7	T	3.64E+24	80	294	10	113	0	203
2003	7	19	-8.68	111.23	56.2	5.9	0	T	6.72E+24	70	359	3	97	20	188
2003	9	7	-5.7064	102.0247	3.8	5.5	5.2	T	9.37E+23	70	323	16	107	11	200
2003	10	17	-5.0148	102.4964	44.9	5.7	5.7	N	4.85E+24	30	20	13	282	57	171
2004	1	1	-8.31	115.79	44	5.5	5.4	S	6.58E+24	31	311	58	114	7	216
2004	2	22	-1.56	100.49	42	6.3	5.7	N	1.20E+25	1	105	34	14	56	196
2004	4	16	-5.21	102.72	44	5.6	5.8	S	1.13E+25	45	50	11	309	43	208
2004	5	11	0.41	97.82	21	5.6	6.2	T	1.54E+25	59	35	3	130	31	222
2004	7	29	12.45	95	22	5.7	5.5	N	5.83E+24	12	327	33	66	54	219
2004	7	29	12.44	95	24	5.5	5	N	1.74E+24	7	323	22	56	67	216
2004	8	2	-5.47	102.62	40	5.5	5	S	2.25E+24	13	45	39	145	48	300
2004	8	6	12.43	95	23	5.7	5.2	S	2.72E+24	9	322	36	58	52	220
2004	10	28	-4.91	103.21	42	5.6	4.9	T	9.93E+23	77	7	5	121	12	213
2004	12	26	3.3	95.98	30	7	8.8	T	3.95E+29	52	36	3	130	38	222

2004	12	26	6.91	92.96	39	6.1	7.5	T	7.23E+26	65	21	14	143	20	238
2004	12	26	8.88	92.38	16	6	6.6	T	9.77E+25	81	101	5	340	8	249
2004	12	26	13.46	92.74	26	6.1	6	N	3.22E+25	7	290	17	22	72	178
2004	12	26	13.53	92.84	13	6.3	6.3	S	2.37E+25	38	355	50	155	10	257
2004	12	26	2.78	94.47	30	5.5	5.9	T	8.62E+24	79	65	4	313	11	223
2004	12	26	13.59	92.91	30	5.8	5.7	S	4.40E+24	33	352	53	201	14	91
2004	12	26	3.65	94.09	17	5.6	6.1	S	1.07E+25	49	300	39	143	11	44
2004	12	26	2.79	94.16	30	5.5	6.2	T	1.76E+25	58	341	25	119	19	218
2004	12	27	5.48	94.47	33	6	5.4	T	4.84E+24	69	55	1	321	21	230
2004	12	27	12.98	92.39	23	6	5.5	N	4.95E+24	10	297	27	32	62	189
2004	12	27	5.35	94.65	35	6.2	5.9	T	1.31E+25	66	38	3	134	24	225
2004	12	27	4.72	95.11	49	5.8	5.6	T	4.65E+24	75	46	1	312	15	221
2004	12	27	12.35	92.47	19	5.8	5.3	N	2.68E+24	28	81	8	346	61	242
2004	12	27	11.59	92.5	25	5.5	5.1	N	1.93E+24	26	282	4	190	64	91
2004	12	27	2.93	95.61	28	5.7	5.8	T	4.88E+24	79	148	11	324	1	54
2004	12	28	4.73	95.21	36	5.8	5.5	T	4.60E+24	71	54	4	313	19	221
2004	12	29	9.11	93.76	8	6	5.7	N	1.30E+25	11	99	28	4	60	208
2004	12	29	5.53	94.28	47	5.5	4.9	T	1.53E+24	72	35	4	136	17	228
2004	12	29	5.23	94.62	29	5.7	5.3	S	2.55E+24	28	35	32	144	45	273
2004	12	30	4.23	94.22	16	5.5	4.9	N	7.64E+23	16	35	13	301	69	174
2004	12	30	5.53	94.3	30	5.5	4.9	T	6.68E+23	69	31	6	137	20	229
2004	12	30	12.24	92.51	30	5.8	5.2	T	3.35E+24	53	59	10	161	36	258
2004	12	31	7.12	92.53	14	5.7	6.3	T	1.50E+25	79	139	11	330	2	240
2004	12	31	6.2	92.91	11	5.5	6.1	T	1.13E+25	55	348	30	133	16	233
2004	12	31	5.11	94.86	49	5.6	4.9	T	1.20E+24	73	36	2	132	17	223
2005	1	1	5.47	94.4	36	5.8	5.5	T	3.63E+24	69	16	10	134	18	228
2005	1	1	5.1	92.3	11	6	6.7	S	1.05E+26	6	65	79	186	9	334
2005	1	1	7.34	94.46	55	5.6	5.9	S	1.54E+25	1	111	86	222	4	21

2005	1	2	3.24	95.46	8	5.6	5.9	T	4.79E+24	82	145	7	291	4	22
2005	1	2	6.36	92.79	30	5.7	6.2	T	3.43E+25	73	73	1	341	17	251
2005	1	4	10.67	92.36	23	6	5.9	T	1.57E+25	57	75	1	167	33	258
2005	1	4	4.92	94.79	44	5.5	5.6	T	8.80E+23	68	29	8	139	20	232
2005	1	4	10.56	91.73	10	5.6	5.3	T	3.39E+24	66	83	1	175	24	266
2005	1	5	5.49	94.39	48	5.7	5.8	T	8.49E+24	67	33	6	139	22	231
2005	1	6	5.59	93.15	24.6	5.7	5.7	N	1.77E+24	4	246	6	336	83	121
2005	1	6	5.32	94.83	49	6.1	5.5	T	3.83E+24	69	20	9	135	19	228
2005	1	7	8.77	93.56	30	5.5	4.9	N	7.70E+23	1	287	17	18	73	194
2005	1	9	4.93	95.11	40	6	5.8	T	1.08E+25	69	30	4	131	20	222
2005	1	12	5.55	94.62	29	5.6	5.1	T	1.38E+24	72	10	11	136	14	229
2005	1	15	-6.46	105.24	58	5.5	0	T	3.65E+24	60	29	0	299	30	209
2005	1	24	7.33	92.48	30	6.1	6.2	S	2.57E+25	4	67	84	291	4	158
2005	1	26	8.25	94.04	23	5.6	5.2	S	2.47E+24	1	117	65	209	25	27
2005	1	26	2.7	94.6	22	5.6	6	T	7.73E+24	74	68	6	316	15	225
2005	1	27	7.94	94.06	38	5.5	5.2	S	2.29E+24	2	300	81	197	8	30
2005	1	27	7.88	94.09	30	5.5	5.5	S	4.44E+24	9	102	81	298	3	192
2005	1	27	7.97	94.12	30	5.6	4.8	N	1.49E+24	4	116	34	23	55	211
2005	1	27	5.51	94.31	30	5.6	5.2	T	1.72E+24	66	22	11	137	21	231
2005	1	27	8.04	94.11	30	5.5	4.8	N	1.01E+24	2	121	13	31	77	219
2005	1	28	7.9	93.99	16	5.5	5.2	S	2.10E+24	11	97	66	213	21	3
2005	1	29	13.1	93	30	5.5	4.8	T	8.05E+23	59	309	28	156	12	59
2005	1	29	3.33	93.7	29	5.5	5.2	T	1.83E+24	85	87	2	330	5	240
2005	1	30	8.12	94.06	18	5.6	4.7	N	1.61E+24	1	297	32	28	58	206
2005	2	1	5.18	94.56	24	5.6	4.8	T	1.32E+24	61	11	12	124	26	219
2005	2	5	8.06	94.05	17	5.7	5	N	1.09E+24	1	122	22	31	68	214
2005	2	5	8.11	94.18	30	5.5	5.8	S	8.10E+24	11	315	79	154	4	46
2005	2	6	13.85	93.58	35	5.6	5.1	T	1.73E+24	58	22	22	153	22	252
2005	2	9	4.8	95.12	44	5.7	5.5	T	1.09E+25	69	35	2	131	21	222

2005	2	13	5.08	94.79	48	5.7	4.5	T	1.39E+24	72	23	7	135	16	227
2005	2	13	5.07	94.8	51	5.5	0	T	7.61E+23	71	16	9	135	16	228
2005	2	14	-0.13	98.73	47	6	5.9	S	4.77E+24	43	31	34	262	28	151
2005	2	16	8.11	93.97	0	5.6	5.7	S	7.90E+24	4	307	85	102	2	217
2005	2	17	4.7	95.16	47	5.9	5.4	T	3.62E+24	73	43	1	309	17	219
2005	2	18	5.45	94.42	48	5.8	4.9	T	3.20E+24	70	23	7	133	18	226
2005	2	19	-5.64	101.61	29	5.5	4.7	T	5.05E+23	57	350	17	109	27	208
2005	2	22	10.83	91.77	30	5.6	5.4	T	1.93E+24	75	104	4	358	14	267
2005	2	24	2.89	95.73	30	5.6	5.5	T	4.14E+24	51	52	3	319	39	226
2005	2	26	2.91	95.59	36	6	6.7	T	1.31E+26	51	47	2	315	39	223
2005	3	17	4.86	95.09	60	5.5	5.6	T	4.77E+24	70	33	3	130	20	221
2005	3	25	5.49	94.37	39	5.9	5.7	T	6.98E+24	70	34	6	140	19	232
2005	3	28	2.09	97.11	30	7.2	8.4	T	1.11E+29	51	37	2	130	38	222
2005	3	29	2.65	96.58	30	5.8	5.9	T	7.57E+24	67	4	7	112	22	205
2005	3	30	1.77	97.1	27	5.5	5.5	T	4.04E+24	54	39	1	130	36	220
2005	3	30	2.99	95.41	22	5.9	6.2	T	4.56E+25	52	43	1	312	38	221
2005	3	30	2.93	95.42	25	5.6	5.7	T	2.93E+24	71	46	1	313	19	223
2005	3	31	1.7	97.12	22	5.7	5.8	T	4.40E+24	69	32	4	132	21	224
2005	4	1	0.32	98.11	29	5.6	5	S	2.59E+24	0	88	89	196	1	358
2005	4	3	0.37	98.32	30	5.9	5.9	T	1.17E+25	62	26	7	130	27	223
2005	4	3	2.02	97.94	36	6	5.9	T	2.97E+25	66	21	8	128	23	221
2005	4	4	1.61	97.87	30	5.5	5.3	T	2.58E+24	68	28	8	138	21	231
2005	4	6	-3.98	102.42	67	5.7	0	T	3.13E+24	68	349	16	125	15	219
2005	4	7	0.61	97.42	26	5.9	5.7	S	2.61E+24	43	97	47	275	1	6
2005	4	8	-0.22	97.73	20	5.7	6.3	S	1.64E+25	30	300	56	92	13	202
2005	4	10	-1.64	99.61	19	6.4	6.7	T	1.33E+26	74	242	3	142	16	52
2005	4	10	-1.71	99.78	30	6.2	6.3	T	6.27E+25	82	245	6	103	5	13
2005	4	10	-1.59	99.72	30	5.9	6.2	T	1.54E+25	58	203	2	296	32	27

2005	4	11	2.17	96.76	24	5.9	6	T	1.67E+25	59	46	0	315	31	225
2005	4	11	2.08	96.83	26	5.5	5.1	T	1.81E+24	61	40	2	134	29	225
2005	4	14	-1.91	99.95	33	5.8	5.6	T	5.59E+24	58	27	5	125	32	218
2005	4	16	1.81	97.66	31	6	6.2	T	4.51E+25	59	16	11	125	28	221
2005	4	17	0.31	97.66	25	5.7	5.2	N	1.57E+24	33	76	8	341	56	239
2005	4	17	-1.63	99.62	21	5.8	5.1	T	1.26E+24	84	273	3	148	5	57
2005	4	28	2.13	96.8	22	5.9	6.2	T	3.46E+25	55	45	1	314	35	224
2005	5	9	5.1	94.84	30	5.5	4.8	T	6.00E+23	74	28	4	133	16	225
2005	5	10	-6.23	103.14	17	5.9	6.4	T	2.59E+25	84	332	5	125	3	215
2005	5	14	0.59	98.46	34	6.4	6.8	T	1.58E+26	65	57	0	147	25	237
2005	5	16	-8.31	117.51	41	5.5	0	T	1.04E+24	72	147	4	249	17	340
2005	5	18	5.59	93.27	9	5.7	0	S	1.56E+25	24	234	62	88	14	331
2005	5	19	1.99	97.04	30	6.2	6.9	T	2.46E+26	52	44	2	312	38	221
2005	5	21	5.28	94.8	55	5.9	0	T	3.14E+24	69	22	9	136	19	229
2005	5	26	5.69	93.21	30	5.5	5.3	S	3.25E+24	12	62	67	184	19	328
2005	5	31	5.24	94.43	30	5.5	5.2	T	2.38E+24	48	109	9	9	40	272
2005	6	8	2.17	96.72	23	5.8	5.7	T	1.49E+25	60	43	0	133	30	223
2005	6	13	2.74	94.17	18	5.5	5.4	T	7.07E+24	84	253	2	138	5	48
2005	7	5	1.82	97.08	21	6.2	6.8	T	1.12E+26	51	36	3	130	39	222
2005	7	23	5.11	94.8	48	5.6	4.6	T	1.07E+24	70	17	11	140	16	234
2005	7	24	7.92	92.19	16	6.6	7.5	S	8.80E+26	8	76	71	189	17	344
2005	7	29	2.86	93.56	32	5.8	5	S	2.09E+24	17	64	39	168	46	315
2005	7	30	5.18	94.48	38	5.8	5.2	T	5.61E+24	60	19	15	137	25	235
2005	9	10	4.86	95.04	41	5.8	5.5	T	5.46E+24	69	33	3	129	20	220
2005	10	3	5.54	94.39	47	5.5	0	T	1.80E+24	68	16	9	130	20	223
2005	10	11	10.89	92.3	22	5.5	5.1	T	8.70E+23	72	42	7	154	17	247
2005	10	11	4.82	95.1	30	6	5.3	T	8.16E+24	69	37	1	130	21	221
2005	11	19	2.16	96.79	21	6	6.1	T	5.37E+25	54	47	1	316	36	225

Publications

Seismically active deformation in the Sumatra–Java trench-arc region: geodynamic implications

S. Lasitha[1], M. Radhakrishna[1,*] and T. D. Sanu[1,2]

[1]Department of Marine Geology and Geophysics, School of Marine Sciences, Fine Arts Avenue, Cochin 682 016, In dia
[2]Present address: ONGC, Karaikal , India

Crustal deformation rates (1900–2000) estimated for the Sumatra–Java arc region highlight (i) large variations in dextral shear motion (seismic slip) from 1 mm/yr to 29 mm/yr along the Sumatran Fault Zone (SFZ), (ii) dominantly compression with deformation velocities as high as 19 mm/yr near the equator along offshore Sumatra fore-arc and, (iii) dominance of compression (average 19 mm/yr) in the western part of offshore Java fore-arc that gradually changes to extension (average 3 mm/yr) towards east. While seismic slip rates match well with the geological or GPS derived slip rates between 0° and 2°S along SFZ, the values are much lower for the fault segments north of equator. The deformation pattern in the offshore Sumatra indicates that the Mentawai fault partly accommodates motion due to oblique subduction and suggests local interaction of the Investigator Fracture Zone near the equator. However, north of 2°N, the low deformation velocities in the offshore Sumatra can be attributed to the absence of significant earthquakes during the period of investigation. This long-term seismic quiescence might have caused lock up of stresses that resulted in highly devastating 26 December 2004 earthquake.

Keywords: Deformation, Indian Ocean, Java–Sumatra, moment tensors, seismotectonics.

THE highly devastating and tsunamigenic Sumatran earthquake of 26 December 2004 (~ M_w 9.3) and the large series of aftershock events since then, with another major earthquake of 28 March 2005 (M_w 8.6), have ruptured nearly 1300 km long portion of the plate boundary between the Indo-Australian and the Southeastern Eurasian plates[1–4]. The 26 December 2004 event has given rise to an estimated average slip of more than 5–10 m throughout the rupture length and produced significant static offsets at several far-away permanent GPS sites[5,6]. This abnormally high recent seismic activity has brought to fore, the seismicity of the Indonesian arc system and its extension into the Andaman–Nicobar region. The normal subduction below Java is characterized by the development of typical fore-arc basins. The oblique subduction beneath Sumatra and further north results in partitioning of the convergent motion into thrust and strike-slip faulting. Along the arc, the age and thickness of the lithosphere increase considerably from west to east; from 49–96 Ma below Sumatra to the west to 96–134 Ma below Java[7]. The depth of the Wadati–Benioff Zone (WBZ) also increases in the same manner, from 200 km beneath Sumatra to 670 km beneath Java. This change in the hypocentral depth has been explained as due to the increase in age and subduction zone velocity[8,9].

The 1900 km long trench parallel Sumatran Fault Zone (SFZ) continues northward into the Andaman Sea, where it most likely joins the fracture zones of the back arc-spreading centre near the Andaman Islands[10]. The shape and location of the Sumatran fault, the presence of active volcanic arc and the fore-arc structures are well correlated with the shape and characteristics of the underlying subducting oceanic lithosphere[11].

A 300-km wide strip of the lithosphere exists as a fore-arc sliver plate between the Sumatran fault and the Sumatran deformation front (Figure 1)[13–15]. Seismic reflection data in this region reveal a 600 km long strike-slip fault parallel to the SFZ called the Mentawai Fault Zone (MFZ), just east of Mentawai islands[12]. The MFZ is a zone of weakness that separates the oceanic and continental crust.

In the present study, we have carried out a detailed seismotectonic evaluation of the region by separating the events of the upper plate (h £ 70 km) from that of the WBZ. Nearly 100 years of hypocentral data of such shallow earthquakes within the upper plate and a large number of focal mechanism solutions occurring in the Java–Sumatra subduction zone have been considered in order to study the spatial variation in deformation pattern using the method of summation of the moment tensor.

Data and method of analysis

The method of analysis followed in the present study has been proposed by Papazachos and Kiratzi[16], based on the formulations of Kostrov[17], and Jackson and McKenzie[18]. Many previous workers have subsequently applied this method in seismically active regions[19–23] and therefore details on methodology are not reproduced here.

*For correspondence. (e-mail: mr_radhakrishna@hotmail.com)

This method requires two sets of data. (i) Seismicity data for estimation of seismic moment rate. (ii) Focal mechanism data for determining the shape of the deformation. We have considered hypocentral data from the NOAA epicentral listing and prepared an earthquake dataset of all shallow earthquakes (*h* £ 70 km) during 1900–2000 for the present analysis. Events before 1964 have been compiled from Rothe[24], and Gutenberg and Richter[25]. For the period between 1953 and 1965, magnitudes from Rothe's listing have been recalculated by Newcomb and McCann[13]. Similarly, Engdahl *et al.*[26] precisely determined hypocentral parameters from the ISC listing for the period 1964–95. We considered these revised magnitudes with events *Ms* ‡ 4.5 for the present analysis. For events where *Ms* value is not available, it is obtained from *Mb* using the *Mb–Ms* relation derived for the region. The magnitudes estimated by Gutenberg and Richter[25] and Rothe[24] are equivalent to 20-s *Ms*[27]. The seismicity map of the region shown in Figure 2 is for 100 years (1900–2000), which includes all revised estimates of magnitudes and moments by previous workers.

For preparation of the second dataset, about 240 focal mechanism solutions pertaining to the region have been considered from Harvard CMT listings. For clarity, we have shown 86 events of *Ms* > 5.5 as plotted in Figure 3 (ref. 29). It can be seen from the seismicity map that several large earthquakes display distinct correlation with the SFZ as well as the Sumatran Offshore region. While focal mechanisms of earthquakes along the SFZ show mainly right lateral faulting, in the Sumatran fore arc the mechanisms show mostly thrust-faulting.

Identification of seismogenic belts/sources and deformation velocities

Previous studies on seismicity in relation to overall tectonics of the Sumatra–Java arc region gave valuable information on the first-order segmentation of the arc[30], seismic potential and seismicity in different parts of the arc[13] and seismically active domains within the overriding plate[28]. This information along with other geophysical data has been utilized to identify broad and distinct seismogenic belts/sources. These are (i) the SFZ (ii) the Sumatran fore-arc sliver plate consisting of MFZ, (iii) The Sunda Strait region, (iv) Java onshore region termed as Java Fault Zone (JFZ) and (v) the offshore Java fore-arc region. For belts 1 and 4, the

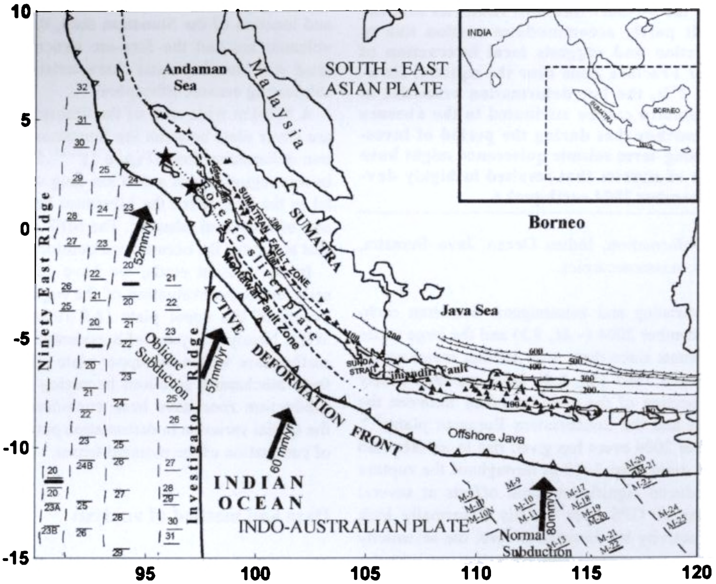

Figure 1. Tectonic sketch map of the Sumatra–Java trench-arc region in eastern Indian Ocean Benioff Zone configuration. Hatched line with numbers indicates depth to the top of the Benioff Zone (after Newcomb and McCann[13]) Magnetic anomaly identifications have been considered from Liu *et al.*[14] and Krishna *et al.*[15]. Magnitude and direction of the plate motion is obtained from Sieh and Natawidjaja[11]. O indicates the location of the recent major earthquakes of 26 December 2004, i.e. the devastating tsunamigenic earthquake (M_w = 9.3) and the 28 March 2005 earthquake (M_w = 8.6).

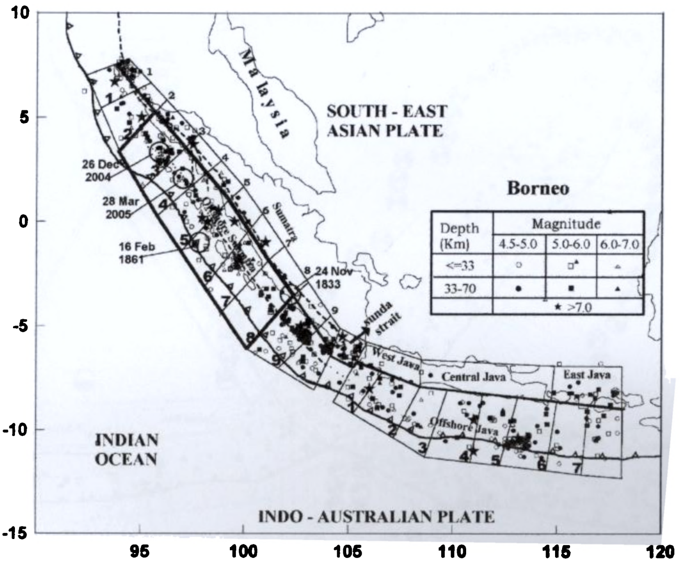

Figure 2. Map showing seismicity and moving window configuration of sources in the Sumatra -Java trench-arc region. The boundary defining the Sumatra and Java Fault zones has been adopted from Slancova *et al.*[28]. The most significant shallow earthquakes in the Sumatran offshore seismic belt are shown as large open circles. The active part of the Sumatran offshore belt is highlighted by a thick line.

boundaries have been defined by Slancova *et al.*[28]. The offshore belts 2 and 5 have been extended up to the deformation front below the Sumatra–Java trench. As seismicity is variable and no segmentation is possible in the case of belts 1, 2 and 5, it is difficult to demarcate individual seismogenic sources. Hence, we employed a moving-window method having a window length of 3–4° and with 50% overlapping, starting from one end to the other. The advantage of this method is that we obtain a continuous variation in deformation pattern along the length of the active seismic belts and also selecting a different window length does not alter the deformation pattern significantly. We succeeded in defining such sources (moving windows); nine sources each along the SFZ and Sumatran fore arc region, and seven sources in the offshore Java region. Due to low seismicity along the JFZ, it is separated into three seismogenic sources, namely West Java, Central Java and East Java. The Sunda strait is considered as a single seismogenic source. Each window representing the seismogenic source along the arc has been numbered as shown in the Figure 2. The deformation velocities (velocity tensor) have been estimated for each of these seismogenic sources. The eigen values and the corresponding eigen vectors represent the magnitude and direction of the principal components of deformation. For a better understanding of the horizontal plate velocities, only those eigen vectors with a plunge less than 25° have been presented in Figure 4.

Results and discussion

Estimation of the moment release pattern and crustal deformation rates based on 100 years of shallow seismicity in comparison with previous studies, brings out significant information about the Sumatra–Java arc region. Some salient results on the deformation pattern are discussed with a view to understanding the geodynamics of the region.

Sumatran Fault Zone

Most of the focal mechanism solutions along the SFZ show pure right lateral strike-slip faulting, which agrees well with the geological observations. All along its length, the deformation velocities suggest nearly N–S compression and E–W extension.

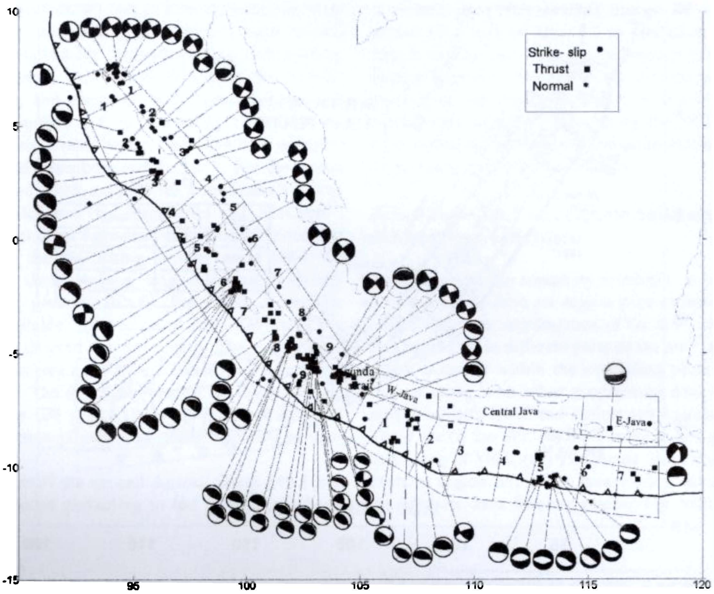

Figure 3. Map showing events for which focal mechanism solutions are available from the Harvard CMT catalogue. For clarity, the mechanisms have been plotted for only those events with $Ms \geq 5.5$. Classification of mechanisms into strike-slip, thrust and normal events is from Kumar *et al.*[29].

The slip rate along the SFZ should range between 30 and 50 mm/yr, assuming that the fault accommodates all the trench-parallel components of convergence between the Indo-Australian and Eurasian plates[31]. Based on SPOT images and topographic maps, Bellier and Sebrier[32] estimated slip rates along SFZ, showing a value of about 23 mm/yr in the north that decreases to 6 mm/yr in the south. Combined analysis of historical triangulation and recent GPS measurements along the SFZ indicate slip rates of 23 to 24 mm/yr[33]. There is a general northward increase in slip rate along the SFZ[34,35]. It is suggested that no significant fore-arc stretching occurs due to slip rate variation along the SFZ and oblique convergence may be accommodated by deformation of 500 km wide zone between the fore-arc to the back-arc domains[35]. The estimated velocity values along the SFZ seismic belt indicate variation in seismically active deformation with maximum dextral shear motion (seismic slip) of 29 mm/yr in the central part to 1 and 8 mm/yr both southward and northward respectively. Except between 0 and 2°S, the estimated velocities are significantly less than the geologically estimated slip rates as well as geodetically measured slip rates, which suggests that considerable amount of slip along the fault may be taken up aseismically.

Sumatran fore-arc region

The Sumatran fore-arc region constitutes the Mentawai islands and the regionally extending MFZ. Majority of strong earthquakes in both the historic and instrumental catalogues of Sunda arc are located in this region. A close examination of the deformation pattern shows that compressive stresses dominate here. The focal mechanism solutions obtained from Harvard CMT catalogue since 1977 in this region and the large 1935 and 1984 events show thrust-faulting mechanisms in the offshore Sumatra[36]. The Sumatran fore-arc perhaps is the most active deformation belt in the region characterized by the occurrence of large historical (1833 and 1861), recent (1935 and 1984) and most recent (2004 and 2005) seismic events. The arc-parallel shear in the Sumatran fore-arc may be taken up on more than one strike-slip fault or shear zone[12]. However, McCaffrey *et al.*[37] observed that this additional strike-slip required might not be accommodated along the MFZ, as the GPS network along the northern part of MFZ does not indicate such large transverse motions. Samuel and Harbury[38] interpreted the trace of the MFZ on the Nias Island to be a reverse fault. Also, there is a significant component of dip-slip in Pliocene along the MFZ[11].

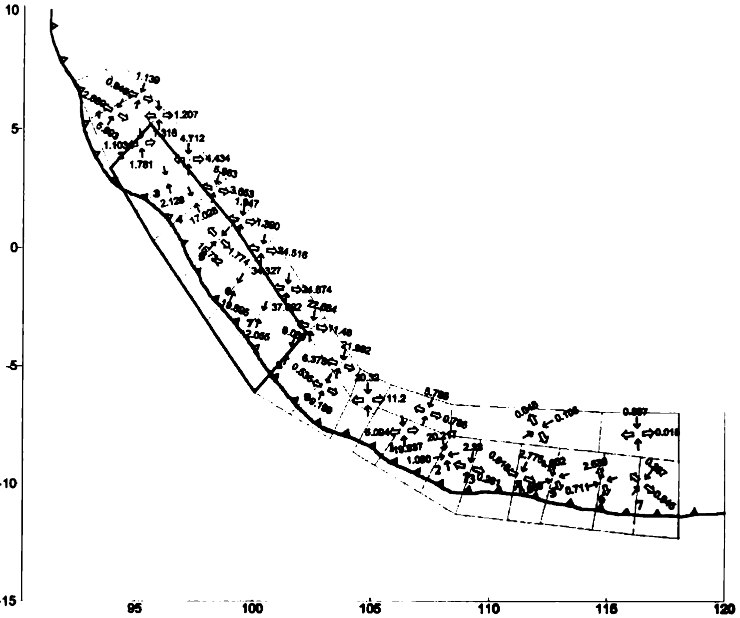

Figure 4. Distribution of deformation velocities calculated for overlapping seismogenic sources in the Sumatra–Java trench-arc region. Values are in mm/yr. Converging arrows indicate compression, while diverging arrows indicate extension.

The deformation velocities estimated for the offshore Sumatra fore-arc region indicate dominantly compression, with higher compressional velocities of 19 mm/yr along N45° near the equator. The deformation pattern further indicates that a portion of the motion is taken up by strike-slip or oblique slip, which means that the MFZ partly accommodates motion due to oblique subduction. Higher deformation velocities (sources 4–6) near the equator may imply the effect of local interaction of the Investigator Fracture Zone, as evidenced by the occurrence of the 1935 and 1984 events[36]. Such subducted ridges or seamounts may act as a mechanical barrier and produce large earthquakes[39]. Newcomb and McCann[13] suggested that the interaction of the Investigator Fracture Zone might have increased interplate coupling in the region. Based on GPS observations, Prawirodirdjo *et al.*[40] observed abrupt change in coupling of the fore-arc to the subducting plate on either side of the equator. This boundary coincides with the rupture zones of the 1833 and 1861 thrust earthquakes. Geodetic data of Bock *et al.*[41], and coral growth around Batu islands region[42] have been used by Simoes *et al.*[43] to identify the locked fault zone down to a depth between 35 and 57 km. However, north of 2°N, the Sumatran fore-arc region (sources 2 and 3) is characterized by the absence of any significant earthquakes in the historical as well as recent earthquake catalogues, which give rise to low deformation values in this region. The long quiescence in this region indicates lock-up stresses over large time intervals, which subsequently resulted in the occurrence of the highly devastating earthquake of 26 December 2004. This mega thrust earthquake caused increase in co-seismic stress on thrust planes in the subduction zone further southeast[44,45] and gave rise to the second major event on 28 March 2005.

Sunda Strait

The Sunda Strait is a consequence of the northwestward motion of the southwestern part of the Sumatran block along the Central Sumatran Fault. The extension zone widens southwestward and changes into a composite zone of strike-slip as well as normal faulting[46]. It is observed that the area is subjected to NW–SE extension because of the motion along Sumatran Fault and to NE–SW compression because of subduction. The region is a comparatively quiet zone with a cluster of moderate and large earthquakes immediately adjacent to the west coast of Java. Some studies indicate southward extension of the SFZ in the Sunda Strait[11,47].

The region shows a compressional deformation of 20.32 – 2.73 mm/yr along the north direction and extensional deformation of 11.2 – 1.5 mm/yr along N 88°, giving rise to a dextral slip of 13 mm/yr in the region.

Java Fault Zone

Seismicity in this region is extremely low compared to that along the SFZ. Lack of major events in the Java region has been ascribed to differential motion at the plate margin, which is principally being taken up either aseismically or by small-magnitude earthquakes[13]. As seismicity is sparse, the JFZ has been divided into three individual segments as mentioned previously. The eigen system of the velocity tensor for the JFZ indicates dominance of compressional deformation. While western Java shows a compression of 5.7 – 0.8 mm/yr along N20° direction and extension of 0.8 – 0.1 mm/yr along N110° direction, deformation in central and eastern Java is negligible due to the absence of large earthquakes within the upper plate.

Java fore-arc region

Offshore Java region shows considerable seismicity and earthquake focal mechanisms show thrust and strike-slip events with few normal faulting events. The strike-slip events may account for the presence of the Cimanderi Fault in Western Java (sources 1 and 2). Deformation velocities indicate dominance of compression (average 19 mm/yr) in the western part, which gradually changes to extension (average 3 mm/yr) towards the eastern part. The deformation pattern further indicates that the Java segment of the arc is seismically less active than the Sumatran segment during the period of investigation, as also observed by Newcomb and McCann[13] based on historical earthquake records. They attribute this difference due to variation in interplate coupling related to the age of the subducting lithosphere in these two regions.

Conclusions

Based on 100 years of hypocentral data of shallow earthquakes in the Sumatra–Java trench-arc region, a detailed seismotectonic evaluation in terms of active crustal deformation pertaining to five major seismogenic belts/sources is made using the method of summation of moment tensors. The results indicate large variation in dextral shear motion from 1 to 29 mm/yr along the SFZ. The estimated slip rates are in good agreement with the geological or GPS-derived slip rate estimates along the fault between 0 and 2°S. Very low slip rates in other segments of the fault suggest that considerable amount of slip along the fault may be taken up aseismically. The deformation velocities estimated for the offshore Sumatra fore arc region indicate dominantly compression with higher compressional velocities of 19 mm/yr along N45° near the equator due to the local interaction of the Investigator Fracture Zone. The deformation pattern further indicates that the MFZ partly accommodates motion due to oblique subduction. Deformation velocities for the Sunda Strait show compression of 20 – 2.7 mm/yr along N–S and extension of 11 – 1.5 mm/yr along E–W direction and give rise to dextral slip of 13 mm/yr. Western Java shows considerable compressional deformation, whereas deformation in the central and eastern Java is negligible. In the offshore Java fore arc region, deformation velocities indicate dominance of compression (19 mm/yr) in the western part, which gradually changes to extension (3 mm/yr) towards the east. The crustal deformation pattern further indicates that the Java segment of the arc is seismically less active than the Sumatran segment during the period of investigation.

1. Lay, T. *et al.*, The great Sumatra–Andaman earthquake of 26 December 2004. *Science*, 2005, **308**, 1127–1133.
2. Ammon, C. J. *et al.*, Rupture process of the 2004 Sumatra–Andaman earthquake. *Science*, 2005, **308**, 1133–1139.
3. Ishii, M., Shearer, P. M., Houston, H. and Vidale, J. E., Extent, duration and speed of the 2004 Sumatra–Andaman earthquake imaged by Hi-Net array. *Nature*, 2005, **435**, 933–936.
4. Kruger, F. and Ohrnberger, M., Tracking the rupture of the *Mw* 9.3 Sumatra earthquake over 1150 km at teleseismic distance. *Nature*, 2005, **435**, 937–939.
5. Banerjee, P., Pollitz, F. F. and Burgmann, R., The size and duration of the Sumatra–Andaman earthquake from far-field static offsets. *Science*, 2005, **308**, 1769–1771.
6. Catherine, J. K., Gahalaut, V. K. and Sahu, V. K., Constraints on rupture of the 26 December 2004, Sumatra earthquake from far-field GPS observations. *Earth Planet. Sci. Lett.*, 2005, **237**, 673–679.
7. Veevers, J. J., Powell, C. M. and Roots, S. R., Review of seafloor around Australia, synthesis of the patterns of spreading. *Aust. J. Earth Sci.*, 1991, **38**, 373–389.
8. Kirby, S. H., Stein, S., Okal, E. A. and Rubie, D. C., Meta stable mantle phase transformations and deep earthquakes in subducting oceanic lithosphere. *Rev. Geophys.*, 1996, **34**, 261–306.
9. Schoffel H. J. and Das, S., Fine details of the Wadati–Benioff zone under Indonesia and its geodynamic implications. *J. Geophys. Res. B*, 1999, **104**, 13101–13114.
10. Curray, J. R., Moore, D. G., Lawver, L., Emmel, E., Raith, R., Henry, M. and Kieckhefer, R., Tectonics of the Andaman sea and Burma. *Am. Assoc. Pet. Geol. Mem.*, 1979, **29**, 189–198.
11. Sieh, K. and Natawidjaja, D., Neotectonics of the Sumatran fault, Indonesia. *J. Geophys. Res. B*, 2000, **105**, 28295–28326.
12. Diament, M., Harjono, H., Karta, C., Deplus, C., Gerard, M. and Malod, J., Mentawai fault zone off Sumatra: A new key to the geodynamics of the western Indonesia. *Geology*, 1992, **20**, 259–262.
13. Newcomb, K. R. and McCann, W. R., Seismic history and seismotectonics of the Sunda arc. *J. Geophys. Res.*, 1987, **92**, 421–439.
14. Liu, C. S., Curray, J. R. and McDonald, J. M., New constraints on the tectonic evolution of the eastern Indian Ocean. *Earth Planet. Sci. Lett.*, 1983, **65**, 331–342.
15. Krishna, K. S. *et al.*, Tectonic model for the evolution of oceanic crust in the northeastern Indian Ocean from the late Cretaceous to the early Tertiary. *J. Geophys. Res. B*, 1983, **100**, 20011–20024.
16. Papazachos, C. B. and Kiratzi, A., A formulation for reliable estimation of active crustal deformation and its application to central Greece. *Geophys. J. Int.*, 1992, **111**, 424–432.

17. Kostrov, V. V., Seismic moment and energy of earthquakes and seismic flow of rocks. *Phys. Solid Earth, Lzv. Acad. Sci., USSR*, 1974, **1**, 23–44.
18. Jackson, J. and McKenzie, D. P., The relationship between plate motion and seismic moment tensors, and the rates of active deformation in the Mediterranean and Middle East. *Geophys. J. Int.*, 1988, **93**, 45–73.
19. Papazachos, C. B., Kiratzi, A. and Papazachos, B., Rates of active crustal deformation in the Aegean and the surrounding area. *J. Geodyn.*, 1992, **16**, 147–179.
20. Kiratzi, A., A study on the active crustal deformation of the north and east Anatolian fault zones. *Tectonophysics*, 1993, **218**, 375–381.
21. Kiratzi, A. and Papazachos, C. B., Active crustal deformation from the Azores triple junction to the Middle East. *Tectonophysics*, 1995, **243**, 1–24.
22. Papazachos, C. B. and Kiratzi, A., A detailed study of the active crustal deformation in the Aegean and surrounding area. *Tectonophysics*, 1996, **253**, 129–153.
23. Radhakrishna, M. and Sanu, T. D., Shallow seismicity, stress distribution and crustal deformation pattern in the Andaman-West Sunda arc and Andaman Sea, northeastern Indian Ocean. *J. Seismol.*, 2002, **6**, 25–41.
24. Rothe, J. P., *The Seismicity of the Earth*, UNESCO, Paris, 1969, p. 336.
25. Gutenberg, G. and Richter, C. F., *Seismicity of the Earth and its Associated Phenomena*, Princeton University Press, Princeton, NJ, USA, 1954, p. 310.
26. Engdahl, E. R., van der Hilst, R. D. and Buland, R., Global teleseismic earthquake relocation with improved travel times and procedures for depth determination. *Bull. Seismol. Soc. Am.*, 1998, **88**, 722–743.
27. Geller, R. J. and Kanamori, H., Magnitudes of great shallow earthquakes from 1902 to 1952. *Bull. Seismol. Soc. Am.*, 1977, **67**, 587–598.
28. Slancova, A., Spicak, A., Hanus, V. and Vanek, J., How the state of stress varies in the Wadati-Benioff Zone: indications from focal mechanisms in the Wadati-Benioff Zone beneath Sumatra and Java. *Geophys. J. Int.*, 2000, **143**, 909–930.
29. Kumar, M. R., Rao, N. P. and Chalam, S. V., A seismotectonic study of the Burma and Andaman arc regions using centroid moment tensor data. *Tectonophysics*, 1996, **253**, 155–165.
30. Chandra, U., Tectonic segmentation of the Burmese Indonesian arc. *Tectonophysics*, 1984, **105**, 279–289.
31. Jarrad, R. D., Relations among subduction parameters. *Rev. Geophys.*, 1986, **24**, 217–284.
32. Bellier, O. and Sebrier, M., Relationship between tectonism and volcanism along the Great Sumatran Fault zone deduced by SPOT image analyses. *Tectonophysics*, 1994, **233**, 215–231.
33. Prawirodirdjo, L., Bock, Y., Genrich, J. F., Puntodewo, S. S. O., Rais, J., Subarya, C. and Sutisna, S., One century of tectonic deformation along the Sumatran fault from triangulation and global positioning system surveys. *J. Geophys. Res. B*, 2000, **105**, 28343–28361.
34. McCaffrey, R., Slip vectors and stretching of the Sumatran fore arc. *Geology*, 1991, **19**, 881–884.
35. Bellier, O. and Sebrier, M., Is the slip rate variation on the Great Sumatran Fault accommodated by fore-arc stretching? *Geophys. Res. Lett.*, 1995, **22**, 1969–1972.
36. Rivera, L., Sieh, K., Helmberger, D. and Natawidjaja, D., A comparative study of the Sumatran subduction-zone earthquakes of 1935 and 1984. *Bull. Seismol. Soc. Am.*, 2002, **92**, 1721–1736.
37. McCaffrey, R. *et al.*, Strain partitioning during oblique plate convergence in northern Sumatra: Geodetic and seismologic constraints and numerical modeling. *J. Geophys. Res. B*, 2000, **105**, 28363–28376.
38. Samuel, M. A. and Harbury, N. A., The Mentawai Fault Zone and deformation of the Sumatra fore arc in the Nias area, in *Tectonic Evolution of Southeast Asia* (eds Hall, R. and Blundell, D. J.), Geol. Soc. Spl. Publ., 1996, vol. 106, pp. 337–351.
39. Kelleher, J. and McCann, W., Buoyant zones, great earthquakes, and unstable boundaries of subduction, *J. Geophys. Res.*, 1976, **81**, 4885–4898.
40. Prawirodirdjo, L. *et al.*, Geodetic observations of inter seismic segmentation at the Sumatra subduction zone. *Geophys. Res. Lett.*, 1997, **24**, 2601–2604.
41. Bock, Y. *et al.*, Crustal motion in Indonesia from GPS measurements. *J. Geophys. Res. B*, 2003, **108**, 2367.
42. Natawidjaja, D. H., Sieh, K., Ward, S. N., Cheng, H., Edwards, R. L., Galetzka, J. and Suwargadi, B. W., Pale geodetic records of seismic and aseismic subduction from central Sumatra micro atolls, Indonesia. *J. Geophys. Res. B*, 2004, **109**.
43. Simoes, M., Avouac, J. P. and Henry, R. C. P., The Sumatra subduction zone: A case for a locked fault zone extending into the mantle. *J. Geophys. Res.*, 2004, **109**, doi: 10.1029/2003JB002958.
44. McCloskey, J., Nalbant, S. S. and Steacy, S., Earthquake risk from co-seismic risk. *Nature*, 2005, **434**, 291.
45. Gahalaut, V. K. and Kalpna, 28 March 2005 Sumatra earthquake: expected, triggered or aftershock? *Curr. Sci.*, 2005, **89**, 452–454.
46. Huchon, P. and Le Pichon, X., Sunda Strait and Central Sumatra Fault. *Geology*, 1984, **12**, 668–672.
47. Pramumijoyo, S. and Sebrier, M., Neogene and Quaternary fault kinematics around the Sunda strait area, Indonesia. *J. SE Asian Earth Sci.*, 1991, **6**, 137–145.

ACKNOWLEDGEMENTS. S.L. thanks Cochin University of Science and Technology and CSIR, New Delhi for awarding research fellowship.

Received 28 April 2005; revised accepted 28 November 2005